

Biogenesis of Interleukin 10 in Macrophages exposed to *Schistosoma mansoni* cercarial products

David Esteban Sanín Peña

Ph.D.

University of York

Biology

July 2014

Abstract

The interaction between antigen presenting cells in the skin with molecules secreted by cercariae of *Schistosoma mansoni* constitutes the first point of contact between the host's immune system and the pathogen. High levels of IL-10 are produced in infected skin, and macrophages, which readily take up the molecules secreted by cercariae, are among the first population recruited to the site of infection.

Macrophages produce high levels of IL-10 when exposed to cercarial excreted/secreted (E/S) products, as well as other cytokines and chemokines (i.e. IL-1 β , IL-6, TNF- α and CCL2), but it is unknown what signalling pathway(s) drive the production of IL-10, rather than other pro-inflammatory cytokines such as IL-12p40, or how they are linked to innate recognition of E/S antigens. Our findings demonstrate that TLRs, particularly TLR4 and TLR2, play a fundamental role in the induction of IL-10. Furthermore, MyD88 is essential for the activation of multiple MAPK pathways which in turn control E/S product-induced IL-10. Selective chemical inhibition of specific pathways allowed us to determine the contribution of each signalling cascade. We established that the activation of MEK/Erk and p38 induced the production of IL-10, whilst it negatively affected IL-12p40. Furthermore, the activation of these kinases leads to the phosphorylation of CREB, which is responsible for the observed effects on IL-10 by being recruited to the promoter of the IL-10 gene. Finally, we show that TLR4 and TLR2 are directly implicated in the activation of these pathways and that macrophages in the skin produce IL-10 as a result of cercarial invasion.

From these findings we propose a mechanism by which *S. mansoni* E/S products induce a specific MAPK signalling cascade that triggers IL-10 production in macrophages by binding their TLRs, thus polarizing the immune response in the skin.

Table of contents

Abstract	2
Table of contents	3
List of figures	9
List of tables	14
List of diagrams	15
Acknowledgements	16
Author's declaration	18
1 Introduction	19
1.1 Schistosomiasis	19
1.1.1 Overview.....	19
1.1.2 Pathology, treatment and vaccination	20
1.1.3 Immune response.....	21
1.2 <i>S. mansoni</i> cercarial skin infection	24
1.2.1 Immune responses in the skin.....	24
1.2.2 Cercarial structure and E/S products.....	26
1.2.3 Immune responses in the skin to invading cercariae.....	28
1.3 Macrophages	30
1.3.1 Macrophage activation	30
1.3.2 Endocytosis	31
1.3.3 Macrophages in <i>S. mansoni</i> infection.....	32
1.4 Innate immune signaling	34
1.4.1 TLRs.....	34
1.4.2 Mitogen activated protein kinases	36
1.4.3 Innate immune signaling in <i>S. mansoni</i> infection	37
1.5 IL-10	39
1.5.1 IL-10 in <i>S. mansoni</i> infection	40
1.6 Setting the scene	41
2 Materials and Methods	42
2.1 Animals and bone marrow	42
2.2 Parasites and parasite derived material	42
2.2.1 Generation of cercarial E/S products (0-3hRP).....	43
2.3 <i>In vitro</i> culture and stimulation of Bone marrow derived macrophages ..	43
2.4 Flow cytometric analysis of antibody-labeled cells	44

2.4.1	Labeling of cells for intracellular molecules	44
2.4.2	Labeling of cells for intracellular phosphorylated proteins.....	44
2.5	Enzyme linked immune absorbent assays	45
2.6	RNA extraction and gene expression analysis by Polymerase Chain Reaction	45
2.7	Statistical analysis	46
3	Global changes in the expression of genes and proteins in BMMφs stimulated with cercarial E/S products	49
3.1	Introduction.....	49
3.2	Chapter specific materials and methods	52
3.2.1	Label free quantitative proteomics of membrane proteins.....	52
3.2.1.1	Membrane protein extraction	52
3.2.1.2	Label free quantitative proteomics.....	52
3.2.1.3	Gene ontology (GO) term enrichment and subcellular localization analysis of regulated proteins	53
3.2.2	Kinase proteome profiler array	53
3.2.3	qPCR array for MAPK and Toll-like receptor signaling.....	54
3.3	Results	55
3.3.1	In vitro differentiation of bone marrow cells into macrophages	55
3.3.2	Cytokine production by BMMφs in response to overnight stimulation with 0-3hRP and other PAMPs	56
3.3.2.1	Endotoxin contamination present in 0-3hRP is neutralized by Polymixin B....	56
3.3.2.2	0-3hRP induces a distinct cytokine response in BMMφs	56
3.3.3	Changes to the membrane proteome of BMMφs after stimulation with 0- 3hRP and LPS.....	57
3.3.3.1	Membrane protein extraction and LC-MS/MS pre-run.....	57
3.3.3.2	Label-free quantitative proteomics of membrane enriched protein samples ..	59
3.3.3.3	Validation of protein expression using flow cytometric analysis of antibody- labelled 0-3hRP treated BMMφs	60
3.3.4	Phosphorylation of MAPKs in BMMφs after stimulation with 0-3hRP	61
3.3.4.1	Kinase proteome profiler array of BMMφs treated with 0-3hRP	61
3.3.4.2	Densitometry analysis of kinase proteome profiler array.....	62
3.3.4.3	Fold changes in kinase activation after stimulation with 0-3hRP.....	62
3.3.5	Rapid gene expression changes in BMMφs after stimulation with 0-3hRP; analysis by qPCR array.....	63
3.3.5.1	BMMφs treated with 0-3hRP alter the expression of several genes	64
3.3.5.2	qPCR for specific gene transcripts corroborate PCR array	64
3.4	Discussion	66
3.4.1	0-3hRP elicits a unique response in BMMφs.....	66

3.4.2	Changes in membrane proteins in BMMφs stimulated with 0-3hRP	68
3.4.3	Activation of MAPKs in BMMφs stimulated with 0-3hRP is tightly regulated 69	
3.4.4	Gene expression in BMMφs exposed to cercarial E/S products.....	71
3.5	Summary	73
4	Signaling pathways in BMMφs exposed to cercarial E/S products	95
4.1	Introduction.....	95
4.2	Chapter specific material and methods	98
4.2.1	MAPKs inhibitors	98
4.2.2	Chromatin Immunoprecipitation.....	98
4.2.2.1	PCR of precipitated DNA.....	99
4.3	Results	100
4.3.1	Dynamics of cytokine production in BMMφs exposed to 0-3hRP	100
4.3.2	BMMφs require TLRs to produce cytokines in response to 0-3hRP	100
4.3.2.1	BMMφs from MyD88, TLR4 or TLR2 deficient mice are phenotypically comparable to WT BMMφs, but respond differentially to innate immune ligands/stimuli. 100	
4.3.2.2	MyD88, TLR4 and TLR2 are required for IL-10 and IL-12p40 production in BMMφs exposed to 0-3hRP	101
4.3.3	Dynamics of BMMφ activation of several signaling molecules in response to 0-3hRP	102
4.3.3.1	Levels of phosphorylated Erk1/2 but not total Erk1/2 change in BMMφs exposed to 0-3hRP	102
4.3.3.2	Levels of phosphorylated p38, CREB and RSK are increased in BMMφs stimulated with 0-3hRP	102
4.3.3.3	BMMφs require MyD88, TLR4 and TLR2 to phosphorylate MAPKs in response to 0-3hRP	103
4.3.4	Hierarchy of signaling pathways in BMMφs exposed to 0-3hRP	103
4.3.4.1	Phosphorylation of Erk1/2 in BMMφs exposed to 0-3hRP depends on NF-κB activation and Tpl2 release	103
4.3.4.2	Chemical inhibition of Erk1/2 and p38 pathways reduces the phosphorylation of CREB and RSK.....	104
4.3.4.3	Other components of NF-κB are activated by 0-3hRP in BMMφs	105
4.3.5	Signaling pathways modulate the production of cytokines in BMMφs exposed to 0-3hRP.....	105
4.3.5.1	Chemical inhibition of signaling pathways results in modulation of cytokine responses	106
4.3.5.2	Abrogation of Erk1/2 phosphorylation in Tpl2 ^{-/-} BMMφs in response to 0-3hRP modulates the production of IL-10 and IL-12p40	107

4.3.5.3 MAPK signaling in BMMφs limits IL-12p40 production independently of IL-10
108

4.3.6 CREB is recruited to the IL-10 promoter to induce the activation of its
transcription in BMMφs exposed to 0-3hRP109

4.4 Discussion111

4.4.1 BMMφs carefully orchestrate the production of IL-10 and IL-12p40 in
response to 0-3hRP111

4.4.2 BMMφs use MAPKs downstream of TLRs to produce IL-10 in response to
0-3hRP112

4.4.3 Phosphorylated CREB is recruited to the IL-10 promoter to modulate its
transcription in BMMφs exposed to 0-3hRP113

4.5 Summary115

**5 Internalization of *S. mansoni* cercarial E/S products by BMMφs is
required for cytokine production..... 140**

5.1 Introduction.....140

5.2 Chapter specific material and methods142

5.2.1 Fluorescent labeling of *S. mansoni* cercarial E/S products142

5.2.2 Uptake inhibitors.....142

5.2.3 Confocal microscopy of BMMφs exposed to fluorescently labeled cercarial
E/S products142

5.3 Results143

5.3.1 BMMφs internalize 0-3hRP143

5.3.1.1 0-3hRP is internalized by BMMφs via endocytosis in an actin dependent
manner. 143

5.3.1.2 0-3hRP uptake by BMMφs depends partly on PI3K signaling144

5.3.2 MAPK activation in BMMφs exposed to 0-3hRP is partly dependent on
internalization144

5.3.3 IL-10 and IL-12p40 production is dependent on internalization of 0-3hRP
by BMMφs145

5.4 Discussion147

5.4.1 Uptake of 0-3hRP by BMMφs requires actin polymerization and intact PI3K
signaling147

5.4.2 MAPK activation and cytokine production in BMMφs exposed to 0-3hRP is
dependent on uptake.....148

5.5 Summary151

**6 Macrophages in the skin condition the immune response to *S.*
mansoni cercariae by producing IL-10 162**

6.1	Introduction.....	162
6.2	Chapter specific materials and methods	164
6.2.1	Skin infection with <i>S. mansoni</i> cercariae	164
6.2.2	Dermal exudate cells	164
6.2.2.1	Detection of intracellular IL-10 in DEC.....	164
6.3	Results	166
6.3.1	Different populations of cells in the skin change after <i>S. mansoni</i> infection 166	
6.3.1.1	Global changes in DEC populations after <i>S. mansoni</i> cercariae infection....	166
6.3.1.2	Further characterization of monocyte populations in the skin after <i>S. mansoni</i> cercariae infection.....	167
6.3.2	IL-10 is produced by whole skin biopsies after <i>S. mansoni</i> infection	168
6.3.2.1	Skin infected with <i>S. mansoni</i> cercariae produces IL-10 and IL-12p40.....	168
6.3.2.2	Dynamics of IL-10 production by infected skin in culture.....	168
6.3.2.3	IL-10 producing cells are increased in skin infected with <i>S. mansoni</i> cercariae 168	
6.3.3	F4/80 ⁺ cells in the skin produce IL-10 in response to <i>S. mansoni</i> cercariae 169	
6.3.4	Higher proportion CD3 ⁺ CD4 ⁺ T cells in the skin produce IL-10 in response to <i>S. mansoni</i> cercariae.....	170
6.4	Discussion	171
6.4.1	<i>S. mansoni</i> infection alters the proportions and numbers of immune cells in the skin	171
6.4.2	<i>S. mansoni</i> infection triggers the production of IL-10 by tissue resident macrophages.....	173
6.5	Summary	177
7	Discussion	191
7.1	<i>S. mansoni</i> cercarial E/S products have a profound impact on macrophage phenotype.....	191
7.2	TLR2 and TLR4 drive the production of IL-10 by macrophages in response to cercarial E/S products	193
7.3	Endosomal recognition of cercarial E/S products by macrophages is likely to play an important role in cytokine responses.....	196
7.4	Macrophages in the skin are an important source of IL-10 in <i>S. mansoni</i> cercarial infection.....	199
	Concluding remarks	202
8	Appendices	204

8.1	Membrane protein analysis using label free proteomics	205
8.2	Kinase proteome profiler	231
8.3	Fractionation of <i>S. mansoni</i> cercarial E/S products	233
8.3.1	Fractionation of 0-3hRP	233
8.3.2	SDS polyacrylamide gel electrophoresis (PAGE) of fractions	233
8.3.3	Differential effects of soluble and pellet fractions of <i>S. mansoni</i> E/S products on cytokine production.....	233
8.3.4	0-3hRP _p inhibits TLR4 mediated IL-12p40 production in BMM ϕ exposed to LPS	234
8.3.5	Protein profile of different fractions <i>S. mansoni</i> E/S products	235
8.3.6	0-3hRP _p fluoresces naturally	235
8.4	Sm16, a protein in 0-3hRP_p, inhibits BMMϕ activation by TLR ligands ..	245
8.4.1	Western blot analysis of fractions	245
8.4.2	Sm16 is present in 0-3hRP _p	245
8.4.3	Sm16 blocks cytokine production in response to TLR4 and TLR3, but not TLR2 ligands in BMM ϕ s	246
8.4.4	Sm16 is able to prevent BMM ϕ activation in the context of IFN- γ stimulation	247
8.4.5	TLR2 is not required for rSm16 effect on cytokine production in BMM ϕ s	248
8.4.6	Sm16 is taken up by BMM ϕ s into a distinct processing pathway	249
	List of Abbreviations	260
	References.....	265

List of figures

Figure 3.1 Production of macrophages by differentiation of bone marrow cells from femurs and tibia of C57BL/6 mice.....	74
Figure 3.2 Cytokine production by BMM ϕ s in response to 0-3hRP is not due to endotoxin contamination	75
Figure 3.3 Cytokine production by BMM ϕ s exposed to different PAMPs.....	76
Figure 3.4 Venn diagram depicting the protein hits for the membrane proteome of BMM ϕ s after stimulation with 0-3hRP, LPS, or Media	77
Figure 3.5 Comparison of regulated proteins in BMM ϕ s stimulated with 0-3hRP or LPS	78
Figure 3.6 (continued) Expression of CD14, CD36, and MSR1 in BMM ϕ s exposed to 0-3hRP	80
Figure 3.7 Kinase proteome profiler array of BMM ϕ s exposed to 0-3hRP	81
Figure 3.8 Densitometry analysis of kinase proteome profiler array	82
Figure 3.9 Fold changes in MAPK phosphorylation	83
Figure 3.10 Regulated genes in treated BMM ϕ s	84
Figure 3.11 Gene expression differences in stimulated BMM ϕ s.....	85
Figure 3.12 Validation of transcript levels in stimulated BMM ϕ s.....	86
Figure 3.13 Time course of transcription of regulated genes in BMM ϕ s treated with 0-3hRP	87
Figure 4.1 Time course of cytokine production in BMM ϕ s exposed to 0-3hRP	116
Figure 4.2 BMM ϕ s deficient on MyD88, TLR4 or TLR2 are phenotypically similar to WT BMM ϕ s.....	117
Figure 4.3 BMM ϕ s deficient on MyD88, TLR4 or TLR2 are selectively able to respond to specific PAMPS	118
Figure 4.4 BMM ϕ s require TLRs for cytokine production in response to 0-3hRP	119
Figure 4.5 Changes in levels of tErk in BMM ϕ s exposed to 0-3hRP	120

Figure 4.6 Changes in levels of P-Erk in BMMφs exposed to 0-3hRP.....	121
Figure 4.7 BMMφs activate p38, CREB and RSK, but not Akt, in response to 0-3hRP	122
Figure 4.8 Quantitation of phosphorylated p38, CREB, RSK and Akt in BMMφs exposed to 0-3hRP	123
Figure 4.9 Phosphorylation of Erk1/2 in response to 0-3hRP is dependent on TLR signaling	124
Figure 4.10 Phosphorylation of p38 in response to 0-3hRP is dependent on TLR signaling.....	125
Figure 4.11 Phosphorylation of CREB in response to 0-3hRP is dependent on TLR signaling	126
Figure 4.12 NF-κB (p105) is activated in BMMφs exposed to 0-3hRP	127
Figure 4.13 BMMφs deficient for Tpl2 are similar to WT BMMφs.....	128
Figure 4.14 Phosphorylation of Erk1/2 and CREB in response to 0-3hRP is dependent on Tpl2.....	129
Figure 4.15 Chemical inhibition of MAPKs in BMMφs exposed to 0-3hRP reveals pathway hierarchy	130
Figure 4.16 Activation of NF-κB (p65) in BMMφs exposed to 0-3hRP is not dependent on Erk1/2 or p38 signaling	131
Figure 4.17 Chemical inhibition of signaling pathways regulates cytokine production in BMMφs exposed to 0-3hRP	132
Figure 4.18 Tpl2 deficient BMMφs have reduced IL-10 production and increased IL-12p40 production in response to 0-3hRP	134
Figure 4.19 BMMφs deficient for IL-10 are similar to WT BMMφs	135
Figure 4.20 Chemical inhibition of signaling pathways regulates IL-12p40 production in IL-10 ^{-/-} BMMφs exposed to 0-3hRP	136
Figure 4.21 Chemical inhibition of signaling pathways regulates IL-10 and IL-12p40 mRNA in BMMφs exposed to 0-3hRP	137
Figure 4.22 Fragment size of sonicated chromatin in BMMφs	138

Figure 4.23 Phosphorylated CREB is recruited to the promoter of IL-10 in BMMφs exposed to 0-3hRP	139
Figure 5.1 0-3hRP uptake by BMMφs requires actin polymerization	152
Figure 5.2 PI3K inhibition of BMMφs limits uptake of 0-3hRP	153
Figure 5.3 Chemical inhibition of uptake in BMMφs exposed to 0-3hRP limits Erk1/2 phosphorylation	154
Figure 5.4 Chemical inhibition of uptake in BMMφs exposed to 0-3hRP limits p38 phosphorylation.....	155
Figure 5.5 Chemical inhibition of uptake in BMMφs exposed to 0-3hRP limits CREB phosphorylation.....	156
Figure 5.6 PI3K inhibition of BMMφs exposed to 0-3hRP limits Erk1/2 phosphorylation.....	157
Figure 5.7 PI3K inhibition of BMMφs exposed to 0-3hRP limits p38 phosphorylation.....	158
Figure 5.8 PI3K inhibition of BMMφs exposed to 0-3hRP limits CREB phosphorylation.....	159
Figure 5.9 Chemical inhibition of 0-3hRP uptake inhibits cytokine production in BMMφs.....	160
Figure 5.10 Chemical inhibition of PI3K regulates cytokine production in BMMφs exposed to 0-3hRP	161
Figure 6.1 Flow cytometric analysis of cell populations in DEC after <i>S. mansoni</i> cercariae invasion.....	179
Figure 6.2 Total cell numbers in DEC after infection of pinnae with <i>S. mansoni</i> cercariae	180
Figure 6.3 Proportions of cell populations in DEC after infection of pinnae with <i>S. mansoni</i> cercariae	181
Figure 6.4 Numbers of cell populations in DEC after infection of pinnae with <i>S. mansoni</i> cercariae.....	182
Figure 6.5 CD11c expression on MHC-II ⁺ DEC populations recovered from mice 4 days after exposure of pinnae to <i>S. mansoni</i> cercariae.....	183

Figure 6.6 Cytokine production from <i>in vitro</i> cultured skin biopsies from mice infected with <i>S. mansoni</i> cercariae	184
Figure 6.7 IL-10 production time course from skin infected with <i>S. mansoni</i> cercariae	185
Figure 6.8 Proportions of GFP ⁺ DEC after infection with <i>S. mansoni</i> cercariae	186
Figure 6.9 Proportions of GFP ⁺ cell populations in DEC after exposure of pinnae to <i>S. mansoni</i> cercariae	187
Figure 6.10 Number of GFP ⁺ F4/80 ⁺ MHC-II ^{high} cells in DEC from mice after exposure <i>S. mansoni</i> cercariae	188
Figure 6.11 CD11c expression on MHC-II ⁺ GFP ⁺ DEC populations from mice 4 days after exposure to <i>S. mansoni</i> cercariae	189
Figure 6.12 Percentages and number of GFP ⁺ CD3 ⁺ CD4 ⁺ cells in DEC from mice after exposure <i>S. mansoni</i> cercariae	190
Figure 8.1 BMMφs exposed to 0-3hRP fractions secrete differing quantities of IL-10 and IL-12p40.....	237
Figure 8.2 0-3hRP _p blocks IL-12p40 production by BMMφs exposed to LPS	238
Figure 8.3 0-3hRP does not impair IL-12p40 production in BMMφs exposed to LPS	239
Figure 8.4 0-3hRP fractions retain different levels of proteins	240
Figure 8.5 0-3hRP naturally emits red fluorescence	241
Figure 8.6 0-3hRP fluorescence is detectable inside BMMφs	243
Figure 8.7 0-3hRP naturally emits red fluorescence which can be detected on a protein gel as discrete bands.....	244
Figure 8.8 0-3hRP fractions protein profile comparison to rSm16	250
Figure 8.9 Sm16 abundance in 0-3hRP fractions	251
Figure 8.10 rSm16 blocks cytokine production in BMMφs exposed to LPS....	252
Figure 8.11 rSm16 blocks cytokine production in BMMφs exposed to TLR4 and TLR3, but not TLR2 ligands.....	253

Figure 8.12 rSm16 blocks both cytokine production and oxidative burst in BMM ϕ exposed to LPS and IFN- γ	254
Figure 8.13 rSm16 has differential effect on cytokine production in BMM ϕ s exposed to 0-3hRP	255
Figure 8.14 rSm16 blocks IL-12p40 production in BMM ϕ s exposed to TLR4 and TLR3 ligands in a TLR2 independent manner	256
Figure 8.15 Uptake of fluorescently labelled rSm16 by BMM ϕ s	257
Figure 8.16 High resolution image of vesicles containing rSm16 in BMM ϕ s ..	258
Figure 8.17 Intracellular trafficking of rSm16 is delayed compared to dextran processing.....	259

List of tables

Table 2.1 Flow cytometry antibodies.....	47
Table 2.2 PCR Primers	48
Table 3.1 Cellular localization of protein hits (k) and percentages (out 404 hits)	88
Table 3.2 Regulated proteins in 0-3hRP stimulated BMMφs compared to Media	89
Table 3.3 Regulated proteins in LPS stimulated BMMφs compared to Media..	91
Table 3.4 GO term enrichment analysis in terms of biological process	92
Table 3.5 Cellular localization GO term enrichment analysis	93
Table 3.6 qPCR array genes.....	94
Table 8.1 LC-MS/MS pre-run of membrane protein enriched samples sorted based on Mascot score for hits in 0-3hRP treatment.....	205
Table 8.2 Biological process GO terms for regulated proteins	225
Table 8.3 Cellular localization GO terms for regulated proteins	228
Table 8.4 Kinase proteome profiler coordinates and phosphorylation sites ...	231

List of diagrams

Diagram 1.1 World distribution of Schistosomiasis. Taken from Colley et al, 2014	19
Diagram 1.2 <i>Schistosoma mansoni</i> life cycle. Taken from Pearce & MacDonald 2002	20
Diagram 1.3 Immune cells in the skin. Adapted from Pasparakis et al, 2014 ...	25
Diagram 1.4 Schematic of <i>S. mansoni</i> cercaria. Adapted from Dorsey et al, 2002	26
Diagram 1.5 Fluorescent labeling of <i>S. mansoni</i> cercariae revealing pre- and post-acetabular glands. Taken from Paveley et al, 2009	27
Diagram 1.6 Toll like receptor signaling pathway. Taken from Akira et al, 2004	35
Diagram 1.7 TLR activation of MAPKs. Taken from Arthur et al, 2013	37
Diagram 3.1 Previously reported links between MAPKs	70
Diagram 3.2 Summary of global changes in stimulated BMMφs	73
Diagram 4.1 Signaling pathways in BMMφs exposed to 0-3hRP	106
Diagram 4.2 IL-10 biogenesis in BMMφs exposed to cercarial E/S products .	115
Diagram 7.1 IL-10 biogenesis in macrophages exposed to <i>S. mansoni</i> cercarial E/S products	195

Acknowledgements

My nearly 4 years in the University of York have been absolutely incredible. The experience of producing science in such a nurturing and collaborative environment with the full support and guidance I received will be hard to match in the future. I have had the chance to mature as a researcher and interact with a wide community of scientists that influenced and enriched my work. My gratitude has to be expressed to my funding bodies COLFUTURO and COLCIENCIAS, for facilitating my studies. Nonetheless it is the individuals that have helped me throughout this experience that I must truly express my gratitude to.

First and foremost there is my supervisor Dr Adrian Mountford. Words fail to describe my gratitude towards him. His respect of my own ideas, his guidance in making them happen, and his unfailing support when I experience a set back made him truly invaluable. I felt guided but never controlled. He constantly made sure that my work was the best it could be through critical (but gentle) examination of everything I produced. However, his mentorship was not limited to my academic activities. I am indebted to him for his genuine concern for my wellbeing when things got difficult, his encouragement to balance my academic commitments with fun and his support towards my future career. Thanks Adrian! I am extremely grateful for having worked with you!

Thanks also to all the staff in the Technology Facility, but particularly Karen Hogg, Karen Hodgkinson and Graeme Park, who provided essential technical advice (and occasionally a good laugh) to make my work be the best it could be. Dr Harv Isaacs and Dr Nathalie Signoret, both members of my Training Advisory Panel, patiently read my reports and provided amazing feedback on my findings.

I have an immense debt of gratitude to the rest of the Mountford lab: Cat Prendergast, Claire Bourke and Ann Bamford. Ann's help with the life cycle and maintaining the lab tidy was important, but not as much as the caring and fun conversations we shared constantly. Thanks for making sure (or at least trying) to get me to eat healthy! Cat and Claire became invaluable friends. Always there to celebrate or commiserate after an experiment, and provide technical and moral support. I will miss you both a lot! I learned tons from both of you!

My time in York was a lot of fun. I made a lot of great friends in York, and this space is too small to list you all. The friends I made on my first week in York, who opened their houses and hearts to me, made this experience incredible. Louise, Mike, Ryan, Sarah and Sean thank you! You were my surrogate family in this country and it would not have been the same with out you! Thanks also to Eleanor, Dan and Clare for so many fun nights in the pub when we complained about doing a PhD! Ben, Manolo and Ronnie looked after me far too often when we went out to dance! Thanks also to my friends back home, especially Caro, Juli, Freddy y Laura, who received me with open arms every time I could fly over.

Finally, I must express my immense gratitude towards my parents and siblings. Hermanitas, las adoro! Cada conversación por teléfono o por chat fue una fuente de apoyo y felicidad! Ustedes son como dos solecitos brillantes que me llenan de amor! Papi y Mami, gracias por todo! Ustedes me han apoyado de forma incondicional desde el principio, con sacrificios económicos grandes, pero más que eso con su constante orgullo y ánimo para seguir adelante! Esto es un logro de los tres. Los amo!

Author's declaration

"I solemnly swear that I am up to no good" – J.K. Rowling

All experimental work presented in this document was performed in the University of York between September 2010 and June 2014 by the candidate, and has not been submitted for award before to this or any other institution. Technical assistance from the staff of the Technology Facility in the Department of Biology was sought in several instances, yet the author was present and responsible during all work carried out. Experiments around IL-10 production in the skin were performed in close collaboration with Dr Catriona Prendergast. Preparation of samples for LC-MS/MS of membrane proteins was performed by the author and James Chamberlain, a project student under the author's supervision.

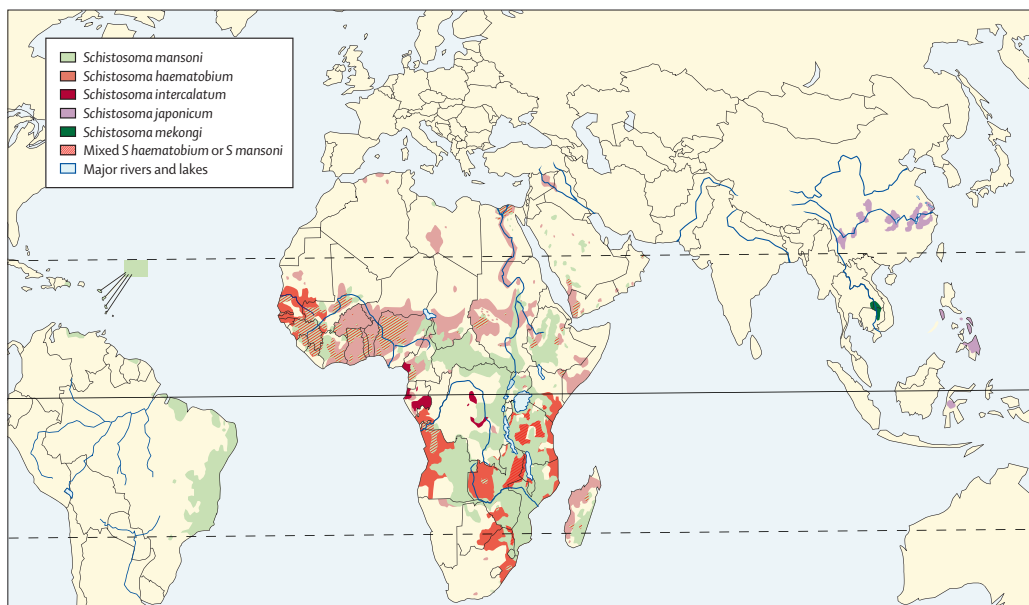
1 Introduction

1.1 Schistosomiasis

1.1.1 Overview

Schistosomiasis, also known as bilharzia, is a parasitic disease caused in humans primarily by three species of trematodes: *Schistosoma haematobium*, *S. mansoni* and *S. japonicum*, but also by *S. intercalatum*, and *S. mekongi*. The disease affects 230 million people distributed in tropical and subtropical regions of the world (Diagram 1.1) (Colley et al, 2014; Fairfax et al, 2012; Gryseels et al, 2006). Unlike Central and South America, and East Asia, there is significant geographical overlap of different schistosome parasite species in Africa. Urogenital schistosomiasis is caused by *S. haematobium*, whereas *S. mansoni* is responsible for intestinal schistosomiasis (Colley et al, 2014; Gryseels et al, 2006).

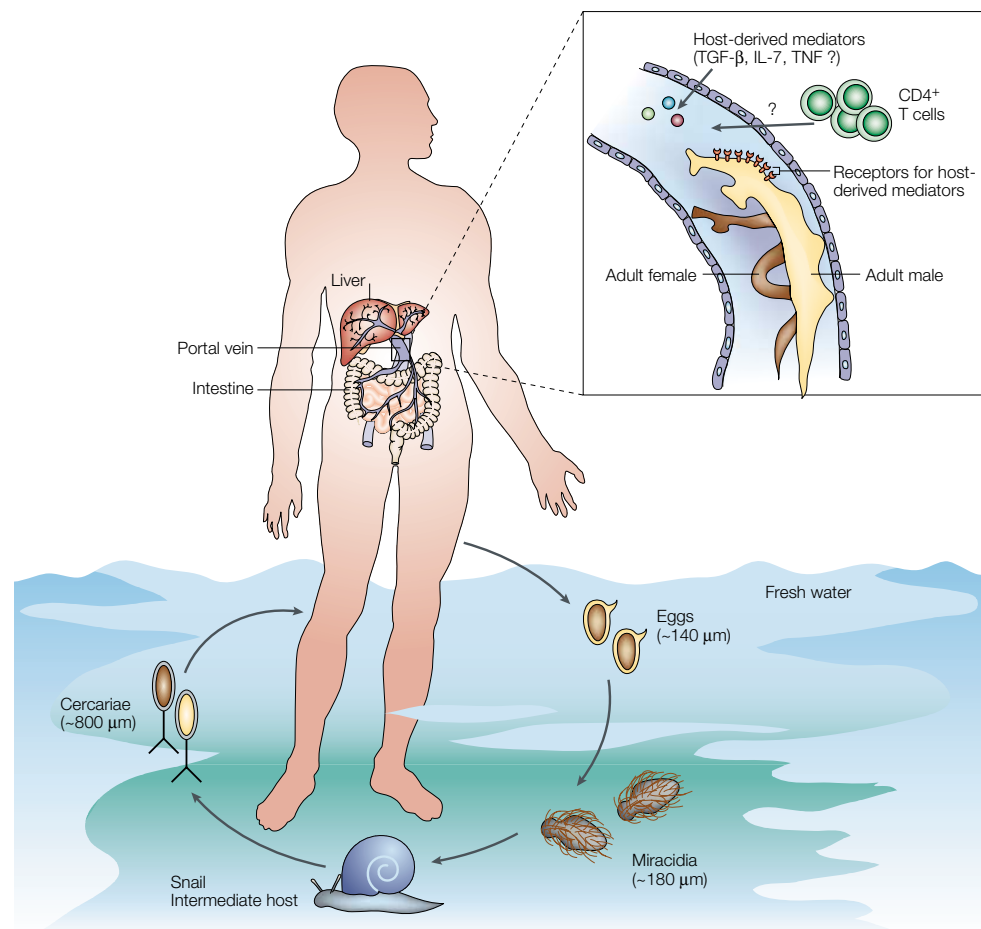
Diagram 1.1 World distribution of Schistosomiasis. Taken from Colley et al, 2014



World distribution of schistosome species is limited by the availability of ecological niches for the intermediate hosts of the parasite, which are different species of fresh water dwelling snails. *S. haematobium* and *S. mansoni* require snails from the *Bulinus* and *Biomphalaria* genera respectively (Colley et al, 2014). Infected snails release the free-swimming form of the parasite, called cercariae, which are able to locate the mammalian host and start infection following percutaneous exposure (Diagram 1.2). Cercariae penetrate the skin

and transform into schistosomula, a larval stage of the parasite that is able to migrate through the dermis and epidermis, to reach the host's vasculature. Larvae then migrate to the lungs and complete their maturation by pairing and lodging in the venous plexus of the bladder, for *S. haematobium*, or in the portal vein system near the intestines, for *S. mansoni*. Adult worms release several hundred eggs per day, which are excreted through urine or faeces allowing them to reach fresh water. At this stage the eggs hatch into miracidia that are able to infect the snail host, thereby completing their life cycle (Fairfax et al, 2012; Pearce & MacDonald, 2002).

Diagram 1.2 *Schistosoma mansoni* life cycle. Taken from Pearce & MacDonald 2002



1.1.2 Pathology, treatment and vaccination

Schistosome parasites cause pathology as eggs are trapped in tissues or are expelled into the gut or bladder lumen. Trapped eggs induce severe local inflammatory processes that are characterized by the influx of several types of leucocytes and the deposition of collagen, forming immune-mediated granulomas (Colley et al, 2014; Girgis et al, 2014; Hotez et al, 2008; Pearce &

MacDonald, 2002). These granulomas limit the movement of eggs, which eventually die, leaving behind a fibrotic plaque in the tissue (Pearce & MacDonald, 2002). As these processes continually occur in the liver and the gut, in the case of *S. mansoni*, host organ functionality is severely compromised leading to complications and in some cases death of the infected host (Richter et al, 1998). Additionally, in urogenital schistosomiasis the extent of tissue damage in the bladder is positively correlated with bladder cancer (Schwartz, 1981).

Adult worms ingest erythrocytes, causing anemia, and their location in the portal vein can lead to periportal fibrosis and hypertension, as well as portal shunting (Colley et al, 2014; Wilson, 1990). Moreover, larval migration through the lungs can severely impact the aerobic capacity of infected individuals, even several decades post infection (Bustinduy et al, 2011). Long lasting effects of early chronic infection have an important impact on physical performance and educational attainment (Colley et al, 2014).

Current therapy for schistosomiasis is restricted to one isoquinolinone drug called praziquantel (Gryseels et al, 2006; Mutapi et al, 2011; Wilson et al, 2011). The drug allows efficient clearance of adult worms, but it requires intact antibody responses (Colley et al, 2014; Gryseels et al, 2006). The drug has no proven effect on developing larvae or eggs (Hotez, 2009), consequently it has limited efficacy for long term control of the disease in endemic areas.

Vaccine development efforts are still ongoing, but there have not been any successful clinical trials in humans (Colley et al, 2014). Historically, there has been significant focus on vaccines using irradiated cercariae (Hewitson et al, 2007; Mountford & Harrop, 1998). Only recently the full genome of the parasite was sequenced (Berriman et al, 2009; Protasio et al, 2012), and there is hope that its characterization will aid the development of a prophylactic vaccine.

1.1.3 Immune response

As with other helminthic infections, schistosomiasis is characterized by a strong Th2 response, marked by elevated levels of interleukin (IL-) 4, eosinophilia in the blood and increased levels of Immunoglobulin (Ig) E (Fairfax et al, 2012; Hotez et al, 2008; Pulendran & Artis, 2012).

As *S. mansoni* is patent in mice, this host species provides an important infection model, and consequently the immune response to *S. mansoni* is relatively well characterized. Soluble *S. mansoni* egg antigen (SEA) obtained from mature eggs is a potent driver of T helper (Th) 2 responses by CD4⁺ T cells (MacDonald et al, 2002; Perona-Wright et al, 2006). Eggs trapped in the liver release antigens that are picked up by dendritic cells (DCs), which are then able to polarize CD4⁺ T cells towards a Th2 phenotype (de Jong et al, 2002; Everts et al, 2010; Phythian-Adams et al, 2010). Molecular characterization of SEA has highlighted the role of some proteins (e.g. Omega-1) that might be responsible for the induction of Th2 responses (Everts et al, 2009). C-type lectin receptors and Toll like receptors have also been implicated in the recognition of SEA by DCs (Everts et al, 2012; Everts et al, 2010; Meevissen et al, 2011; van Liempt et al, 2007).

Leucocytes involved in granuloma formation around eggs following chronic *S. mansoni* infection in the mouse include DCs and CD4 T cells, but also eosinophils and macrophages (Pearce & MacDonald, 2002). As this environment is strongly biased towards a Th2 phenotype, IL-4 is able to drive DCs and macrophages into an alternatively activated state (Barron & Wynn, 2011; Cook et al, 2012; Girgis et al, 2014). In macrophages, this is represented by an increase in the expression of Arginase 1 (Arg-1), Resistin like molecule α (Relm α) and chitinase like 3 (Ym1) (Gordon & Martinez, 2010; Martinez et al, 2009). Granuloma structures are also present in the gut, where eggs utilize Peyer's patches to escape into the intestinal lumen (Turner et al, 2012).

The consequences of the immune processes against *S. mansoni* in later stages of the disease, which collectively fall under what is being termed type 2 immunity (Allen & Maizels, 2011; Pulendran & Artis, 2012), are neither protective for the host, nor entirely beneficial for the pathogen. Adult worms are able to live in infected hosts for years in the case of humans (Colley et al, 2014), yet immune responses are necessary for the worms to fully mature. However, lack of IL-4 receptor alpha (IL-4R α) or alternatively activated macrophages, have been shown in mice to significantly increase the egg output (Herbert et al, 2004; Ramalingam et al, 2008). Effectively, *S. mansoni* chronic infection is a balance between host fitness and tolerance of the parasite, limiting the amount of damage caused in tissues.

This description of immune responses to *S. mansoni* in the chronic phase is by no mean exhaustive, yet the main focus of this thesis is on the early stages of the infection, as cercariae penetrate the skin, which will be discussed in greater detail.

1.2 *S. mansoni* cercarial skin infection

Most immunological studies have focused on the chronic phase of *S. mansoni* infection, leaving the larval (prior to worm maturation and egg deposition) phase of disease largely uncharacterized, and often broadly referred to as Th1 (Fairfax et al, 2012; Hotez et al, 2008). However, the process of cercarial penetration of the skin has been investigated in the context of radiation-attenuated larvae as putative vaccines.

1.2.1 Immune responses in the skin

The skin is a complex stratified tissue that modulates the interplay between the immune system and the environment. As such, it plays host to a plethora of non-pathogenic microorganism (Belkaid & Naik, 2013; Naik et al, 2012) and immune cells that are in constant interaction, both of which have the potential to shape the immune responses to invading parasites (Pasparakis et al, 2014).

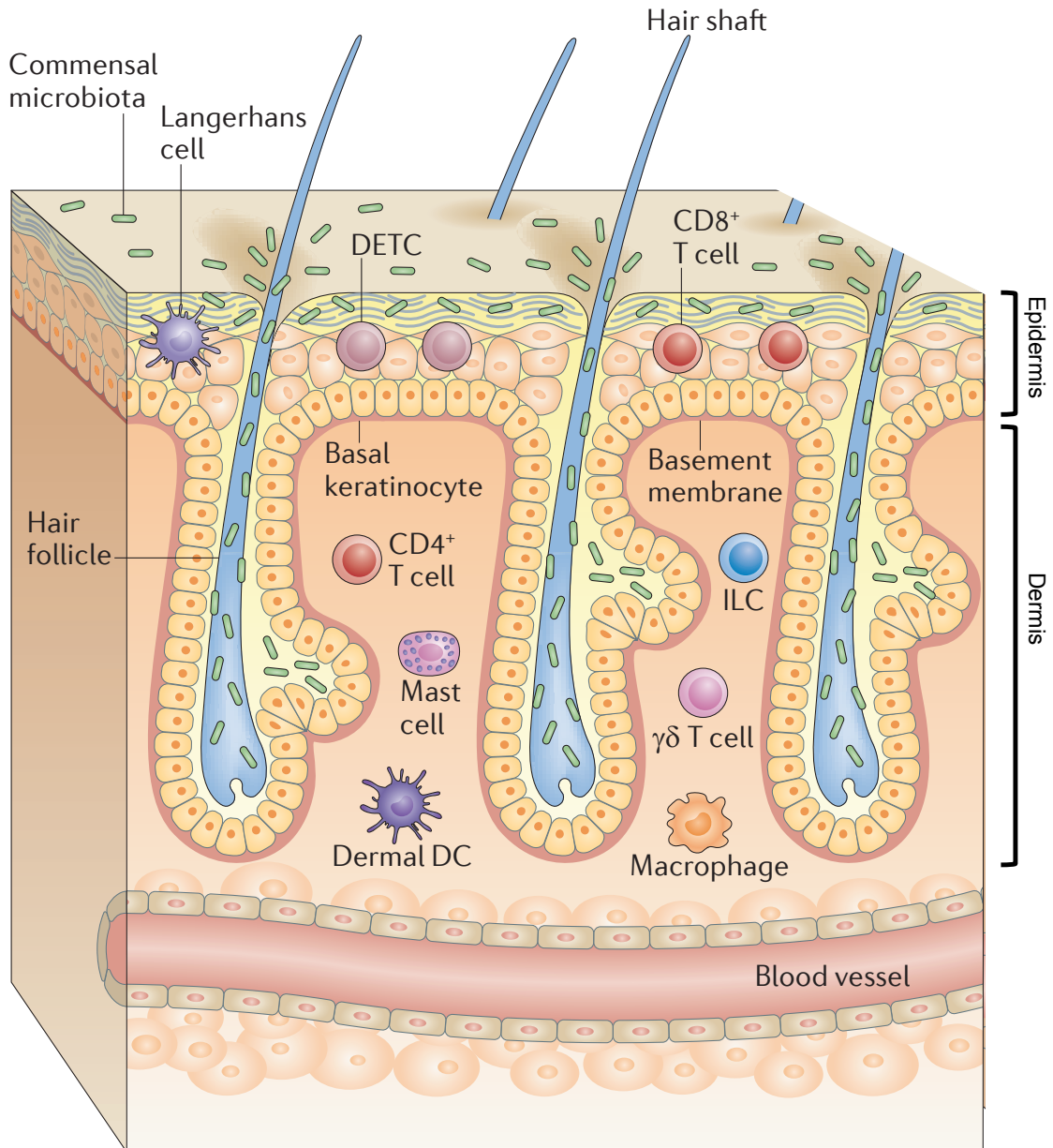
The skin is divided into two layers. The outer superficial epidermis is primarily comprised of keratinocytes, langerhans cells (LCs) and certain types of T cells (like Dendritic epidermal T cells (DETC) or CD8⁺ T cells). The underlying dermis is composed of stromal cells, like fibroblasts, and several types of immune cells such as macrophages, DCs, T cells, mast cells and innate lymphoid cells (ILCs) (Diagram 1.3) (Nestle et al, 2009; Pasparakis et al, 2014).

In the epidermis, LCs are seeded from the Yolk sac and fetal liver (Ghigo et al, 2013) and whilst they are normally thought to be a type of DC, can be thought of as tissue resident macrophages (Davies et al, 2013). These cells are actively monitoring the skin to find pathogens and can act as antigen presenting cells (Kumkate et al, 2007; Pasparakis et al, 2014).

The source of DCs and macrophages in the dermis is contentious, with a significant input from the bone marrow (Jakubzick et al, 2013; Malissen et al, 2014). Both groups of cells are similarly poised to respond to infections, and pro-inflammatory macrophages in particular have been implicated in several pathogenic settings both as driving inflammation, or having a host protective role (Fuentes-Duculan et al, 2010; Meng et al, 2009). Keratinocytes, in the epidermis, and ILCs in the dermis, are a source of cytokines for other immune cells (Pasparakis et al, 2014), and act as early warning systems against infection. Neutrophils can be recruited to the dermis by keratinocytes (Albanesi

et al, 2005), and are associated with severe inflammatory processes in the skin (Abram et al, 2013). Mast cells on the other hand, are always in the dermis, and are quick to respond to any infection by de-granulating and facilitating pathogen clearance (Nestle et al, 2009; Pasparakis et al, 2014).

Diagram 1.3 Immune cells in the skin. Adapted from Pasparakis et al, 2014



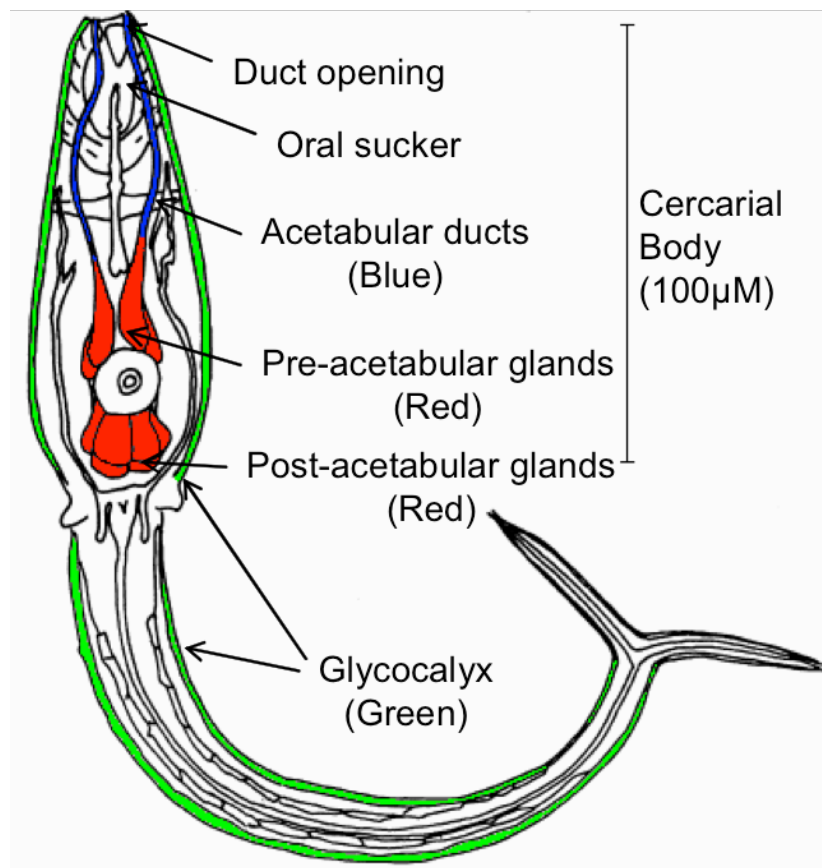
T cells in the skin are varied in composition and can be found both in the dermis and epidermis. An important proportion are memory antigen specific T cells, both CD8⁺ and CD4⁺ (Mackay et al, 2013; Sanchez Rodriguez et al, 2014) which are generally found in the epidermis. CD4⁺ T cells in the dermis can be regulatory T cells (Belkaid et al, 2002; Campanelli et al, 2006) or memory T cells.

An additional important component of the skin is the bacterial flora covering it. The role of commensal microbiota on immune response in the skin is not fully understood. Unlike the gut, defects in innate signaling have no effect on the composition of skin flora (Belkaid & Naik, 2013), but the numbers of regulatory T cells and the fate of infections are severely affected by commensal bacteria (Naik et al, 2012).

1.2.2 Cercarial structure and E/S products

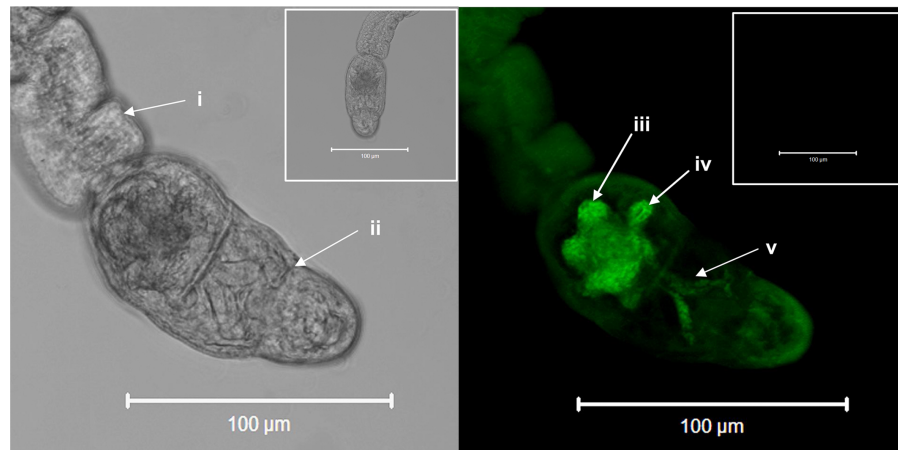
S. mansoni cercariae are macroparasites with several specialized tissues that are designed to facilitate invasion of the host (Diagram 1.4) (Dorsey et al, 2002).

Diagram 1.4 Schematic of *S. mansoni* cercaria. Adapted from Dorsey et al, 2002



The tail (Diagram 1.5, i), which permits the movement of the cercariae in fresh water, is lost upon penetration of the skin, leaving the body (Diagram 1.5, ii) to burrow through the tissue (Paveley et al, 2009). This body is covered in a carbohydrate rich coating, called the glycocalyx that could protect larvae from immune attack (McKerrow et al, 2006).

Diagram 1.5 Fluorescent labeling of *S. mansoni* cercariae revealing pre- and post-acetabular glands. Taken from Paveley et al, 2009



The contents of the post and pre-acetabular glands (Diagram 1.5, iii & iv respectively) of the parasite are released through the acetabular ducts (Diagram 1.5, v) into the skin and are called Excretory/Secretory (E/S) products (aka 0-3hRP) (Paveley et al, 2009). Cercariae penetrate the skin by releasing these molecules to remodel the extracellular matrix (Curwen et al, 2006; Paveley et al, 2009; Wilson, 2012) and aid migration of larvae through the skin to reach blood vessels thereby facilitating onward migration (McKerrow & Salter, 2002; Salter et al, 2000).

S. mansoni cercarial E/S products have been shown to contain more than 50 different proteins (Curwen et al, 2006; Knudsen et al, 2005), that are expressed in different proportions and released in the first three hours after mechanical transformation.

Of the identified proteins in 0-3hRP the most often mentioned are the enzymes in the mixture, which allow remodeling of extracellular matrix necessary for parasite penetration of the skin. Of this group, the best studied is cercarial elastase, which has chymotrypsin activity enabling it to break skin elastin (Salter et al, 2000). Nonetheless, at least seven other elastases are secreted into the skin, alongside five metalloproteases one of which is Invadolysin (Wilson, 2012). The specificity of these enzymes is unknown. In addition to aiding penetration, they could be responsible for degradation of antibodies directed at cercariae (McKerrow et al, 2006).

Several of the proteins present in 0-3hRP are heavily glycosylated (Jang-Lee et al, 2007), and glycans could play an important role in the immunomodulatory

properties of 0-3hRP (Hokke & Deelder, 2001; Jenkins et al, 2005). Consensus in the scientific community is that glycans in cercarial secretions are responsible for their immunomodulatory effects. However, the only protein in 0-3hRP with a defined immunomodulatory role, Sm16, is not glycosylated (Jang-Lee et al, 2007). Sm16 is able to induce apoptosis if it reaches the cytosol of cells (Holmfeldt et al, 2007), and effectively blocks signaling downstream of TLR4 and TLR3 (Brännström et al, 2009).

1.2.3 Immune responses in the skin to invading cercariae

S. mansoni cercariae are not fast in penetrating human skin. They first crawl on the surface for ~40s before starting penetrating movements, which they only achieve after several minutes (Haas & Haeberlein, 2009). As stated before, most studies of immune processes in the skin to invading cercariae have concentrated on responses after vaccination with irradiated parasites. The exceptions are studies where the tools employed were limited (i.e. before flow cytometry or fluorescent microscopy were available). From these early studies, it is possible to ascertain that an influx of primarily neutrophils, but also macrophages and DCs is apparent at the site of infection (Incani & McLaren, 1984). Evidence from more recent studies using irradiated parasites, shows that LCs are able to migrate to the skin-draining lymph node and present antigen (Kumkate et al, 2007). Indeed, the skin exposed to radiation-attenuated parasites appears to develop a Th1-type immune response, with IL-12p40 playing an important role (Hewitson et al, 2007). These findings were supported by two more recent studies, which confirmed the appearance of neutrophils, DCs and macrophages at this early stage (Paveley et al, 2009), accompanied by the recruitment of a substantial population of eosinophils following repeated infection (Cook et al, 2011). Neutrophils, DCs and macrophages all appear to take up cercarial E/S products released by the invading larvae, and the latter two cell types then migrate to the skin draining lymph nodes (Paveley et al, 2009).

The data on cytokine and chemokine production from the skin is again originally available from earlier studies with irradiated cercariae. Cytokines are produced in the skin as a cascade including MIP1 α , eotaxin, IL-6, IL-1, IL-18 and IL-12p40 and IL-10, several of which reached their peak production 4 days after parasite exposure (Hogg et al, 2003a). The crosstalk between IL-12p40 and IL-

10 in particular was investigated showing that IL-10 in the skin was able to limit IL-12p40 production, thus preventing efficacy of Th1 vaccine-induced immune responses (Hogg et al, 2003a; Hogg et al, 2003b). In studies using normal parasites, modest increases in the production of IL-10, IL-4 and IL-13 were shown in the first few days after infection compared to naïve skin, whilst markedly elevated levels were detected for IL-12p40, tumor necrosis factor alpha (TNF- α) and thymic stromal lymphopoietin (TSLP) (Cook et al, 2011).

CD4⁺ T cells in the skin draining lymph nodes proliferate in response to *S. mansoni* cercarial antigen and produce interferon gamma (IFN- γ), IL-10 and IL-4 (Cook et al, 2011; Pemberton et al, 1991). The antigen-specific proliferative response can be supported by DCs from the skin after *S. mansoni* infection, adding evidence to the hypothesis that these cells prime CD4⁺ T cells by migrating from the skin (Cook et al, 2011).

In summary, the immune response in the skin to invading *S. mansoni* cercariae exhibits features from a classical inflammatory setting with neutrophil and monocyte influx, but also has characteristics of type 2 immunity with recruitment of eosinophils and production of IL-4. This mixed Th1/Th2 response after a primary infection in the skin is further supported by the proliferative responses in the skin draining lymph nodes, where both IFN- γ and IL-4 are being produced.

1.3 Macrophages

Macrophages are phagocytic cells that reside in different organs, or circulate in the blood (Wynn et al, 2013). Macrophages exhibit different phenotypes in between tissues and within a tissue, as is the case for the spleen (Davies et al, 2013; Murray & Wynn, 2011). Tissue resident macrophages are seeded in most tissues from an embryonic stage, and maintain their numbers through local proliferation (Jenkins et al, 2013; Schulz et al, 2012). Alternatively, these cells can differentiate from circulating monocytes that are recruited to the sites of infection during inflammatory processes (Girgis et al, 2014; Jenkins et al, 2011).

Unlike DCs, macrophages are unable to prime naïve CD4⁺ T cells, but they present antigen in the tissues and are an important source of cytokines at the sites of infection (Benoit et al, 2008; Chow et al, 2011; Davies et al, 2013; Gordon & Martinez, 2010). Consequently, these cells have the ability to condition the adaptive immune response, so study of their biology has been closely examined in recent decades (Davies et al, 2013; Gordon, 2003; Gordon & Martinez, 2010; Wynn et al, 2013). Moreover, macrophages are also the target of cytokines released by effector T cells. They can become activated in an IFN- γ -dependent manner, or an IL-4-dependent manner, and in both instances become important effector cells of the adaptive immune response (Barron & Wynn, 2011).

1.3.1 Macrophage activation

IFN- γ activation of macrophages, or classical activation, occurs following bacterial infections leading to a strong Th1 phenotype in CD4⁺ T cells (Barron & Wynn, 2011). Classically activated macrophages (CAM ϕ s) have increased bactericidal capacity as they have enhanced expression of inducible nitric oxide synthase (iNOS), which leads to higher levels of nitric oxide (NO) production. These cells are able to mediate pathogen clearance and produce increased levels of IL-12p70, further supporting the Th1 environment (Benoit et al, 2008).

IL-4 activation of macrophages, or alternative activation, occurs in helminth infections, but also when there is extensive tissue damage, or during allergy. Alternatively activated macrophages (AAM ϕ s) have increased expression of Arg-1, Relm α and Ym1. These cells also proliferate *in situ*, have increased phagocytic capacity and elevated levels of major histocompatibility complex

class II (MHC-II) expression (Balce et al, 2011; Davies et al, 2013; Gordon & Martinez, 2010; Jenkins & Allen, 2010; Jenkins et al, 2013; Loke et al, 2007; Rojas López & Duque Correa, 2007).

Macrophages are able to recognize many different stimuli using pattern recognition receptors (PRR) to discern the most appropriate route of activation they should undergo. Three clearly defined families of PRRs have been described, including toll-like receptors (TLRs), C-type lectin receptors (CLRs) and nucleotide oligomerization domain (NOD)-like receptors (NLRs) (Akira & Takeda, 2004; Davicino et al, 2011; Kufer & Sansonetti, 2011).

Stimulation with PRRs ligands results in the production of cytokines such as IL-1 β , IL-6, TNF α , IL-10 and IL-12 (Benoit et al, 2008; Gordon, 2003; Martinez et al, 2009) and the expression of several markers of activation, such as MHC-II, CD80 and CD86 (Wynn et al, 2013). Nonetheless, changes in the levels of these molecules are only a subset of the activation that macrophages undergo upon ligand binding, which have only now been partly characterized through the analysis of the proteome and secretome of activated macrophages (Li et al, 2011; Meissner et al, 2013).

1.3.2 Endocytosis

Macrophages constantly sample their environment by actively internalizing molecules and particles via endocytosis. That process can be energy costly (Watts, 2011), and severely impact signaling pathways (Kagan & Iwasaki, 2012; Shilo & Schejter, 2011). Endocytosis and endosomal trafficking depend on actin polymerization and Ca⁺ signaling (Huotari & Helenius, 2011; Watts, 2011). Thus, endocytosis involves the remodeling of the cytoskeleton and the rearrangement of membranes, which necessitates a series of organized signaling events (Traub, 2011; Watts, 2011). The phosphatidylinositol-4,5-bisphosphate 3-kinase (PI3K) family of kinases participate in the rearrangement of membrane structures and trafficking in cells by phosphorylating lipids on the cell membrane and endosomes (Stephens et al, 2002; Vanhaesebroeck et al, 2012). As such, this family of kinases contributes to triggering signaling pathways leading to phagocytosis and other processes.

Several families of phagocytic receptors are available to macrophages to initiate endocytosis (Baranova et al, 2012; Goodridge et al, 2011; Joshi et al, 2006;

Kagan & Iwasaki, 2012). Some of these receptor families require opsonization of the material before they can be engaged, which is usually achieved via complement or antibodies, and is typically directed at extracellular bacteria and dying cells (Joshi et al, 2006). In addition to their role in activating macrophages, CLRs, such as DC-specific intercellular adhesion molecule-3-grabbing non-integrin (DC-SIGN) on dendritic cells or the macrophage mannose receptor (MR) in macrophages and dendritic cells, directly bind carbohydrates on the surface of proteins on pathogens (Gringhuis et al, 2007; Martinez-Pomares et al, 2001; Svajger et al, 2011). Scavenger receptors can also bind to foreign or modified lipids and mediate their internalization (Baranova et al, 2012; Oury, 2014).

1.3.3 Macrophages in *S. mansoni* infection

Macrophages play a fundamental role in *S. mansoni* infection at all stages of the disease. They are able to partly mediate protective immunity induced by irradiated cercariae by increased production of nitric oxide (Caulada-Benedetti et al, 1991; James et al, 1998), although this has been contested (Coulson et al, 1998). Furthermore, if LCs are regarded as tissue resident macrophages (Davies et al, 2013), they have also been shown to migrate to the skin-draining lymph nodes where they can to present antigen after exposure to vaccinating parasites (Kumkate et al, 2007). F4/80⁺ cells in the skin after infection, which include LCs as well as macrophages, take up cercarial E/S products and migrate to the lymph node (Paveley et al, 2009). Moreover, after multiple exposure to invading cercariae, F4/80⁺ macrophages become alternatively activated in the skin (Cook et al, 2011), most likely to control the excessive tissue damage caused by the migrating parasite and in the process conditioning the overall immune response in the skin. In addition, during the pre-patent phase of the adult worm infection prior to egg deposition, these mononuclear cells have significantly impaired function as APCs, leading to hypo-responsiveness from T cells in the mesenteric lymph nodes, in a mechanism dependent on IL-12p40 production (Ferragine et al, 2013).

AAMφs are essential for host survival during *S. mansoni* infection, by maintaining barrier function in the gut during the acute phase and limiting Th1 responses and pathology during the chronic phase of the disease (Herbert et al, 2004). Furthermore, they are involved in limiting fibrosis through the expression

of Arg-1, as enhanced liver fibrosis as well as granulomatous inflammation was evident in infected mice when macrophages were unable to produce this protein (Pesce et al, 2009). These cells are partly recruited from the blood to establish granulomas around the eggs (Girgis et al, 2014), although AAMφs are not required for these structures to be maintained (Herbert et al, 2004). Nonetheless, their increased production of Arg-1 and IL-10 limits the extent of Th2 responses, thus limiting inflammation and limiting scarring potentially by acting on fibroblasts (Barron & Wynn, 2011).

1.4 Innate immune signaling

1.4.1 TLRs

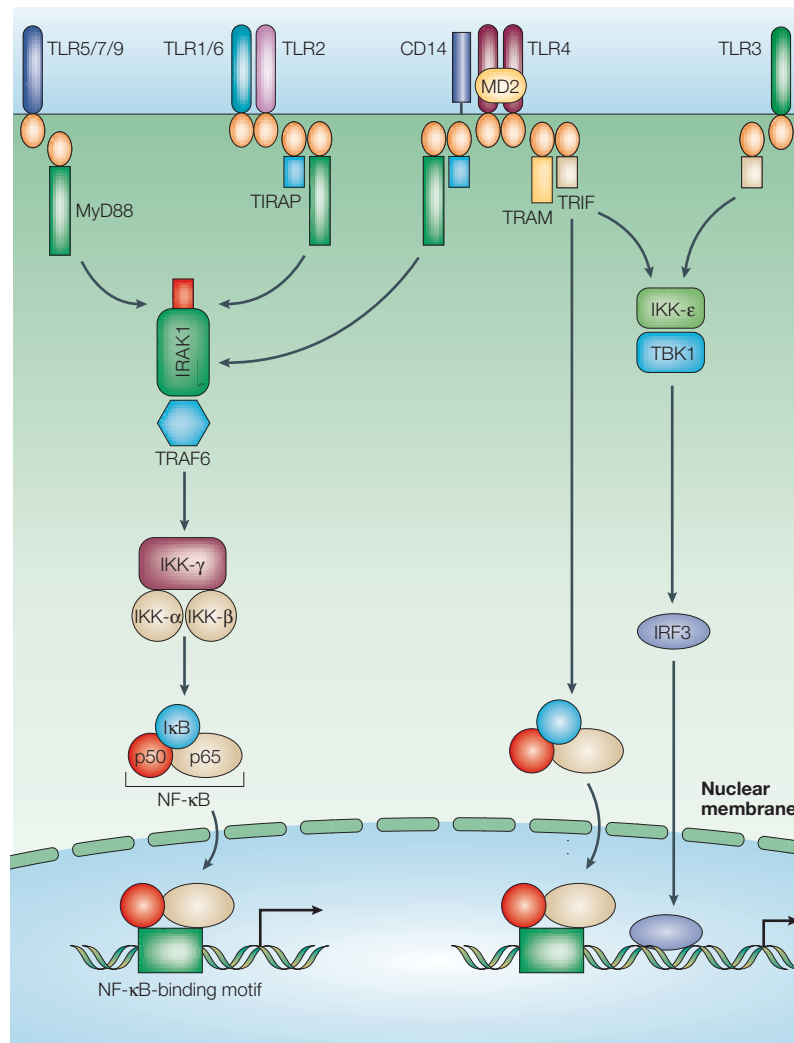
Toll was initially discovered in *Drosophila melanogaster*, when it was found that the lack of this protein made that organism susceptible to fungal infection (Valanne et al, 2011). Since, TLRs have been found in several organisms and are now recognized as a well-conserved system of receptors that control innate immune responses in many cells of the immune system. Several ligands have been identified for the existing 13 TLRs in mice, 10 of which have human homologues (Adachi et al, 1998; Akira & Takeda, 2004; Dillon et al, 2004; Downes & Marshall-Clarke, 2010; Hoshino et al, 1999; Ioannou & Voulgarelis, 2010; Shi et al, 2011; Takeuchi et al, 1999).

TLRs can be localized in the cell surface (e.g. TLR1, 2, 4 & 6) or in endosomes (e.g. TLR3, 7, 9, 10 & 11), which is related to the ligands they are associated with. TLR2 and TLR4 recognize products of the outer walls of extracellular bacteria and fungi (Sato et al, 2003; Takeuchi et al, 1999), whereas endosomal TLRs usually recognize nucleic acids or products of intracellular pathogens (like flagellin from *Toxoplasma gondii*) (de Jong et al, 2002; Yarovinsky et al, 2005). Upon recognition of their ligand, TLRs can form homodimers (e.g. TLR4) or heterodimers with more than one TLR (e.g. TLR2/1 or TLR2/6) (Akira & Takeda, 2004; Kagan & Iwasaki, 2012). Upon dimerisation several adaptor proteins can be recruited to the intracellular domains of TLRs to activate multiple signaling pathways (Diagram 1.6) (Bonham et al, 2014).

Most TLRs utilize MyD88 as their main adaptor molecule, which is recruited to the plasma membrane by toll-interleukin 1 receptor (TIR) domain containing adaptor protein (TIRAP), however TLR4 and TLR3 can also use TIR-domain-containing adapter-inducing interferon β (TRIF), which is a recruited alongside TRIF related adaptor molecule (TRAM) (Adachi et al, 1998; Bonham et al, 2014; Donnelly et al, 2010; Kagan & Iwasaki, 2012; Laird et al, 2009; Liu et al, 2012; Muzio et al, 1997; Shi et al, 2011; Warner & Nunez, 2013; Wesche et al, 1997). TLR-ligand binding triggers a cascade of kinases which involves the activation of interleukin-1 receptor-associated kinase 1 (IRAK1), and then mitogen activated protein kinase (MAPK) kinase kinase 7 (MAP3K7) (or TAK1), alongside several scaffolding proteins like TNF-receptor associated factor 6

(TRAF6) (Diagram 1.6). MAP3K7 phosphorylates of inhibitor of nuclear factor kappa B Kinase β (IKK β) leading to the activation of the nuclear factor kappa B (NF- κ B) system, which is made out of several different proteins (such as p65, p105 and its degradation product p50). These subunits, which remain in the cytoplasm when inactive, form homodimers or heterodimers upon release and direct transcription of pro-inflammatory cytokines (such as IL-12, IL-6 and IL-1), chemokines, as well as other transcription factors (Adachi et al, 1998; Hinz & Scheidereit, 2014; Hoesel & Schmid, 2013; Iwasaki et al, 2011; Muzio et al, 1997; Oeckinghaus et al, 2011; Ruland, 2011; van Berlo et al, 2010; Warner & Nunez, 2013; Wesche et al, 1997; Yu et al, 2011).

Diagram 1.6 Toll like receptor signaling pathway. Taken from Akira et al, 2004



TLRs also employ several different accessory receptors that either facilitate ligand binding or modulate the activation of TLRs and recruitment of adaptor molecules. These co-receptors include membrane bound proteins like CD14

and CD36, or soluble factors such as lymphocyte antigen 96 (MD2) and lipopolysaccharide (LPS) binding protein (LBP) (Lee et al, 2012).

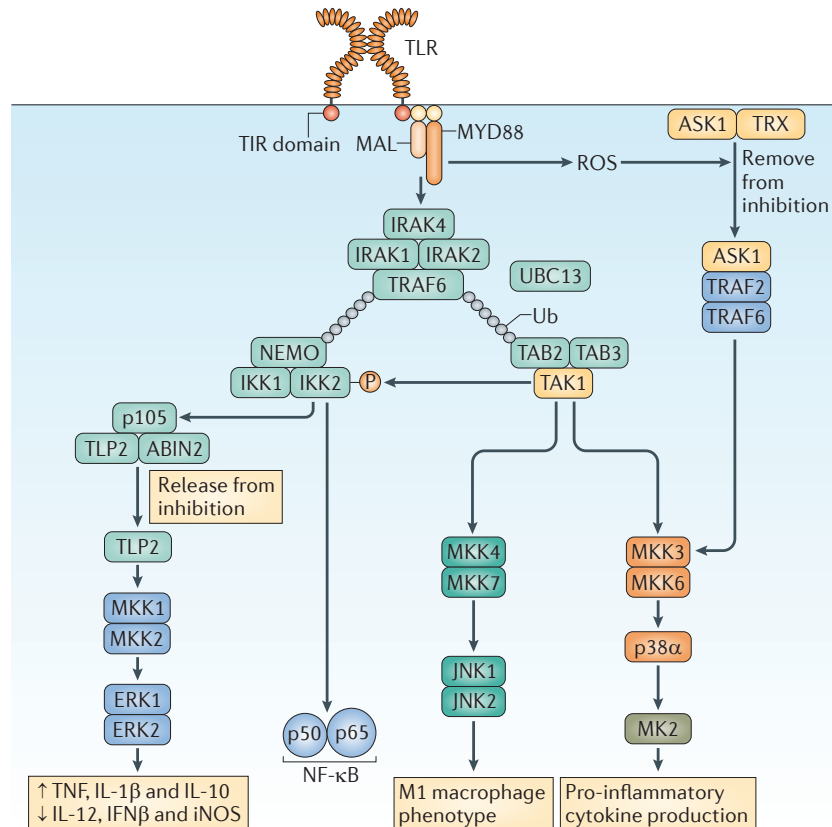
1.4.2 Mitogen activated protein kinases

Mitogen activated protein kinases (MAPKs) are a diverse family of proteins that transport signals received from the environment by becoming phosphorylated, and phosphorylating others kinases in turn. These proteins are involved in growth, development, cell cycle, metabolism and immune signaling and can be activated downstream of several receptors including TLRs (Arthur & Ley, 2013). These signaling cascades lead to the phosphorylation of transcription factors that trigger gene expression. MAPKs are incredibly versatile because they are an interwoven network of signaling pathways that feed into each other (Arthur & Ley, 2013; Bandyopadhyay et al, 2010; Deak et al, 1998; Farhan et al, 2010; Gehart et al, 2010). These proteins are highly stratified: MAPK kinase kinases (MAP3K) phosphorylate MAPK kinases (MAP2K), which in turn phosphorylate MAPKs that further phosphorylate MAPK activate-protein kinases (MAPKAP) (i.e. Proto-oncogene serine/threonine-protein kinase (RAF) activates Mitogen activated protein kinase kinase 1/2 (MEK1/2), which activates Extracellular signal-regulated kinase (Erk1/2), which phosphorylates Ribosomal s6 kinase (RSK1/2)) (Arthur & Ley, 2013; Bain et al, 2007). Multiple MAPKs have more than one isoform, and it is often difficult to study the role, if any, of each one (Beardmore et al, 2005; Braem et al, 2011; Deak et al, 1998).

MAPKs can be directly activated downstream of TLRs by MAP3K7 (Diagram 1.7), which phosphorylates the kinases upstream of p38 and JNK. MAP3K7 (TAK1) also mediates the phosphorylation of p105, which is then degraded, releasing Tumor progression locus 2 (Tpl2) or MAP3K8 to phosphorylate MEK1/2, which then phosphorylates Erk1/2 (Arthur & Ley, 2013; Braem et al, 2011; Elcombe et al, 2013; Laird et al, 2009; Lawrenz et al, 2012; Mayer et al, 2013; Medina et al, 2010; Pinto et al, 2011; Rommel et al, 1999; Salmeron et al, 1996; Yan et al, 2010; Yang et al, 2010).

MAPKs regulate transcription through the phosphorylation of several transcription factors, such as cAMP response element binding protein (CREB), Activator protein 1 (AP-1) and c-Jun (Elcombe et al, 2013; MacKenzie et al, 2013; Mayer et al, 2013; Strippoli et al, 2012; van Vliet et al, 2013; Wen et al, 2010).

Diagram 1.7 TLR activation of MAPKs. Taken from Arthur et al, 2013



1.4.3 Innate immune signaling in *S. mansoni* infection

Only a few differences have been described in *S. mansoni* infection of TLR-deficient mice compared to wild type animals. TLR2-deficient mice have significantly fewer eosinophils in granulomas measured after 5 weeks, but survival of the infected hosts is largely unaffected (Magalhães et al, 2010). Nonetheless, SEA has a well-documented potent effect on TLR signaling in DCs. Thus, SEA is able to block LPS induced IL-12p40 production in an IL-10 independent manner (Kane et al, 2004). Despite being a “silent” antigen in terms of cytokine expression and overall gene expression changes, SEA is able to modulate DC and macrophage cytokine responses and gene expression, when these cells are exposed to SEA in conjunction with various TLR ligands, including LPS (Correale & Farez, 2009; Kane et al, 2004; van Riet et al, 2009) and Pam₃CSK₄ (Agrawal et al, 2003). The modulation of those responses was often attributed to being mediated by TLR2. Indeed, lipids in SEA bind directly to TLR2 and are able to condition DCs and consequently affect T-cell responses (Magalhães et al, 2010; van der Kleij et al, 2002).

The effects of SEA on these cells are at least partly mediated by Erk1/2 and p38 (Agrawal et al, 2003; Correale & Farez, 2009; Goh et al, 2009; van Riet et al, 2009), and the ratio between the phosphorylation of these two MAPKs in the context of stimulation with LPS, could be indicative of the ability of DCs to polarize T cells towards a Th2 phenotype (van Riet et al, 2009). In particular, p38 has been implicated in coordinating SEA processing in DCs (Marshall & Pearce, 2008).

Other than TLRs, receptors involved in the recognition of SEA by macrophages include several CLRs, particularly macrophage galactose-type lectin (MGL) and MR (van Liempt et al, 2007). However, the role of these receptors is mostly associated with the uptake of the antigens (Meevissen et al, 2012; Meevissen et al, 2011).

The role of TLRs and CLRs in the recognition or uptake of cercarial E/S products is much more limited, and there is no knowledge of the involvement of MAPKs. The MR is partly responsible for the uptake of cercarial E/S *in vitro* and *in vivo*, with a modest effect on the cytokine production by macrophages deficient for this CLR (Paveley et al, 2011). Moreover, IL-6 and IL-12p40 production by macrophages exposed to 0-3hRP is entirely dependent on MyD88, but only partly dependent on TLR4 (Jenkins et al, 2005).

1.5 IL-10

IL-10 has a very well defined role in the immune system. It acts as a master regulator of inflammatory processes, by limiting the extent of the immune response and encouraging resolution of inflammation (Saraiva & O'Garra, 2010). It has a fundamental role in maintaining tolerance at barrier sites and its absence leads to chronic pathological inflammatory conditions that severely affect the fitness of affected individuals (Kuhn et al, 1993).

IL-10 can be expressed by all T-cells subsets and is a primary effector mechanism employed by regulatory or suppressive T cells, particularly Type 1 regulatory cells (Tr1) (Sabat et al, 2010). IL-10 expression in all Th subsets is governed by the transcription factor c-MAF (Saraiva et al, 2009; Saraiva & O'Garra, 2010; Xu et al, 2009). GATA3 has also been implicated in the initiation of IL-10 transcription in Th2 cells, particularly by inducing chromatin remodeling (Chang et al, 2007; Shoemaker et al, 2006).

IL-10 can also be expressed by macrophages and DCs, although the signaling pathways that allow this have been less well defined, with different kinases, such as Erk, p38, Mitogen- and stress-activated protein kinases (MSK) (Ananieva et al, 2008; Elcombe et al, 2013) and transcription factors, like CREB, c-MAF, NF- κ B p50 homodimers and CCAAT/enhancer binding protein β (C/EBP β) implicated (Ananieva et al, 2008; Cao et al, 2005; Cao et al, 2006; MacKenzie et al, 2013; Nandan et al, 2012). IL-10 production in macrophages and DCs has been described in response to TLR and CLR ligands, particularly ligands for DC SIGN and MGL in combination with LPS, or LPS alone (Cao et al, 2006; Elcombe et al, 2013; van Vliet et al, 2013). Extensive chromatin remodeling also occurs in the IL-10 promoter of macrophages, including hyper-phosphorylation, with this last feature being Erk dependent (Lucas et al, 2005; Saraiva et al, 2005; Zhang et al, 2006).

The IL-10 receptor signals in cells using Janus kinase 1 (JAK1), tyrosine kinase 2 (TYK2) and Signal transducer and activator of transcription 3 (STAT3) (Sabat et al, 2010). It also activates Dual specificity phosphatases (DUSPs) and Src homology region 2 domain-containing phosphatase-1 (SHP1), which are well known inhibitors of TLR signaling (Hammer et al, 2006; Okazawa et al, 2005; Yuk et al, 2011). IL-10 blocks the production of pro-inflammatory cytokines, the

proliferation of T cells and the expression of MHC-II. However, IL-10 also promotes the uptake of dead/apoptotic cells through the up-regulation of scavenger receptors (de Waal Malefyt et al, 1991; Sabat et al, 2010).

1.5.1 IL-10 in *S. mansoni* infection

The role of IL-10 in parasitic infections has been well studied. In *S. mansoni* mouse models, IL-10 has been shown to modulate the immune response in the liver and in the mesenteric lymph nodes, primarily by preventing excessive pathology (Redpath et al, 2014). Indeed, animals deficient for IL-10 presented excessive liver fibrosis, succumbed to infection faster (week 10) than wild type controls, and had significantly enlarged liver granulomas at later stages of the disease (week 15) (Mentink-Kane et al, 2011; Sadler et al, 2003; Wynn et al, 1998). Further more, T cell derived IL-10 and non-T cell derived IL-10 were important limiting pathology (Hesse et al, 2004). IL-10 has also been found to prevent mice from becoming resistant to the parasite after praziquantel treatment, as second challenge of mice treated with the drug and an anti-IL-10 receptor antibody were able to clear 50% more worms than praziquantel only treated controls (Wilson et al, 2011). Moreover, IL-10 is able to partly drive macrophages in the granulomas towards an incomplete alternative activated phenotype (Dewals et al, 2010). Evidence for a potential role of IL-10 in humans is also available from a recent study that showed that blood cultures from infected individuals produced more IL-10 in response to *S. mansoni* antigens than cultures from healthy controls (Turner et al, 2013). Interestingly, lower levels of IL-10 positively correlated with higher periportal fibrosis in infected individuals (Booth et al, 2004). Moreover, IL-10 significantly limits IL-12p40-mediated Th1 responses in the skin after vaccination with irradiated cercariae (Hogg et al, 2003b), and can block IFN- γ -induced nitric oxide killing of schistosomula in vitro (Gazzinelli et al, 1992).

Finally, the cellular source of IL-10 is known only in later stages (after 4 weeks) of the disease, where primarily CD4⁺ T cells (often CD25⁺) produce it in the liver or mesenteric lymph nodes (Redpath et al, 2014; Scheer et al, 2014).

1.6 Setting the scene

S. mansoni cercarial E/S products have been shown to be internalized *in vitro* by bone marrow derived DCs and macrophages, as well as *in vivo* by some cell populations in the skin, including F4/80⁺ macrophage-like cells (Paveley et al, 2009). It has also been shown that the uptake of cercarial E/S products by macrophages is partly mediated by the mannose receptor (Paveley et al, 2011). *S. mansoni* cercarial E/S products elicit a strong cytokine response from *in vitro* stimulated macrophages and DCs, and the production of these cytokines is dependent on MyD88, which implies a significant role for TLRs in the detection of cercarial E/S products (Jenkins et al, 2005).

Skin immune responses to *S. mansoni* cercariae warrant further examination, with particular attention placed on the role of E/S products and macrophages, which become alternatively activated after multiple infections, with a concomitant increase in the production of IL-10 by whole skin explants (Cook et al, 2011).

This project aims to demonstrate that an *in vitro* model of macrophages allows investigation of the ability of *S. mansoni* cercarial E/S products to induce the production of IL-10 in preference to IL-12p40. This model will be used to interrogate the intracellular signaling events that occur in macrophages leading to the production of IL-10, and implicate the role of TLRs in the recognition of helminth antigens. Finally, the *in vivo* cellular sources of IL-10 will be determined in a single skin infection with *S. mansoni* cercariae.

2 Materials and Methods

2.1 Animals and bone marrow

All animals were bred and maintained in the Biological Services Facility at the Department of Biology, University of York, according to the standards laid out in the Animal's Scientific Procedures Act 1986. All strains were housed in filter-topped cages and under specific pathogen free conditions. The University of York Ethics committee approved all experimental work carried out. Age matched female C57BL/6 strain mice between 6-10 weeks old were used for all experimental procedures. The outbred strain of mouse, NMR-I, which was used to maintain the parasite life cycle, was routinely bought from Harlan Laboratories, UK.

All transgenic strains were on a B6 genetic background. Transgenic mice with the IL-10 protein tagged with green fluorescent protein (GFP) (IL-10^{+gfp}) (Kamanaka et al, 2006) and TLR2 deficient (TLR2^{-/-}) (Takeuchi et al, 1999) mice were initially purchased from the Jackson Laboratory, USA, and then maintained in the Biological Services Facility. IL-10^{+gfp} mice were kept as a heterozygote line to avoid reported deficiencies in IL-10 production (Kamanaka et al, 2006). IL-10 deficient (IL-10^{-/-}) mice (Kuhn et al, 1993) were obtained from Dr Marika Kullberg (University of York), whilst Prof Paul Kaye (University of York) provided Rag deficient (Rag^{-/-}) mice, which lack T and B cells.

Bones from TLR4 deficient (TLR4^{-/-}) (Hoshino et al, 1999) and MyD88 deficient (MyD88^{-/-}) (Adachi et al, 1998) mice were obtained from Prof Andrew MacDonald, from mice housed in University of Edinburgh, UK. Tpl-2 deficient (Tpl2^{-/-}) (Dumitru et al, 2000) mice were obtained from Dr Mark Wilson from mice housed in the National Institute of Medical Research, Mill Hill, London, UK.

2.2 Parasites and parasite derived material

A Puerto Rican strain of *Schistosoma mansoni* (*S. mansoni*) was maintained in the laboratory by routinely infecting NMR-I mice and *Biomphalaria glabrata* snails.

To obtain infective cercariae, latent snails were placed in the dark for a minimum of 24h and then exposed to incandescent light for 2h to induce the release of the parasites. For the purposes of mouse infection cercariae were

collected, counted and diluted to a concentration of approximately 150 parasites per milliliter (ml).

Alternatively, cercariae were used to prepare two types of antigen preparations used for *in vitro* stimulation.

2.2.1 Generation of cercarial E/S products (0-3hRP)

Cercarial E/S products were produced as described previously (Curwen et al, 2006; Jang-Lee et al, 2007; Jenkins et al, 2005; Paveley et al, 2009). Briefly, cercariae were chilled for 1 hour in a large volume of water (~500ml) in order to allow them to sediment. Excess liquid (parasite-free) was removed and the concentrated parasites washed with chilled filter-sterilized water 3 times. After the third wash, cercariae were mechanically transformed by vortexing for 90s and then cultured in RPMI® (Gibco) containing 50U/ml penicillin and 50µg/ml streptomycin for 3 hours at 37°C 5% CO₂. Culture supernatants were collected, further removing transformed cercariae (schistosomula) and parasite tails from the preparation by centrifugation (800g for 8min at 4°C). Supernatants were stored at -20°C until needed. Up to 80ml of pooled supernatants from parasites shed on different dates were concentrated to 1ml using a filter spin column with a molecular weight cut off of 3kDa (GE Life Sciences). This concentrated preparation, retaining all molecules above 3kDa, was subsequently referred to as cercarial Excretory/Secretory (E/S) products (a.k.a. 0-3hRP). The protein concentration of 0-3hRP was measured using a BCA® protein assay (Thermo Scientific) according to the manufacturer's instructions.

2.3 *In vitro* culture and stimulation of Bone marrow derived macrophages

Femurs and tibias were obtained from animals described in 2.1; muscle was scraped from bones and the bone marrow was flushed out with PBS using a 25G needle. Cell suspensions were filtered to remove bone and tissue debris and then enumerated using a hemocytometer. Aliquots of 5x10⁶ cells were re-suspended in 10ml of DMEM® medium (Gibco) containing 10% FCS, 2mM L-Glutamine (Gibco), 50U/ml penicillin, 50µg/ml streptomycin and 50µM 2-mercaptoethanol (Complete DMEM). This was supplemented (1:5) with Macrophage colony stimulating factor (M-CSF) obtained from culture

supernatants of L929 murine fibroblast cell line. Bone marrow cell suspensions were subsequently cultured at 37°C and 5%CO₂ in 10cm culture dishes.

After 7 days, media was discarded and adherent cells washed with cold PBS before being left for 10min in warm PBS in order to let the cells detach. Cultured cells were then collected by scraping the plastic surface to further detach cells and prepared for subsequent applications by spinning them down at 1000g at 4°C and re-suspending them in complete DMEM. Cells obtained in this manner were subsequently used as bone marrow derived macrophages (BMMφ).

2.4 Flow cytometric analysis of antibody-labeled cells

Cells obtained from tissues, or *in vitro* cultures, were incubated in round bottom 96 well plates with goat serum and anti CD16/CD32 monoclonal antibody (mAb) (eBioscience), for 10min at 4°C to prevent non-specific mAb binding to Fc-receptors. Cells were then labeled with the appropriate mAb dilution in 10μl of 1% FCS in PBS (FACS buffer) for 30-45min at 4°C (see Table 2.1). Cells were washed with FACS buffer at 1000g for 7min at 4°C and then re-suspended in 350μl of FACS buffer for immediate acquisition by flow cytometry, or fixed in 100μl 2% paraformaldehyde (PFA) in PBS prior to flow cytometry acquisition at a later point.

2.4.1 Labeling of cells for intracellular molecules

Cells already labeled for surface markers were subsequently stained for intracellular proteins using Foxp3 Fixation/Permeabilization (Fix/Perm) Concentrate and Diluent (eBioscience) adapting the manufacturer's protocol. Briefly, cells were placed in Fix/Perm solution for 1 hour (or ON) at 4°C. Cells were then washed once (as described above) with 1X Permeabilization (Perm) buffer (eBioscience) and stained in 50μl of Perm buffer with appropriate antibody dilution (see Table 2.1) for 1 hour at 4°C. Finally, cells were washed once with Perm buffer and re-suspended in PBS for subsequent analysis.

2.4.2 Labeling of cells for intracellular phosphorylated proteins

Stimulated BMMφ were washed with cold PBS and then fixed in 2% PFA in PBS for 10min at 37°C. Fixed cells were then recovered by scrapping and left ON at 4°C in round bottom 96 well plates.

After ON incubation, cells were spun as described above, then incubated in 50µl fresh Fix/Perm buffer for 1 hour before being spun again and incubated with relevant anti-phospho Ab diluted 1:200 in 100µl of Perm buffer for 1 hour at room temperature. Cells were washed again with Perm buffer and then incubated for 1 hour at room temperature with goat anti-rabbit Alexa Fluor 488 diluted 1:200 in Perm buffer. Finally, cells were washed and re-suspended in 300µl of PBS for later analysis by flow cytometry.

2.5 Enzyme linked immune absorbent assays

Culture supernatants were analyzed for the amount of cytokines present using commercially available enzyme linked immune absorbent assays (ELISA). IL-10 and IL-12p40 ELISA kits were purchased from R&D Systems and performed according to their specifications.

Briefly, flat bottom 96 well plates were incubated with capture mAb ON and then washed with 0.1% Tween PBS (PBS_T) 3 times. Plates were blocked for 2 hours with 1% Bovine Serum Albumin (BSA) prior to the addition of culture supernatants and/or recombinant cytokine standards for a further 2 hours. After 3 more washes with PBS_T, biotinylated detection mAb was added to the wells and incubated for 2 hours. Plates were washed again, and incubated for 20min with streptavidin conjugated to horseradish peroxidase. Three final washes were performed and 50µl of TMB® substrate (KPL) added to each well. Reactions were stopped with 2N NaH₂SO₄ and the optical density measured using a Dynex 5000 microplate reader. Cytokine concentrations were established based on a standard curve within each assay. Limits of detection for each cytokine were at 32pg/ml.

2.6 RNA extraction and gene expression analysis by Polymerase Chain Reaction

Ribonucleic acid (RNA) from 2x10⁶ stimulated BMMφ was obtained using the High Pure RNA isolation kit (Roche) following the manufacturer's instructions. Purified RNA was quantified using a Nanodrop (Thermo Scientific), and based upon these readings the same amount of RNA (typically 1 µg) from each sample was made into cDNA (complementary deoxyribonucleic acid) using SuperScript® (Life Technologies).

cDNA was diluted 1:5 and used for gene expression analysis via quantitative real time polymerase chain reaction (qPCR) using primers listed in Table 2.2 and Fast Sybr Green® master mix (Life Technologies) with three technical replicates per sample. Melting temperatures were always 60°C and primers were used at 0.8µM in the reaction. qPCR was carried out using a StepOnePlus PCR system.

Changes in gene expression were calculated using the delta-delta Ct method (Livak & Schmittgen, 2001) with glyceraldehyde-3-phosphate dehydrogenase (GAPDH) as a housekeeping gene.

2.7 Statistical analysis

Two tailed t-tests (for experiments with only two experimental groups) or analysis of variance (ANOVA) and then multiple comparisons tests (Bonferroni's, Tukey's, Sidak's and Dunnett's) (when experiment included more than 2 groups) were performed to establish significant differences between the groups (* = $p < 0.05$, ** = $p < 0.01$; *** = $p < 0.001$, **** = $p < 0.0001$) using the software package GraphPad Prism®. Error bars represent the standard error of the mean (SEM), based on technical replicates for *in vitro* experiments, or biological replicates for *in vivo* experiments.

Table 2.1 Flow cytometry antibodies

Bone marrow derived macrophages - Surface markers				
Antigen	Fluorochrome	Clone	Isotype	Supplier
F4/80	eF-450	BM8	IgG2a,k	eBioscience
	APC	BM8	IgG2a,k	eBioscience
CD11b	PE-Cy7	M1/70	IgG2b,k	eBioscience
MHC-II	PE	M5/114	IgG2b,k	eBioscience
CD11c	FITC	HL3	IgG1	BD Pharmigen
CD80	APC	16-10A1	Ham. IgG	eBioscience
CD86	PE	GL1	IgG2a,k	eBioscience
CD40	FITC	3/23	IgG2a,k	Pharmigen
CD14	PerCP-eF710	Sa2-8	IgG2a,k	eBioscience
SR-AI/MSR1	PE	268318	IgG2b,k	R&D Systems
CD36	α IgA-PE*	JC63.1	IgA	Cayman
Egr1	GoRb AF488**	44D5	Rabbit IgG	CST***
Bone marrow derived macrophages - Intracellular signaling Proteins				
Antigen	Secondary	Clone	Isotype	Supplier
Erk 1/2	GoRb AF488	Rabbit	Rabbit IgG	CST
P-Erk 1/2		Rabbit		CST
P-p38		Rabbit		CST
P-RSK		D5D8		CST
P-CREB		87G3		CST
P-p105		18E6		CST
P-p65		93H1		CST
P-Akt		Rabbit		CST
Dermal Exudate Cells				
Antigen	Fluorochrome	Clone	Isotype	Supplier
CD11b	BV711	M1/70	IgG2b,k	BD Horizon
MHC-II	APC	M5/114	IgG2b,k	eBioscience
	FITC	269	IgG2a,k	BD biosciences
CD4	APC	GK1.5	IgG2b,k	eBioscience
	PerCP Cy5.5	RM4-5	IgG2a,k	eBioscience
CD3	BV785	17A2	IgG2b,k	BioLegend

*Anti-mouse IgA – PE (eBioscience)

**Goat anti Rabbit AlexaFluor 488 (Life Technologies)

***Cell Signaling Technology

Table 2.2 PCR Primers

Bone marrow derived macrophages - Gene expression		
Gene	Forward Primer (5' - 3')	Reverse Primer (5' - 3')
<i>IL10</i>	GGTCTTGGGAAGAGAAACCAG	GCCACAGTTTTTCAGGGATGA
<i>IL12b</i>	ATCAAGAGCAGTAGCAGTTC	TACTTCTCATAGTCCCTTTG
<i>GAPDH</i>	CCATGTTTGTGATGGGTGTG	CCTTCCACAATGCCAAAGTT
<i>IL10</i> promoter 1	AGAGGAGAGTTCTGGTGCCT	GGTGACTTCCGAGTCAGCAA
<i>IL10</i> promoter 2	AGAGGCCCTCATCTGTGGAT	GCAGAAGTTCATTCCGACCA
<i>IL10</i> promoter 3	TGTGGCTTTGGTAGTGCAAG	TGCTGCCTGCTCTTACTGAC
<i>IL10</i> promoter 4	CTAGGAGCATGTGGCTCTGG	GTCTACCCGACAGCACAGAG

3 Global changes in the expression of genes and proteins in BMM ϕ s stimulated with cercarial E/S products

3.1 Introduction

Macrophages are an important source of cytokines at the site of infection and are among the main initial responders to parasite invasion. These cells have the ability to condition the innate immune response and are also activated by the adaptive immune response. Consequently, the study of their biology has been closely scrutinized in recent decades (Davies et al, 2013; Gordon, 2003; Gordon & Martinez, 2010; Wynn et al, 2013).

Macrophages are able to recognize many different stimuli and their response is tailored to the situation they encounter. Macrophages use pattern recognition receptors (PRR) to discern the most appropriate route of activation they should undergo. Of the known families of PRRs, by far the best characterized is the TLR family. Several ligands have been identified for the existing 13 TLRs in mice, 10 of which have human homologues (Adachi et al, 1998; Akira & Takeda, 2004; Dillon et al, 2004; Downes & Marshall-Clarke, 2010; Hoshino et al, 1999; Ioannou & Voulgarelis, 2010; Shi et al, 2011; Takeuchi et al, 1999).

Upon stimulation with TLR ligands, macrophages will produce cytokines, such as IL-1, IL-6, TNF α , IL-10 and IL-12 (Benoit et al, 2008; Gordon, 2003; Martinez et al, 2009). These cells also modify the expression of several markers of activation (Wynn et al, 2013). In order to characterize possible changes that result from TLR stimulation, unbiased approaches that offer a broad coverage of changes need to be employed. Several of those studies have centered on gene expression analysis using microarrays (Pena et al, 2011; Thomas et al, 2006). Nonetheless, analysis of the proteome and secretome of macrophages have also been performed mainly through the use of mass spectrometry (Li et al, 2011; Meissner et al, 2013). However, these instruments are not inherently quantitative and so different methods have been employed to utilize their potential to identify novel activation markers in combination with accurate estimation of protein level changes (Mallick & Kuster, 2010). In recent years, two approaches have been gaining ground: iTRAQ labeling and label-free quantitative proteomics. Of the two approaches, label-free proteomics offers a similarly accurate but significantly cheaper alternative (Aebersold & Mann,

2003; Bodenmiller & Aebersold, 2010; Domon & Aebersold, 2006; Ferret-Bernard et al, 2012; Mallick & Kuster, 2010; Patel et al, 2009; Robitaille et al, 2013). Label-free quantitative proteomics works by generating an average chromatogram of all the peaks identified across all MS runs, which is then used to assess the relative abundance of each peptide based on a control sample. This method can be used to detect modest changes in protein expression, down to a 20% fold change (Mallick & Kuster, 2010).

Analysis of the results produced by either of these proteomic techniques requires the use of bioinformatic tools. These tools allow exploration of links between the identified hits that are not immediately apparent. Gene ontology (GO) term enrichment has been a preferred method for large protein lists, as it reveals functional protein clusters and cellular localization of the identities (Ferret-Bernard et al, 2012; Li et al, 2011; Meissner et al, 2013).

Bioinformatic analyses offer a window into the balance between the expression patterns of several proteins produced as a consequence of the signals triggered in macrophages upon exposure to TLR ligands. The transduction of these signals is made through several families of kinases, such as MAPKs, which transport signals received from the environment by becoming phosphorylated and phosphorylating others in turn. Eventually, signaling cascades lead to the activation of several transcription factors that trigger gene expression. MAPKs are incredibly versatile because they are an interwoven network of signaling pathways that feed into each other (Arthur & Ley, 2013; Bandyopadhyay et al, 2010; Deak et al, 1998; Farhan et al, 2010; Gehart et al, 2010). Therefore, an understanding of their activation can only be achieved if several of them are measured dynamically. Consequently, proteomic approaches are best accompanied by a study of posttranslational modification of proteins and also changes in gene expression. With this information, activation of macrophages upon stimulation with TLR ligands can be presented as a clearer picture.

In the following chapter, the response of macrophages to *S. mansoni* cercarial E/S products is explored by using several unbiased large-scale techniques. After characterizing macrophages obtained by differentiating bone marrow precursors, BMM Φ s were exposed to the excretory/secretory (E/S) products released by schistosome cercariae and changes in the membrane proteome, the activation of several MAPKs and the expression of an array of genes is

measured. In the end, a holistic view of the events that occur in macrophages exposed to cercarial E/S products is presented.

3.2 Chapter specific materials and methods

3.2.1 Label free quantitative proteomics of membrane proteins

3.2.1.1 *Membrane protein extraction*

BMMΦs were cultured in 10cm culture dishes in complete DMEM as described in 2.3 with 5×10^6 cells per dish, and then stimulated with 50µg/ml 0-3hRP supplemented with 2µg/ml Polymixin B (PMB; Sigma), 1ng/ml of LPS (Sigma), or left un-stimulated (Media). After overnight culture, media was discarded and cells washed with cold PBS before being left in 10ml of warm PBS for 10min at 37°C. Cells were then scraped from the dish, pooled together as duplicates and finally centrifuged at 1000g for 7min at 4°C to concentrate them and remove the PBS. The cells were washed again before use.

BMMΦs were finally re-suspended in 1ml of sonication buffer containing 250mM sucrose, 10mM Tris, 0.5mM KCl, pH 7.2, supplemented with a protease inhibition cocktail (Thermo Scientific) and then sonicated (Sonopuls® Bandelin) on ice at 40-50% power with continuous 1s pulses for 1min.

Cell lysates were centrifuged at 800g for 10min to remove larger membrane structures (i.e. nuclei) and any intact cells. The supernatant was recovered and spun again under the same conditions before being transferred to new tubes and centrifuged at 14000g at 4°C for 20min. Supernatants (containing crude cytosolic fraction) were removed and remaining pellets (enriched for membrane proteins) prepared for mass spectrometry by filtered aided sample preparation (FASP).

3.2.1.2 *Label free quantitative proteomics*

Membrane protein samples were prepared for proteomic analysis using FASP by the staff in the Centre for Excellence in Mass Spectrometry (Department of Biology, University of York). During FASP, all cellular components other than proteins are removed using a filter unit in which proteins are kept throughout processing. In the filter, proteins are denatured, disulfide bonds are broken and peptides are generated using trypsin. Peptides are then eluted in an appropriate solvent.

Samples were analyzed using a liquid chromatography – mass spectrometry (LC-MS) system, comprised of a Waters nanoAcquity ultra pressure liquid

chromatography (UPLC) and a Bruker maXis high-performance quadrupole – time of flight (Q-TOF) mass spectrometer. For data analysis using the label-free quantitative (expression) proteomics approach, the Nonlinear Dynamics Progenesis software was used (Patel et al, 2009). Protein searches were made against the International Protein Index (IPI) mouse database to identify any hits/identities.

3.2.1.3 *Gene ontology (GO) term enrichment and subcellular localization analysis of regulated proteins*

Subcellular classifications were performed with Gene Ontology classification (<http://www.ebi.ac.uk/GOA/>) according to the accession number of protein identities in Uniprot. If no classification was found, the Mouse Genome Informatics website (<http://www.informatics.jax.org/>) was used. Proteins were analyzed according to Gene Ontology (GO) classification using Visual Annotation Display (VLAD; proto.informatics.jax.org/prototypes/vlad-1.0.3/). Significant hits were selected on the basis of the number of proteins (k) found within each category.

3.2.2 **Kinase proteome profiler array**

BMMΦs were stimulated in a 6 well plate (2×10^6 cells per well) with 50µg/ml 0-3hRP supplemented with 2µg/ml PMB for 5, 30 and 60 minutes. After stimulation, samples were prepared for analysis with the Proteome Profiler Array according to the manufacturer's instructions (R&D Systems).

Briefly, cells were lysed with the lysis buffer supplied by the manufacturer for 30min on ice before cell debris was removed by centrifugation at 800g for 10min. The final lysate was mixed with a biotinylated mAb cocktail and incubated for 1 hour at room temperature. Lysate/mAb mixtures were then incubated with pre-blocked Proteome Profiler membranes overnight at 4°C. The membranes were then washed several times with the manufacturer's wash buffer and finally incubated with streptavidin conjugated with horseradish peroxidase (HRP). SuperSignal® West Pico (Thermo Scientific) chemiluminescence reagent was used to reveal the antibody labelling of proteins on the membranes using X-ray film imaging (GE Healthcare). Equal volumes of Luminol/Enhancer Solution and Stable Peroxidase solution were mixed and incubated with labelled/probed membranes for 5min.

Chemiluminescence reagent was removed by washing and X-ray film finally exposed for different lengths of time prior to development.

Densitometry analysis of the blots was performed using a BIO-RAD Gel Doc™ EZ system with the Image Lab® software package (Bio-Rad Laboratories). Pixel intensity was measured over a fixed area for each mAb in the array (i.e. same number of pixels were analyzed) and adjusted based on a global background subtraction. Different membranes were normalized based on the positive controls in the array.

3.2.3 qPCR array for MAPK and Toll-like receptor signaling

BMMΦs were stimulated with 50µg/ml of 0-3hRP supplemented with 2µg/ml of PMB, 1ng/mL of LPS, or simply cultured in media for 30min in 24 well plates (1×10^6 cells per well). Each treatment was performed in triplicate. Replicates were pooled and RNA extracted as described before (2.6) for analysis using RT² Profiler PCR Array (QIAGEN) following the manufacturer's instructions.

Briefly, 0.6µg of RNA from each sample was reverse-transcribed into cDNA using the RT² first strand kit. The cDNA was mixed with the RT² SYBR Green Master Mix and distributed to a 96 well plate pre-coated with primer pairs for target genes. ABI Prism 7300 was used to perform qPCR, and the resulting Ct values were obtained using Applied Biosystems SDS Software (Life Technologies) with the same threshold for all genes and samples. Ct values were used to calculate the differences in gene expression and perform relevant quality control checks (genomic DNA contamination, retro-transcription controls and negative PCR controls) using the PCR Array Data Analysis Template Excel provided by the manufacturer.

3.3 Results

3.3.1 In vitro differentiation of bone marrow cells into macrophages

Bone marrow (routinely) obtained from femurs and tibias of 6 week old female C57BL/6 mice was cultured as described in 2.3 to obtain BMMφs used throughout the project. The culture conditions described in 2.3 rely heavily on the quality of the M-CSF used, which in this case was sourced from supernatants of L929 (L-Sup) fibroblast cultures (Deryugina et al, 1995). Stable and reproducible results for BMMφs were obtained by supplementing complete DMEM with 20% L-Sup from a single stock. Bone marrow cells successfully differentiated into viable F4/80⁺CD11b⁺MHC-II^{low}CD11c^{low} cells (Figure 3.1). Cell yields averaged 20x10⁶ BMMφs per mouse. The expression of the surface markers F4/80, CD11b, and CD11c was consistent in all experiments, however, MHC-II levels were the most variable.

The general gating strategy (Figure 3.1A) used throughout the project included selecting for events on the basis of size and granularity using the forward scattering (FSC), and side scattering (SSC) of light, respectively. Single cells were selected by analyzing the quadratic distribution of events using the FSC. Finally, viable cells were gated using a viability dye as described in 2.4.

A typical phenotype of differentiated bone marrow cells (Figure 3.1B) is presented alongside a bar graph showing the percentage of positive cells for each marker from 7 independent experiments (Figure 3.1C). CD11b was expressed in all BMMφs, as this protein is found in all myeloid cells. F4/80, also expressed in all BMMφs, is a well-established marker of macrophages in tissues, but is present in other immune cells (i.e. DCs and eosinophils). MHC-II expression was low and variable, and as this marker can be up regulated upon activation and stress, its low levels confirmed the naïve nature of BMMφs (Benoit et al, 2008; Galli et al, 2011; Gordon, 2003; Gordon & Martinez, 2010; Jenkins & Allen, 2010). Percentage of CD11c positive BMMφs was low (~10%), so contamination from DCs was ruled out, as all bone marrow derived DCs are positive for this marker (data not shown) (Downes & Marshall-Clarke, 2010; Jenkins & Mountford, 2005).

3.3.2 Cytokine production by BMMΦs in response to overnight stimulation with 0-3hRP and other PAMPs

3.3.2.1 *Endotoxin contamination present in 0-3hRP is neutralized by Polymixin B*

S. mansoni cercarial E/S products (aka 0-3hRP) obtained as described in 2.2.1 come from a non-sterile environment. Although cercariae are extensively washed and cultured in sterile media containing antibiotics, low levels of endotoxin contamination are still detectable (Jenkins & Mountford, 2005) and have been neutralized using PMB (Cardoso et al, 2007; Cooperstock, 1974; Jenkins et al, 2005). To investigate the effect of 0-3hRP in the absence of endotoxin LPS was neutralized using PMB.

BMMΦs (1×10^5 cells per well in 96 well plates) were stimulated overnight with 50µg/ml of 0-3hRP or 1ng/ml of LPS, with or without 2µg/ml of PMB, or left unstimulated (Media). Supernatants were collected and analyzed for the presence of IL-10 and IL-12p40 by ELISA (see 2.5).

Addition of PMB resulted in a significant but partial decrease in the production of both IL-12p40 and IL-10 by BMMΦs in response to 0-3hRP (Figure 3.2) whilst the same quantity of PMB totally neutralized LPS-induced cytokine production in the cells. Since in the presence of PMB, 0-3hRP was still able to induce significantly elevated levels of both cytokines, it is clear that BMMΦs respond to components of 0-3hRP and not exclusively to any potential endotoxin contamination present in the antigen preparation. Consequently, to ensure that the immune responses measured were specific to components of 0-3hRP of helminthic origin, PMB was included in all subsequent experiments.

3.3.2.2 *0-3hRP induces a distinct cytokine response in BMMΦs*

Macrophages respond to many innate stimuli that allow them to condition the immune response. Several TLR antagonists have been described (Akira & Takeda, 2004; Hoshino et al, 1999; Takeuchi et al, 1999) and each induces a distinct response from these cells. To investigate how *S. mansoni* cercarial E/S products compare to other innate stimuli, BMMΦs were exposed to 0-3hRP alongside several different TLR ligands (Figure 3.3).

BMMΦs (1×10^5) were exposed overnight to 0-3hRP (50µg/ml), LPS (1ng/ml), Zymosan A (50µg/ml), Poly I:C (25µg/ml), Pam₃CSK₄ (5µg/ml), or left un-stimulated (Media).

0-3hRP induced a distinct response in BMMΦ cytokine production, with relatively low levels of IL-12p40 and high levels of IL-10 (Figure 3.3). Classically pro-inflammatory stimuli like LPS or Pam₃CSK₄ induced higher levels of IL-12p40 than any other ligand. Likewise, they induced a significantly smaller production of IL-10. Poly I:C induced modest levels of IL-12p40 (similar to those induced by 0-3hRP) and low levels of IL-10. BMMΦs exposed to Zymosan A, a complex mixture of proteins and glycans from yeast, exhibited the greatest amounts of anti-inflammatory IL-10. In summary, the increased levels of IL-10 secreted by BMMΦs in response to 0-3hRP, without a correspondingly high IL-12p40 production, show this antigenic preparation is different from other PAMPs.

3.3.3 Changes to the membrane proteome of BMMΦs after stimulation with 0-3hRP and LPS

Proteins on the cell surface of macrophages mediate communication with other cells. Investigations into changes in the levels of MHC-II, CD80, CD86 and CD40 using flow cytometry in BMMΦs exposed to 0-3hRP yielded no significant results (data not shown). As IL-10, but not IL-12p40, production by these stimulated cells has the potential of modulating the immune response, the regulation of receptors in the membrane of these 0-3hRP stimulated cells warranted investigation. Consequently, an unbiased approach was pursued to investigate the changes in membrane protein expression in macrophages exposed to cercarial E/S products. LPS, a pro-inflammatory stimulus, was used alongside 0-3hRP to compare how these two stimuli affected the membrane proteome of stimulated BMMΦs.

3.3.3.1 *Membrane protein extraction and LC-MS/MS pre-run*

BMMΦs were stimulated overnight with 0-3hRP (50µg/ml), LPS (1ng/ml) or left un-stimulated (Media) as described in 3.2.1. After membrane protein enrichment, samples were pooled and prepared for label free quantitative proteomics.

To assess the quality of protein samples, and the result of membrane enrichment protocol, the preparations were analyzed using LC-MS/MS. In total 416 proteins were identified across the three different samples using the IPI mouse database (Table 8.1). Of the 416 proteins identified, 39 (9.4%) were only present in BMMφs stimulated with 0-3hRP, whereas LPS and Media had 51 (12.3%) and 52 (12.5%) unique proteins, respectively (Figure 3.4). Importantly, 60% of all proteins identified were present in two or more samples, which enables comparisons between levels of expression using the label free proteomics approach, especially as 190 (45.7%) hits were present in all samples, which the analysis will focus on.

To evaluate the success of membrane protein enrichment in the samples, protein hits were analyzed for GO term enrichment using VLAD, as described in 3.2.1.3. The number of proteins associated with a GO term (k) and the percentage of proteins in the sample that mapped to each term were used to choose relevant cellular localizations.

Of 416 identified hits, only 404 proteins had associated GO terms, which is the value to which reported percentages refer to from here on. From that total, 71% of identified hits were associated with membranes (Table 3.1), and 39% mapped to the plasma membrane. This result suggests that the strategy employed to achieve enrichment of membrane proteins from the cell lysates was successful, especially as only 12.9% of proteins associated with the cytosol.

Proteins from membrane-bound organelles were abundant, with 35% of proteins associated with the mitochondrion and 25% with the nucleus. Of the detected proteins, 49.3% can be associated with membrane-bounded vesicles, while small structures such as lysosomes were also represented with 13.9% of proteins mapping to this GO term.

As for molecular processes in which detected proteins were involved with, 39% (152) of hits were associated with “responses to stimulus” (GO:0050896), with 21.3% (83) associated with “signaling” (GO:0023052) and 7.4% (39) with “immune response” (GO:0006955).

3.3.3.2 *Label-free quantitative proteomics of membrane enriched protein samples*

The samples described above were used for quantitation of protein changes using a novel, label-free, mass spectrometry approach (Li et al, 2011; Meissner et al, 2013; Patel et al, 2009). As the method requires further repetition of MS runs, coverage was increased and 436 proteins were identified by MS/MS across the samples, of which quantitation data were obtained for 254. Hits were ranked based on Mascot Score and filtered for significance ($p < 0.05$; i.e. a Mascot Score greater than 67) guaranteeing that mass spectra was accurately matched to identified proteins and reducing the chances of false discovery. Only hits that met that criteria and had at least two peptides from each protein used for quantitation are reported. Coefficients of variation (CV%) of the peptide quantitation for each protein are also given. Hits with a 30% or lower variation are included in the GO term enrichment analysis. Regulated proteins reported are those with more than a 1.5 fold up or down regulation, with a median ratio greater than 1.5 or lower than 0.67. Detailed lists of the association of regulated proteins in both treatments with each GO term for biological processes (Table 8.2) or cellular localization (Table 8.3) are presented in the appendix.

Thirty four proteins were up-regulated in BMM ϕ s exposed to 0-3hRP and only 3 were down-regulated compared to Media (Table 3.2). Conversely, LPS stimulated 7 proteins to be up-regulated with the same number being down-regulated compared to Media (Table 3.3). These results are summarized in Figure 3.5, where quantified proteins in BMM ϕ s stimulated with 0-3hRP and LPS are directly compared to one another. Missing bars correspond to proteins for which good quality data was not available. No error bar is presented when only 1 peptide was used for quantitation.

Similarities between samples obtained using the two different stimulation regimes are evident. Immune response proteins, such as the Macrophage scavenger receptor 1 (MSR1), CD14 and H2-Q2 were up-regulated in both samples. However, LPS treated BMM ϕ s had several down-regulated proteins, more than for 0-3hRP treated cells (Figure 3.5). Only ATP synthase subunit beta (Atp5b) was down-regulated in LPS and up-regulated in 0-3hRP.

These changes are revealed as a pattern when regulated proteins in each sample are analyzed for GO term enrichment. Both treatments had similar

proportions of up-regulated proteins associated with “biological regulation” (70.4% in 0-3hRP vs. 71.4% in LPS), “response to stimulus” (51.9% in 0-3hRP vs. 57.1% in LPS) and “response to stress” (40.7% in 0-3hRP vs. 42.9% in LPS). However, 0-3hRP treated macrophages had a greater number of up-regulated proteins mapping to “metabolic process” with 48.1% compared to 28.6% in LPS (Table 3.4). As a consequence, proteins related to “immune system process” were enriched in LPS treated macrophages with 57.1% compared to 25.9% in 0-3hRP. However, 0-3hRP treated BMM ϕ s up-regulated proteins associated with “regulation of MAPK” (11.1%), a category that was absent in LPS treated cells. In contrast with the observations reported above, LPS treated macrophages down-regulated several proteins mapping to metabolic process (66.7%) compared to none in 0-3hRP treated cells (Table 3.4).

Finally, in accordance with the earlier GO term enrichment analysis (see Table 3.1), several proteins up and down regulated in both treatments were associated with membranes or membrane structures (Table 3.5). Proteins associated with organelles were up and down-regulated to a greater extent in 0-3hRP treated BMM ϕ s than in LPS stimulated cells. Notably, an association with the mitochondrion (66.7%) was only recorded in down-regulated proteins after LPS treatment. This corroborates the down-regulation of metabolic processes associated proteins in LPS treated cells but not in 0-3hRP treated BMM ϕ s.

3.3.3.3 *Validation of protein expression using flow cytometric analysis of antibody-labelled 0-3hRP treated BMM ϕ s*

From the results obtained above, three proteins were selected to partially validate the observations made. CD36 (Baranova et al, 2012; Fonager et al, 2012; Leelahavanichkul et al, 2012) and CD14 (Baumann et al, 2010) were both regulated on BMM ϕ s and have well-established associations with innate immune responses in macrophages, particularly with the Toll-like receptor system (Lee et al, 2012). MSR1 on the other hand, has been reported to have various roles in responses to pathogens (Blanchet et al, 2014; Mukhopadhyay et al, 2011). All three proteins are expressed on the surface of macrophages and specific antibodies were commercially available.

BMM ϕ s were exposed to 0-3hRP (50 μ g/mL) for 18 hours, or left untreated (Media) in three independent experiments. Cells were labeled as described in 2.4 for surface expression of CD36, MSR1 and CD14.

All three markers corroborated the results obtained by mass spectrometry (Figure 3.6). Expressed as the percentage of positive cells (Figure 3.6A & C) and as the median fluorescence intensity (MFI) (Figure 3.6B & D), both approaches identified the differential expression of CD36, MSR1 and CD14 in accordance with the calculations made using the label-free proteomics approach. CD14 and MSR1 were significantly up-regulated on BMM ϕ s stimulated with 0-3hRP compared to Media, whilst the expression of CD36 was significantly down-regulated (Figure 3.6A & C). The MFI values further confirm the modest nature of the changes in the expression of these markers (as seen in Figure 3.5), with changes not exceeding 2 fold up or down regulation.

3.3.4 Phosphorylation of MAPKs in BMM ϕ s after stimulation with 0-3hRP

Investigation into phenotypic changes in BMM ϕ s exposed to *S. mansoni* cercarial E/S products has thus far emphasized that these cells only subtly change the expression of different molecules, despite the marked differences in cytokine production. The differences detected by proteomics indicated a strong association with metabolic processes in BMM ϕ s, and importantly with regulation of MAPKs, which are a well characterized signaling family of proteins. Therefore, the activation status of MAPKs was evaluated using a commercially available kinase proteome profiler array.

3.3.4.1 Kinase proteome profiler array of BMM ϕ s treated with 0-3hRP

BMM ϕ s were stimulated with 0-3hRP (50 μ g/ml) for 5, 30 and 60min and proteins then extracted from lysed cells and tested for the activation of MAPKs as described in 3.2.2. To avoid overexposure or arrays, X-ray films were exposed to membranes for various lengths of time, with 1min being selected based on signal quality (i.e. avoiding overexposure of positive controls and maximizing detection of phosphorylated proteins). Images of x-ray film of membranes are presented in Figure 3.7. Positive and negative controls (PBS) were consistent across all membranes. Due to limited number of membranes, 0 time point was not included.

Several MAPKs were active, as seen by phosphorylation, at 5min (e.g. JNK pan), however stronger signals were apparent after 30 and 60min of stimulation with 0-3hRP (such as CREB, ERK or TOR) (Figure 3.7). Intriguingly, not all detected signals remained strong after 60min of exposure to cercarial E/S products (e.g. JNK 2 and p38 α).

3.3.4.2 *Densitometry analysis of kinase proteome profiler array*

To more accurately measure the levels of phosphorylation of the detected signals in the membranes, a densitometry analysis was performed on the exposed X-ray films. Pixel density was quantified on each coordinate of the array using identical circular areas followed by global background subtraction (which led to some negative values). Values were normalized based on the positive controls on each blot to account for inter-membrane variation, as recommended by the manufacturer. Finally, technical replicates (n=2) in each membrane were used to calculate the mean and standard deviation for each of the 26 proteins in the array.

The strongest signal detected corresponded to ERK2 (Figure 3.8), followed by CREB, JNK pan, JNK2, p38 α , RSK1 and TOR. After exposure to 0-3hRP, the strongest signals for individual kinases corresponded to the 5min time point in 7 cases (p70 S6K, p38 δ , p38 β , MKK3, HSP27, JNK pan and JNK 3), to the 30min time point in 3 cases (p38 α , JNK 2 and CREB) and to the 60min time point also in 3 cases (RSK2, MKK6, ERK2). Sustained activation was clear in TOR, GSK-3 α/β , GSK-3 β and MSK2 where signal strength at 30 and 60min were equally high. Other kinases had a dip in the signal after 30min of exposure (RSK1 and p53) with levels returning to the initial time point after 60min. Notably, no changes between time points were detected in the Akt family, or for ERK1, p38 γ and JNK1.

3.3.4.3 *Fold changes in kinase activation after stimulation with 0-3hRP*

The segregation of kinases into different dynamics of activation implied a temporal regulation as part of different signaling cascades. To further explore this feature of the response to 0-3hRP, densitometry data was analyzed as fold changes in phosphorylation compared to the earliest available time point (5min). Normalized densitometry data was used to calculate fold changes in protein phosphorylation using 5min (arbitrarily set to 1) as a reference point.

MAPKs were segregated into 4 groups according to peaks of activation, as described above. Mean fold changes and SD for activated proteins at each time point are presented (Figure 3.9).

Proteins that were phosphorylated at 5min (Figure 3.9A) showed a pronounced reduction in activation at both 30 and 60min, with levels at 60min being lowest for 4 out of 7 proteins in this group. Conversely, MAPKs that had a dip in the signal at 30min (Figure 3.9B) recovered initial levels of phosphorylation after 60min of stimulation.

The remaining three groups were remarkably similar. All proteins had consistently similar fold changes in activation between 30min and 60min (Figure 3.9D), excluding p38 α (Figure 3.9C) and RSK2 (Figure 3.9D), which differed between this two time points. Thus, these 8 proteins (p38 α , CREB, RSK2, ERK2, MSK1, TOR, GSK-3 α/β and GSK-3 β) appeared dynamically linked (JNK2 excluded as it did not exceed the 2 fold change threshold of activation).

3.3.5 Rapid gene expression changes in BMM ϕ s after stimulation with 0-3hRP; analysis by qPCR array

BMM ϕ s exposed to 0-3hRP activated several kinases through phosphorylation with a very tight temporal regulation. This activation was most apparent after 30min. Furthermore, 0-3hRP modulated various proteins that regulate signal transduction and are involved with the TLR system (3.3.3.2). Therefore, the expression of genes related to MAPK activation and TLR stimuli was tested after 30min of exposure to 0-3hRP using a qPCR array with 156 genes (see 3.2.3).

BMM ϕ s were stimulated with 0-3hRP (50 μ g/ml), LPS (1ng/ml) or left unstimulated (Media) for 30min. RNA was extracted from these cells and prepared for analysis as described in 3.2.3. RNA transcripts for 156 test genes, plus 5 house-keeping genes (HKGs), were tested using a qPCR array (for full list of genes see Table 3.6). Samples met all relevant quality controls, which included testing for genomic DNA contamination, retro-transcription controls and negative PCR controls. Changes in gene expression were calculated based on Ct values as specified in 2.6 using all 5 HKGs (*Hprt*, *Gapdh*, *Gusb*, *Actb* and *Hsp90ab1*) by using their average Ct values for each sample.

3.3.5.1 *BMMφs treated with 0-3hRP alter the expression of several genes*

Using un-stimulated macrophages (Media) to calculate fold differences in transcript levels (Figure 3.10), 55 genes were found to be regulated in 0-3hRP and LPS stimulated BMMφs using a 2-fold change threshold. Unlike LPS, which mainly caused up-regulation of various genes (such as *Il12a*, *Mapk13*, *Lta*), 0-3hRP had a powerful effect on the expression of multiple transcripts both by inducing (Figure 3.10A) or repressing (Figure 3.10B) expression. Notably, LPS stimulated BMMφs up-regulated the expression of several proteins of the MAPK family, whereas cells stimulated with 0-3hRP down-regulated their transcription or did not affect their expression at all (e.g. *Map3k7*, *Mapk8ip2*, *Mapk13*).

Differences in IL-10 and IL-12p40 protein production reported earlier (3.3.2.2) were consistent with expression of their genes at the transcript level, with 0-3hRP stimulated BMMφs producing more *Il10* and less *Il12a* transcript than LPS treated cells (Figure 3.10A). 0-3hRP powerfully induced the expression of several cytokines (e.g. *Il1a*, *Il1b*, *Il10*, *Il6*), although LPS also activated their transcription.

Ct value differences between target transcripts and HKGs within each sample were calculated ($2^{-\Delta Ct}$) for BMMφs exposed to 0-3hRP and LPS. A direct comparison of the value for each gene between the two treatments was made (Figure 3.11). Genes with a greater than 2-fold change in either direction fall outside the dotted lines which represent the 2-fold threshold. HKGs were constant between the samples (Figure 3.11 in red), however several target genes were differentially regulated between the two samples. For example, the differences in *Il10* and *Il12a* mentioned above remained apparent in this new analysis (Figure 3.11 in blue). CD14, which was found to have similar protein levels in LPS and 0-3hRP stimulated BMMφs (Figure 3.5), also had similar levels of transcript (Figure 3.11 in orange).

3.3.5.2 *qPCR for specific gene transcripts corroborate PCR array*

To verify the results obtained using the qPCR array for genes related to MAPKs and TLRs, RNA was obtained from 0-3hRP stimulated BMMφs and tested specifically for 4 of the regulated transcripts.

BMMφs were stimulated with 0-3hRP (50μg/ml), LPS (1ng/ml) or left un-stimulated (Media). RNA was extracted and used for gene expression analysis

as described in 2.6 using primers for *I110* and *I12b* (see Table 2.2) or with primers purchased from QIAGEN (equal to the primers in the array) for mitogen activated protein kinase kinase kinase 7 (*Map3k7*) and early growth response protein 1 (*Egr1*), which were selected for being the most down or up-regulated transcripts in 0-3hRP stimulated BMMφs, respectively (Figure 3.10). Changes in gene expression were quantified relative to un-stimulated (Media) BMMφs using *Gapdh* as a HKG.

Initial experiments were performed to examine the expression of *Egr1* (Figure 3.12A) and *Map3k7* (Figure 3.12B) in BMMφs after 30min exposure to 0-3hRP or LPS. The results for *Egr1* confirmed earlier observations (Figure 3.10), with a pronounced expression of this transcription factor in response to 0-3hRP but not LPS (Figure 3.12A). However, the expression of *Map3k7* by qPCR did not agree with the qPCR array data as no changes of expression were detected although by array this kinase was reduced after stimulation with 0-3hRP (Figure 3.12B).

Due to the dynamic temporal nature of MAPK activation (see 3.3.4.3), changes in the timing of expression for *Egr1* and *Map3k7* transcripts, as well as *I110* and *I12b*, were investigated (Figure 3.13). The expression of *I110* after 30min of exposure to 0-3hRP was significantly higher than response to Media (Figure 3.13A), thus confirming the array results. Moreover, this transcript continued to increase at 100min of exposure. However, *I12b* was only marginally increased compared to Media after 30min exposure to 0-3hRP (Figure 3.13B; averaging 1.6 fold increase) and the increase was only significant after 100min exposure.

The dramatic induction of *Egr1* by 30min was evident, however its expression decreased back to levels for cells cultured with Media only after 100min (Figure 3.13C). The expression of *Map3k7* was not statistically different in BMMφs treated with 0-3hRP and their un-stimulated counterparts at any of the time points tested (Figure 3.13D).

3.4 Discussion

BMM ϕ s stimulated with 0-3hRP exhibit a strikingly unique activation state. These cells produced high levels of anti-inflammatory cytokine IL-10 and low levels of pro-Th1 cytokine IL-12p40. They also changed the way in which they regulated their metabolism, potentially to fuel immune processes differently. Furthermore, BMM ϕ s exposed to 0-3hRP activated and regulated several MAPKs whose activation profile matches that of the transcription of *I110* and *Egr1*. Finally, they appear to regulate these features using components of the TLR system, such as CD14 and CD36, which have altered expression levels in stimulated cells compared to resting cells.

3.4.1 0-3hRP elicits a unique response in BMM ϕ s

The number of studies addressing the effects of 0-3hRP on immune cells is limited. *S. mansoni* cercarial secretions are a complex mixture of proteins that can be obtained for *in vitro* studies in more than way, which has led to some discrepancies in findings by different groups around the world. The focus of this work was the effect of 0-3hRP, prepared by mechanical disruption of cercariae, on murine macrophages. 0-3hRP obtained in that manner has been shown to contain at least one bacterial product (LPS) (Jenkins et al, 2005), which was successfully neutralized using PMB throughout this study. Nonetheless, other PAMPs of microbial origin are undoubtedly present in 0-3hRP, however completely controlling experimentally for their effect is not currently possible. This issue is partly addressed by washing cercariae extensively and by incubating the parasite with antibiotics. However, in a natural environment, individuals will be exposed to cercariae in an unsterile environment, which could support the idea of a “dirty” 0-3hRP having more physiological relevance. Determining the exact nature and levels of “contaminants” in 0-3hRP would require complex mass spectrometric analysis of the preparation, targeting a broad range of molecules of different biochemical nature. Those experiments are beyond the scope of the current work.

This study employed BMM ϕ s to study the effects of 0-3hRP. Several methods exist for the isolation and production of other macrophage for *in vitro* studies (Bailey et al, 2011; Jenkins et al, 2005; John et al, 2013; Mukhopadhyay et al, 2011). All methods available should be judged on the basis of physiological

relevance, cell yield, homogeneity of the results, being of naive phenotype, and having plasticity upon maturation with specific ligands. Conditioning bone marrow cells with CSF-1, which drives the differentiation and proliferation of macrophages *in vivo* (Jenkins et al, 2011; Jenkins et al, 2013) and has been used for the same purpose *in vitro*, produces cells that have the required plasticity to respond differentially to a plethora of stimuli that mature macrophages may encounter *in vivo* in the tissues and blood (Bailey et al, 2011; Deryugina et al, 1995). BMM ϕ s prepared in this manner were found to have a homogeneous and high expression of CD11b (myeloid cell marker) and F4/80, which is expressed by macrophages in tissues and by other immune cells like eosinophils and dendritic cells. A small percentage of BMM ϕ s expressed CD11c compared to bone marrow derived DCs (data not shown) and expression of MHC-II was similarly low. Furthermore, these cells were readily available, as yields were high in every culture, and were able to produce cytokines when challenged with 0-3hRP and a range of PAMPs. Thus, this system provided a physiologically relevant, homogeneous, naïve and plentiful experimental platform to assess the effect of stimulation with *S. mansoni* cercarial E/S products.

0-3hRP elicited cytokine production in BMM ϕ s that was significantly different from other PAMPs, and was independent of possible endotoxin contamination. The low levels of IL-12p40 and high levels of IL-10 detected in culture supernatants after overnight exposure to the antigenic preparation, suggest that 0-3hRP is driving a mixed response. IL-12p40 is essential to induce Th1 responses from the adaptive immune system (Cook et al, 2011; de Jong et al, 2002; Yang et al, 2010). However, IL-10 is a master regulator of the immune response that dampens inflammation, limits T cell activation and induces tissue repair (Antoniv & Ivashkiv, 2011; Belkaid et al, 2001; Kamanaka et al, 2006; Kuhn et al, 1993; Sabat et al, 2010; Saraiva & O'Garra, 2010; Specht et al, 2012). This duality in the response from BMM ϕ s exposed to 0-3hRP matches the mixed responses often encountered at infection sites of schistosome infections, in which both cytokines are present (Cook et al, 2011; Hewitson et al, 2007; Pearce & MacDonald, 2002; Perona-Wright et al, 2006). Cells from the immune system in the skin will encounter 0-3hRP as larvae migrate through this tissue. Therefore, immune cells in the skin could be driven to this mixed

cytokine response by exposure to the secretions of invasive larvae. Evidence for the presence in *S. mansoni* infected skin of IL-10 and IL-12p40, but also IL-1 β and IL-6 that were also induced (at transcript level) by 0-3hRP, is already available (Hogg et al, 2003b), and 0-3hRP could be partly responsible for the induction of all these cytokines *in vivo*.

3.4.2 Changes in membrane proteins in BMM ϕ s stimulated with 0-3hRP

Label-free quantitative proteomics was used to investigate membrane proteins from stimulated BMM ϕ s in an effort to further elucidate changes in response to 0-3hRP. This method provided sufficient coverage and accuracy to measure changes in hundreds of membrane proteins simultaneously in BMM ϕ s stimulated with 0-3hRP or LPS. The effectiveness of the membrane enrichment was evidenced by the over-representation of these proteins in the samples (71%). However, the association of some proteins with the GO term “membrane” is not limited to integral membrane proteins, but rather to proteins that interact or are part of the membrane. Moreover, no input sample (i.e. pre-membrane enrichment) was analyzed, and that would be required to rigorously assess the success of the process.

Relative changes (with respect to resting cells) revealed that BMM ϕ s stimulated with 0-3hRP up-regulated the expression of proteins involved in metabolic processes, which was not the case in cells stimulated with LPS. BMM ϕ s exposed to 0-3hRP increase the expression of proteins linked with the GO term “metabolism of organic substances”, which could mean that processing and responding to 0-3hRP is costly from an energy point of view, to a greater extent than responding to LPS. However, due to the limited number of protein hits that mapped to metabolism, it is not possible to determine exactly how 0-3hRP is affecting these processes. Further experiments measuring the uptake of carbohydrates and lipids, as well as the consumption of oxygen and production of lactate would commence to address this feature of 0-3hRP stimulated macrophages. Indeed, understanding the energy requirement of 0-3hRP activated macrophages would shed light on potential differences and similarities with cells activated by other ligands. Others have explored the interplay and intimate linkage between metabolism and the immune response (Arnoult et al, 2011; Everts et al, 2014; Ferret-Bernard et al, 2012; Gehart et al, 2010; Pulendran & Artis, 2012; Vanhaesebroeck et al, 2012; West et al, 2011).

Hypoxic conditions are often associated with inflammation (Bartels et al, 2013), consequently immune cells will need to fundamentally change the way they obtain energy. The possibility these finding raise with respect to the regulation of metabolism of macrophages by 0-3hRP is in line with previous reports of the effect of other *S. mansoni* antigenic preparations (i.e. SEA) on DCs (Ferret-Bernard et al, 2012).

0-3hRP stimulated macrophages up-regulated surface proteins with known immunological functions. Changes in MSR1, CD36 and CD14 were validated using flow cytometry. These three proteins have been reported to mediate macrophage responses to different stimuli. MSR1 and CD36 are both scavenger receptors that could be implicated in uptake of 0-3hRP, as is the case with other ligands (Baranova et al, 2012; Blanchet et al, 2014; Fonager et al, 2012; Mukhopadhyay et al, 2011; Oury, 2014; Sulahian et al, 2008). However, as CD36 expression is reduced, 0-3hRP might be exerting its anti-inflammatory properties by reducing the availability of this receptor on the surface of macrophages. CD14 is perhaps the best characterized co-receptor for the TLR system (Akira & Takeda, 2004; Ambarus et al, 2012; Baumann et al, 2010; Ioannou & Voulgarelis, 2010; Valanne et al, 2011). CD14 up-regulation in 0-3hRP treated BMMφs provides a starting point for the implication of TLRs in the recognition of parasite secretions.

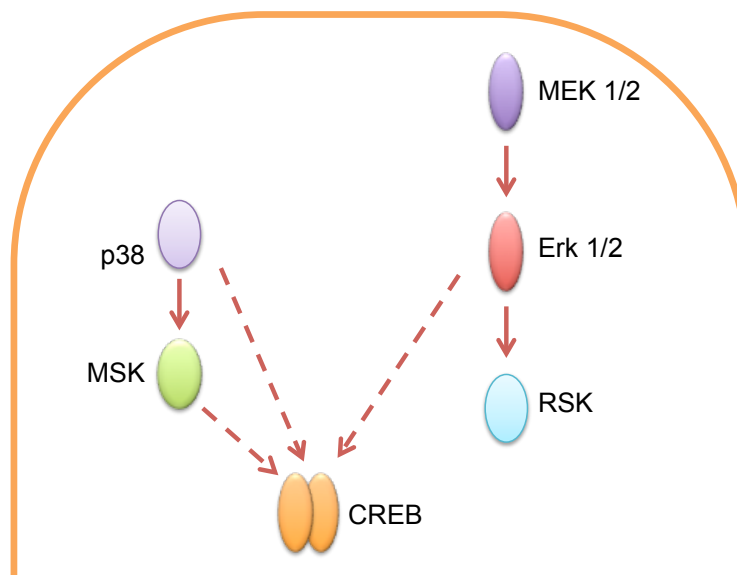
Finally, the GO term enrichment analysis revealed that BMMφs stimulated with 0-3hRP up-regulated proteins that modulate MAPK responses, a category absent from LPS treated cells. In conjunction with the up-regulation of elements of the TLR system and the distinct cytokine production elicited by the parasite secretions, MAPKs appeared to be a likely link between the exposure to 0-3hRP and the downstream immune response.

3.4.3 Activation of MAPKs in BMMφs stimulated with 0-3hRP is tightly regulated

Activation of MAPKs in BMMφs exposed to 0-3hRP was diverse. Although unstimulated BMMφs were not included in this analysis (i.e. no time point 0 was performed), a clear temporal regulation of activation of MAPKs was evidenced across the three time points measured. The most interesting feature of these findings was the dynamic link observed between p38α, MSK2, ERK2, RSK2 and CREB, suggesting that these proteins might be part of the same signaling

pathway. Others have reported links (see Diagram 3.1) between p38 α and MSK2 (Yang et al, 2010) or ERK2 and RSK2 (Bain et al, 2007; Mayer et al, 2013; van Vliet et al, 2013). Moreover, CREB has been reported to be downstream of both p38 and Erk1/2 (Deak et al, 1998; Elcombe et al, 2013; Mayer et al, 2013; van Vliet et al, 2013; Wen et al, 2010). However, the association made in the present study between all these molecules, with a common activator and similar dynamics of phosphorylation, is novel. The implications of these associations and how they relate to the production of cytokines in response to 0-3hRP *in vivo* and *in vitro* will be explored fully in subsequent chapters. The relative contribution of these kinases to the phenotype observed in stimulated macrophages will be obtained through a combination of genetically deficient animals and chemical inhibitors.

Diagram 3.1 Previously reported links between MAPKs



Demonstrated associations (solid lines) and proposed links (dashed lines) by previous studies between MAPKs.

Other kinases were also active in macrophages exposed to 0-3hRP. The strong and prolonged activation of TOR, which started after 30min of stimulation with 0-3hRP, is unclear as other members of the TOR signaling pathway were not active (such as the Akt family) or had very low levels of activation (p70 S6K) (Gwinn et al, 2008). Furthermore, GSK-3 was also active, as discussed further down, but reports suggest TOR blocks this kinase (Alessandrini et al, 2011; Cremer et al, 2011; Wang et al, 2011). Consequently, the role of the activation of TOR in the context of 0-3hRP-stimulation would require further exploration.

Chemical inhibition of stimulated macrophages through rapamycin would provide a starting point for these experiments.

GSK-3 α/β is a well-known regulator of signaling events in macrophages. It functions mainly as an inhibitor of the transcription of numerous genes and has been described to act in concert with IL-10 to suppress the activation of certain transcripts in favor of others (Antoniv & Ivashkiv, 2011; Park et al, 2011; Wang et al, 2011). GSK3- α/β is activated in response to 0-3hRP in BMM ϕ s after 30min and remains highly active after 60min. In that way, it could be cooperating with the other triggered signals to favor an anti-inflammatory response, similar to the known ability of p38 α to maintain low levels of IL-12 (Yang et al, 2010).

Overall, 0-3hRP stimulated BMM ϕ s activate several MAPKs that are regulated differently, resulting in different temporal dynamics. A group of these kinases appears to act in concert, peaking at 30min of activation and then maintaining those high levels of activity for at least 30 more minutes. This group contains several kinases that have been linked to TLRs and cytokine production, particularly that of IL-10. Therefore, the gene expression of macrophages after 30min exposure to 0-3hRP was investigated, targeting genes that are linked with MAPKs and the TLR system.

3.4.4 Gene expression in BMM ϕ s exposed to cercarial E/S products

The gene expression profile of macrophages exposed to 0-3hRP was dramatically different from that elicited by LPS after 30min of exposure. 0-3hRP induced a stronger cytokine response from macrophages, which had higher levels of TNF α , IL-1 and IL-6 transcript than LPS stimulated cells. These cytokines have been conventionally associated with the innate immune system (Benoit et al, 2008; Hertzog et al, 2011; Ioannou & Voulgarelis, 2010; Rathinam et al, 2012; Ruland, 2011). They are produced faster than other cytokines and often their levels drop as the inflammatory process evolves.

The increase in cytokine transcript levels was also true for IL-10, which unlike TNF α , IL-1 and IL-6, dampens the immune response and is associated with the resolution of inflammation, not its commencement (Belkaid et al, 2001; Kuhn et al, 1993; Sabat et al, 2010; Saraiva & O'Garra, 2010). Unlike all other cytokines, IL-12 was higher in LPS stimulated macrophages than in 0-3hRP stimulated

ones. These results confirm the observations made when the levels of these cytokines were measured in culture supernatants. 0-3hRP consistently induced higher levels of IL-10 and lower levels of IL-12 than LPS. This contrast underpins the difference between 0-3hRP and LPS as innate stimuli. Cercarial E/S products are a potent immune stimulus, however they deviate from classic pro-inflammatory PAMPs.

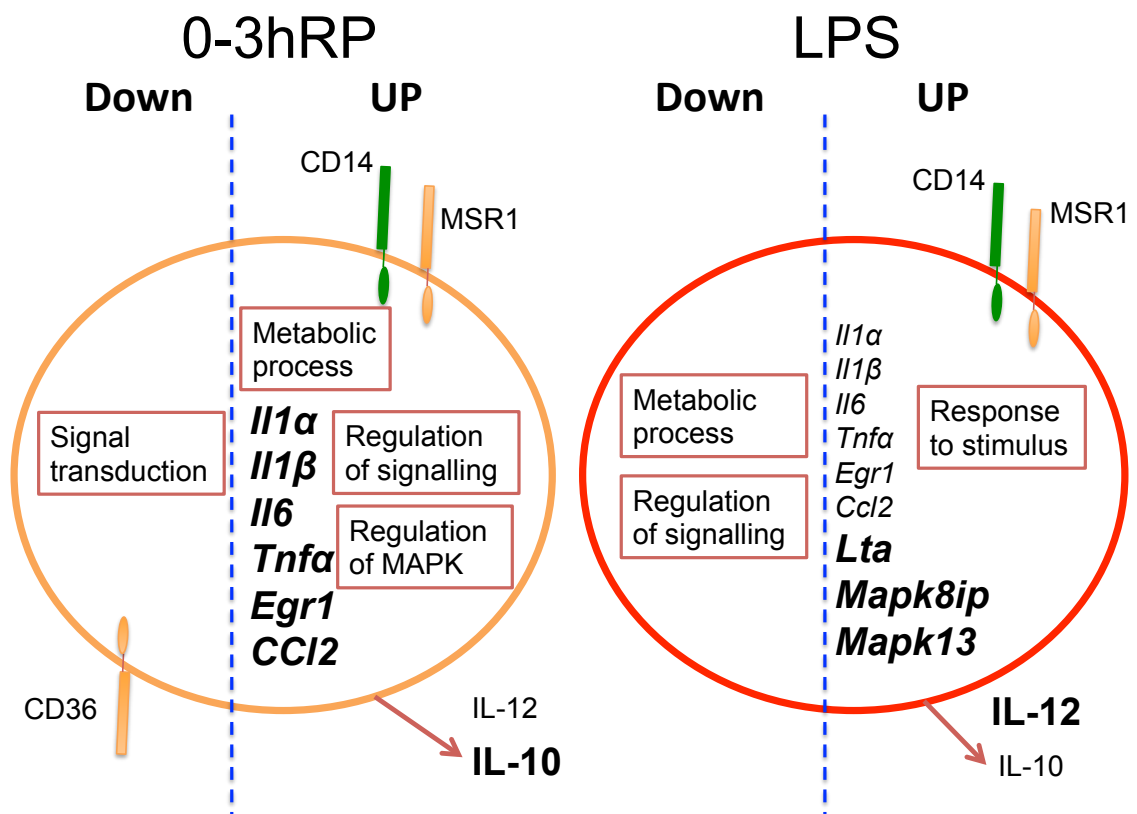
The most highly expressed transcript in 0-3hRP stimulated BMMφs was *Egr1*. This transcription factor is known to be induced by several signaling cascades in response to growth factors, sheer stress and oxygen deprivation (Pagel & Deindl, 2011), and both Erk and CREB are upstream from it (Pagel & Deindl, 2011; Shen et al, 2011). *Egr1* targets several hundred genes, some of which are related to inflammation, however, its role in this process is not clear and is more often associated with tissue damage (Fu et al, 2003). The production of this transcript was validated using qPCR and tested at different times after stimulation with 0-3hRP, alongside *Il10* and *Il12b*.

The transcription of *Il10* and *Egr1* was reminiscent of the phosphorylation of MAPKs, which peaked at 30min. *Egr1* activation was transient, and after 100min not different from Media, unlike *Il10* transcription that continued to increase. *Il12b*, on the other hand, was only significantly elevated after 100min. This evidence links IL-10 and Egr1 to the phosphorylation of the MAPKs described earlier, as their dynamic of activation matches each other.

3.5 Summary

BMMφs exposed to 0-3hRP dramatically altered the expression and synthesis of a varied array of proteins that differ from the activation elicited by LPS (Diagram 3.2). Those differences included the potent induction by 0-3hRP of an array of cytokines (at the transcript level), including IL-10. However, this was not the case for IL-12. LPS on the other hand induced the expression of MAPK that were not up-regulated by 0-3hRP. Moreover, 0-3hRP up-regulated proteins associated with the regulation of signaling and MAPK cascades, a category absent from LPS.

Diagram 3.2 Summary of global changes in stimulated BMMφs



Summary of up and down regulated transcripts (*italics*), protein and processes (*boxes*) in 0-3hRP (orange) and LPS (red) stimulated BMMφs. Bold text identifies transcripts/proteins where levels were higher in either treatment.

LPS and 0-3hRP also differentially regulated proteins associated with metabolic processes. Finally, receptors like CD14 and MSR1 were up-regulated by both, yet only 0-3hRP down-regulated the expression of CD36, a TLR co-receptor. Together these findings highlight the distinctiveness of 0-3hRP as an innate stimulus and suggest that both MAPKs and TLRs play a role in the response to 0-3hRP by macrophages, a feature that will be explored in the next chapter.

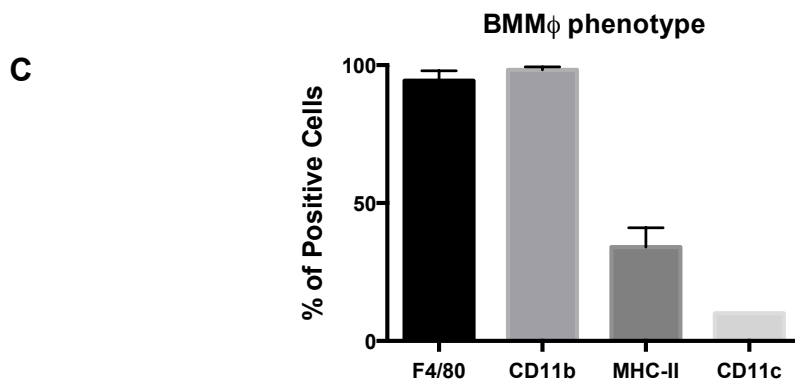
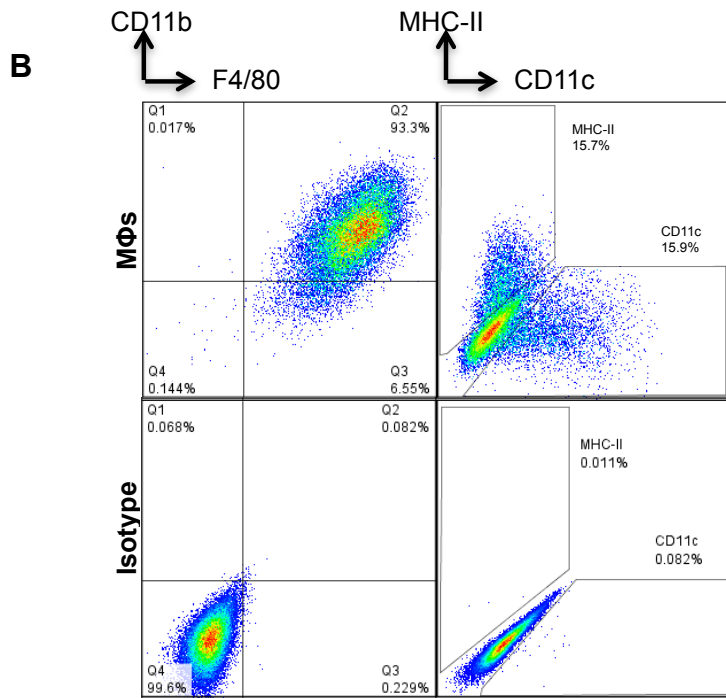
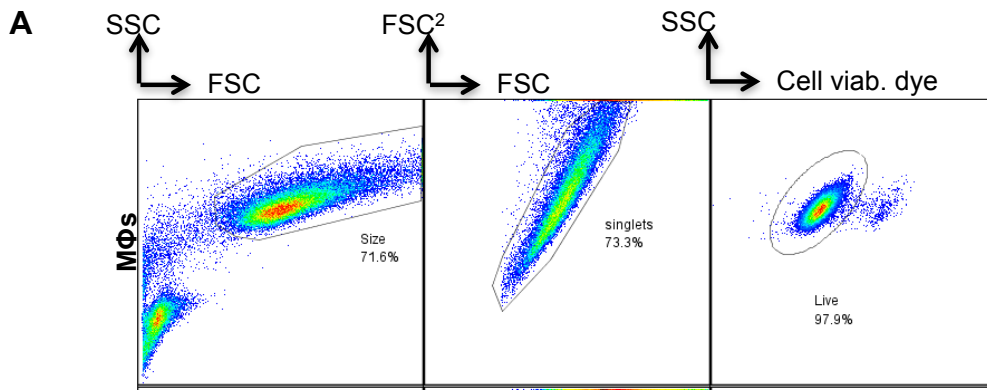


Figure 3.1 Production of macrophages by differentiation of bone marrow cells from femurs and tibia of C57BL/6 mice

Bone marrow cells cultured for 7 days were stained with (A) a viability dye and (B) labeled with antibodies against F4/80, CD11b, MHC-II and CD11c or relevant isotype controls. Representative flow plots (A, B) with percentages for numbers of cells within each gate and (C) bar graph showing mean values (+SD) of percentage of positive cells from 7 independent experiments are presented.

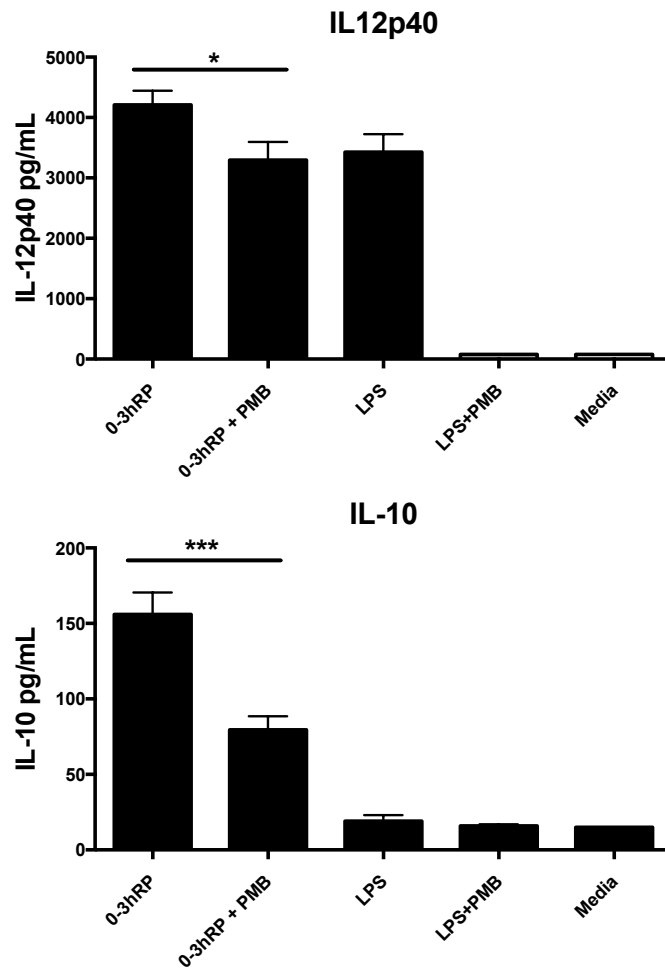


Figure 3.2 Cytokine production by BMMΦs in response to 0-3hRP is not due to endotoxin contamination

Supernatants from BMMΦs stimulated overnight with 0-3hRP (50µg/ml) or LPS (1ng/mL) with or without PMB (2µg/ml) were analyzed for IL-12p40 and IL-10 by cytokine specific ELISA. Means +SEM of three technical replicates are presented. ANOVA and then Dunnett's multiple comparisons test were performed to examine differences between mean of 0-3hRP alone or with the addition of PMB (***) = $p < 0.01$). The result is representative of three independent experiments.

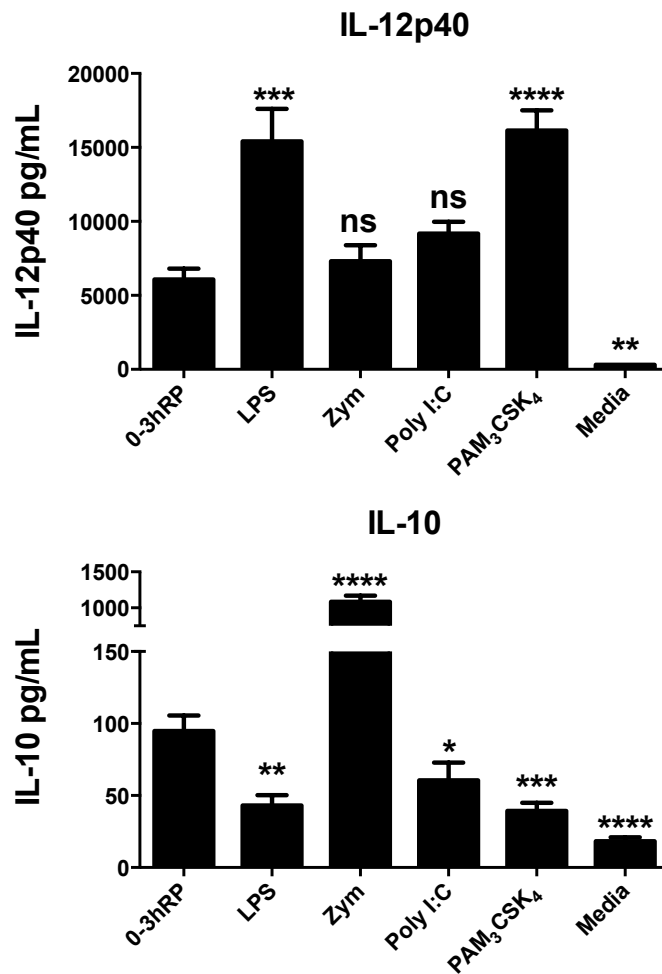


Figure 3.3 Cytokine production by BMMΦs exposed to different PAMPs

Culture supernatants from BMMΦs exposed overnight to 0-3hRP (50µg/ml), LPS (1ng/ml), Zymosan A (50µg/ml), Poly I:C (25µg/ml), Pam₃CSK₄ (5µg/ml) or left un-stimulated (Media) were tested for IL-12p40 and IL-10. Means +SEM of three technical replicates are presented. ANOVA and then Dunnett's multiple comparisons test were performed to examine differences between the means compared to 0-3hRP (* = p<0.05; ** = p<0.01; *** = p<0.001; **** = p<0.0001; ns = p>0.05). The result is representative of three independent experiments.

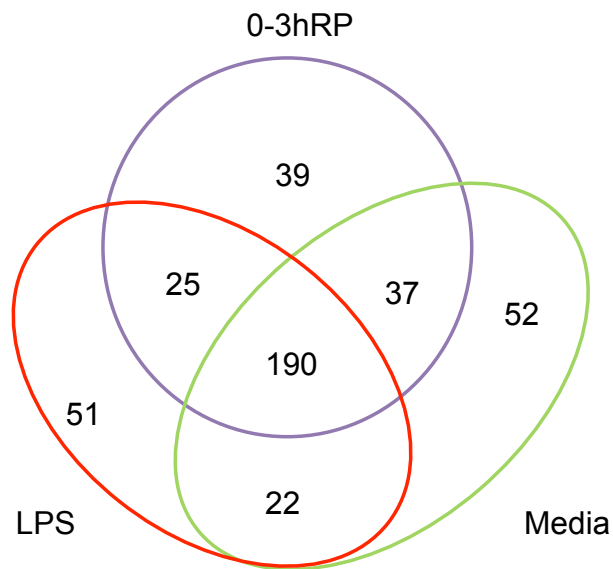


Figure 3.4 Venn diagram depicting the protein hits for the membrane proteome of BMMφs after stimulation with 0-3hRP, LPS, or Media

Membrane protein enriched samples from BMMφs stimulated overnight with 0-3hRP (50μg/ml), LPS (1ng/ml) or left un-stimulated (Media) were analyzed with LC-MS/MS to identify changes in expressed proteins. In total, 416 different proteins were identified. BMMφs for each treatment regime presented unique proteins, whilst others were shared by more than one treatment regime

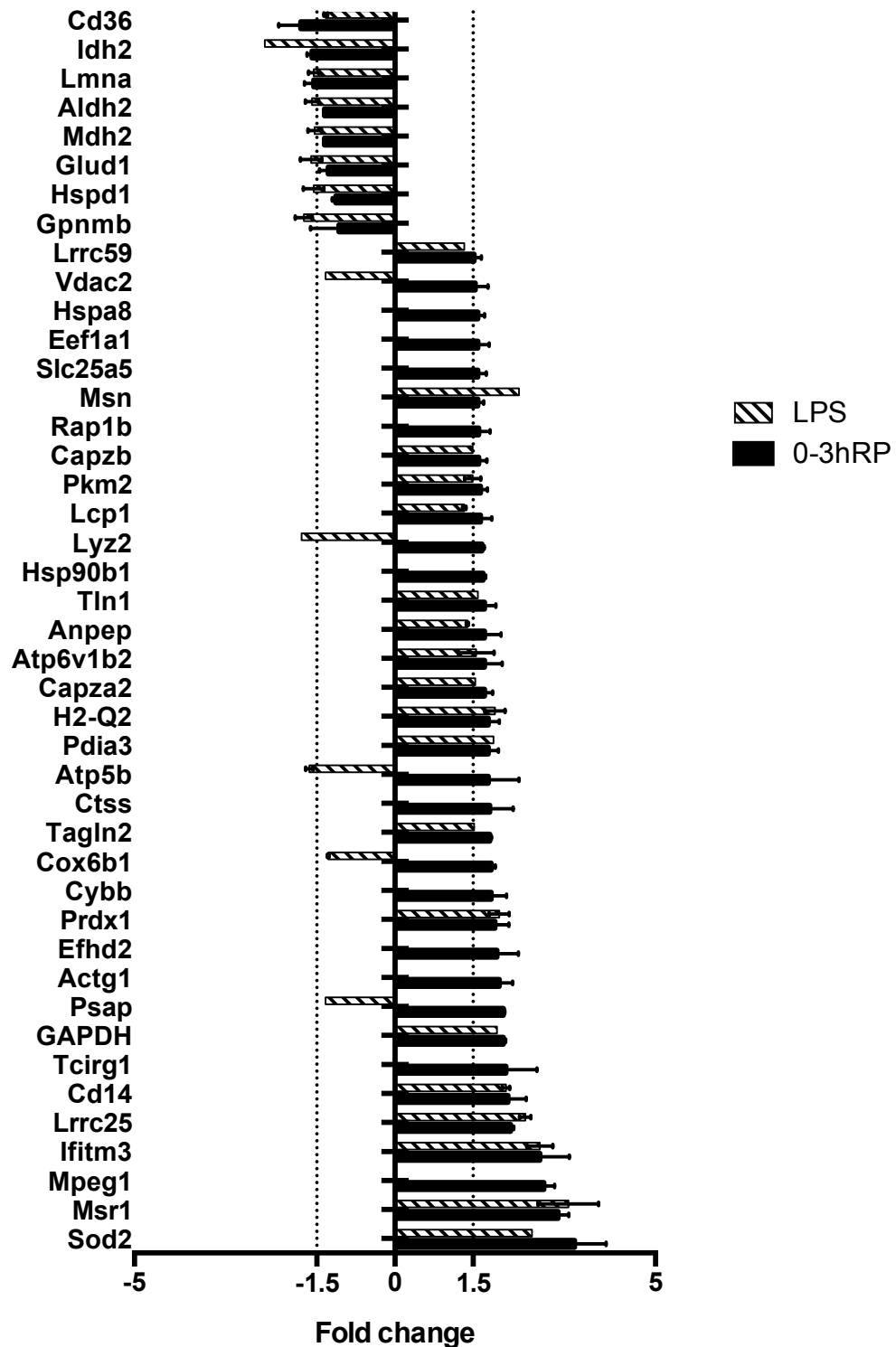


Figure 3.5 Comparison of regulated proteins in BMMφs stimulated with 0-3hRP or LPS

BMMφs were stimulated for 18 hours with 0-3hRP (50μg/ml), LPS (1ng/ml) or left un-stimulated. Cells were lysed, three independent samples from for treatment were pooled, and after membrane protein enrichment, the proteome quantified using a label-free approach. Results were filtered for significance ($p < 0.05$) and low variation ($CV\% < 30\%$) with at least 2 peptides used for quantitation (except when no error bar is given). Median fold changes calculated based on samples from un-stimulated BMMφs for each protein and SD are presented. Missing bars correspond to poor data quality.

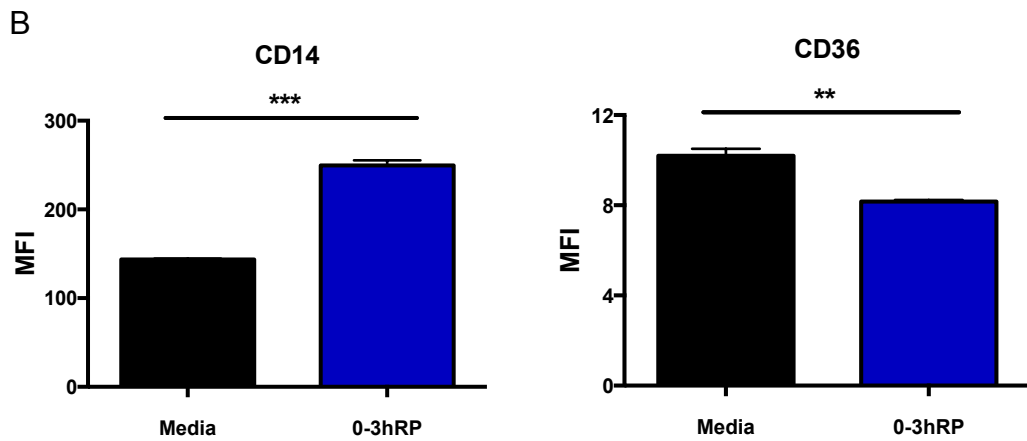
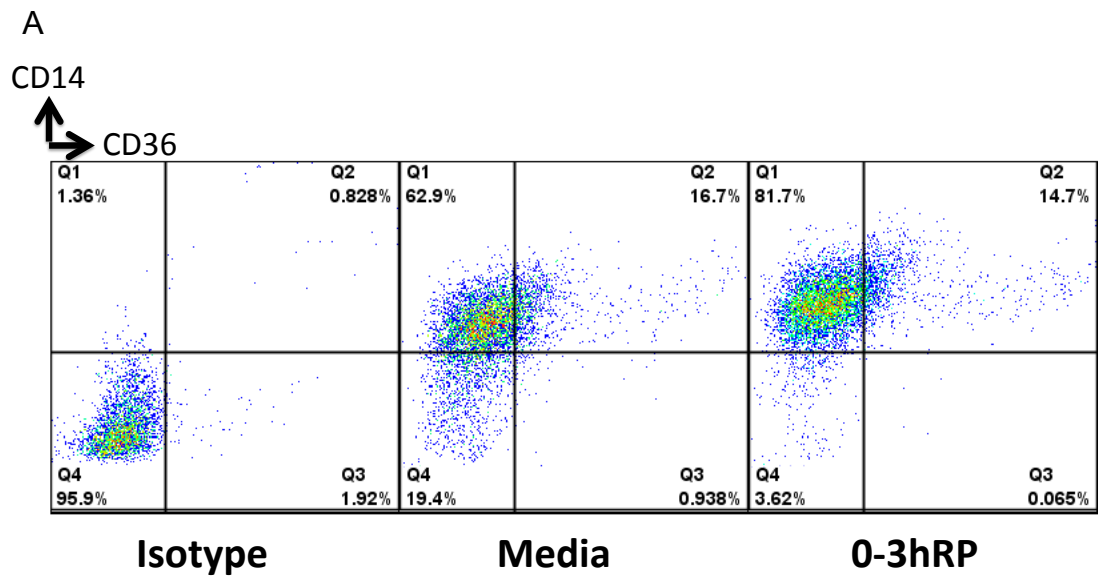


Figure 3.6 Expression of CD14, CD36, and MSR1 in BMMφs exposed to 0-3hRP (Continued in the next page)

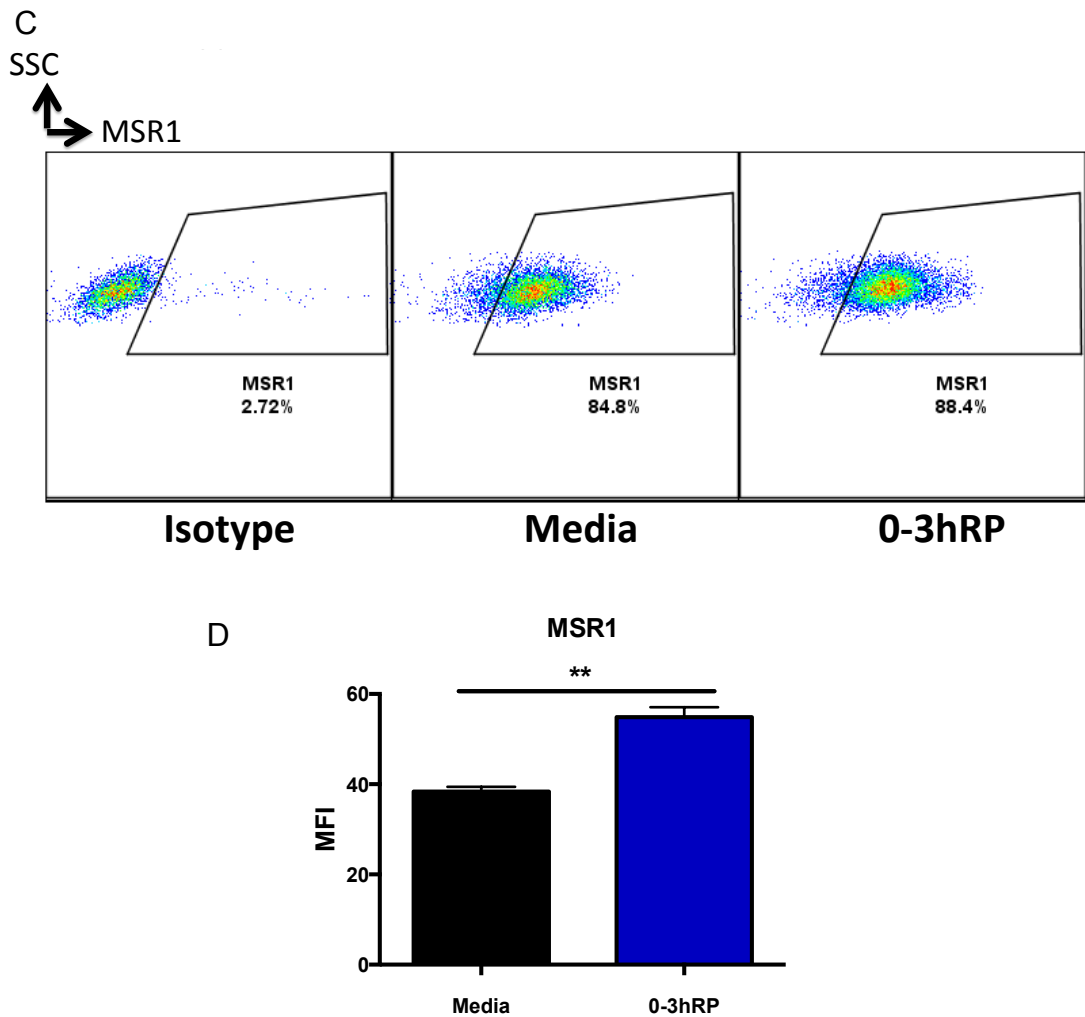


Figure 3.6 (continued) Expression of CD14, CD36, and MSR1 in BMMφs exposed to 0-3hRP

BMMφs were exposed for 18 hours to 0-3hRP (50μg/ml) or left un-stimulated (Media) and then labeled with antibodies for CD36, CD14 and MSR1. Representative flow plots for cells expressing CD14, CD36 and MSR1 (**A & C**), and bar charts depicting their mean MFI values (**B & D**). Means +SEM of three technical replicates for each protein are given. Unpaired two tailed t-tests were performed to examine differences between means of 0-3hRP and Media (** = $p < 0.01$; *** = $p < 0.001$). The result is representative of three independent experiments.

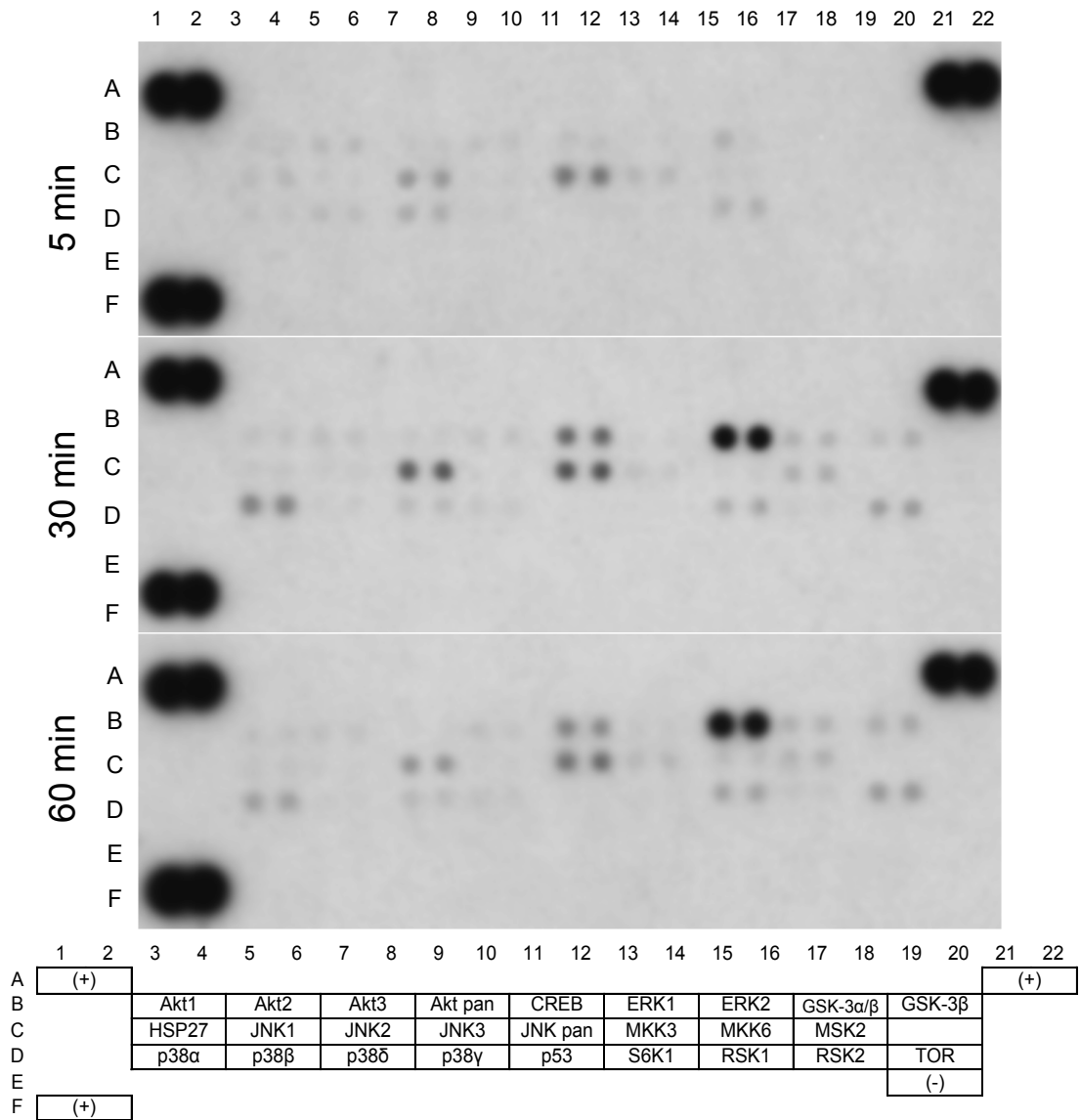


Figure 3.7 Kinase proteome profiler array of BMMφs exposed to 0-3hRP
 BMMφs were exposed to 0-3hRP (50μg/ml) for 5, 30 or 60 minutes before being lysed and MAPK phosphorylation measured using a kinase proteome profiler array (R&D). Membranes from each time point and the coordinates for the proteins are presented; each protein is in duplicate in the array. Positive controls for the assay are in the corners.

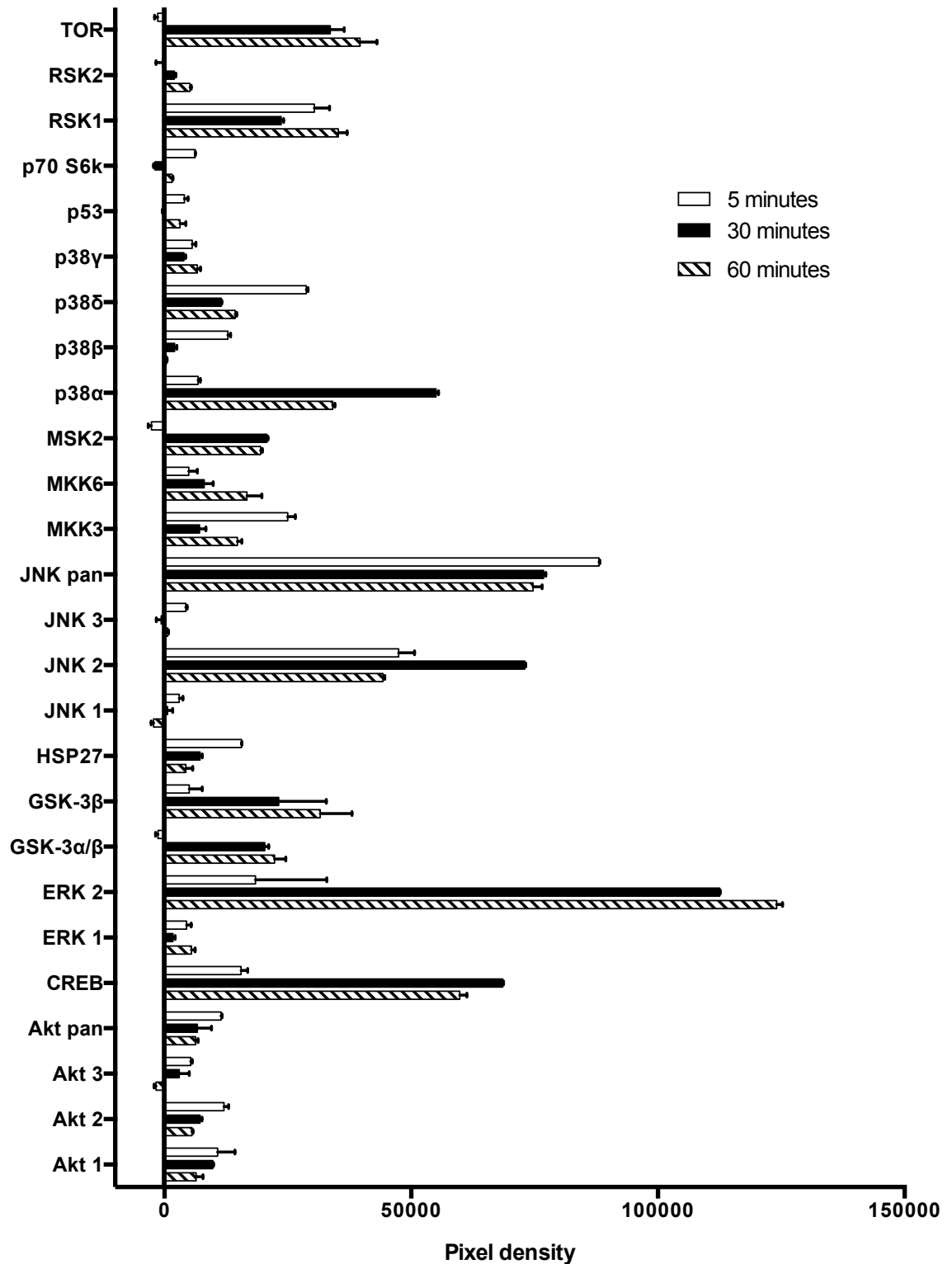


Figure 3.8 Densitometry analysis of kinase proteome profiler array

Densitometry analysis of MAPK phosphorylation measured using a kinase proteome profiler array. Positive controls in each membrane were used to normalize the results and a global background subtraction was performed. Means between technical replicates (duplicates) and SD are presented.

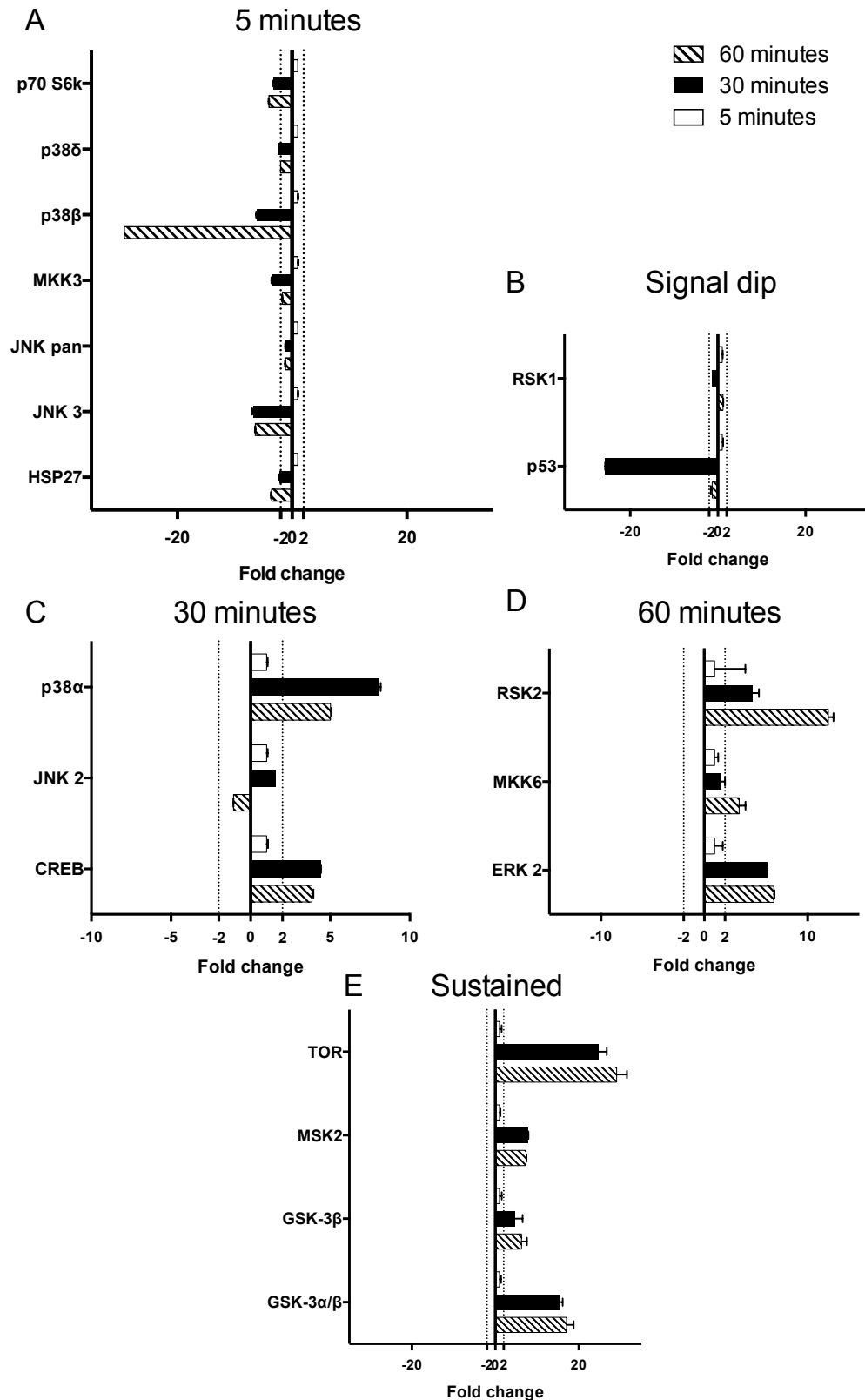


Figure 3.9 Fold changes in MAPK phosphorylation

Fold changes in phosphorylation of MAPKs were calculated using the 5-minute time point as a reference (arbitrarily set to one). Mean fold changes and SD are presented for each protein. Proteins with peak activation after 5min (A), 30min (C), 60min (D), a dip in activation (B) or sustained activation (E) are segregated to different graphs. Dotted lines correspond to a 2-fold change threshold.

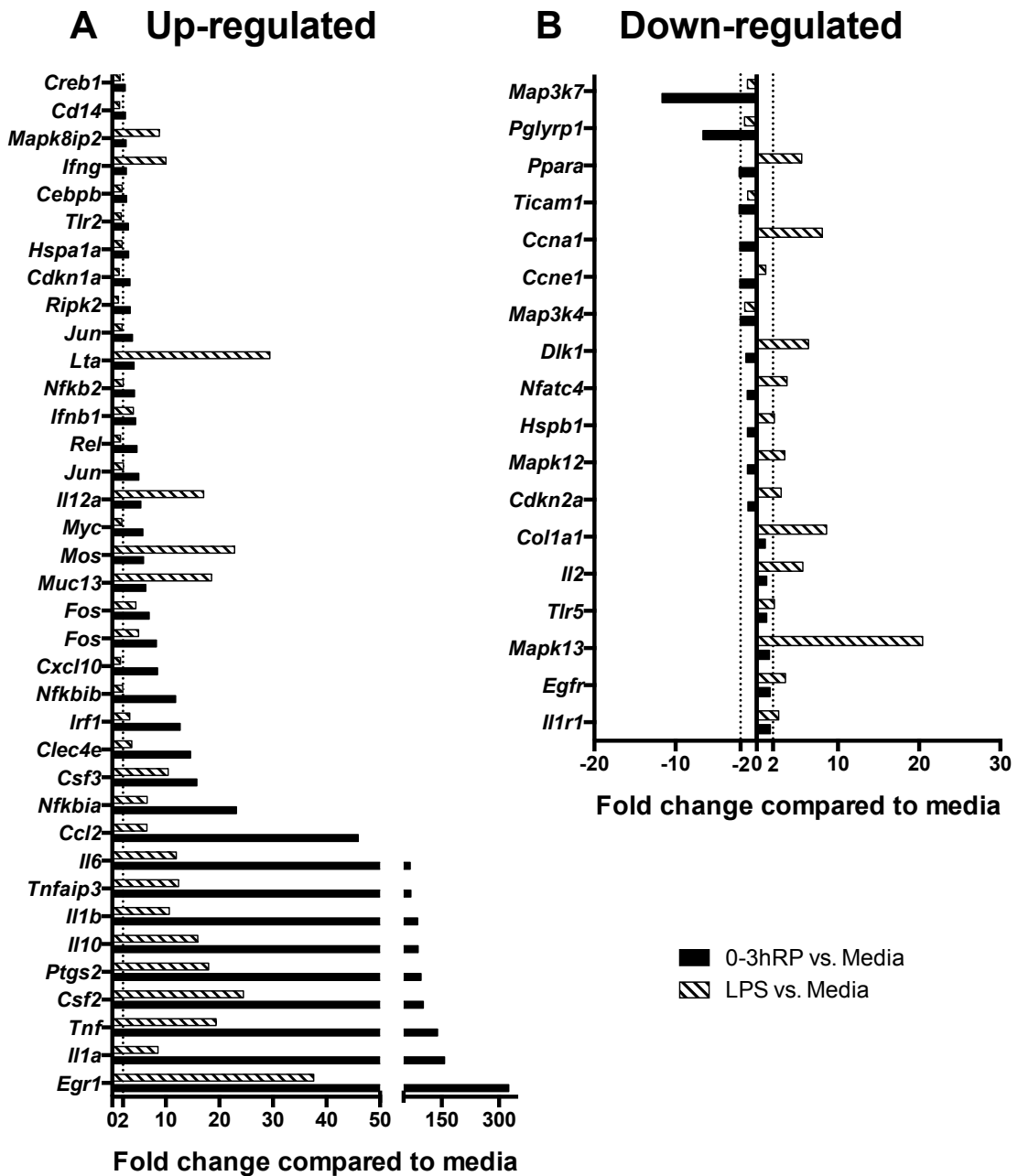


Figure 3.10 Regulated genes in treated BMMφs

Fold changes in the expression of genes related to MAPKs or TLRs were calculated on BMMφs after treatment for 30min with 0-3hRP (50µg/ml) or LPS (1ng/ml) using the un-stimulated BMMφs as a reference, and the average Ct value of 5 HKG (*Hprt*, *Gapdh*, *Gusb*, *Actb* and *Hsp90ab1*) to normalize. Fold changes for up-regulated transcripts (**A**) or down-regulated transcripts (**B**) according to 0-3hRP stimulation, are presented. Dotted line represents the 2 fold change threshold.

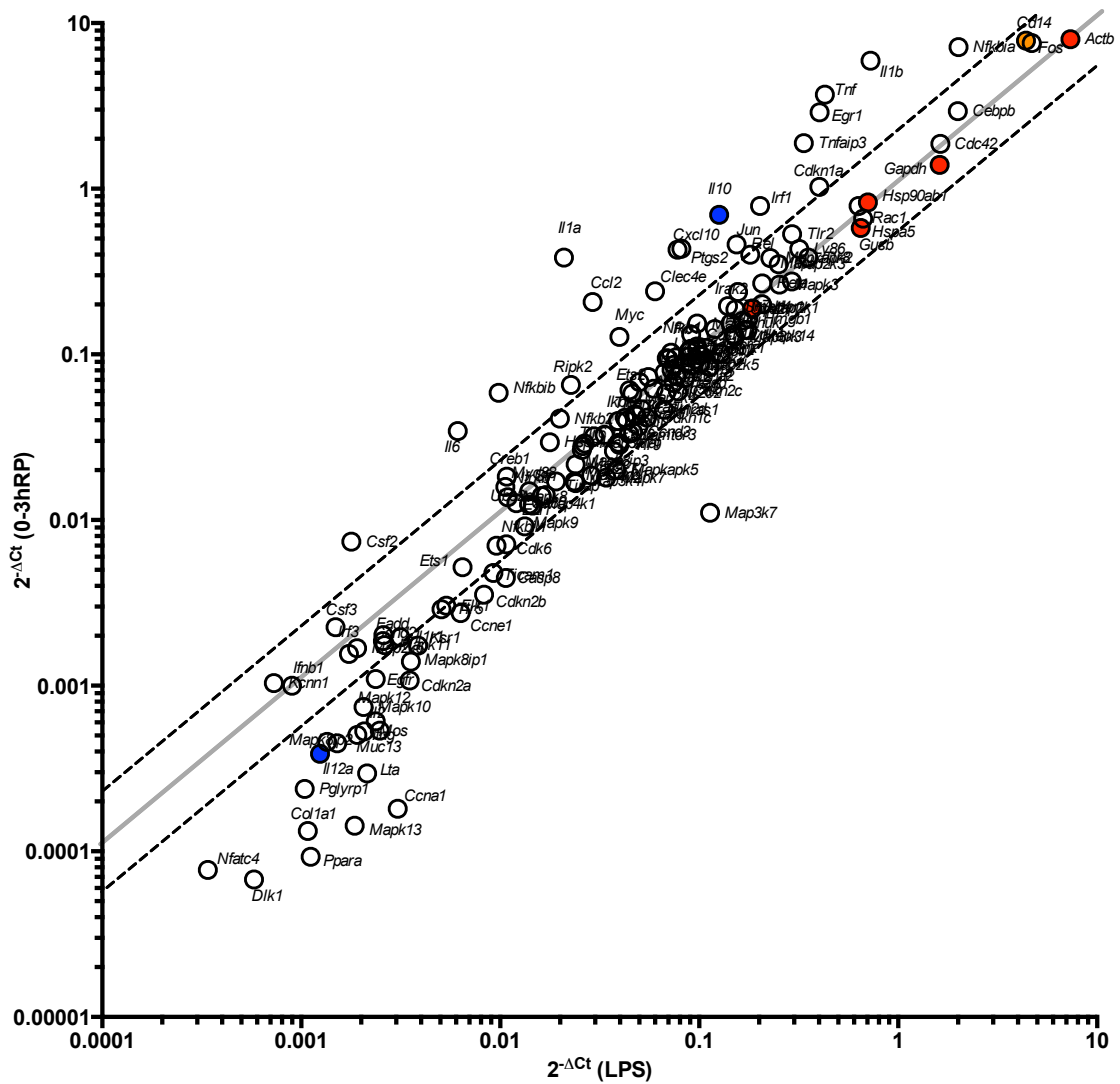


Figure 3.11 Gene expression differences in stimulated BMMφs

BMMφs were exposed for 30min to 0-3hRP (50μg/ml) or LPS (1ng/ml). RNA was extracted and used in a qPCR array to find changes in expression of 161 genes. Differences between Ct values for genes related to MAPKs or TLRs to Ct values for HKGs (*Hprt*, *GAPDH*, *Gusb*, *Actb* and *Hsp90ab1*; in red) were calculated ($2^{-\Delta C_t}$) for each treatment. $2^{-\Delta C_t}$ values for LPS and 0-3hRP are presented against each other for all genes. Transcripts within the dotted lines were not different between the two treatments.

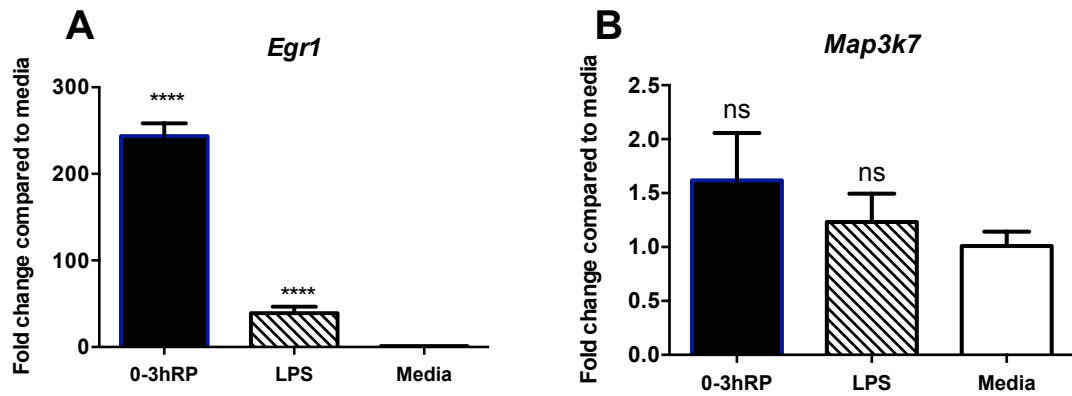


Figure 3.12 Validation of transcript levels in stimulated BMMφs

BMMφs were exposed for 30min to 0-3hRP (50μg/ml), LPS (1ng/ml) or left unstimulated (Media). RNA was extracted and transcript levels of *Egr1* (A) and *Map3k7* (B) calculated using the delta delta Ct method with Media as reference and *Gapdh* as a HKG. Mean fold changes +SEM are presented from three technical replicates. ANOVA and then Dunnett's multiple comparisons test were performed to examine differences between the means of stimulated cells compared to Media (**** = $p < 0.0001$; ns = $p > 0.05$). The result is representative of three independent experiments.

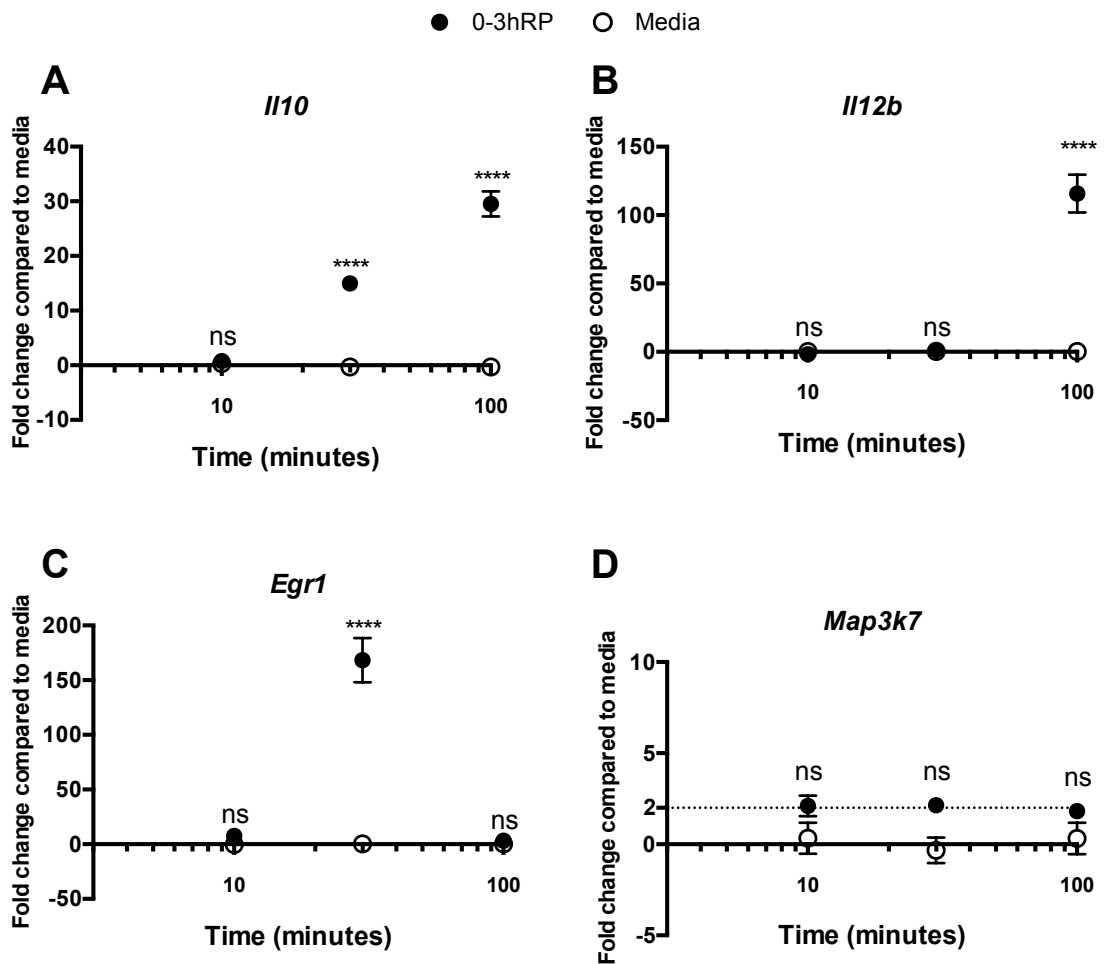


Figure 3.13 Time course of transcription of regulated genes in BMMφs treated with 0-3hRP

BMMφs were exposed for 10, 30 or 100min to 0-3hRP (50μg/ml) or left unstimulated (Media). RNA was extracted and transcript levels of *Il10* (A), *Il12b* (B), *Egr1* (C) and *Map3k7* (D) calculated using the delta delta Ct method with Media as reference and *Gapdh* as a HKG. Means ±SEM are presented from three technical replicates. ANOVA and then Sidak's multiple comparisons test were performed to examine differences between the means of 0-3hRP treated cells compared to Media at each time point (**** = $p < 0.0001$; ns = $p > 0.05$). The result is representative of three independent experiments.

Table 3.1 Cellular localization of protein hits (k) and percentages (out 404 hits)

Cellular localization		
GO term	%	k
GO:0016020: membrane	71.0	287
Plasma Membrane		
GO:0005886: plasma membrane	34.9	141
GO:0009986: cell surface	10.4	42
GO:0042995: cell projection	17.3	70
Endosomes		
GO:0000323: lytic vacuole	13.9	56
GO:0005764: lysosome	13.9	56
GO:0031988: membrane-bounded vesicle	49.3	199
GO:0005765: lysosomal membrane	7.2	29
Organelles		
GO:0005739: mitochondrion	35.6	144
GO:0005634: nucleus	25.0	101
GO:0005783: endoplasmic reticulum	15.1	61
GO:0005794: Golgi apparatus	9.4	38
GO:0005829: cytosol	12.9	52

Table 3.2 Regulated proteins in 0-3hRP stimulated BMMφs compared to Media

Accession	Protein	Peptides	Fold change	Number of Peptides used for quantitation	CV [%]
Up-regulated					
MGI:98352	Sod2 Superoxide dismutase [Mn]	3	3.45	2	17.49
MGI:98257	Msr1 macrophage scavenger receptor 1 isoform a	3	3.13	2	6.65
MGI:1333743	Mpeg1 macrophage expressed gene 1	3	2.86	2	7.06
MGI:1913391	Ifitm3 Interferon-inducible protein homolog	4	2.78	4	20.5
MGI:2445284	Lrrc25 Leucine-rich repeat-containing protein 25 precursor	2	2.22	2	2.85
MGI:88318	Cd14 Monocyte differentiation antigen CD14 precursor	9	2.17	4	16.18
MGI:1350931	Tcirg1 T-cell, immune regulator 1	11	2.13	2	28.01
MGI:3649467	Glyceraldehyde-3-phosphate dehydrogenase (GAPDH) isoform 1	2	2.08	2	2.08
MGI:97783	Psap Sulfated glycoprotein 1 precursor	9	2.08	2	1.34
MGI:87906	Actg1 Actin, cytoplasmic 2	2	2.00	2	12.85
MGI:106504	Efhd2 Swiprosin 1	11	1.96	4	20.95
MGI:99523	Prdx1 Peroxiredoxin-1	14	1.92	7	13.78
MGI:88574	Cybb Cytochrome b-245 heavy chain	5	1.85	2	15.67
MGI:107460	Cox6b1 Cytochrome c oxidase subunit VIb isoform 1	4	1.85	2	4.19
MGI:1312985	Tagln2 Transgelin-2	4	1.82	2	1.76
MGI:107341	Ctss cathepsin S	8	1.82	3	24.84
MGI:95834	Pdia3 Protein disulfide-isomerase A3 precursor	16	1.79	4	10.82
MGI:95896	H2-Q2; H2-L; H2-Q1; H-2D cell surface glycoprotein (Fragment)	7	1.79	3	12.02
MGI:106222	Capza2 F-actin-capping protein subunit alpha-2	10	1.72	4	9.03
MGI:109618	Atp6v1b2 Vacuolar ATP synthase subunit B	13	1.72	6	19.73
MGI:96749	Anpep Aminopeptidase N	18	1.72	4	18.49

MGI:1099832	Tln1 Talin-1	25	1.72	2	12.54
MGI:98817	Hsp90b1 Endoplasmic precursor	9	1.69	2	3.01
MGI:96897	Lyz2 Lysozyme C	6	1.67	2	2.52
MGI:104808	Lcp1 Plastin-2	26	1.64	8	13.46
MGI:97591	Pkm2 Isoform M2 of Pyruvate kinase isozymes M1/M2	10	1.64	2	8.14
MGI:104652	Capzb Isoform 2 of F-actin-capping protein subunit beta	10	1.61	3	9.52
MGI:894315	Rap1b Ras-related protein Rap-1b precursor	9	1.61	3	13.29
MGI:97167	Msn Moesin	26	1.59	5	7.17
MGI:3644836	Slc25a5 ADP/ATP translocase 2	19	1.59	3	10.36
MGI:3648808	Eef1a1 Elongation factor 1-alpha 1	7	1.59	2	13.57
MGI:105384	Hspa8 Heat shock cognate 71 kDa protein	14	1.59	3	8.28
MGI:106915	Vdac2 Voltage-dependent anion-selective channel protein 2	8	1.54	3	16.01
MGI:2138133	Lrrc59 Leucine-rich repeat-containing protein 59	5	1.52	2	9.11
Down-regulated					
MGI:96794	Lmna Isoform A of Lamin-A/C	34	-1.56	2	11.39
MGI:96414	Idh2 Isocitrate dehydrogenase [NADP], mitochondrial precursor	3	-1.59	2	5.96
MGI:107899	Cd36 Platelet glycoprotein 4	9	-1.81	3	23.17

Table 3.3 Regulated proteins in LPS stimulated BMMφs compared to Media

Accession	Protein	Peptides	Fold change	Number of Peptides used for quantitation	CV [%]
Up-regulated					
MGI:98257	Msr1 macrophage scavenger receptor 1 isoform a	3	3.33	2	17.42
MGI:1913391	Ifitm3 Interferon-inducible protein homolog	4	2.78	3	9.06
MGI:2445284	Lrrc25 Leucine-rich repeat-containing protein 25 precursor	2	2.50	2	4.38
MGI:88318	Cd14 Monocyte differentiation antigen CD14 precursor	9	2.13	2	3.38
MGI:99523	Prdx1 Peroxiredoxin-1	14	2.00	5	9.69
MGI:95896	H2-Q2; H2-L; H2-Q1; H-2D cell surface glycoprotein (Fragment)	7	1.92	3	10.08
MGI:109618	Atp6v1b2 Vacuolar ATP synthase subunit B	13	1.56	2	21.88
Down-regulated					
MGI:97050	Mdh2 Malate dehydrogenase	14	-1.54	3	8.55
MGI:3651246	Hspd1 Isoform 1 of 60 kDa heat shock protein	16	-1.57	3	12.72
MGI:96794	Lmna Isoform A of Lamin-A/C	34	-1.57	3	6.43
MGI:99600	Aldh2 Aldehyde dehydrogenase	20	-1.58	4	8.03
MGI:95753	Glud1 Glutamate dehydrogenase 1	12	-1.61	3	12.75
MGI:107801	Atp5b ATP synthase subunit beta	33	-1.65	2	4.38
MGI:1934765	Gpnmb Transmembrane glycoprotein NMB precursor	6	-1.76	2	9.34

Table 3.4 GO term enrichment analysis in terms of biological process

Biological process					
0-3hRP			LPS		
Up-regulated					
Term	% (27*)	k**	Term	% (7)	k
GO:0065007: biological regulation	70.4	19	GO:0065007: biological regulation	71.4	5
GO:0050896: response to stimulus	51.9	14	GO:0050896: response to stimulus	57.1	4
GO:0008152: metabolic process	48.1	13	GO:0002376: immune system process	57.1	4
GO:0044237: cellular metabolic process	44.4	12	GO:0006950: response to stress	42.9	3
GO:0071704: organic substance metabolic process	40.7	11	GO:0045087: innate immune response	42.9	3
GO:0006950: response to stress	40.7	11	GO:0008152: metabolic process	28.6	2
GO:0023051: regulation of signaling	25.9	7	GO:0002252: immune effector process	28.6	2
GO:0002376: immune system process	25.9	7	GO:0009605: response to external stimulus	28.6	2
GO:0045087: innate immune response	14.8	4			
GO:0009605: response to external stimulus	14.8	4			
GO:0043408: regulation of MAPK cascade	11.1	3			
GO:0002252: immune effector process	11.1	3			
Down-regulated					
Term	% (3)	k	Term	% (6)	k
GO:0050896: response to stimulus	100	3	GO:0008152: metabolic process	66.7	4
GO:0006950: response to stress	100	3	GO:0071704: organic substance metabolic process	50	3
GO:0023052: signaling	66.7	2	GO:0044237: cellular metabolic process	50	3
GO:0007165: signal transduction	66.7	2	GO:0050896: response to stimulus	33.3	2
			GO:0023051: regulation of signaling	33.3	2

* Number in parenthesis represents total number of hits based on which percentages are calculated.

** k is the number of hits that associate to a category.

Table 3.5 Cellular localization GO term enrichment analysis

Cellular localization					
0-3hRP			LPS		
Up-regulated					
Term	% (30*)	k**	Term	% (7)	k
GO:0016020: membrane	76.7	23	GO:0005575: cellular_component	100	7
GO:0031982: vesicle	66.7	20	GO:0016020: membrane	85.7	6
GO:0005886: plasma membrane	43.3	13	GO:0031982: vesicle	85.7	6
GO:0005739: mitochondrion	30.0	9	GO:0005886: plasma membrane	71.4	5
GO:0042995: cell projection	30.0	9	GO:0005829: cytosol	42.9	3
GO:0005829: cytosol	20.0	6	GO:0009986: cell surface	42.9	3
GO:0009986: cell surface	20.0	6	GO:0005634: nucleus	28.6	2
GO:0005783: endoplasmic reticulum	20.0	6	GO:0005764: lysosome	28.6	2
GO:0005634: nucleus	16.7	5			
GO:0005764: lysosome	16.7	5			
GO:0005794: Golgi apparatus	6.7	2			
Down-regulated					
Term	% (3)	k	Term	% (6)	k
GO:0016020: membrane	66.7	2	GO:0016020: membrane	66.7	4
GO:0005739: mitochondrion	66.7	2	GO:0005739: mitochondrion	66.7	4
			GO:0031982: vesicle	66.7	4
			GO:0005886: plasma membrane	50.0	3

* Number in parenthesis represents total number of hits based on which percentages are calculated.

** k is the number of hits that associate to a category.

Table 3.6 qPCR array genes

Genes				
<i>Actb</i>	<i>Col1a1</i>	<i>Il1b</i>	<i>Mapk11</i>	<i>Pglyrp1</i>
<i>Agfg1</i>	<i>Creb1</i>	<i>Il1r1</i>	<i>Mapk12</i>	<i>Ppara</i>
<i>Araf</i>	<i>Crebbp</i>	<i>Il2</i>	<i>Mapk13</i>	<i>Ptgs2</i>
<i>Atf2</i>	<i>Csf2</i>	<i>Il6</i>	<i>Mapk14</i>	<i>Rac1</i>
<i>Btk</i>	<i>Csf3</i>	<i>Il6ra</i>	<i>Mapk3</i>	<i>Raf1</i>
<i>Casp8</i>	<i>Cxcl10</i>	<i>Irak1</i>	<i>Mapk6</i>	<i>Rb1</i>
<i>Ccl2</i>	<i>Dlk1</i>	<i>Irak2</i>	<i>Mapk7</i>	<i>Rel</i>
<i>Ccna1</i>	<i>E2f1</i>	<i>Irf1</i>	<i>Mapk8</i>	<i>Rela</i>
<i>Ccna2</i>	<i>Egfr</i>	<i>Irf3</i>	<i>Mapk8ip1</i>	<i>Ripk2</i>
<i>Ccnb1</i>	<i>Egr1</i>	<i>Jun</i>	<i>Mapk8ip2</i>	<i>Sfn</i>
<i>Ccnb2</i>	<i>Eif2ak2</i>	<i>Kcnn1</i>	<i>Mapk8ip3</i>	<i>Smad4</i>
<i>Ccnd1</i>	<i>Elk1</i>	<i>Kras</i>	<i>Mapk9</i>	<i>Tbk1</i>
<i>Ccnd2</i>	<i>Ets1</i>	<i>Ksr1</i>	<i>Mapkapk2</i>	<i>Ticam1</i>
<i>Ccnd3</i>	<i>Ets2</i>	<i>Lamtor3</i>	<i>Mapkapk5</i>	<i>Ticam2</i>
<i>Ccne1</i>	<i>Fadd</i>	<i>Lta</i>	<i>Max</i>	<i>Tirap</i>
<i>Cd14</i>	<i>Fos</i>	<i>Ly86</i>	<i>Mef2c</i>	<i>Tlr1</i>
<i>Cd80</i>	<i>Gapdh</i>	<i>Ly96</i>	<i>Mknk1</i>	<i>Tlr2</i>
<i>Cd86</i>	<i>Grb2</i>	<i>Map2k1</i>	<i>Mos</i>	<i>Tlr3</i>
<i>Cdc42</i>	<i>Gusb</i>	<i>Map2k2</i>	<i>Muc13</i>	<i>Tlr4</i>
<i>Cdk2</i>	<i>Hmgb1</i>	<i>Map2k3</i>	<i>Myc</i>	<i>Tlr5</i>
<i>Cdk4</i>	<i>Hprt</i>	<i>Map2k4</i>	<i>Myd88</i>	<i>Tlr6</i>
<i>Cdk6</i>	<i>Hras1</i>	<i>Map2k5</i>	<i>Nfatc4</i>	<i>Tlr7</i>
<i>Cdkn1a</i>	<i>Hsp90ab1</i>	<i>Map2k6</i>	<i>Nfkb1</i>	<i>Tlr8</i>
<i>Cdkn1b</i>	<i>Hspa1a</i>	<i>Map2k7</i>	<i>Nfkb2</i>	<i>Tlr9</i>
<i>Cdkn1c</i>	<i>Hspa5</i>	<i>Map3k1</i>	<i>Nfkbia</i>	<i>Tnf</i>
<i>Cdkn2a</i>	<i>Hspb1</i>	<i>Map3k2</i>	<i>Nfkbib</i>	<i>Tnfaip3</i>
<i>Cdkn2b</i>	<i>Ifnb1</i>	<i>Map3k3</i>	<i>Nfkbil1</i>	<i>Tnfrsf1a</i>
<i>Cdkn2c</i>	<i>Ifng</i>	<i>Map3k4</i>	<i>Nfrkb</i>	<i>Tollip</i>
<i>Cdkn2d</i>	<i>Ikbkb</i>	<i>Map3k7</i>	<i>Nr2c2</i>	<i>Tradd</i>
<i>Cebpb</i>	<i>Il10</i>	<i>Map4k1</i>	<i>Nras</i>	<i>Traf6</i>
<i>Chuk</i>	<i>Il12a</i>	<i>Mapk1</i>	<i>Pak1</i>	<i>Trp53</i>
<i>Clec4e</i>	<i>Il1a</i>	<i>Mapk10</i>	<i>Peli1</i>	<i>Ube2n</i>
				<i>Ube2v1</i>

4 Signaling pathways in BMMφs exposed to cercarial E/S products

4.1 Introduction

TLRs can be localized on the cell surface (e.g. TLR2 and TLR4) or in endosomes (e.g. TLR3, 7, 9, 10 & 11) and can form homodimers (e.g. TLR4) or heterodimers with more than one TLR (e.g. TLR2/1 or TLR2/6) (Akira & Takeda, 2004; Kagan & Iwasaki, 2012) when binding to specific ligands. Upon dimerisation several adaptor proteins can be recruited to the intracellular domains of TLRs to activate multiple signaling pathways (Bonham et al, 2014). Most TLRs utilize MyD88 as their main adaptor molecule, however TLR4 and TLR3 can also use TRIF (Adachi et al, 1998; Bonham et al, 2014; Donnelly et al, 2010; Kagan & Iwasaki, 2012; Laird et al, 2009; Liu et al, 2012; Muzio et al, 1997; Shi et al, 2011; Warner & Nunez, 2013; Wesche et al, 1997). Typically, a cascade of kinases is triggered upon TLR-ligand binding, particularly MAP3K7, which phosphorylates IKKβ leading to the activation of the NF-κB system, which is made out of several different proteins (such as p65, p105 and its degradation product p50). These subunits form homodimers or heterodimers upon release from the NF-κB complex and direct transcription of pro-inflammatory cytokines (such as IL-12, IL-6 and IL-1), chemokines, as well as other transcription factors (Adachi et al, 1998; Hinz & Scheidereit, 2014; Hoesel & Schmid, 2013; Iwasaki et al, 2011; Muzio et al, 1997; Oeckinghaus et al, 2011; Ruland, 2011; van Berlo et al, 2010; Warner & Nunez, 2013; Wesche et al, 1997; Yu et al, 2011).

The kinase cascades triggered by TLR binding will lead to the activation of several MAPKs. This family of proteins is involved in a broad range of immune processes, as well as in growth and development (Arthur & Ley, 2013; Bandyopadhyay et al, 2010; Deak et al, 1998; Farhan et al, 2010; Gehart et al, 2010). Multiple MAPKs have more than one isoform, and it is often difficult to study the role, if any, of each one (Beardmore et al, 2005; Braem et al, 2011; Deak et al, 1998). Crosstalk between different axes of the MAPK family has often been reported, increasing the complexity and diversity of the system. MAPKs can be directly activated downstream of TLRs by MAP3K7 (which phosphorylates the kinases upstream of p38 and JNK) or by the NF-κB system. Phosphorylated p105 is degraded, releasing Tumor progression locus 2 (Tpl2)

or MAP3K8 to phosphorylate MEK1/2, which then phosphorylates Erk1/2 (Arthur & Ley, 2013; Braem et al, 2011; Elcombe et al, 2013; Laird et al, 2009; Lawrenz et al, 2012; Mayer et al, 2013; Medina et al, 2010; Pinto et al, 2011; Rommel et al, 1999; Salmeron et al, 1996; Yan et al, 2010; Yang et al, 2010). MAPKs regulate transcription through the phosphorylation of several transcription factors, such as CREB, AP-1 and c-Jun (Elcombe et al, 2013; MacKenzie et al, 2013; Mayer et al, 2013; Strippoli et al, 2012; van Vliet et al, 2013; Wen et al, 2010).

The TLR system, leading to the activation of the signals described above, has been traditionally linked with pro-inflammatory mediators and antimicrobial activity. Consequently, the production of anti-inflammatory cytokines by macrophages, such as IL-10, which confers these cells a regulatory function, is poorly understood. Indeed, few studies deal with the initiators and sources of IL-10, compared to IL-10 targets (Ambarus et al, 2012; Ananieva et al, 2008; Antoniv & Ivashkiv, 2011; Elcombe et al, 2013; Kamanaka et al, 2006; Kuhn et al, 1993; MacKenzie et al, 2013; Sabat et al, 2010; Saraiva & O'Garra, 2010; Wilson et al, 2011). Nonetheless, the transcription of IL-10 in macrophages has been shown to require CREB, c-MAF, NF- κ B p50 homodimers and C/EBP β (see 1.5), and some studies have found that the promoter region of the IL-10 gene undergoes significant chromatin remodeling, particularly by phosphorylation of histones (Lucas et al, 2005; Saraiva et al, 2005; Zhang et al, 2006).

The technique of choice to study changes in chromatin and recruitment of transcription factors is chromatin immunoprecipitation (ChIP) (Whitfield et al, 2012; Yip et al, 2012). Covalently linked chromatin is fractionated by sonication into small fragments that can be isolated using antibodies for a specific target, typically histone marks or a transcription factor. Precipitated fragments can then be sequenced or analyzed using PCR to map regions of the genome with which the target was interacting in the cells (Consortium et al, 2007). In this manner, antibodies against transcription factors can be used to demonstrate the role of these molecules in the initiation of the transcription of a gene, such as IL-10.

The association between helminth products and TLRs is not unheard of (Correale & Farez, 2009; Donnelly et al, 2010; Everts et al, 2010; Goodridge et al, 2001; Kane et al, 2004; Puneet et al, 2011; van Riet et al, 2009).

Schistosoma larval and egg antigens have been shown to interact with TLRs in mononuclear phagocytes (Brännström et al, 2009; Burton et al, 2010; Correale & Farez, 2009; Gao et al, 2012; Holmfeldt et al, 2007; Jenkins et al, 2005; Joshi et al, 2008; Meevissen et al, 2011; Retra et al, 2008; Zhang et al, 2011). Only a small fraction of those studies have sought to describe the signaling pathways triggered in the cells, or indeed link them to the production of specific cytokines (Gao et al, 2012; Meevissen et al, 2011; van Liempt et al, 2007).

In the previous chapter, a holistic view of changes that occur in BMMφs exposed to 0-3hRP was presented. A strong modulation of several genes associated with TLR signaling and MAPKs was discovered, both at the mRNA and protein level, as well as a distinct activation state, which is triggered in these cells. IL-10 mRNA was rapidly produced after exposure to cercarial E/S products and its production matched the activation of a subset of MAPKs (p38α, Erk2, RSK2, CREB) that peaked in activity 30min after stimulation with the antigen preparation.

In the following chapter, the links between TLRs and the responses to 0-3hRP observed in BMMφs will be investigated with particular attention placed on the production of IL-10. Ultimately, I will present a mechanism by which BMMφs activate different signaling pathways leading to the production of IL-10.

4.2 Chapter specific material and methods

4.2.1 MAPKs inhibitors

MEK1/2 inhibitor U0126 and p38 inhibitor SB203580 were purchased from Cell Signalling Technology®. JNK inhibitor II was purchased from Calbiochem®.

4.2.2 Chromatin Immunoprecipitation

This protocol was adapted from the instruction manual of the Chromatin Immunoprecipitation Assay kit® (Merck Millipore). BMMφs were generated as described in 2.3 and exposed to 50µg/ml of 0-3hRP with 2µg/ml of PMB for 30min in 6 well plates. BMMφs were washed twice with PBS, removed by scraping and then fixed in suspension with 1% formaldehyde in PBS for 10min at room temperature at a concentration of 1×10^6 cells/ml. Fixation was stopped with 125mM Glycine (from kit). Aliquots of 5×10^6 cells were used per immunoprecipitation (IP). Cells were lysed for 10min on ice in 600µl lysis buffer containing 50mM Tris-HCl pH 8.1, 10mM EDTA and 1% SDS, supplemented with Protease Inhibitor Cocktail® (SIGMA-ALDRICH) and Phosphatase Inhibitor Cocktail Set II® (Calbiochem).

A volume of 900µl dilution buffer containing 20mM Tris-HCl, 150mM NaCl pH 8.1, 1% Triton X-100 and 1mM EDTA was added to give a final volume of 1.5ml. Cells were sonicated on ice using a Bioruptor plus® (Diagenode). The Bioruptor's tank was cooled to 4°C before starting the first round of sonication and it was kept cold by replacing ice every 10min. Samples were sonicated for 45min with the settings as 30s ON and 30s OFF at HIGH setting.

Sonicated cellular lysate was centrifuged at 15000g for 10min at 4°C. Supernatants were transferred to a clean tube and an aliquot was saved as the input control. Supernatants were pre-cleared with 30µl of Protein A Agarose/Salmon sperm DNA (50% slurry) for 30min at 4 °C with agitation. Agarose was removed by brief centrifugation (500g 4°C 1min) and supernatants were incubated with the following antibodies:

Target	Clone	Dilution	Source
P-CREB	87G3	1:50	Cell Signaling Technology
CREB	48H2	1:50	Cell Signaling Technology
RNA Pol II	CTD4H8	1:1500	Merck Millipore
CD36	JC63.1	1:1500	Cayman
No antibody	-	-	-

After overnight incubation (with gentle agitation at 4°C), 30µl of Protein A Agarose/Salmon sperm DNA (50% slurry) were added to the supernatant-antibody mixture and incubated for 1 hour at 4°C with gentle agitation. The agarose pellet with bound DNA was recovered by gentle centrifugation (500g 4°C 1min) and supernatants discarded. Pellets were washed with 1ml of low salt buffer from the kit for 5min at 4°C with agitation and the agarose pellets were recovered by gentle centrifugation (500g 4°C 1min). The same process was repeated for the high-salt buffer, then the LiCl buffer, and finally twice with the TE buffer, all provided by the manufacturer.

DNA was recovered by resuspending the agarose pellet in an Elution Buffer containing 20mM Tris-HCl, pH 7.5, 5mM EDTA, 50mM NaCl, 1% SDS and 50µg/ml proteinase K (Promega). Resuspended pellets were incubated for 2 hours at 68°C with vigorous shaking. Agarose was removed by gentle centrifugation (500g 4°C 1min), and supernatants transferred to a clean tube. DNA was extracted from supernatants (ChIP DNA) or input controls using a phenol-chloroform extraction protocol. Extracted DNA was dissolved in 50µl of PCR grade water and used for PCR.

4.2.2.1 *PCR of precipitated DNA*

ChIP DNA or input controls were tested for the presence of several regions of the IL-10 promoter using conventional PCR (for primer sequences see Table 2.2). Briefly, reactions were carried out in 25µL containing 1X PCR buffer (Invitrogen), 4mM MgCl₂ (Invitrogen), 0.2mM dNTPs (Fermentas), 0.5U Taq Polymerase (Invitrogen), 1µM of each Primer and 5µL of DNA.

Thermal cycler was set for an initial step of 95°C for 3min, followed by 35 cycles of 95°C for 30s, 60°C for 1min and 72°C for 1min. After a final elongation step of 72°C for 3min, samples were analyzed on a 2% agarose gel. Gel was revealed using SYBR® Safe (Life technologies) and densitometry analysis was performed using a GelDoc® and ImageLab® by Biorad.

4.3 Results

4.3.1 Dynamics of cytokine production in BMM ϕ s exposed to 0-3hRP

As seen in chapter III, BMM ϕ s exposed to 0-3hRP tightly regulate the production of *Il10* and *Il12b* mRNA levels. The dynamics of the transcription of those two genes were shown in 3.3.5.2, however secretion of protein has not been explored over a similar time course. To that end, BMM ϕ s were stimulated with 0-3hRP (50 μ g/ml) for different periods of time and culture supernatants analyzed by specific ELISAs (2.5) for these two cytokines.

As with mRNA, IL-10 protein production first appeared at an earlier time point than IL-12p40 (Figure 4.1). IL-10 was initially detected after 100min of stimulation (Figure 4.1A), and continued to increase until 1000min (18h), although the rate of increase declined after 300min. On the other hand, IL-12p40 was only detected in the culture supernatant after 300min (Figure 4.1B) and continued to increase. Unlike IL-10, which eventually started to decrease, IL-12p40 protein production continued to increase until the last time point measured (1000min).

As discussed previously, rapid IL-10 production matches the activation of the kinases seen in 3.3.4 whilst the production of IL-12p40 is comparatively delayed.

4.3.2 BMM ϕ s require TLRs to produce cytokines in response to 0-3hRP

Previous studies have shown that MyD88, an adaptor protein used by several TLRs for signal transduction, is essential for the production of IL-6 and IL-12p40 by peritoneal macrophages in response to 0-3hRP (Jenkins et al, 2005). TLR4 was only partially required, the role of TLR2 was not investigated and no indication was given of the effect of MyD88 or TLR4 on the production of IL-10 (Jenkins et al, 2005).

4.3.2.1 BMM ϕ s from MyD88, TLR4 or TLR2 deficient mice are phenotypically comparable to WT BMM ϕ s, but respond differentially to innate immune ligands/stimuli.

BMM ϕ s from WT or mice deficient for MyD88, TLR4 or TLR2 were made as described in 2.3. After 7 days in culture, cells were labeled with antibodies against F4/80, CD11b and a cell viability discrimination dye (see 2.4). BMM ϕ s

obtained from all strains of mice were positive for F4/80 and CD11b; representative flow plots of 5 independent experiments are shown in Figure 4.2, gated on live single cells.

BMM ϕ s from all strains exposed overnight to 1ng/ml of LPS, a TLR4 ligand, 5 μ g/ml of Pam₃CSK₄, a TLR2 ligand, or left un-stimulated (Media) were tested for their ability to secrete IL-12p40 overnight into the culture supernatant (see 2.5). MyD88^{-/-} BMM ϕ s did not produce IL-12p40 in response to LPS or Pam₃CSK₄ (Figure 4.3). TLR4^{-/-} BMM ϕ s also did not produce IL-12p40 in response to LPS, although they produced equivalent levels of this cytokine as WT BMM ϕ s when exposed to Pam₃CSK₄. On the other hand, TLR2^{-/-} BMM ϕ s produced as much IL-12p40 in response to LPS as WT BMM ϕ s, whilst these cells did not respond to Pam₃CSK₄. Levels of IL-10 in response to both stimuli in all four mouse-strains were below (or just above) the detection limit of the assay (data not shown). Combined, these results indicate that phenotypically comparable BMM ϕ s obtained from MyD88, TLR4 and TLR2 deficient mice were not prevented from responding to TLR ligands specific to receptors other than the one they lacked. Consequently, BMM ϕ s from these strains were used to assess the roles of TLR4 and TLR2, and their associated signaling pathways, in response to stimulation with 0-3hRP.

4.3.2.2 *MyD88, TLR4 and TLR2 are required for IL-10 and IL-12p40 production in BMM ϕ s exposed to 0-3hRP*

BMM ϕ s from WT plus MyD88, TLR4 and TLR2 deficient mice were exposed overnight to 0-3hRP (50 μ g/ml), or left un-stimulated (Media) and the culture supernatants tested for the presence of IL-10 and IL-12p40 by ELISA (2.5).

MyD88^{-/-} BMM ϕ s did not produce IL-10 in response to 0-3hRP (Figure 4.4). These cells also did not produce IL-12p40, which demonstrates that MyD88 is essential for the production of these particular cytokines in response to 0-3hRP. In contrast, TLR4^{-/-} BMM ϕ s exhibited only partially impaired production of both IL-10 and IL-12p40 when compared with WT cells. Similarly, TLR2^{-/-} BMM ϕ s had impaired production of both cytokines, particularly IL-10, which was as low as Media in 2 of the experiments performed.

4.3.3 Dynamics of BMM ϕ activation of several signaling molecules in response to 0-3hRP

The findings described in chapter III highlighted the tight temporal regulation of the production of *I110* and *I12b* transcripts, as well as the activation of several MAPKs by phosphorylation. To validate the results obtained with the Proteome profiler (3.3.4), a flow cytometric approach was taken for different MAPKs that were activated in response to 0-3hRP (2.4.2).

4.3.3.1 Levels of phosphorylated Erk1/2 but not total Erk1/2 change in BMM ϕ s exposed to 0-3hRP

BMM ϕ s exposed to 0-3hRP or left un-stimulated for 0, 10, 30 or 100min were labeled with antibodies against phosphorylated Erk1/2 (P-Erk), or total Erk1/2 (tErk) and analyzed using flow cytometry. Single cells were selected based on size and granularity. Shifts in the MFI of the entire population (presented as histograms) are indicative of phosphorylation of studied proteins.

Levels of tErk remained constant across treatments and time points (Figure 4.5A), with no significant differences in the MFI of the population (Figure 4.5B). Levels of P-Erk changed dramatically in 0-3hRP stimulated macrophages after 30min of exposure, and remained significantly elevated after 100min (Figure 4.6A & B). The increased activation of Erk1/2 matches the dynamic of phosphorylation found in 3.3.4, validating those results.

4.3.3.2 Levels of phosphorylated p38, CREB and RSK are increased in BMM ϕ s stimulated with 0-3hRP

Having validated the activation of Erk1/2 in 3.3.4, the same was performed for other identified MAPKs and so BMM ϕ s stimulated with 0-3hRP, were labeled with antibodies against phosphorylated p38 (P-p38), CREB (P-CREB), RSK (P-RSK) and Akt (P-Akt) and analyzed as above using flow cytometry.

p38 and CREB were highly phosphorylated in BMM ϕ s exposed to 0-3hRP compared to Media. Both MAPKs were active after 10min, peaked by 30min and then decreased after 100min (but remained significantly higher than Media) (Figure 4.7 & Figure 4.8A, B). The phosphorylation of RSK was modest (Figure 4.7), but its dynamic matches that of other measured kinases (Figure 4.8C). BMM ϕ s exposed to 0-3hRP only had significantly higher levels of P-RSK after 30min, and then dropped below Media levels after 100min. Phosphorylation of

Akt was slight and did not follow a dynamic like the others proteins tested (Figure 4.7 & Figure 4.8D), confirming earlier results determined by Proteome profiler (3.3.4). Combined these data reveal that Erk1/2, p38, CREB and RSK1/2, but not Akt, have similar patterns of dynamic regulation in BMMφs shortly after exposure to 0-3hRP, hinting at a common signaling pathway.

4.3.3.3 *BMMφs require MyD88, TLR4 and TLR2 to phosphorylate MAPKs in response to 0-3hRP*

BMMφs from WT plus MyD88, TLR4 and TLR2 deficient mice were exposed for 30min to 0-3hRP were labeled with antibodies against phosphorylated Erk1/2, p38 and CREB for analysis with flow cytometry.

Levels of P-Erk in MyD88^{-/-} BMMφs stimulated with 0-3hRP were no different from Media, and were significantly lower than WT BMMφs stimulated with 0-3hRP (Figure 4.9A & B). Similarly, TLR4 deficient and TLR2 deficient BMMφs had significantly lower levels of P-Erk compared to WT BMMφs (p<0.01-0.001). Levels of total Erk1/2, or other proteins measured in the present study, have not been reported to differ between TLR or MyD88 deficient strains compared to WT. tErk was compared between WT, TLR4 and MyD88 deficient mice on one occasion in the course of this work and no differences were detected (data not shown). Levels of both P-p38 (Figure 4.10) and P-CREB (Figure 4.11) were not increased in MyD88^{-/-} BMMφs in response to 0-3hRP, whilst in TLR4^{-/-} and TLR2^{-/-} BMMφs both proteins were greatly impaired compared to WT cells. Thus, BMMφs phosphorylate Erk1/2, p38 and CREB in response to 0-3hPR with the peak of activation at 30min, by using TLR2 and TLR4, in a MyD88 dependent manner.

4.3.4 **Hierarchy of signaling pathways in BMMφs exposed to 0-3hRP**

4.3.4.1 *Phosphorylation of Erk1/2 in BMMφs exposed to 0-3hRP depends on NF-κB activation and Tpl2 release*

Erk1/2 phosphorylation downstream of TLRs occurs when p105 is phosphorylated by IKKβ. Phosphorylated p105 (P-p105) is degraded, releasing Tpl2 to phosphorylate MEK1/2, which then phosphorylates Erk1/2 (see 4.1).

Flow cytometric analysis of 0-3hRP treated BMMφs revealed that they phosphorylated p105 with a similar dynamic as other kinases measured (Figure

4.12). Peak levels of P-p105 occurred after 30min of exposure to 0-3hRP although they were also significantly elevated at 10 and 100min (Figure 4.12A & B; $p < 0.0001$).

As p105 is being phosphorylated, it is possible that Tpl2 may be responsible for the phosphorylation of Erk1/2 in BMM ϕ s exposed to 0-3hRP. WT and Tpl2^{-/-} BMM ϕ s prepared as before (see 2.3) were determined to exhibit comparable expression of F4/80 and CD11b (Figure 4.13). Levels of P-Erk were significantly reduced in Tpl2^{-/-} BMM ϕ s in response to 0-3hRP compared to WT BMM ϕ s (Figure 4.14 A & B, $p < 0.0001$). Indeed, in Tpl2^{-/-} BMM ϕ s there was no difference in the levels of P-Erk in response to 0-3hRP compared to Media. Levels of P-CREB were also significantly reduced in Tpl2^{-/-} BMM ϕ s exposed to 0-3hRP compared to WT BMM ϕ s (Figure 4.14 C & D, $p < 0.0001$).

These findings complement the information already gathered. BMM ϕ s phosphorylate MAPKs in response to 0-3hRP by using TLR2 plus TLR4 and recruiting MyD88, which triggers the activation of NF- κ B (p105) and p38. The phosphorylation of p105, releases Tpl2 that then phosphorylates MEK1/2, which phosphorylates Erk1/2. CREB is partially activated by the Erk1/2 pathway.

4.3.4.2 *Chemical inhibition of Erk1/2 and p38 pathways reduces the phosphorylation of CREB and RSK*

To further elucidate the contribution of p38 and Erk1/2 to the activation of RSK and CREB, chemical inhibition of both pathways was used. BMM ϕ s were pre-treated for 2 hours with a MEK1/2 inhibitor (U0126 at 10 μ M) or a p38 inhibitor (SB203580 at 1 μ M) and then exposed for 30min to 0-3hRP, or left unstimulated. Concentrations of inhibitors used were in line with manufacturer's recommendations. BMM ϕ s were then labeled with antibodies for P-Erk, P-p38, P-CREB or P-RSK as above.

MEK1/2 inhibition of Erk1/2 phosphorylation effectively abrogated the levels of P-Erk in 0-3hRP treated BMM ϕ s (Figure 4.15 A), whereas inhibition of p38 had no effect on the levels of P-Erk, which is to be expected as p38 is not upstream of Erk1/2. Phosphorylation of p38 (Figure 4.15B) was largely unaffected by both inhibitors. SB203580 prevents p38 from phosphorylating its targets, but does not prevent p38 itself from being phosphorylated (Kumar et al, 1999). MEK1/2

inhibition with U0126 did not affect levels of P-p38, in agreement with Erk1/2 not being upstream of p38 and that the inhibitor does not have off target effects on this protein.

Phosphorylation of RSK was greatly affected by inhibition of MEK1/2 but not p38 (Figure 4.15C). MEK1/2 inhibition significantly reduced the levels of P-RSK in response to 0-3hRP ($p < 0.0001$). Consequently, RSK is downstream of Erk1/2. Both MEK1/2 and p38 inhibition had significant, and comparable, effects on the levels of phosphorylated CREB (Figure 4.15D, $p < 0.05$). Both inhibitors reduced the levels of P-CREB by half, indicating that this transcription factor is downstream from both pathways.

4.3.4.3 *Other components of NF- κ B are activated by 0-3hRP in BMM ϕ s*

In 4.3.4.1, phosphorylation of p105, a component of NF- κ B, was reported. This suggests that additional proteins of this complex are likely to be activated in response to 0-3hRP. To test this, BMM ϕ s were exposed to 0-3hRP and then labeled with antibodies for phosphorylated p65 (P-p65). In some experiments, BMM ϕ s were pre-treated for 2 hours with the MEK1/2 inhibitor U0126 (10 μ M) or the p38 inhibitor SB203580 (1 μ M) before being exposed for 30min to 0-3hRP.

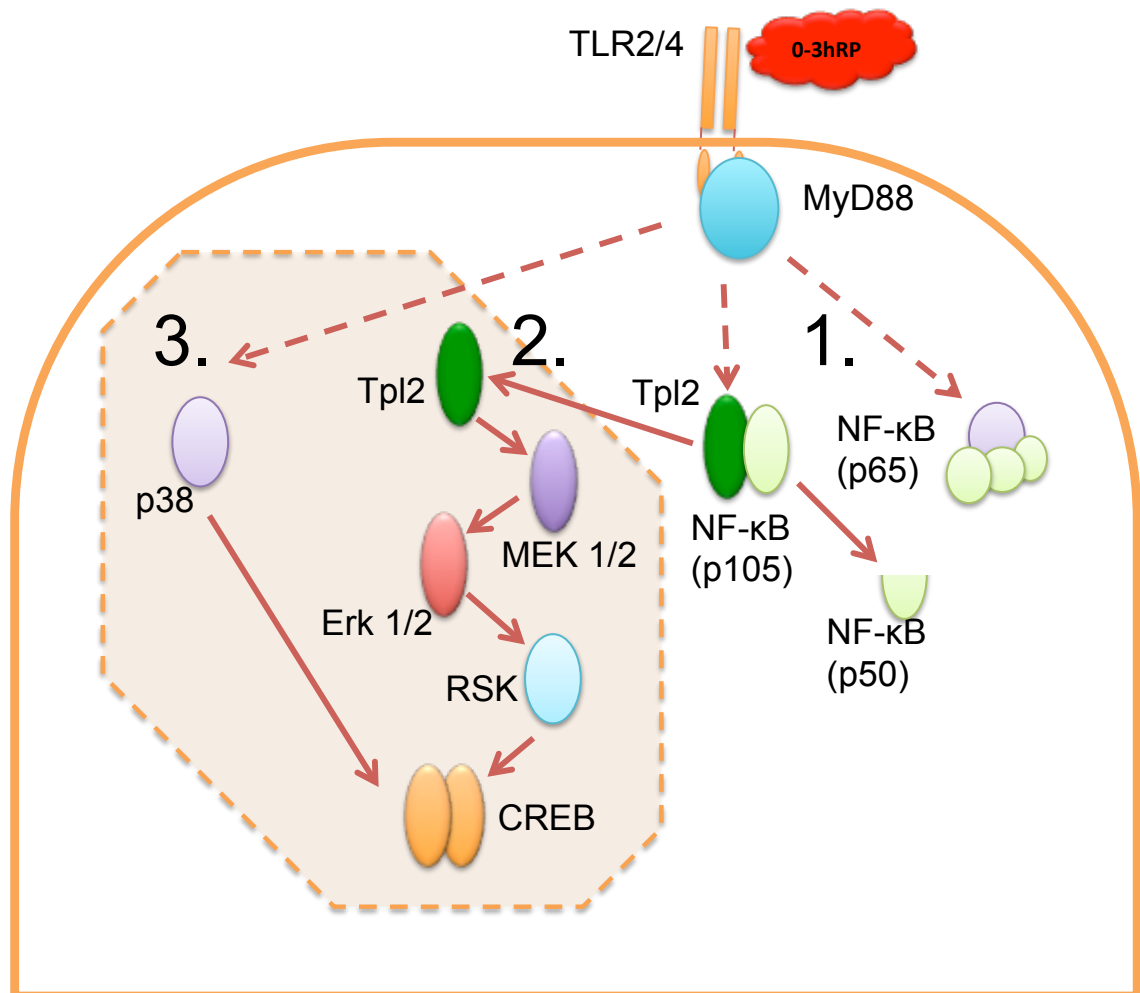
Like P-p105 (Figure 4.12), p65 becomes phosphorylated in BMM ϕ s after exposure to 0-3hRP by 30min (Figure 4.16A&B, $p < 0.0001$). However, unlike P-p105, the levels of P-p65 remain significantly elevated even after 100min (Figure 4.16B, $P < 0.0001$). Neither MEK1/2 or p38 inhibition diminished phosphorylation of p65, indicating that p65 is not downstream of either of those pathways (Figure 4.16). With MEK1/2 inhibition, there was a slight, yet significant ($p < 0.01$), increase in the MFI of P-p65 in 0-3hRP-stimulated BMM ϕ s compared to untreated controls (Figure 4.16B), however this is unlikely to be biologically relevant, as it is minimal compared to differences in MFI as a result of stimulating cells with 0-3hRP or Media controls.

4.3.5 Signaling pathways modulate the production of cytokines in BMM ϕ s exposed to 0-3hRP

Findings in the previous section demonstrated that 0-3hRP binds TLR2 and TLR4 in BMM ϕ s, which results in the recruitment of MyD88 and subsequent activation of NF- κ B and MAPKs (Diagram 4.1). Three distinct signaling cascades have been identified.

First (Diagram 4.1, 1.), at least two components of the NF- κ B system are activated. Phosphorylation of p65 is quick and sustained, whereas phosphorylation of p105 is transient. Second (Diagram 4.1, 2.), phosphorylation of p105 results in the release Tpl2, which triggers MEK1/2, which activates Erk1/2, which phosphorylates RSK. Third (Diagram 4.1, 3.), p38 is activated, most likely by MAP3K7, which is upstream from NF- κ B as well. Finally both the Tpl2-MEK-Erk-RSK axis and the p38 axis result in the phosphorylation of CREB. Some of these associations had already been made with other ligands, as discussed in Diagram 3.1, but they had not all been integrated into the same pathway, with a common activator and in response to a helminth antigen.

Diagram 4.1 Signaling pathways in BMM ϕ s exposed to 0-3hRP



4.3.5.1 *Chemical inhibition of signaling pathways results in modulation of cytokine responses*

In 4.3.2.2, TLR signaling was linked with the production of cytokines in response to 0-3hRP, however the activation of MAPKs has not been directly

associated with cytokine production. Consequently, BMM ϕ s were pre-treated for 2 hours with increasing doses of the MEK1/2 inhibitor U0126, the p38 inhibitor SB203580, and a JNK inhibitor (JNK inhibitor II). BMM ϕ s were then exposed overnight to 0-3hRP, or left un-stimulated (Media) and their culture supernatants tested for IL-10 and IL-12p40 by ELISA.

MEK1/2 inhibition resulted in a significant decrease in the production of IL-10 by BMM ϕ s exposed to 0-3hRP (Figure 4.17A). As the dose of the inhibitor increased, the production of this cytokine was further reduced. Conversely, IL-12p40 production increased significantly as the dose of the inhibitor increased. Inhibition of p38 had a strikingly similar effect on cytokine production (Figure 4.17B). As the dose of inhibitor administered increased, IL-10 was reduced whilst IL-12p40 was increased. The effects of this inhibitor were more potent, likely due to its modest effect on Erk1/2 (see 4.3.4.2).

JNK inhibition did not have a significant effect on the production of either cytokine in BMM ϕ s exposed to 0-3hRP (Figure 4.17C). The observed reductions were minimal and not a function of the inhibitor dose. Results obtained with the proteome profiler showed that JNK2 was activated in response to 0-3hRP (see 3.3.4.3), however, its inhibition did not have a decisive effect on IL-10 and IL-12p40 production. No positive control for JNK inhibition was included in the experiments, but doses used were in line with instructions by manufacturers.

In summary, the phosphorylation of Erk1/2 and p38, and importantly, their downstream targets, primarily CREB, lead to the production of IL-10 and limit the induction of IL-12p40.

4.3.5.2 Abrogation of Erk1/2 phosphorylation in Tpl2^{-/-} BMM ϕ s in response to 0-3hRP modulates the production of IL-10 and IL-12p40

BMM ϕ s exposed to 0-3hRP require Tpl2 to phosphorylate Erk1/2 (see 4.3.4.1). Therefore, in light of the results outlined above, Tpl2^{-/-} BMM ϕ s exposed to 0-3hRP should have reduced production of IL-10 and increased production of IL-12p40 compared to WT BMM ϕ s. As expected, Tpl2^{-/-} BMM ϕ s significantly reduced the levels of IL-10 produced in response to 0-3hRP (Figure 4.18A), albeit this reduction was very modest. Conversely, IL-12p40 was dramatically increased in Tpl2^{-/-} BMM ϕ s (Figure 4.18B). Both observations confirm the

results obtained with chemical inhibition (4.3.4.1). Moreover, the slight decrease in IL-10, matches the phosphorylation of CREB in Tpl2^{-/-} BMMφs exposed to 0-3hRP, that was also only modestly reduced compared to WT BMMφs (Figure 4.14D).

4.3.5.3 *MAPK signaling in BMMφs limits IL-12p40 production independently of IL-10*

Preventing the phosphorylation of Erk1/2 and p38 through chemical inhibition or by using genetically modified mice, results in a significant increase in the production of IL-12p40 (Figure 4.17). This increase was accompanied by a reduction in IL-10, raising the possibility that its reduction causes the increase of pro-inflammatory IL-12p40. An alternative explanation is that MAPKs directly limit the production of IL-12p40 by negatively regulating its transcription.

Consequently, BMMφs were derived from IL-10 deficient mice (see 2.3). As with other protein deficient strains, IL-10^{-/-} BMMφs were comparable to WT BMMφs with regards to F/4/80 and CD11b percentages of positive cells (Figure 4.19). Subsequently, IL-10^{-/-} BMMφs were pre-treated for 2 hours with the MEK1/2 inhibitor U0126 or the p38 inhibitor SB203580 and then exposed overnight to 0-3hRP. IL-10^{-/-} BMMφs exposed to 0-3hRP produced significantly higher levels of IL-12p40 compared to WT BMMφs (Figure 4.20), however, MEK1/2 inhibition also resulted in a significant increase in the production of IL-12p40 in both strains of mice (Figure 4.20A). Similarly, p38 inhibition significantly increased the production of IL-12p40 in both WT and IL-10^{-/-} BMMφs (Figure 4.20B).

As IL-12p40 production increased as a result of the inhibition of MEK1/2 and p38 in the absence of IL-10, it follows that both signaling pathways are limiting the production of IL-12p40 in an IL-10 independent manner, potentially by preventing *Il12b* transcription. Therefore, mRNA was extracted from both WT and IL-10^{-/-} BMMφs and transcript levels of *IL10* and *IL12b* measured (see in 3.3.5.2). After 100min of stimulation, which is the earliest time point when both transcripts are abundant (see Figure 3.13), and levels of IL-10 protein are still low (see 4.3.1), both MEK1/2 and p38 inhibition significantly reduced IL-10 mRNA in BMMφs exposed to 0-3hRP (Figure 4.21A). Importantly, the use of both inhibitors also significantly increased the levels of IL-12p40 mRNA (Figure 4.21B). In summary, TLR mediated activation of MAPKs in BMMφs exposed to

0-3hRP limits the amount of IL-12p40 produced by these cells independently of IL-10.

4.3.6 CREB is recruited to the IL-10 promoter to induce the activation of its transcription in BMMφs exposed to 0-3hRP

Evidence presented thus far shows that BMMφs use TLR2 and TLR4 to recognize 0-3hRP, leading to MyD88 mediated activation of two axes of MAPKs signaling that converge in the phosphorylation of CREB. Therefore, it is possible that CREB, which is a transcription factor, is recruited to the IL-10 promoter where it participates in the initiation of IL-10 mRNA synthesis.

In order to investigate this hypothesis, BMMφs stimulated with 0-3hRP for 30min were processed for ChIP as described in 4.2.2. Fragment size of sonicated chromatin was estimated to be ~200bp using agarose gel electrophoresis (Figure 4.22), which is the recommended size for ChIP (Landt et al, 2012). After an aliquot of sonicated chromatin was saved as input DNA control, ChIP was carried out with antibodies against phosphorylated CREB (α -P-CREB) and total CREB (α -CREB). Antibodies against RNA Polymerase II (α -Pol II) were used as positive controls, given that the IL-10 gene is transcriptionally active after 30min of stimulation with 0-3hRP. Antibodies against a non-nuclear protein (CD36) were used as a negative control (α -CD36) alongside a no antibody control (No Ab).

Precipitated DNA and input DNA were used for PCR with 4 sets of primers mapping the IL-10 promoter region (for sequences see Table 2.2) and densitometry analysis performed as described in 4.2.2.1. Designed primers provided coverage of 1000bp of the IL-10 promoter (Figure 4.23A). In the schematic diagram, genomic DNA (black) is divided into 4 regions by each primer set (red dashed boxes). The portion of *IL10* covered includes the start of transcription (0bp, RNA in green) and translation (+64bp, protein in blue). Of the four fragments analyzed, only the 4th region was detected by PCR (Figure 4.23B, red arrows). This was the case for chromatin precipitated with both α -P-CREB and α -CREB, indicating that a regulatory element for CREB is likely to be in that region of the gene, and not elsewhere. Densitometry analysis of PCR results confirmed the initial observations, with enrichment only apparent in the 4th region investigated (Figure 4.23C). Although the experiment was performed in 4 separate occasions with similar results, densitometry measures were not

combined due to differences in background levels and exposure times. Chromatin precipitated with α -Pol II only produced a strong signal with the 4th set of primers (Figure 4.23D), just as with α -P-CREB and α -CREB. Negative controls (i.e. α -CD36 and No Ab) were negative for all the primer pairs.

It is therefore concluded that phosphorylated CREB is recruited to the IL-10 promoter in BMM ϕ s after 30min of exposure to 0-3hRP, where it is likely to modulate the transcription of this cytokine.

4.4 Discussion

4.4.1 BMM ϕ s carefully orchestrate the production of IL-10 and IL-12p40 in response to 0-3hRP

The results presented in this chapter highlight the very detailed control macrophages stimulated with *S. mansoni* cercarial E/S products have over the production of IL-10 and IL-12p40. Rather than producing both cytokines shortly after encountering the stimulus, BMM ϕ s stagger their synthesis, initially producing anti-inflammatory IL-10 prior to the production of IL-12p40. The production of IL-10 peaks and then starts to decrease even when IL-12p40 continues to rise. This difference in dynamics of cytokine production is likely to be the cause of the regulation of the signaling pathway described in this chapter. IL-10 is triggered earlier by MAPKs that at the same time limit the activation of IL-12p40. Moreover, different components of 0-3hRP might be responsible for the induction of different cytokines. IL-10 production significantly affects the course of *S. mansoni* infection, preventing resistance to this parasite from being established (Wilson et al, 2011). The fact that BMM ϕ s first response to cercarial E/S products is to produce IL-10, hints at the importance innate cells might have in conditioning the immune response to *S. mansoni* very early on.

Cercarial invasion of the skin, and the subsequent release of E/S products, occurs within hours of the start of infection (Paveley et al, 2009). Therefore, no T cell-derived signals would reach macrophages exposed to 0-3hRP in the skin at these early time points. Nevertheless, macrophages must respond to cercarial E/S products as soon as they encounter them. These studies have shown that BMM ϕ s directly recognize 0-3hRP using TLRs. Despite their accepted association with pro-inflammatory cytokines, the TLR family of receptors, which includes TLR2 and TLR4, appears responsible for the production of IL-10 in a MyD88 dependent manner. Other studies show that TLR2 can have a more regulatory role than TLR4, by limiting the ability of antigen presenting cells to induce a Th1 response (Agrawal et al, 2003; Gao et al, 2012; van Riet et al, 2009), blocking the production of pro-inflammatory cytokines (Correale & Farez, 2009), regulating susceptibility to bacterial infection (Blanchet et al, 2014) or promoting the production of IL-10 (van Vliet et al, 2013). Indeed, TLR2 deficiency in BMM ϕ s exposed to 0-3hRP resulted in a more pronounced defect in the induction of IL-10, compared to TLR4 deficient

cells. Conversely, the absence of TLR2 had a relatively small effect on IL-12p40, unlike TLR4, which greatly reduced the production of this cytokine in response to 0-3hRP.

Thus, TLR2 mediated IL-10 production by macrophages exposed to *S. mansoni* cercarial secretions, would give macrophages a regulatory phenotype, and limit their ability to contribute to the induction of Th1 responses.

4.4.2 BMMφs use MAPKs downstream of TLRs to produce IL-10 in response to 0-3hPR

Unlike semi-quantitative methods to measure phosphorylation (i.e. Western blotting) that require normalization based on total protein vs. phosphorylated protein and constitutively expressed genes (i.e. GAPDH, α -tubulin), flow cytometry measures directly the amount of phosphorylated protein in individual cells (as fluorescence intensity). Consequently, comparisons can be made between treatments for homogenous populations of cells in the absence of the mentioned normalizers. This is apparent from the results obtained in this chapter where the constant levels of tErk as measured by flow cytometry, albeit informative, bore no significance in the analysis made on the changing levels of P-Erk.

As macrophages rely heavily on the TLR system to produce cytokines, it follows that the activation of MAPKs and NF- κ B would be timed to match the dynamic of cytokine production. In fact, p105, Erk1/2, RSK, p38, and CREB have maximal activity after 30min of stimulation with cercarial E/S products. This activation depended directly on MyD88 and was strongly impacted by the absence of TLR2, whose function was complemented by TLR4. The phosphorylation of p105, which occurred after 30min of exposure to 0-3hRP, results in its degradation into p50, releasing Tpl2 from an inactive cytoplasmic complex. p65 also became phosphorylated after 30min of stimulation. Released p50 and activated p65 are then free to form a heterodimer. The p50/p65 complex is a well-known transcription factor and among its prime targets are pro-inflammatory cytokines such as IL-1 and IL-6 (Hoesel & Schmid, 2013), and as both cytokines, along other pro-inflammatory mediators, were induced at the transcript level by 0-3hRP, it is possible to assume that the p50/p65 dimer is actively directing the transcription of these genes in 0-3hRP treated BMMφs. However, the release of Tpl2 results in the activation of MEK1/2 and

subsequent phosphorylation of Erk1/2. In BMM ϕ s exposed to cercarial E/S products, these events led to the activation of RSK and CREB. The association between Erk1/2 and CREB has been reported in the past with other innate immune stimuli, such as Zymosan or Leishmania parasites, and receptors including TLRs (Elcombe et al, 2013; Nandan et al, 2012; Nandan & Reiner, 2005; van Vliet et al, 2013), however, it has not been reported in the context of helminth antigens.

In the present studies inhibition of MEK1/2 and p38, and their downstream targets, resulted in a significant impairment of the production of IL-10, proving the close link between these signals and the transcription and translation of this regulatory cytokine. This association has been made by others (Arthur & Ley, 2013; Elcombe et al, 2013; Lucas et al, 2005; Mayer et al, 2013; van Vliet et al, 2013; Zhang et al, 2006), but not in the context of a helminth antigen, and only rarely as a result of TLR signaling. However, these MAPKs are also acting to limit the production of IL-12p40 in an IL-10 independent manner. In particular, p38 is well known for causing increased IL-12 p40 secretion in the absence of IL-10 (Deak et al, 1998; Elcombe et al, 2013; Mayer et al, 2013). The disruption of Erk1/2 activation in Tpl2 deficient macrophages had a similar effect, and the use of other MEK1/2 inhibitors (PD98059, AZ6244) also impaired IL-10 production, whilst enhancing IL-12p40 (data not shown).

4.4.3 Phosphorylated CREB is recruited to the IL-10 promoter to modulate its transcription in BMM ϕ s exposed to 0-3hRP

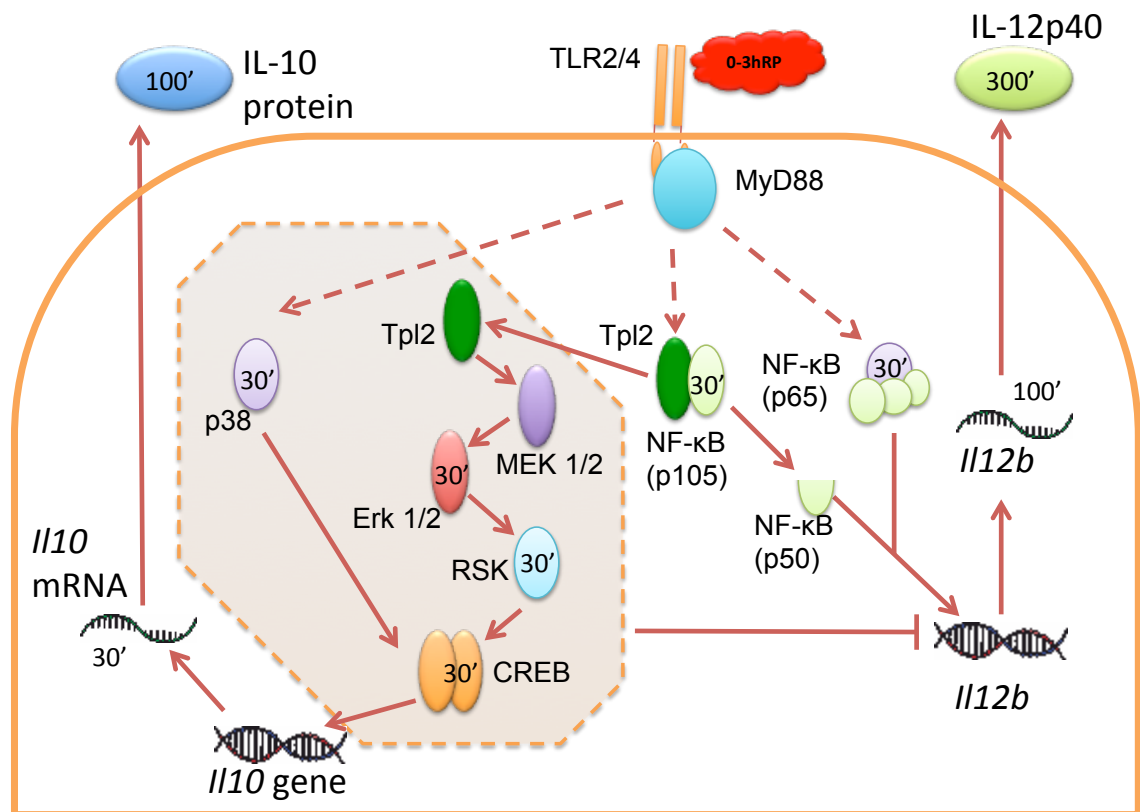
The Tpl2-MEK-Erk-RSK and p38 axes converge on the activation of CREB in BMM ϕ s exposed to 0-3hRP. This convergence and the strong association between these pathways and the production of IL-10, led to the assumption that CREB facilitated the transcription of IL-10. Here it is shown that in BMM ϕ s exposed to cercarial E/S products, phosphorylated CREB is recruited to the IL-10 promoter in a region that overlaps with the first exon of the gene, which is different from what was reported in the past (Ananieva et al, 2008). This recruitment is apparent after 30 minutes of stimulation with the parasite's secretions, at which point there is a peak in the activation of CREB. Both the abundant levels of phosphorylated CREB and its strong interaction with the IL-10 promoter, place this transcription factor in a privileged place to effectively regulate the transcription of this cytokine.

Several other studies have linked CREB and IL-10 (Elcombe et al, 2013; MacKenzie et al, 2013; Mayer et al, 2013; Nandan et al, 2012; van Vliet et al, 2013; Wen et al, 2010) by using chemical inhibition, siRNA or genetically modified cells. However, only two of studies showed an interaction between CREB and DNA from the IL-10 gene. One in a highly artificial system (Nandan et al, 2012) and another in conjunction with another transcription factor (Ananieva et al, 2008). Others have used ChIP to investigate the changes in the IL-10 promoter following stimulation with different antigens, finding interactions with other transcription factors like NF- κ B or cMAF (1.5), and have linked this with Erk1/2, but have confined their studies to histone modification (Lucas et al, 2005; Zhang et al, 2006). In this study a novel regulatory element has been found in the IL-10 promoter, where CREB binds as a result of TLR stimulation in a process that enhances transcription of IL-10.

4.5 Summary

S. mansoni cercarial E/S products bind TLR2 and TLR4 in BMMφs, which results in the recruitment of MyD88 and subsequent activation of NF-κB and MAPKs (Diagram 4.2). Three distinct signaling cascades are triggered by these interactions.

Diagram 4.2 IL-10 biogenesis in BMMφs exposed to cercarial E/S products



Firstly, at least two components of the NF-κB system are activated. Phosphorylation of p65 is quick and sustained, whereas phosphorylation of p105 is transient, peaking after 30 minutes of stimulation. As p105 is degraded into p50, it becomes free to form heterodimers with p65 and orchestrate the transcription of pro-inflammatory genes. Secondly, degradation of p105 also results in the release of Tpl2, which phosphorylates MEK1/2, which activates Erk1/2, which phosphorylates RSK. Thirdly, p38 is activated, most likely by MAP3K7, which is also upstream from NF-κB. Finally both the Tpl2-MEK-Erk-RSK axis and the p38 axis result in the phosphorylation of CREB. This transcription factor is then able to go to nucleus, find the IL-10 promoter and increase the production of this cytokine.

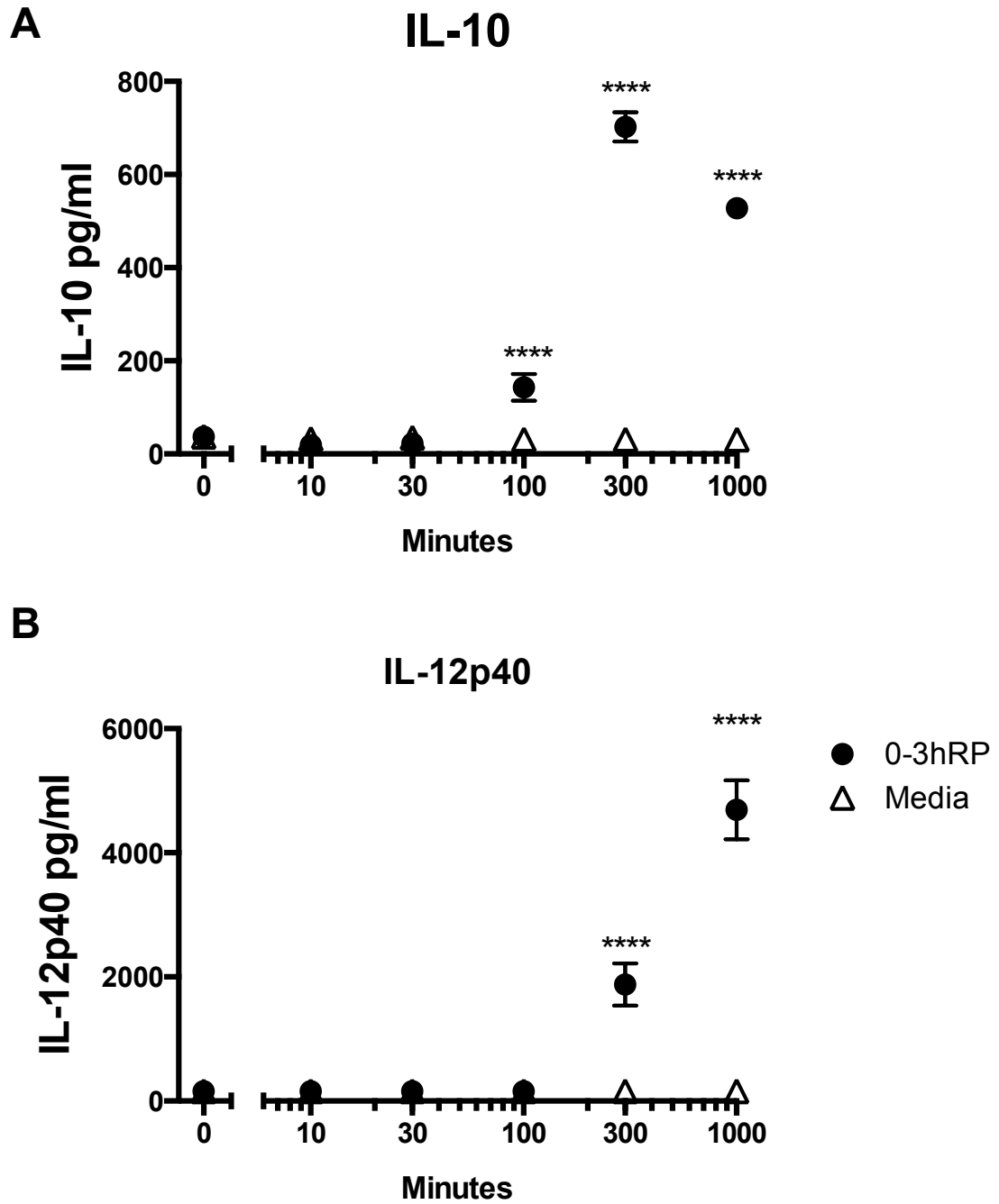


Figure 4.1 Time course of cytokine production in BMMφs exposed to 0-3hRP

Supernatants from BMMφs exposed to 0-3hRP (50μg/ml) or left un-stimulated (Media) were tested for the presence of (A) IL-10 and (B) IL-2p40. Means ±SEM of three technical replicates are presented. ANOVA and then Sidak's multiple comparisons test were performed to examine differences between the means of 0-3hRP stimulated cells compared to Media at each time point (* = $p < 0.05$; ** = $p < 0.01$; *** = $p < 0.001$; **** = $p < 0.0001$; ns = $p > 0.05$). Results are representative of three independent experiments.

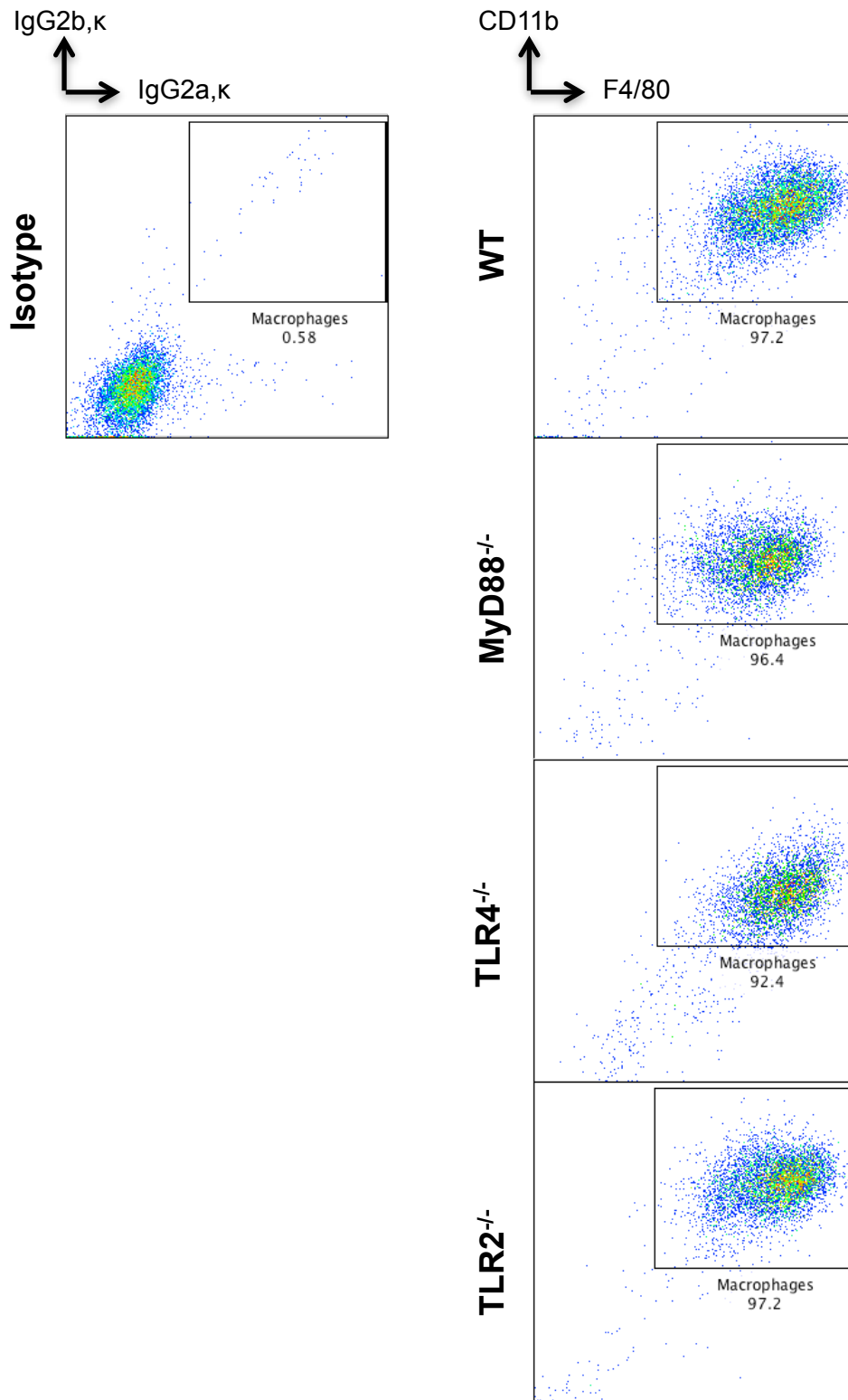


Figure 4.2 BMMφs deficient on MyD88, TLR4 or TLR2 are phenotypically similar to WT BMMφs

WT, MyD88^{-/-}, TLR4^{-/-} or TLR2^{-/-} BMMφs were obtained after 7 days of culture of bone marrow from WT or specific receptor/protein deficient mice. Differentiated cells were labeled with antibodies against F4/80 and CD11b. Representative flow plots of single live cells (based on a cell viability exclusion dye) are shown. Results are representative of five independent experiments.

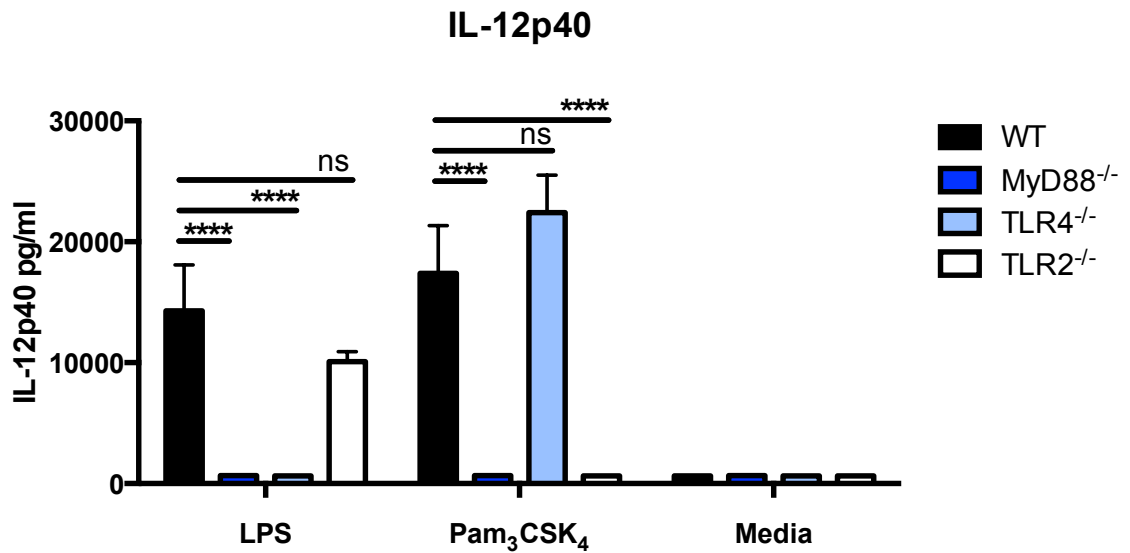


Figure 4.3 BMMφs deficient on MyD88, TLR4 or TLR2 are selectively able to respond to specific PAMPS

WT, MyD88^{-/-}, TLR4^{-/-} or TLR2^{-/-} BMMφs were obtained after 7 days of culture of bone marrow from WT or specific receptor/protein deficient mice. Culture supernatants from BMMφs exposed overnight to LPS (1ng/ml), Pam₃CSK₄ (5μg/ml) or left un-stimulated (Media) were analyzed for IL-12p40 production. Means +SEM of three technical replicates are presented. ANOVA and then Dunnett's multiple comparisons test were performed to examine differences between the means of stimulated cells from all deficient strains compared to WT (**** = p<0.0001; ns = p>0.05). Results are representative of two independent experiments.

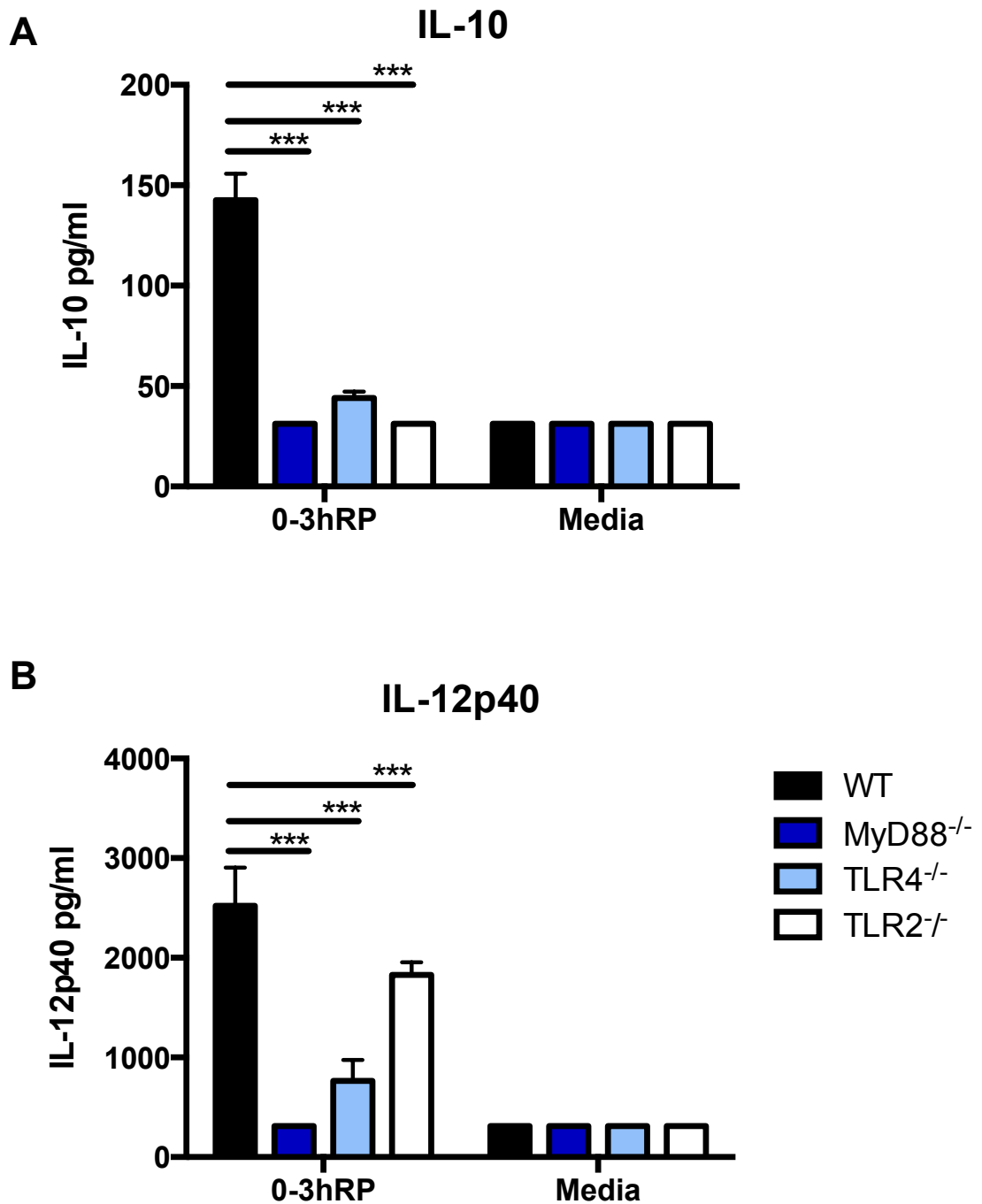


Figure 4.4 BMMφs require TLRs for cytokine production in response to 0-3hRP

Supernatants from WT, MyD88^{-/-}, TLR4^{-/-} or TLR2^{-/-} BMMφs exposed to 0-3hRP (50μg/ml) or left un-stimulated (Media) were tested for the production of (A) IL-10 and (B) IL-12p40. Limits of detection for ELISA were 32pg/ml for IL-10 and IL12p40. Means +SEM of three technical replicates are presented. ANOVA and then Dunnett's multiple comparisons test were performed to examine differences between the means of stimulated protein deficient cells compared to stimulated WT cells (***) = p<0.001). Results are representative of three independent experiments.

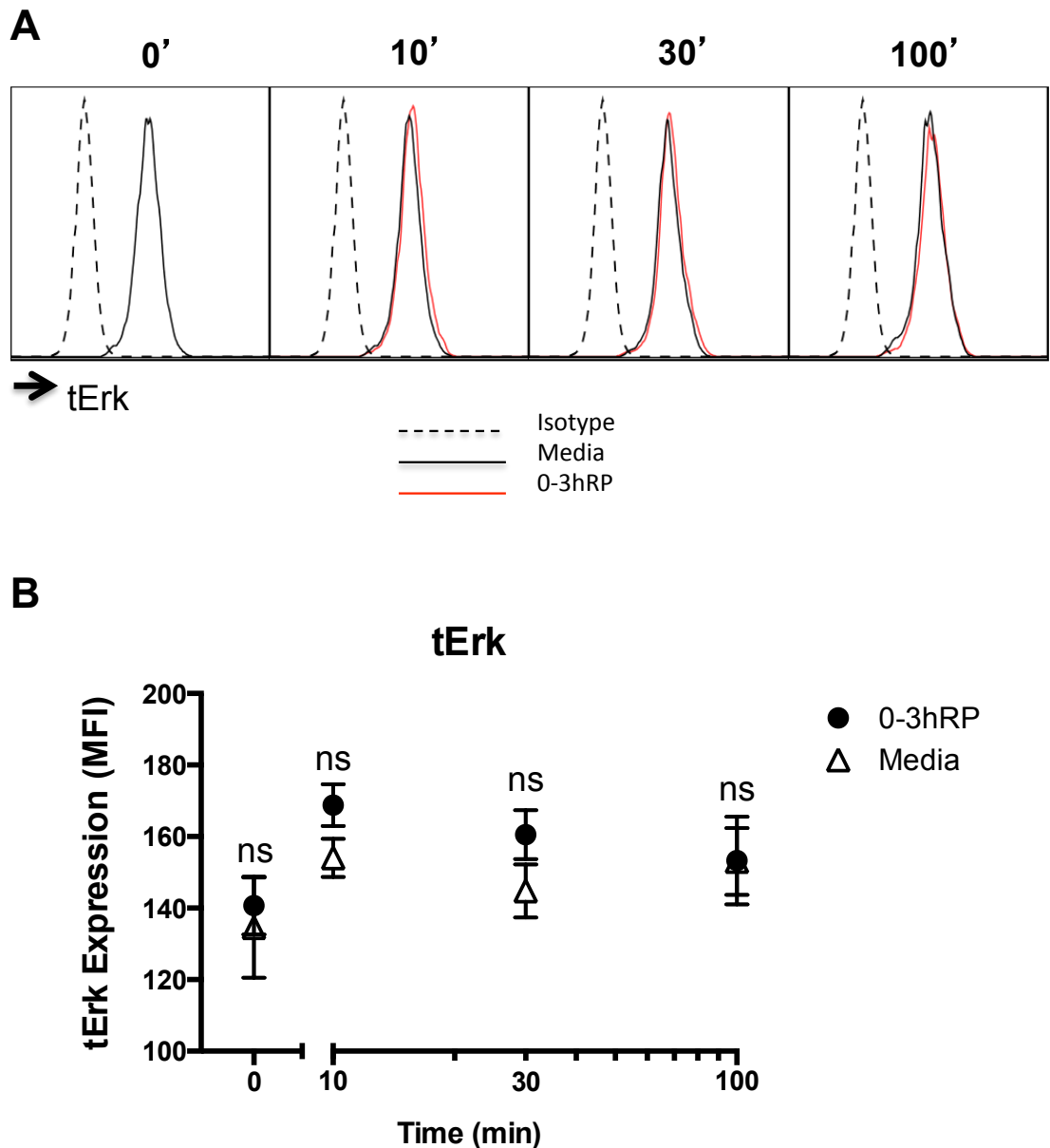


Figure 4.5 Changes in levels of tErk in BMMφs exposed to 0-3hRP

BMMφs exposed to 0-3hRP (50μg/ml) or left un-stimulated (Media) for 0, 10, 30 or 100min were labeled with antibodies against total Erk1/2 (tErk). **(A)** Representative overlaid histograms of single cells are presented from Isotype control (dashed line), Media control (black line) or 0-3hRP treatment (red line). **(B)** Mean ±SEM of MFI for each time point are also given from three technical replicates. ANOVA and then Sidak's multiple comparisons test were performed to examine differences between the means of 0-3hRP treated cells compared to Media control at each time point (ns = $p > 0,05$). Results are representative of three independent experiments.

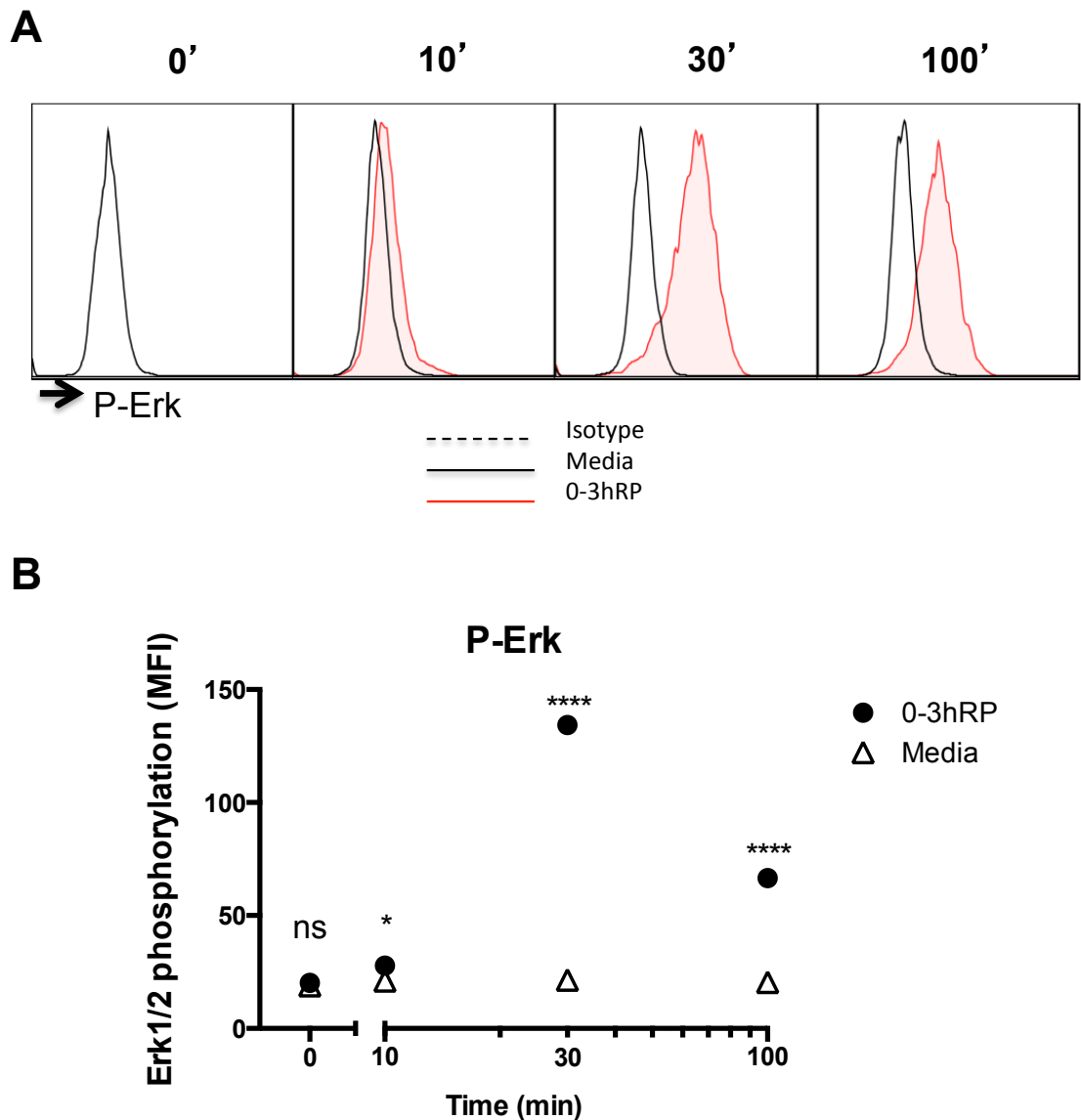


Figure 4.6 Changes in levels of P-Erk in BMMφs exposed to 0-3hRP

BMMφs exposed to 0-3hRP (50µg/ml) or left un-stimulated (Media) for 0, 10, 30 or 100min were labeled with antibodies against phosphorylated Erk1/2 (P-Erk). (A) Representative overlaid histograms of single cells are presented from Media control (black line) or 0-3hRP treatment (red line). (B) Mean ±SEM of MFI for each time point are also given from three technical replicates. ANOVA and then Sidak's multiple comparisons test were performed to examine differences between the means of 0-3hRP treated compared to Media control at each time point (* = $p < 0.05$; **** = $p < 0.0001$; ns = $p > 0,05$). Results are representative of three independent experiments.

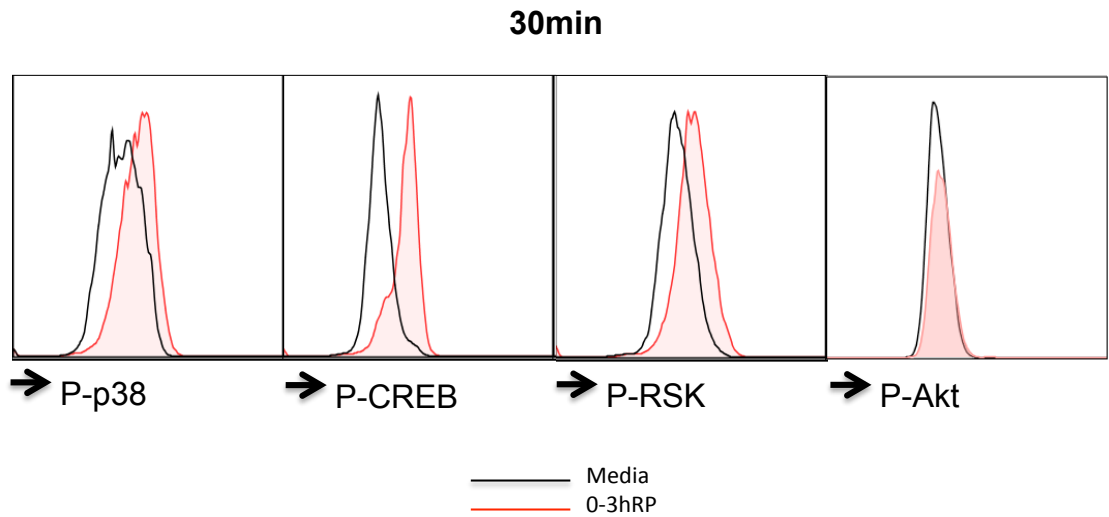


Figure 4.7 BMMφs activate p38, CREB and RSK, but not Akt, in response to 0-3hRP

BMMφs exposed to 0-3hRP (50μg/ml) or left un-stimulated (Media) for 30min were labeled with antibodies against phosphorylated p38, CREB, RSK and Akt. Representative overlaid histograms of single cells from 0-3hRP treated (red) or Media (black) are shown. Results are representative of three independent experiments.

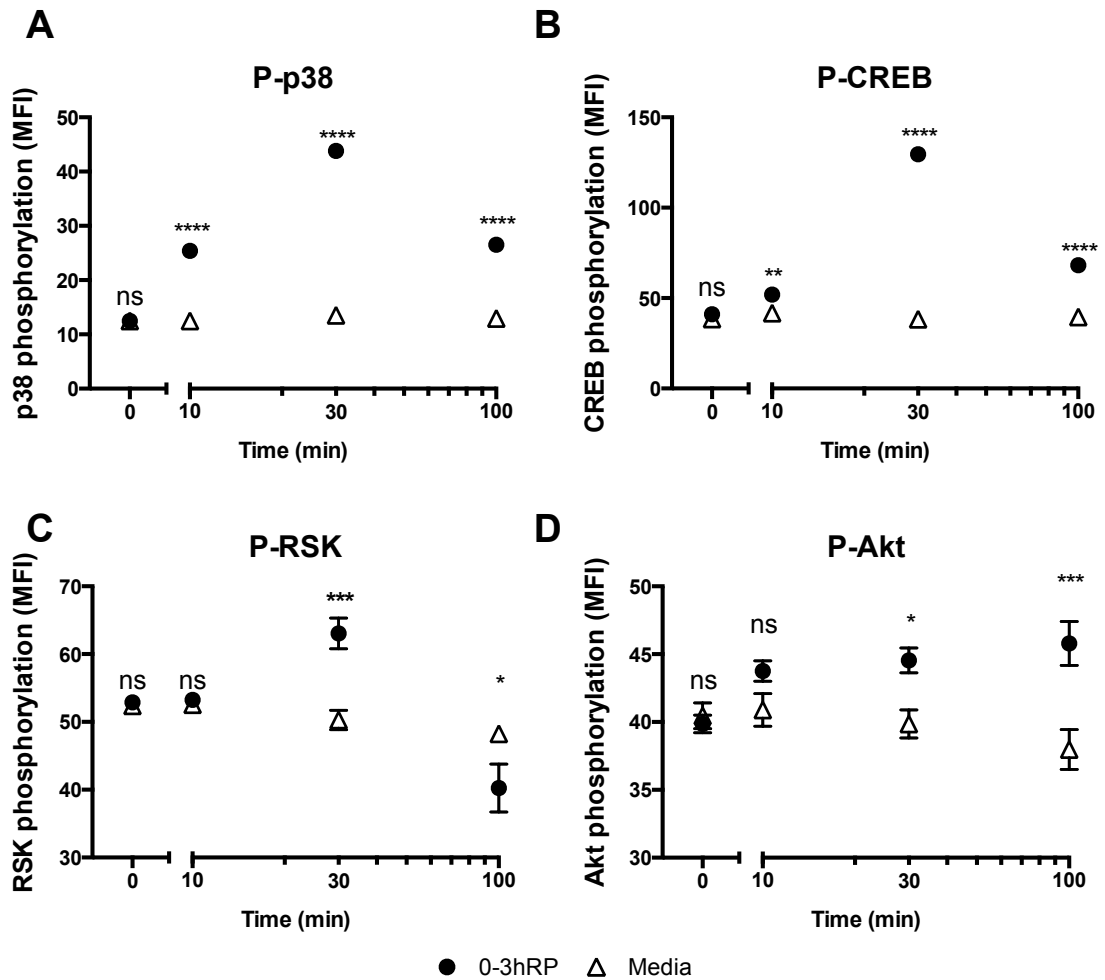


Figure 4.8 Quantitation of phosphorylated p38, CREB, RSK and Akt in BMMφs exposed to 0-3hRP

BMMφs exposed to 0-3hRP (50μg/ml) or left un-stimulated (Media) for 0, 10, 30 or 100min were labeled with antibodies against phosphorylated (A) p38, (B) CREB, (C) RSK and (D) Akt. Means ±SEM of MFIs for each time point are presented from three technical replicates. ANOVA and then Sidak's multiple comparisons test were performed to examine differences between the means of 0-3hRP treated cells at each time point compared to Media (* = $p < 0.05$; ** = $p < 0.01$; *** = $p < 0.001$ **** = $p < 0.0001$; ns = $p > 0.05$). Results are representative of three independent experiments.

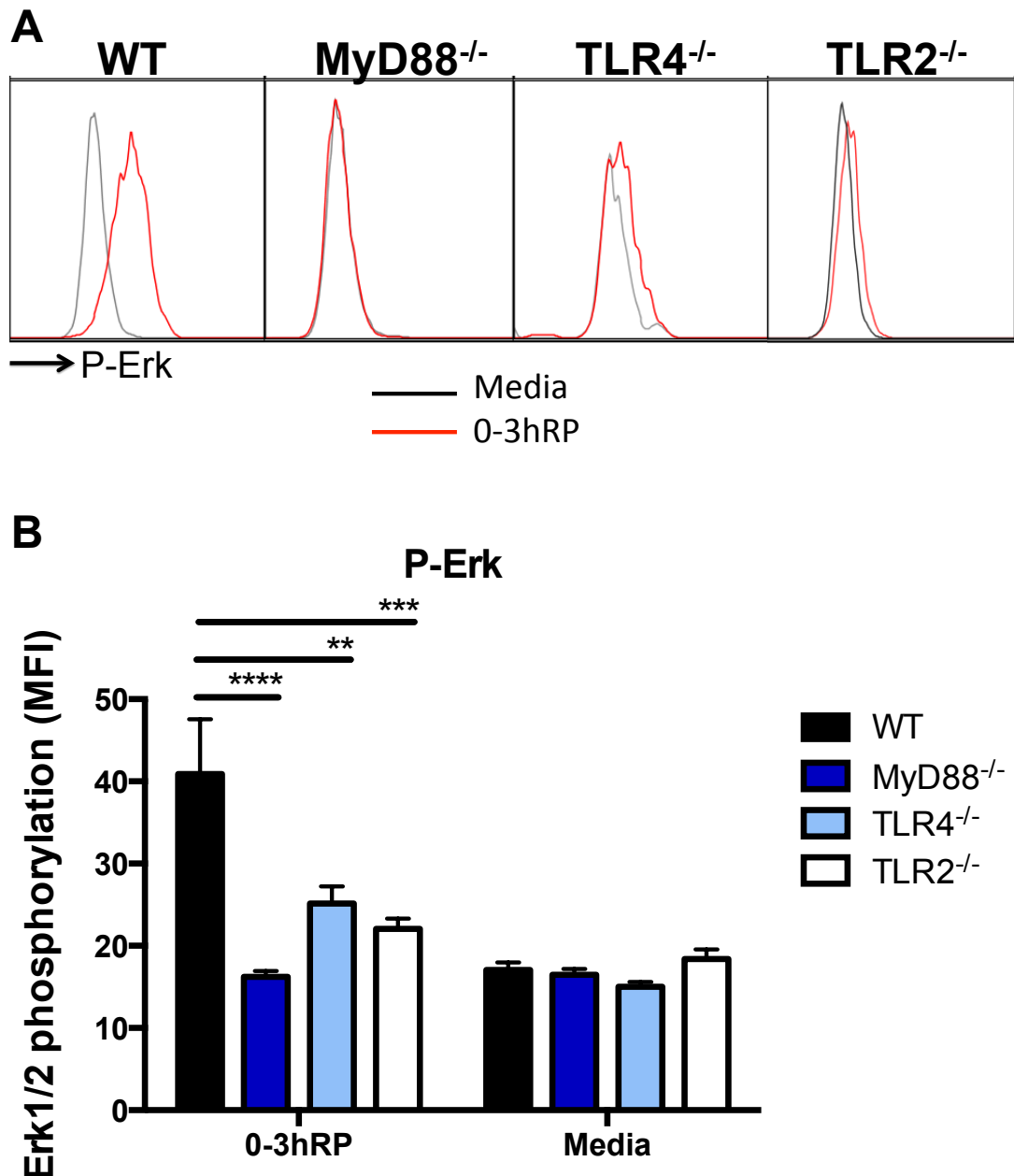


Figure 4.9 Phosphorylation of Erk1/2 in response to 0-3hRP is dependent on TLR signaling

WT, MyD88^{-/-}, TLR4^{-/-} or TLR2^{-/-} BMMφs exposed for 30min to 0-3hRP (50μg/ml) or left un-stimulated (Media) were labeled with antibodies against phosphorylated Erk1/2 (P-Erk). **(A)** Representative overlaid of histograms with 0-3hRP treated cells (red) and Media control (black) and **(B)** means +SEM of MFIs for each mouse strain are given from 3 biological replicates. ANOVA and then Bonferroni's multiple comparisons test were performed to examine differences between the means of stimulated protein deficient cells compared to WT cells (** = p<0.01; *** = p<0.001 **** = p<0.0001; ns = p>0.05). Results are representative of three independent experiments.

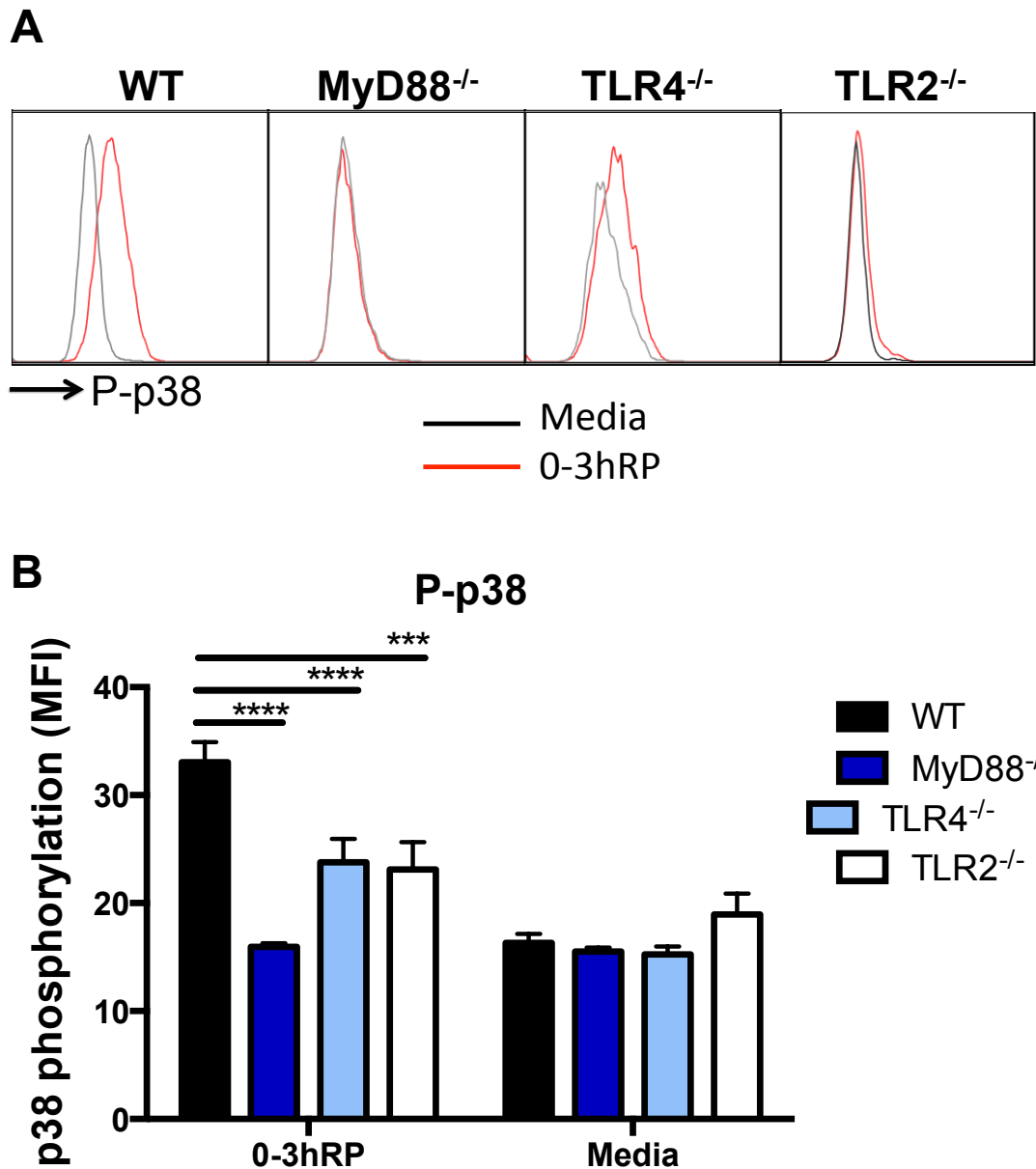


Figure 4.10 Phosphorylation of p38 in response to 0-3hRP is dependent on TLR signaling

WT, MyD88^{-/-}, TLR4^{-/-} or TLR2^{-/-} BMMφs exposed for 30min to 0-3hRP (50μg/ml) or left un-stimulated (Media) were labeled with antibodies against phosphorylated p38 (P-p38). **(A)** Representative overlaid of histograms with 0-3hRP treated cells (red) and Media control (black) and **(B)** means +SEM of MFIs for each mouse strain are given from 3 biological replicates. ANOVA and then Bonferroni's multiple comparisons test were performed to examine differences between the means of stimulated protein deficient cells compared to WT cells (** = p<0.01 **** = p<0.0001; ns = p>0.05). Results are representative of three independent experiments.

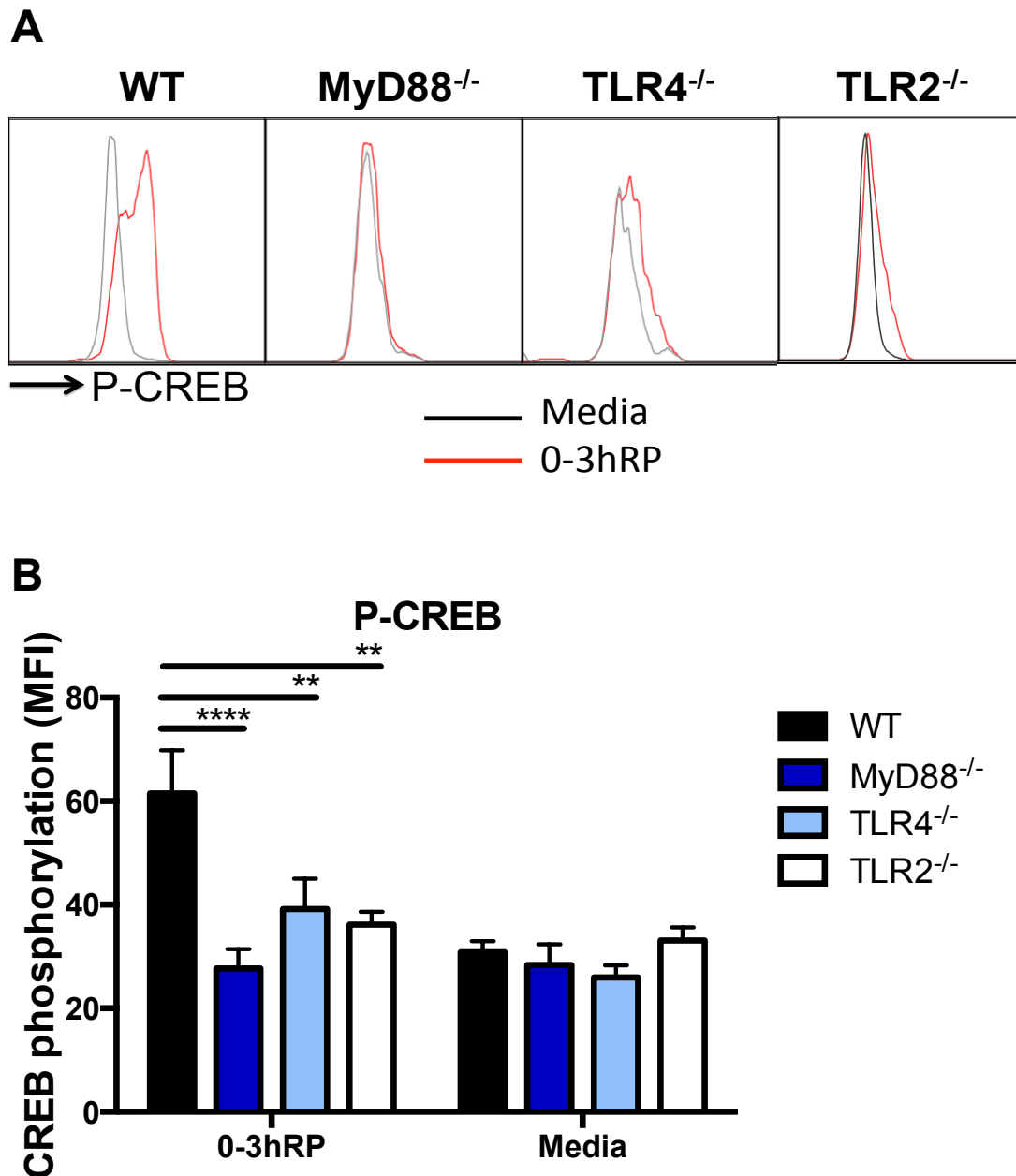


Figure 4.11 Phosphorylation of CREB in response to 0-3hRP is dependent on TLR signaling

WT, MyD88^{-/-}, TLR4^{-/-} or TLR2^{-/-} BMMφs exposed for 30min to 0-3hRP (50μg/ml) or left un-stimulated (Media) were labeled with antibodies against phosphorylated CREB (P-CREB). (A) Representative overlaid histograms with 0-3hRP treated cells (red) and Media control (black) and (B) means +SEM of MFIs for each mouse strain are given from 3 biological replicates. ANOVA and then Bonferroni's multiple comparisons test were performed to examine differences between the means of stimulated protein deficient cells compared to WT cells (** = p<0.001 **** = p<0.0001; ns = p>0.05). Results are representative of three independent experiments.

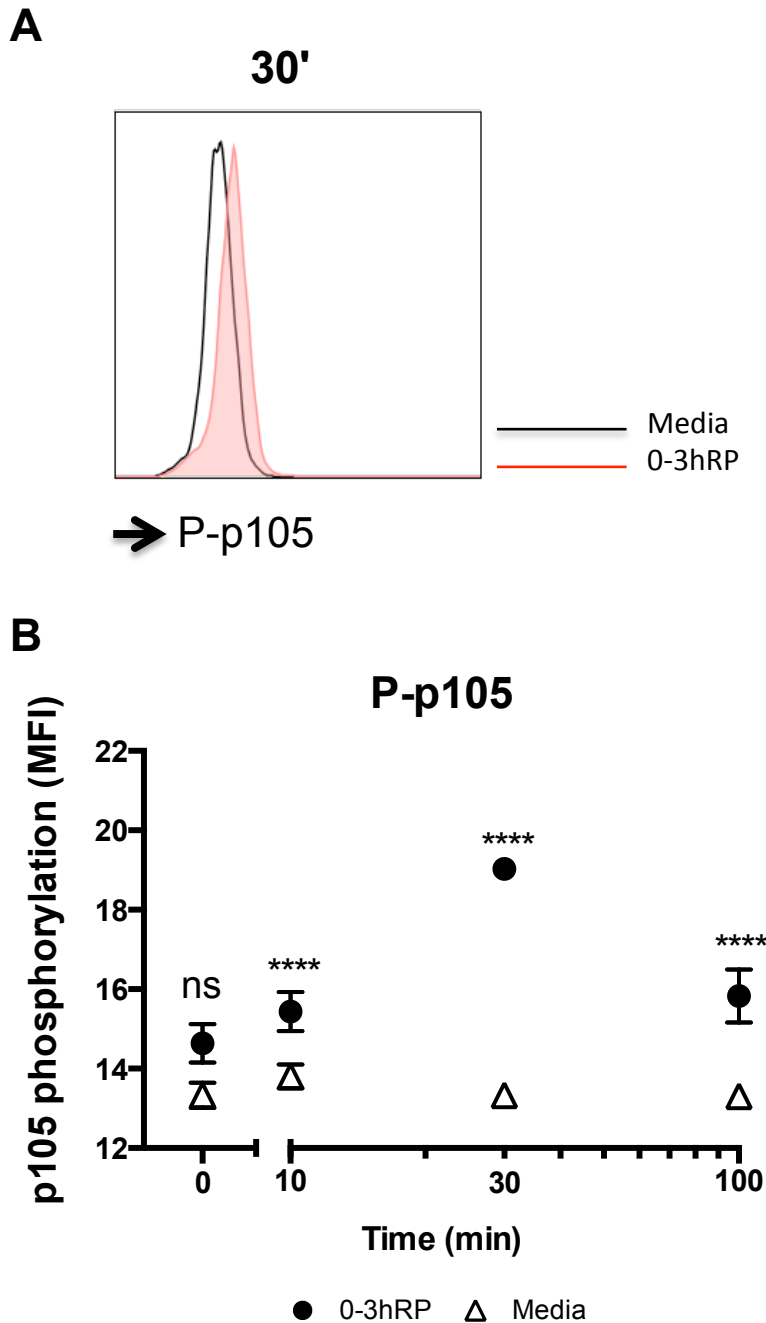


Figure 4.12 NF- κ B (p105) is activated in BMM ϕ s exposed to 0-3hRP

BMM ϕ s exposed to 0-3hRP (50 μ g/ml) or left un-stimulated (Media) for 0, 10, 30 or 100min were labeled with antibodies against phosphorylated p105 (P-p105). (A) Representative overlaid histograms of single cells are presented from Media control (black line) or 0-3hRP treatment (red line) after 30min of stimulation. (B) Mean \pm SEM of MFI for each time point are also given from three technical replicates. ANOVA and then Sidak's multiple comparisons test were performed to examine differences between the means of 0-3hRP treated compared to Media control at each time point (**** = $p < 0.0001$; ns = $p > 0,05$). Results are representative of three independent experiments.

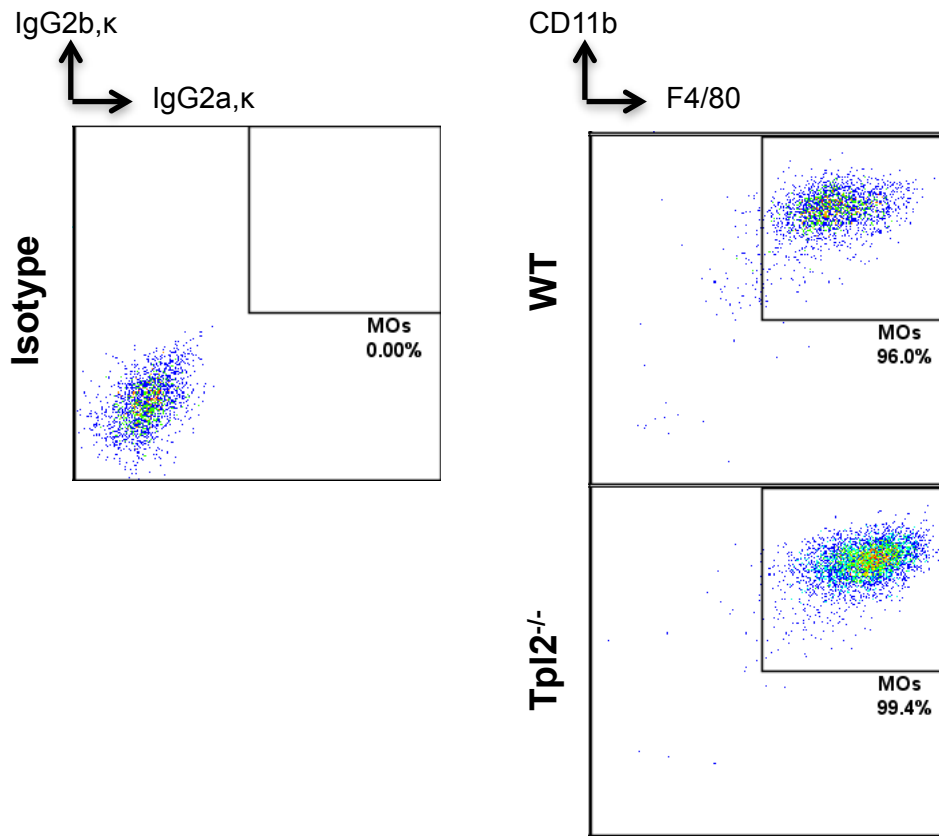


Figure 4.13 BMMφs deficient for Tpl2 are similar to WT BMMφs

WT or Tpl2^{-/-} BMMφs were obtained after 7 days of culture of bone marrow from WT or Tpl2 deficient mice. Differentiated cells were labeled with antibodies against F4/80 and CD11b. Representative flow plots of single live cells (based on a cell viability exclusion dye) are shown. Results are representative of three independent experiments.

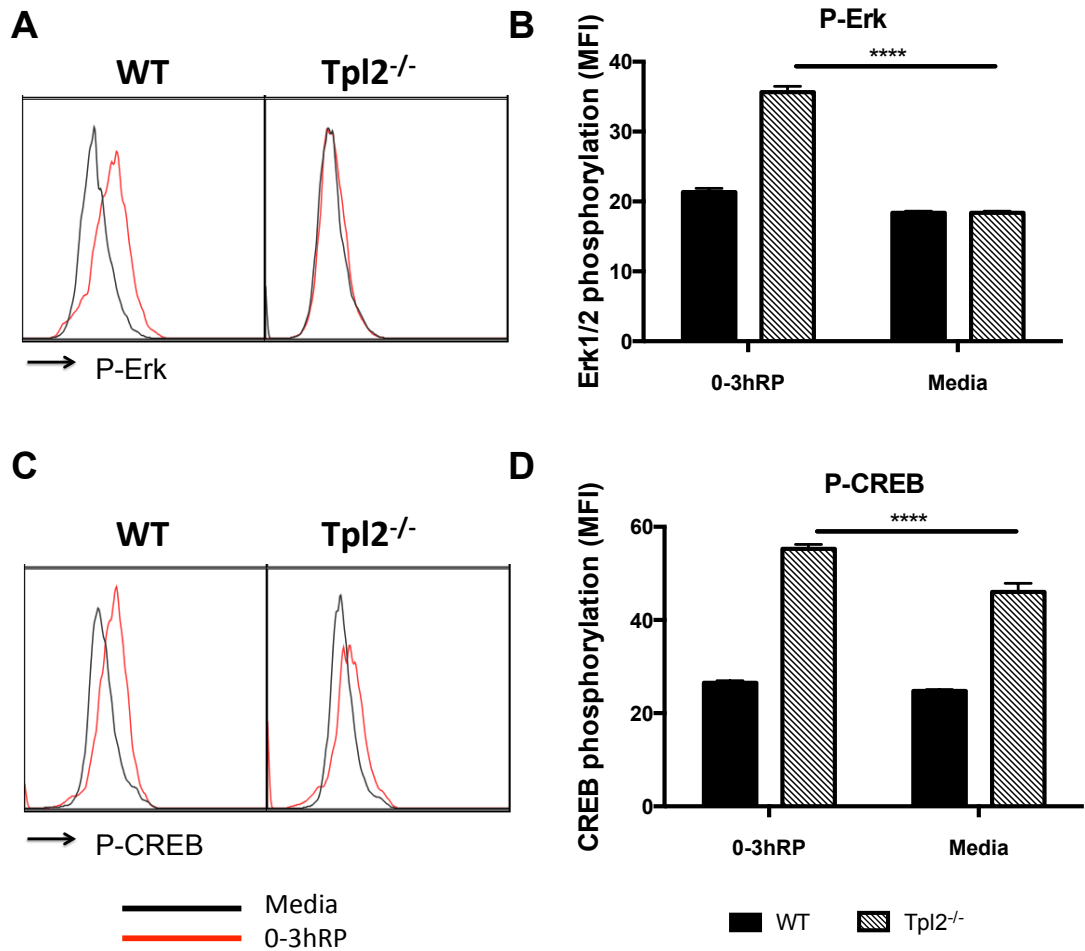


Figure 4.14 Phosphorylation of Erk1/2 and CREB in response to 0-3hRP is dependent on Tpl2

WT or Tpl2^{-/-} BMMφs exposed for 30min to 0-3hRP (50μg/ml) or left unstimulated (Media) were labeled with antibodies against phosphorylated (**A & B**) Erk1/2 (P-Erk) and (**C & D**) CREB (P-CREB). Representative overlaid histograms with 0-3hRP treatment (red) or Media (black) (**A & C**) and means +SEM of MFIs (**B & D**) for each mouse strain are given from three technical replicates. ANOVA and then Dunnett's multiple comparisons test were performed to examine differences between the means of stimulated Tpl2 deficient cells compared to WT cells (** = p<0.01; **** = p<0.0001). Results are representative of three independent experiments.

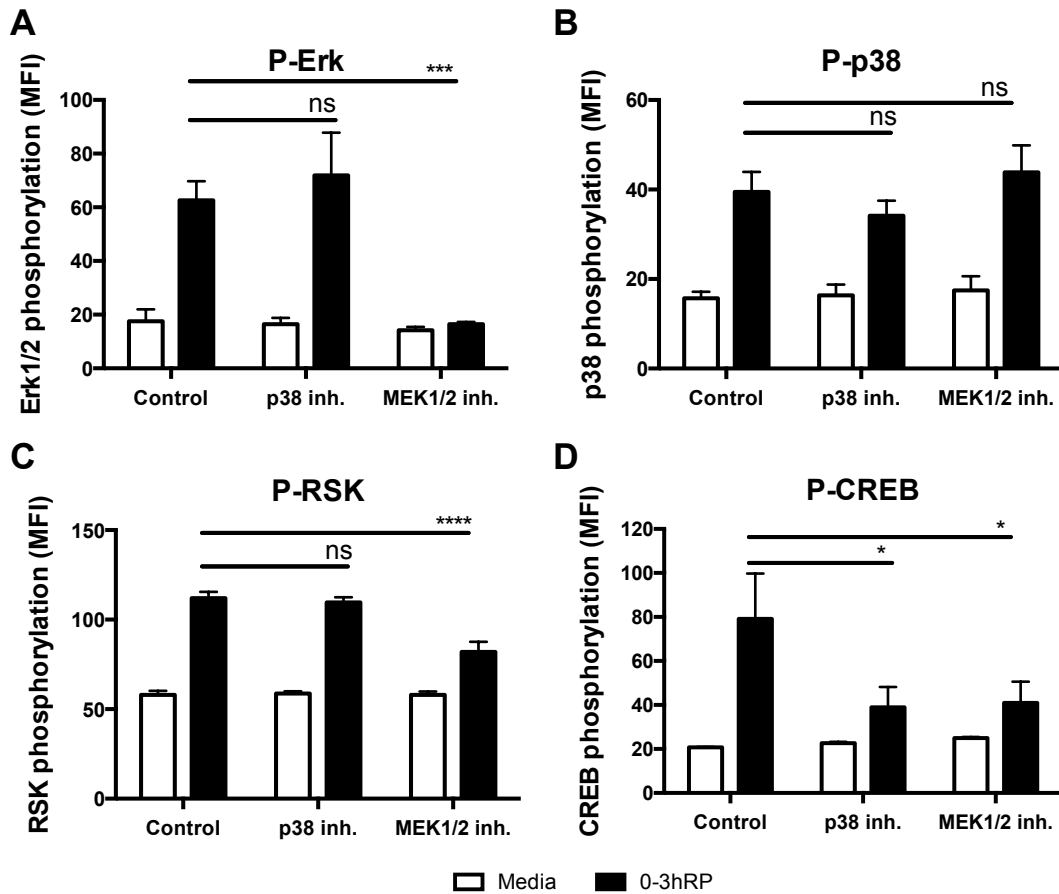


Figure 4.15 Chemical inhibition of MAPKs in BMMφs exposed to 0-3hRP reveals pathway hierarchy

BMMφs pre-treated for 2 hours with a MEK1/2 inhibitor (U0126 at 10μM) or a p38 inhibitor (SB203580 at 1μM) were exposed to 0-3hRP (50μg/ml) or left unstimulated (Media) for 30min. BMMφs were then labeled with antibodies against (A) P-Erk, (B) P-p38, (C) P-RSK and (D) P-CREB. Means +SEM of MFIs are given from three technical replicates. ANOVA and then Tukey's multiple comparisons test were performed to examine differences between the means of inhibitor treated stimulated cells compared to control (* = p<0.05; ** = p<0.01; *** = p<0.001; **** = p<0.0001; ns = p>0.05). Results are representative of three independent experiments.

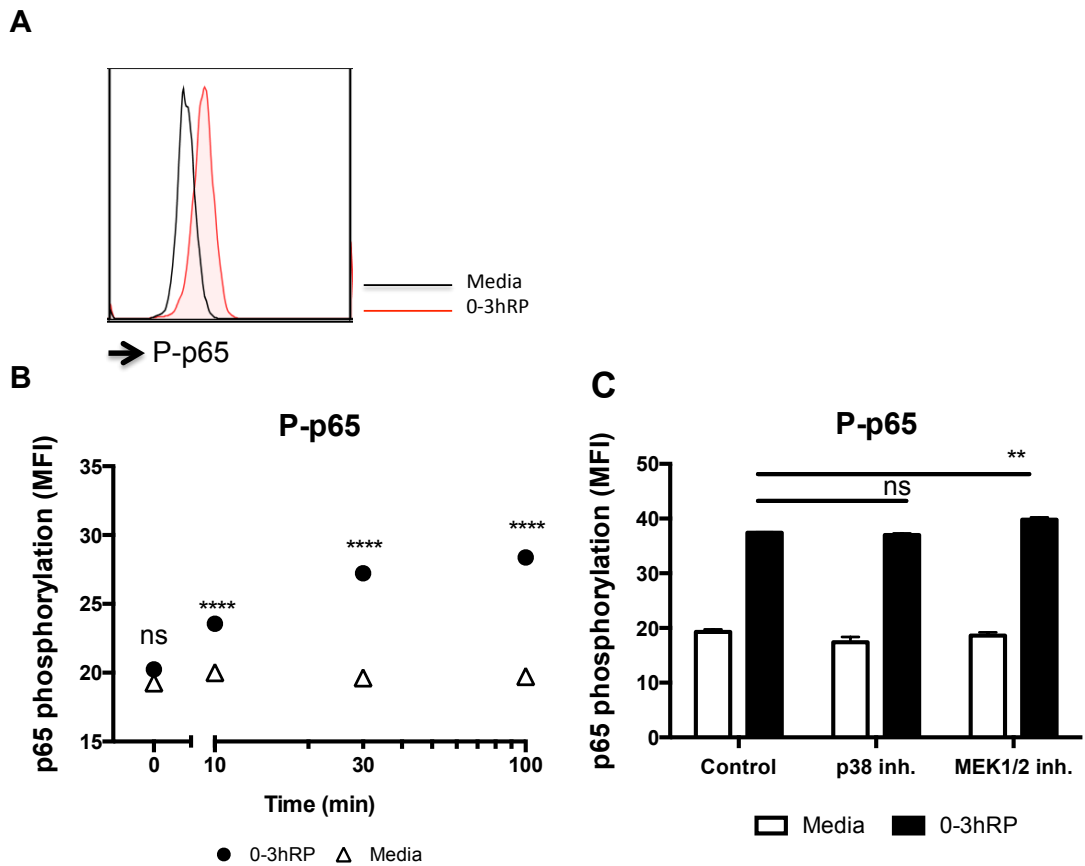


Figure 4.16 Activation of NF- κ B (p65) in BMM ϕ s exposed to 0-3hRP is not dependent on Erk1/2 or p38 signaling

BMM ϕ s were exposed to 0-3hRP (50 μ g/ml) or left un-stimulated (Media) for 0, 10, 30 and 100min and labeled with antibodies against phosphorylated p65 (P-p65). **(A)** Representative overlaid histogram after 30min of stimulation with 0-3hRP (red) or Media control (black) plus **(B)** means \pm SEM of MFIs for each time point are given from three technical replicates. Additionally, BMM ϕ s pre-treated for 2 hours with a MEK1/2 inhibitor (U0126 at 10 μ M) or a p38 inhibitor (SB203580 at 1 μ M) were exposed to 0-3hRP (50 μ g/ml) or left un-stimulated (Media) for 30min. **(C)** BMM ϕ s were then labeled with antibodies against P-p105. Means \pm SEM of percentages are given from three technical replicates. ANOVA and then Sidak's (B) or Dunnett's (C) multiple comparisons test were performed to examine differences between the means of stimulated cells compared to Media control at each time point (B) or between the means of inhibitor treated stimulated cells compared to control cells (** = $p < 0.01$; **** = $p < 0.0001$; ns = $p > 0.05$). Results are representative of three independent experiments.

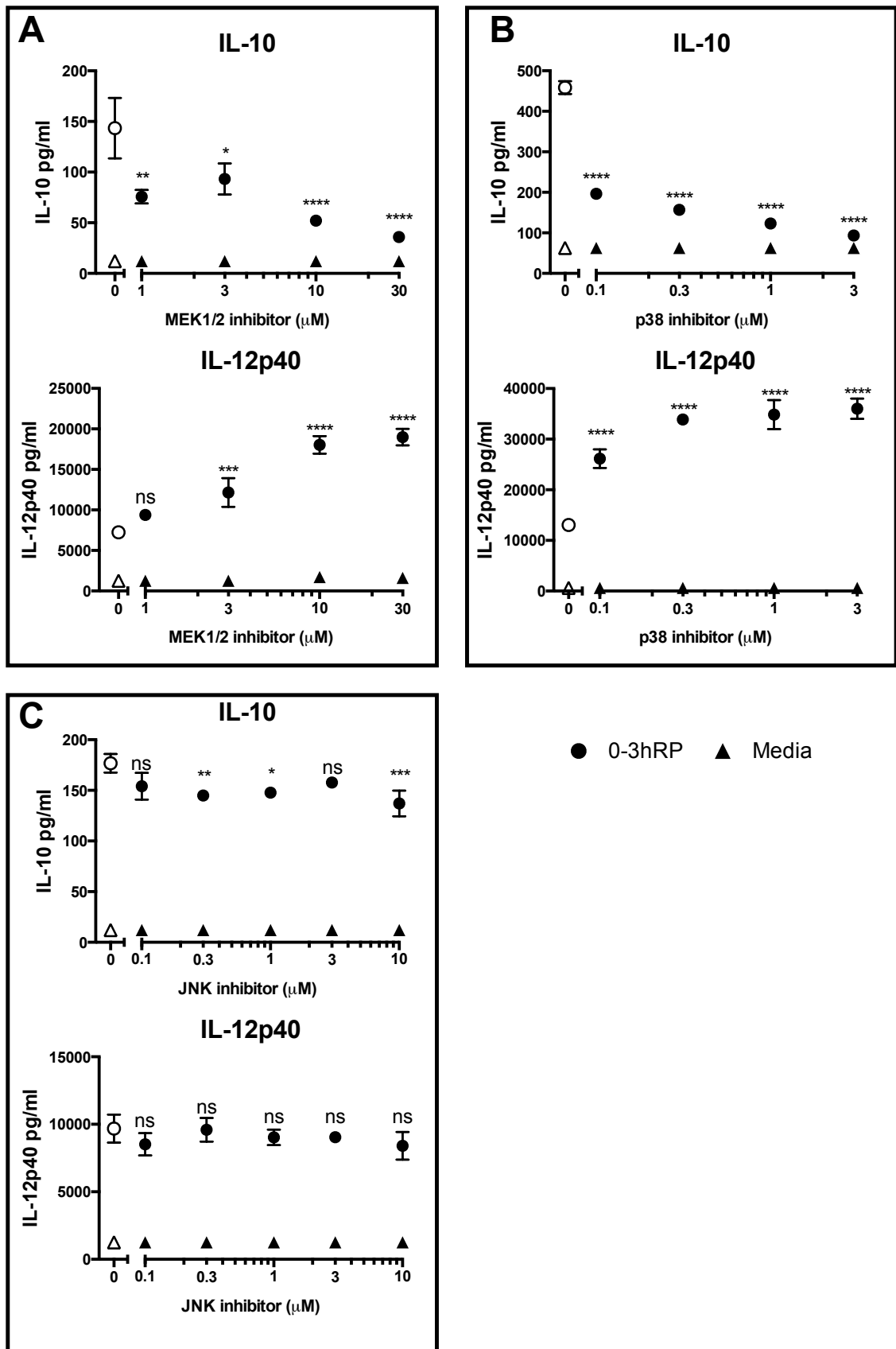


Figure 4.17 Chemical inhibition of signaling pathways regulates cytokine production in BMMφs exposed to 0-3hRP

BMMφs were pre-treated for 2 hours with increasing doses of (A) a MEK1/2 inhibitor (U0126), (B) a p38 inhibitor (SB203580) and (C) a JNK inhibitor (JNK inhibitor II) in separate experiments. BMMφs were then exposed overnight to 0-

3hRP (50 μ g/ml) or left un-stimulated (Media) and culture supernatants tested for IL-10 and IL-12p40 by ELISA. Means \pm SEM from three technical replicates are given. BMM ϕ s without pre-treatment with inhibitors are represented with open circles (0-3hRP) or open triangles (Media). ANOVA and then Dunnett's multiple comparisons test were performed to examine differences between the means of inhibited BMM ϕ s compared to untreated control (* = $p < 0.05$; ** = $p < 0.01$; *** = $p < 0.001$; **** = $p < 0.0001$; ns = $p > 0.05$). Results are representative of three independent experiments.

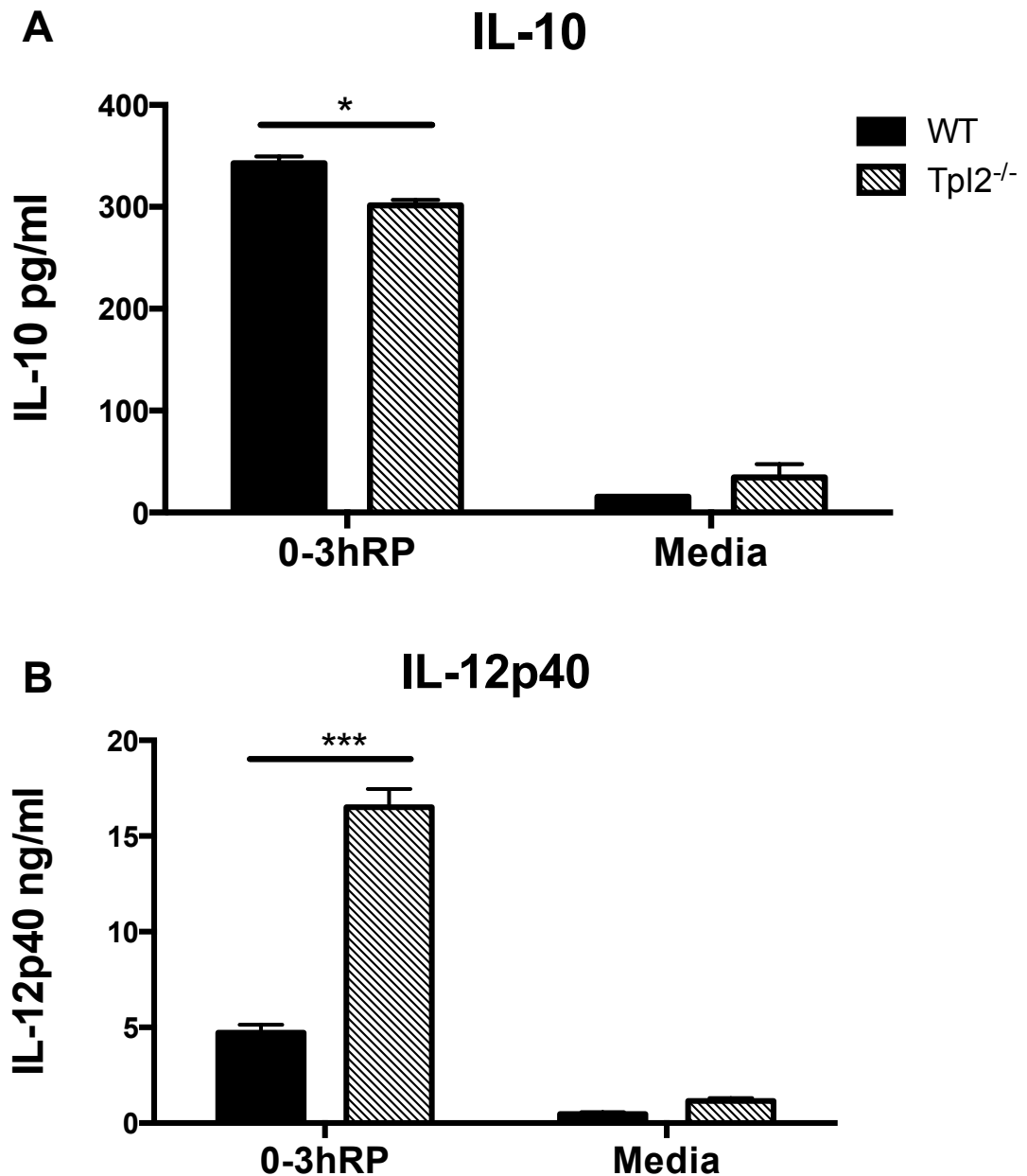


Figure 4.18 Tpl2 deficient BMMφs have reduced IL-10 production and increased IL-12p40 production in response to 0-3hRP

Supernatants from WT or Tpl2^{-/-} BMMφs exposed to 0-3hRP (50μg/ml) overnight or left un-stimulated (Media) were tested for the presence of (A) IL-10 and (B) IL-12p40. Means +SEM of three technical replicates are presented. ANOVA and then Dunnett's multiple comparisons test were performed to examine differences between the means of stimulated Tpl2 deficient cells compared to WT cells (* = p<0.05; *** = p<0.001). Results are representative of three independent experiments.

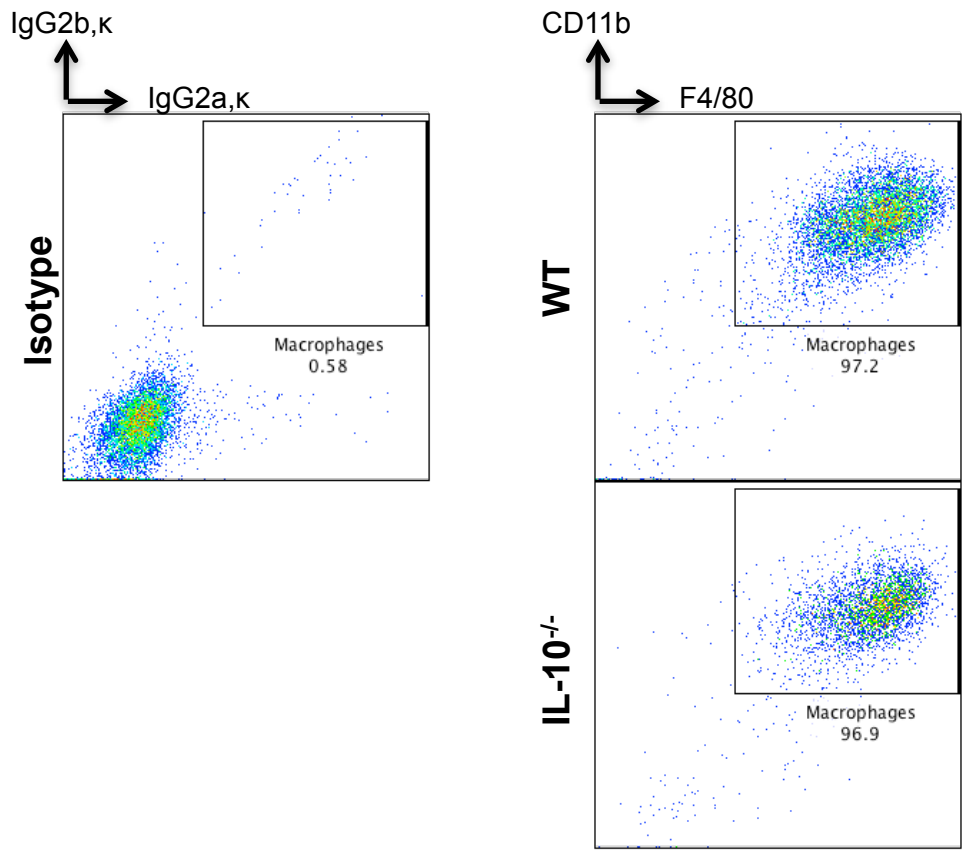


Figure 4.19 BMMφs deficient for IL-10 are similar to WT BMMφs
 WT or IL-10^{-/-} BMMφs were obtained after 7 days of culture of bone marrow from WT or IL-10 deficient mice. Differentiated cells were labeled with antibodies against F4/80 and CD11b. Representative flow plots of single live cells (based on a cell viability exclusion dye) are shown. Results are representative of three independent experiments.

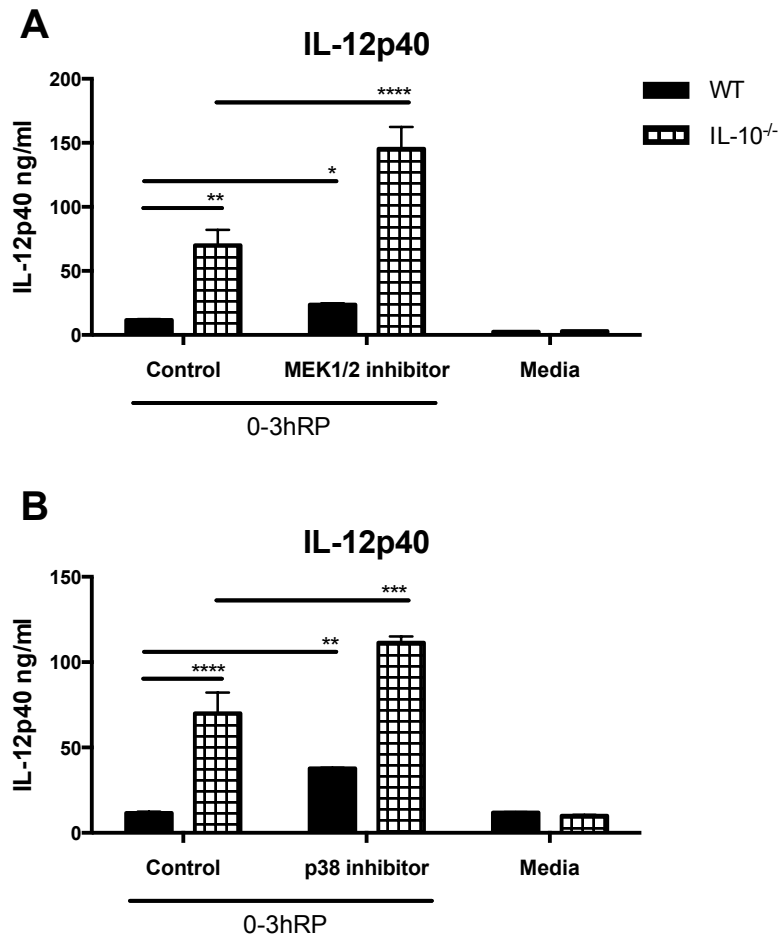


Figure 4.20 Chemical inhibition of signaling pathways regulates IL-12p40 production in IL-10^{-/-} BMMφs exposed to 0-3hRP

WT and IL-10^{-/-} BMMφs were pre-treated for 2 hours with (A) a MEK1/2 inhibitor (U0126 at 10μM) or (B) a p38 inhibitor (SB203580 at 1μM). BMMφs were then exposed overnight to 0-3hRP (50μg/ml) or left un-stimulated (Media) and culture supernatants tested for IL-12p40 by ELISA. Means +SEM from three technical replicates are given. ANOVA and then Dunnett's multiple comparisons test were performed to examine differences between the means of inhibitor treated stimulated cells compared to control cells within each strain, and between 0-3hRP stimulated WT and IL-10 deficient cells (* = p<0.05; ** = p<0.01; *** = p<0.001; **** = p<0.0001). Results are representative of three independent experiments.

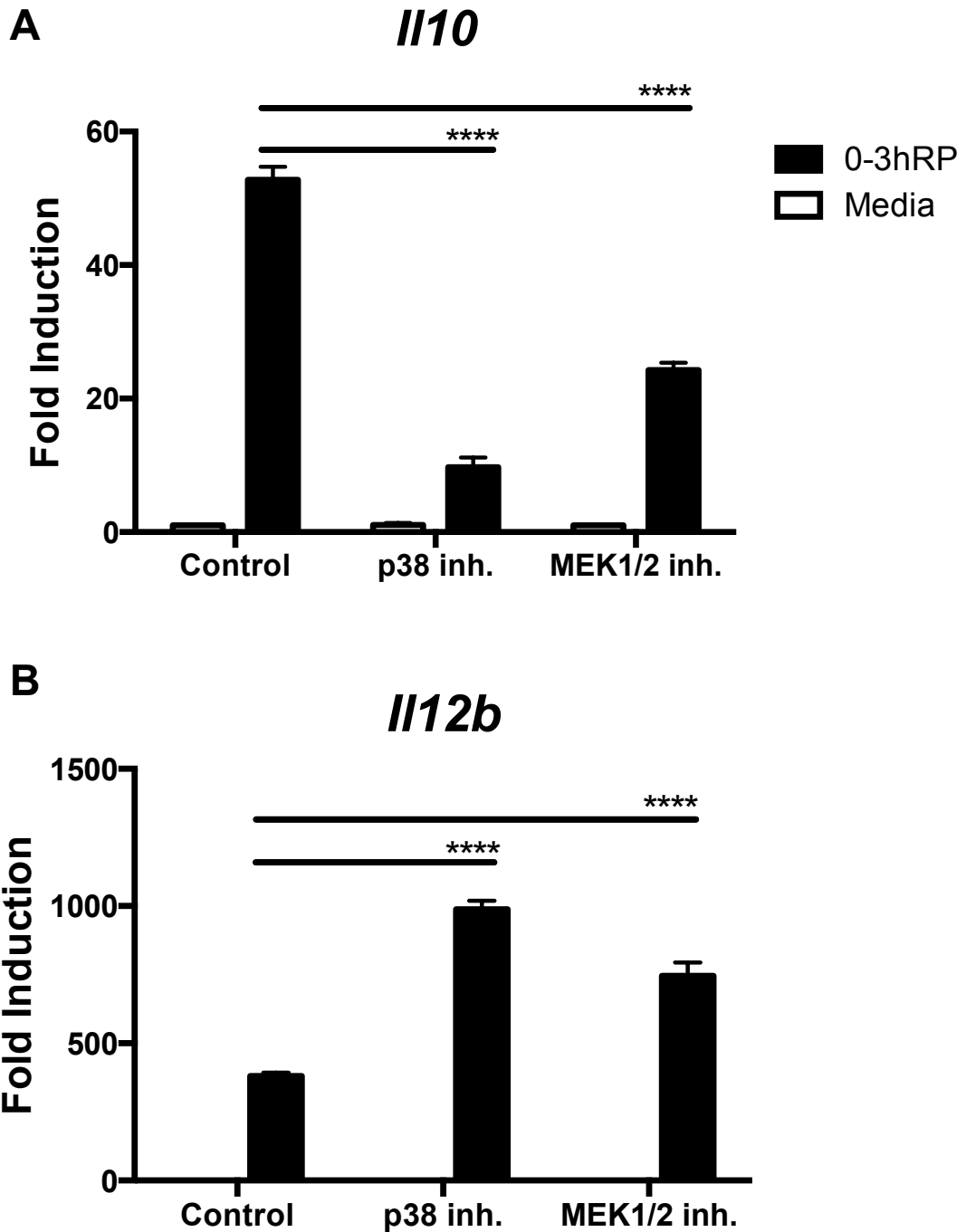


Figure 4.21 Chemical inhibition of signaling pathways regulates IL-10 and IL-12p40 mRNA in BMMφs exposed to 0-3hRP

BMMφs were pre-treated for 2 hours with a MEK1/2 inhibitor (U0126 at 10μM) or a p38 inhibitor (SB203580 at 1μM) and then exposed to 0-3hRP (50μg/ml) or left un-stimulated (Media). After 100min RNA was extracted and transcript levels of (A) *Il10* and (B) *Il12b* calculated using the delta delta Ct method with Media as reference and *Gapdh* as a HKG. Means +SEM are presented for three technical replicates. ANOVA and then Dunnett's multiple comparisons test were performed to examine differences between the means of inhibitor treated stimulated cells compared to control cells (**** = $p < 0.0001$). Results are representative of two independent experiments.

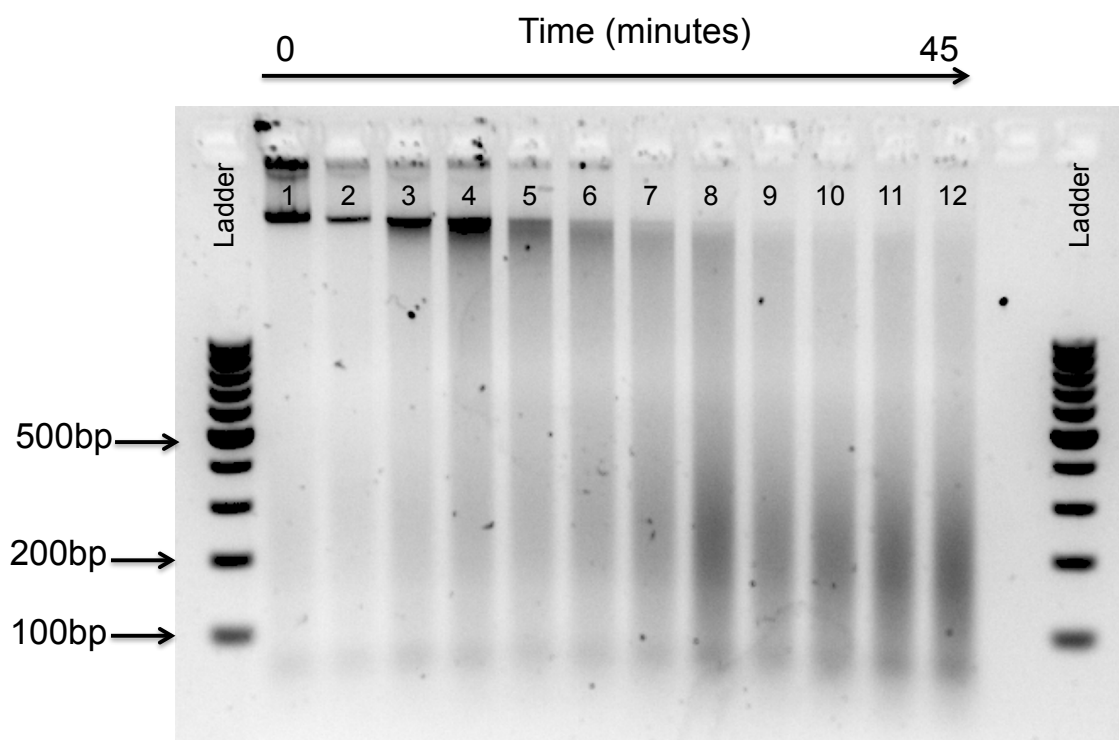


Figure 4.22 Fragment size of sonicated chromatin in BMMφs

Cross-linked chromatin from BMMφ lysates (lanes 1 and 2) was sonicated, taking aliquots every 5min (lanes 3-10). After 45min (lanes 11 and 12) cross-linking was reversed, proteins digested and DNA extracted and run on a 2% agarose gel.

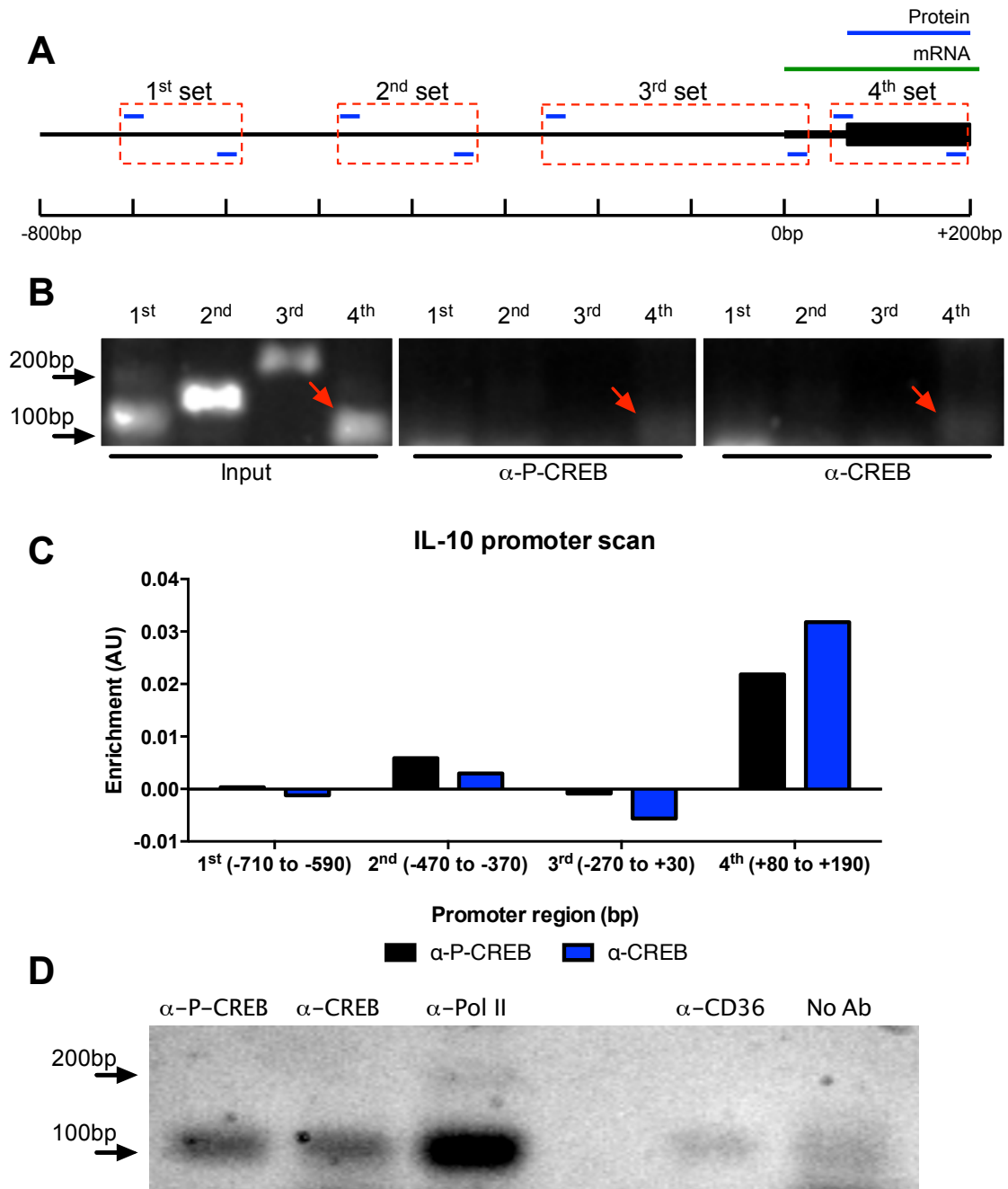


Figure 4.23 Phosphorylated CREB is recruited to the promoter of IL-10 in BMMφs exposed to 0-3hRP

Sonicated chromatin from BMMφs exposed for 30min to 0-3hRP (50μg/ml) was precipitated with antibodies against phosphorylated CREB (α-P-CREB), total CREB (α-CREB), RNA Polymerase II (α-Pol II), CD36 (α-CD36) and a no antibody control (No Ab). (A) Schematic of the IL-10 promoter depicting four regions investigated (red dashed boxes), the start of transcription (0bp, RNA in green) and the start of translation (+64bp, protein in blue) is given. (B) Input, α-P-CREB and α-CREB DNA purified from precipitates was analyzed by PCR for of the specified regions and (C) densitometry analysis of results. (D) α-P-CREB, α-CREB, α-Pol II, α-CD36 and No Ab DNA purified from precipitates were also analyzed by PCR for of the 4th region alone. Results are representative of 4 independent experiments.

5 Internalization of *S. mansoni* cercarial E/S products by BMM ϕ s is required for cytokine production

5.1 Introduction

Macrophages are phagocytic cells that constantly sample their environment by actively internalizing molecules and particles. That process, which is broadly referred to as endocytosis, is tightly regulated as it is energy costly (Watts, 2011), and can severely impact signaling pathways (Kagan & Iwasaki, 2012; Shilo & Schejter, 2011). To accommodate endocytosis, and thereafter traffic of the endosomes to the right compartments in the cells, actin polymerization and Ca⁺ signaling are required (Huotari & Helenius, 2011; Watts, 2011).

Macrophages employ several families of phagocytic receptors to take up pathogen-associated material from their surroundings (Baranova et al, 2012; Goodridge et al, 2011; Joshi et al, 2006; Kagan & Iwasaki, 2012), however some of these receptor families require opsonization of the material (with complement or antibodies) before they can be engaged (Joshi et al, 2006). Other receptor families, such as CLRs (i.e. MR) or scavenger receptors, can interact directly with the particles by binding to carbohydrate (Gringhuis et al, 2007; Martinez-Pomares et al, 2001; Svajger et al, 2011) or lipid (Baranova et al, 2012; Oury, 2014) moieties.

The coordinated process of endocytosis described above, involving remodeling of the cytoskeleton and the recruitment of several adaptor molecules, requires different signaling pathways (Traub, 2011; Watts, 2011). Recruitment of adaptor molecules in particular, is mediated by the phosphorylation of lipids on the membrane, making it accessible to different proteins. The PI3K family of kinases participate in the rearrangement of membrane structures and trafficking in cells by phosphorylating lipids on the cell membrane and endosomes (Stephens et al, 2002; Vanhaesebroeck et al, 2012). As such, this family of kinases contributes to triggering signaling pathways leading to phagocytosis and other processes.

Moreover, a growing body of literature has considered the possibility that TLRs, whose function has been traditionally restricted to the cell surface (i.e. TLR2 and TLR4), are in fact also able to direct signaling pathways from endosomal compartments (Aksoy et al, 2012; Bonham et al, 2014; Kagan & Iwasaki, 2012).

Indeed, some studies reveal the intricate interplay between TLRs on the surface and in the endosomes in the responses to bacterial products, as TLR4 (in the surface) and TLR9 (in the endosome) cooperated to direct signals triggered by these pathogens (Wolf et al, 2011). Furthermore, helminth products can sequester TLR components limiting their responses to other stimuli (Pineda et al, 2014).

S. mansoni cercarial E/S products have been shown to be internalized *in vitro* by bone marrow derived dendritic cells and macrophages, as well as *in vivo* by some cell populations in the skin, including F4/80⁺ macrophage-like cells (Paveley et al, 2009). The uptake of cercarial E/S products by macrophages is partly mediated by the MR (Paveley et al, 2011). Furthermore, the present study has shown that the protein levels of other phagocytic receptors, particularly CD36 and MSRI (see 3.3.3.3), are regulated in response to 0-3hRP.

Thus far, this work has made no reference to the ability of BMMφs to phagocytize 0-3hRP, or indeed how that process could affect the signaling pathways described, or whether TLR recognition of 0-3hRP occurs at the surface or inside the cell. In the current chapter, the impact of 0-3hRP uptake by BMMφs on MAPK activation and cytokine production will be established. As a result, a model of *S. mansoni* cercarial E/S products uptake by BMMφs and its links to the cytokine responses observed in macrophages will be proposed.

5.2 Chapter specific material and methods

5.2.1 Fluorescent labeling of *S. mansoni* cercarial E/S products

Cercarial E/S products were labeled by incubating the protein preparation for 3 hours with Alexa Fluor® 633 (Invitrogen) at a concentration of 1µg of dye per 100µg of 0-3hRP. Excess dye was removed by washing with PBS using a filter spin column with a molecular weight cut off of 5kDa at 4°C and 14000g for 1.5 hours. Flow through was removed at frequent intervals and more PBS was added to the mixture. Media control was treated in the same manner (i.e. 1µg of dye per a medium volume equivalent to that of 100µg 0-3hRP).

5.2.2 Uptake inhibitors

Cytochalasin D was purchased from SIGMA-ALDRICH. PI3K family inhibitor LY294002 was purchased from Cell Signalling Technology® and p110-δ inhibitor was kindly donated by Dr Klaus Okkenhaug, University of Cambridge, Cambridge, UK. Cell viability was checked via trypan blue staining and/or fluorescent live/dead discrimination dyes (see 2.4).

5.2.3 Confocal microscopy of BMMφs exposed to fluorescently labeled cercarial E/S products

BMMφs were obtained as described before (see 2.3) and allowed to adhere to glass cover slips for two hours in 24 well plates (1x10⁶ cells/well). BMMφs were exposed to labeled 0-3hRP (50µg/ml) for 100min and then washed twice with PBS. Cells were fixed on to cover slips for 20min with 4% PFA in PBS at room temperature, and then placed in 0.05% saponin 0.2% BSA (staining buffer) for 30min at room temperature.

Cover slips were incubated for 1 hour at room temperature with polyclonal rabbit antibody against EEA-1 (1:200, Abcam) in staining buffer. Cover slips were washed 3 times with staining buffer (5 min each) and then incubated for 1 hour with goat anti-rabbit Alexa Fluor® 547 (1:1000, Life Technologies) in staining buffer. Finally, cover slips were washed twice (5 min each) in staining buffer, adding DAPI (2µg/ml) (SIGMA) in the second washing step, and then rinsed with deionized water. Cover slips were mounted on glass slides using Prolong® Gold (Life Technologies) and sealed with nail varnish. Images were acquired using a Zeiss LSM 710 invert microscope using ZEN microscope software.

5.3 Results

5.3.1 BMM ϕ s internalize 0-3hRP

To test the ability of macrophages to internalize 0-3hRP, the preparation was linked to AF633 as described (5.2.1) and BMM ϕ s exposed to the labeled material for different periods of time in 96 well plates.

5.3.1.1 *0-3hRP is internalized by BMM ϕ s via endocytosis in an actin dependent manner.*

Flow cytometric analysis of stimulated BMM ϕ s revealed a rapid increase in the fluorescence of the cells, indicative of the amount of fluorescently labeled 0-3hRP bound to, or internalized, by them (Figure 5.1A). Thus, After 30min exposure to the preparation, more than a third of the cells (~34%) were positive for labeled 0-3hRP, which was significantly higher than media control (~0.04%, Figure 5.1A, $p < 0.0001$, significance in purple). Positive cells for labeled 0-3hRP could be quantified as a percentage within the positive gate based on Media (Figure 5.1B), or as an increase on MFI of the whole population (Figure 5.1C), which indicates the amount of labeled 0-3hRP bound, or internalized, by the cells. For both indicators, uptake of the labeled preparation was significant at all time points measured (Figure 5.1B & C, $p < 0.05-0.0001$, significance in purple).

To examine if BMM ϕ s were interacting with 0-3hRP on their surface through a receptor or if the parasite material was indeed internalized, microscopy of BMM ϕ s exposed to labeled 0-3hRP was employed. Confocal microscopy of BMM ϕ s after 60min exposure to labeled 0-3hRP (Figure 5.1D) confirmed internalization of 0-3hRP as it was contained in discreet compartments (Figure 5.1D, red punctae) within the cell and not on the outer plasma membrane. This was further confirmed by z-stack imaging of cells, with 0-3hRP containing vesicles seen at the level of the nucleus of the cell (data not shown). Moreover, plasma membrane staining is not seen as punctae, but rather as elongated arcs. Similar, patterns of internalization were observed at 30min, although the amounts detected were less abundant (data not shown). At least a portion of 0-3hRP remained in early endosomes, as evidenced by co-localization with EEA-1 (Figure 5.1D, white arrow) further confirming that 0-3hRP is taken up by BMM ϕ s via endocytosis.

Treatment with Cytochalasin D (CytD), an actin polymerization inhibitor, revealed that the process of 0-3hRP uptake required actin remodeling. This inhibitor prevented 0-3hRP uptake from as early as 10min after exposure to the secretions (Figure 5.1C, $p < 0.05$, significance in black), but also at all other time points measured (Figure 5.1A, B & C, $p < 0.001-0.0001$, significance in black). Media control with CytD-treated BMM ϕ s was not different from Media control in un-treated cells (data not shown). As stated above, differences in percentages (Figure 5.1B) or MFI (Figure 5.1C) quantify different aspects of the uptake. As a percentage, a significant proportion of CytD-treated BMM ϕ s internalized labeled 0-3hRP after 300min (Figure 5.1B, ~80%), however, the amount of labeled material contained in these BMM ϕ s was reduced more than ten-fold compared to un-treated cells (Figure 5.1C, MFI of 450 vs. 40 in the absence vs. presence of CytD respectively).

5.3.1.2 *0-3hRP uptake by BMM ϕ s depends partly on PI3K signaling*

Kinases of the PI3K family are well known mediators of trafficking and endocytosis. Treatment of BMM ϕ s with PI3K family inhibitor LY294002 (25 μ M) was enough to significantly limit the uptake of labeled 0-3hRP at 30 min (Figure 5.2A). The percentage of 0-3hRP positive cells was significantly lower at 30 and 100min (Figure 5.2B, $p < 0.0001$, significance in black), although not at 300min ($p > 0.05$, significance in black). LY294002 only treatment was not different from Media control (data not shown). The MFI of the cell population incubated with labeled 0-3hRP plus LY294002 inhibitor was reduced at 30min (36 in untreated controls vs. 28 in treated cells) but not significantly. However, the MFI of treated BMM ϕ s greatly reduced at 100min, but also at 300min (Figure 5.2C, $p < 0.0001$, significance in black), indicating that even if all cells contained some 0-3hRP, as evidenced by the percentage of positive cells, the amount of material taken up in the presence of inhibitor was still significantly reduced compared to uninhibited BMM ϕ s (~2-fold reduction).

5.3.2 MAPK activation in BMM ϕ s exposed to 0-3hRP is partly dependent on internalization

As reported in chapter IV, BMM ϕ s employ TLR2 and TLR4 to activate MAPKs in response to 0-3hR, however, as discussed in the introduction to this chapter, TLR signaling can originate from activation of receptors on the cell surface, or from within endosomes. By using CytD to limit the amount of 0-3hRP

internalized by BMM ϕ s, the impact of this process on MAPK activation was addressed.

Levels of P-Erk were greatly reduced after exposure to 0-3hRP in CytD-treated BMM ϕ s compared to untreated control (Figure 5.3, $p < 0.0001$). Slight differences observed between Media and cells treated with CytD only are unlikely to be biologically relevant, as potent stimulation with 0-3hRP induces a much greater response.

Equally significant reductions were observed with P-p38 in CytD-treated BMM ϕ s exposed to 0-3hRP compared to un-treated controls (Figure 5.4, $p < 0.0001$). Similarly, P-CREB levels in CytD-treated BMM ϕ s exposed to 0-3hRP were significantly reduced compared to un-treated cells (Figure 5.5, $p < 0.0001$). Consequently, internalization of 0-3hRP is required for complete activation of MAPK, suggesting that TLR recognition may be occurring within the endosomes.

As PI3K inhibition had an effect on the internalization of 0-3hRP by BMM ϕ s (Figure 5.2), its effect on MAPK activation was tested. Similar to CytD, levels of P-Erk (Figure 5.6), P-p38 (Figure 5.7) and P-CREB (Figure 5.8) were greatly reduced in response to 0-3hRP in BMM ϕ s where the PI3K family inhibitor LY294002 was used. To address which protein in the PI3K family might be involved in this process, a specific inhibitor for the catalytic subunit of the PI3K family p110- δ (IC87114) was used. As before, levels of P-Erk (Figure 5.6), P-p38 (Figure 5.7) and P-CREB (Figure 5.8) were significantly reduced ($p < 0.0001$) in IC87114 treated BMM ϕ s exposed to 0-3hRP compared to un-treated cells.

This evidence further confirms the links between these Erk, p38 and CREB (see chapter IV), however, it highlights the role of internalization on the activation of these MAPKs, and emphasizes the possibility that 0-3hRP-TLR binding occurs in the endosome of macrophages.

5.3.3 IL-10 and IL-12p40 production is dependent on internalization of 0-3hRP by BMM ϕ s

MAPK activation in BMM ϕ s exposed to 0-3hRP is linked to cytokine production (4.3.5). As blocking internalization of cercarial E/S products impairs that

activation, it was possible that production of IL-10 and IL-12p40 would also be affected.

In line with the inhibition of MAPK activation, CytD treatment of BMMφs exposed to 0-3hRP significantly reduced the production of IL-10 and IL-12p40 compared to controls (Figure 5.9, $p < 0.001-0.0001$). However, increasing doses of PI3K family inhibitor LY294002 or p110- δ inhibitor IC87114 only affected IL-10 production (Figure 5.10A & B), which was significantly impaired. IL-12p40 production (Figure 5.10A & B), was neither enhanced, as seen with the inhibition of other kinases (4.3.5.1), nor reduced as detected in the presence of CytD (Figure 5.9). Thus, 0-3hRP internalization is required for complete activation of MAPKs and cytokine production.

5.4 Discussion

5.4.1 Uptake of 0-3hRP by BMMφs requires actin polymerization and intact PI3K signaling

Previous studies have shown that *S. mansoni* E/S products are taken up by macrophages in the skin and by BMMφs *in vitro* (Paveley et al, 2009). Indeed, here it was established that the uptake of 0-3hRP by BMMφs is a rapid process that reaches its zenith after 300min of exposure to the labeled secretions. It is clear, from the MFI measurement, that as early as 10min after stimulation, the whole population of BMMφs contains traces of the material. Nonetheless, after only 30min, a substantial amount of 0-3hRP can be found inside the cells. This coincides with the peak in the activation of several MAPKs reported earlier (see 4.3.3), as well as the earliest detection of IL-10 mRNA in response to 0-3hRP (see 3.3.5.2).

Confocal microscopy of stimulated BMMφs revealed that labeled 0-3hRP was indeed taken by cells into small (2μm) well-defined vesicles located in the cytoplasm, an observation confirmed by 3 dimensional imaging of the cells (data not shown). Some of those vesicles were positive for early endosomal marker EEA-1 after 60min of exposure to 0-3hRP, confirming the cytoplasmic localization of 0-3hRP and its trafficking through endosomes.

This uptake process requires both actin polymerization, as revealed following inhibition with cytochalasin D, and PI3K signaling, as shown by inhibition with a PI3K family inhibitor. Potential toxic effects of the inhibitors employed were partly discarded by checking cell viability via microscopy with trypan blue and via flow cytometry with live/dead discrimination dyes (data not shown). Responsiveness of inhibited BMMφs to stimuli independent from the pathways targeted by the drugs would be required to completely rule out the toxic effects of these inhibitors. However, concentrations used were always in line with published doses (Paveley et al, 2009; Vlahos et al, 1994). Moreover, PI3K inhibition did not prevent IL-12p40 production by BMMφs, meaning cells were not only viable but also able to produce cytokines. Both actin polymerization and PI3K activity require ATP, therefore it is likely that cell surface receptors in BMMφs orchestrate the uptake of 0-3hRP as it will be energetically costly. *S. mansoni* egg antigens have been shown to be internalized by C-type lectin receptors (Everts et al, 2012; van Liempt et al, 2007). Cercarial E/S products

are known for being highly glycosylated (Jang-Lee et al, 2007) and partly require the MR for internalization (Paveley et al, 2011). Earlier, evidence of other phagocytic receptors (CD36 and MSRI) that were regulated by 0-3hRP-stimulation was presented (see 3.3.3.3), so their involvement in the uptake of 0-3hRP warrants further investigation.

0-3hRP is a complex mixture of proteins, some of which are glycosylated and potentially linked to lipids as lipoproteins. It would therefore be unsurprising that more than one of the diverse mechanisms described above is involved in the uptake of this material. Certainly, the macrophage MR is partly involved, despite not having a cytoplasmic signaling domain, but CD36 and MSRI, both scavenger receptors with lipid affinity, which trigger signaling pathways, could play an important role.

5.4.2 MAPK activation and cytokine production in BMMφs exposed to 0-3hRP is dependent on uptake

In this study, *S. mansoni* cercarial E/S products have been shown to affect multiple aspects of macrophage biology, with particular attention given to the production of IL-10. Others have shown that 0-3hRP modulates its trafficking through BMMφs (Paveley et al, 2009), and it is well established that TLR ligands can affect the maturation of phagosomes (Kagan & Iwasaki, 2012). Consequently, the signaling pathways triggered in macrophages as a result of its uptake warranted examination.

Inhibition of uptake using cytochalasin D resulted in significant reductions in the activation of Erk1/2, p38 and CREB. Previously, it was determined that TLR2 and TLR4, both abundantly available in the surface of BMMφs, were responsible for the activation of these signals (see 4.3.3.3). From the evidence presented in this chapter, it is possible to conclude that a significant portion of the activation of MAPKs in BMMφs occurs as a consequence of 0-3hRP uptake, and that these molecules could be recognized in endosomes by TLR2 or TLR4. As mentioned in the introduction of this chapter, the importance of TLR4 signaling from the endosomes is a nascent field, and similar reports for TLR2 are not available. Thus, these findings open up the exciting possibility that TLR2, as well as TLR4, have functional roles in the recognition of 0-3hRP in endosomal compartments. Moreover, the kinetics of activation of MAPKs and production of IL-10 support this hypothesis. 0-3hRP is evident within cells from

10 minutes after exposure, and is abundant in BMM ϕ s at 30min, when MAPKs signals peak and IL-10mRNA is detected. Thus 0-3hRP binding TLRs in the endosomes is a possibility that warrants further examination. Genetic tools that modify the recruitment of TIRAP to the cell membrane, affecting MyD88 interaction with cell surface TLRs, would be ideal to address this question.

Another possibility is that the signaling cascades triggered by TLR2 and TLR4 are sustained by another receptor in an endosomal compartment, as reported by other with respect to a TLR4-TLR9 interplay (Wolf et al, 2011). Of the two possibilities, the first one is more likely, as at least TLR4 has been shown to signal from endosomes and accumulate in phagolysosomes (Kagan & Iwasaki, 2012), however, the use of macrophages deficient in endosomal TLRs would be necessary to rule out any potential contribution from these receptors.

Blocking 0-3hRP using Cytochalasin D also resulted in a significant reduction in the production of IL-10 and IL12p40. This reduction is in line with the observed reduction in MAPK activation, and congruent with the hypothesis that TLR binding to 0-3hRP occurs in endosomal compartments. Moreover, experiments performed with LPS stimulation of BMM ϕ s showed that Cytochalasin D inhibition also resulted in IL-12p40 reduction (data not shown), further supporting the evidence that highlights the role of uptake/endosomal recognition of PAMPs.

Unlike blocking actin polymerization, PI3K inhibition not only prevents phagocytosis, but also impacts the recruitment of adaptor molecules to different cellular compartments (Vanhaesebroeck et al, 2012). In fact, inhibition of p110- δ has been shown to prevent TLR4 internalization and enhance its ability to signal from the cell surface (Aksoy et al, 2012), and PI3K signaling is required for adequate recruitment of TIRAP to TLRs (Bonham et al, 2014). Consequently, the observed effects by inhibiting PI3K signaling in BMM ϕ s exposed to 0-3hRP are not only a result of limiting its uptake, despite this being a consequence of inhibition. It is necessary to assume, in light of the mentioned literature, that the recruitment of adaptor molecules is also affected. Thus, the significant reductions in phosphorylation of Erk1/2, p38 and CREB could be a consequence of the reduced uptake, of blocking TLR receptor trafficking, of blocking TIRAP-MyD88 recruitment, or a combination of the three.

To shed light on ambiguity of the interpretation of the results of this inhibition, it is pertinent to observe the effects of chemical inhibition on cytokine production. IL-10 was greatly impaired by PI3K inhibition in BMMφs exposed to 0-3hRP, whereas IL-12p40 was largely unaffected. As P-Erk, P-p38 and P-CREB are also greatly reduced, a decrease of IL-10 is expected based on previous inhibition of MAPK (see 4.3.5.1), as it is indeed the case with PI3K inhibition. However, earlier findings suggest that IL-12p40 would increase if the levels of MAPKs were reduced. In the context of PI3K inhibition, IL-12p40 in response to 0-3hRP remains unchanged. Nonetheless, blocking 0-3hRP uptake with Cytochalasin D, reduces the amount of IL-12p40. Consequently, PI3K inhibition is having a double effect on BMMφs. First, it is blocking the uptake of 0-3hRP, but to a lesser extent than Cytochalasin D, which results in a reduction of both IL-10 and IL-12p40. Second, PI3K inhibition results in the reduction in MAPKs due to the defect in uptake of 0-3hRP but also by an additional mechanism, further decreasing the levels of IL-10. However, this boosts IL-12p40 production back to the levels of uninhibited cells.

Finally, the maturation of endosomes during 0-3hRP trafficking was not addressed. Earlier reports suggest that endosome maturation is affected by 0-3hRP-stimulation (Paveley et al, 2009) and uptake of *E. coli* particles is indeed affected by exposure to *S. mansoni* cercarial products (data not shown). The acidification of lysosomes, which could also be regulated by 0-3hRP-stimulation was not studied, but could be addressed using chemical inhibitors (i.e. bafilomycin).

5.5 Summary

S. mansoni cercarial E/S products are recognized by BMMφs via one or more phagocytic receptors, which leads to their internalization in an actin dependent manner. This process is also partly dependent on intact PI3K signaling. Both from the surface of the cell, but also from an endosomal compartment, O-3hRP binds to TLR2 and TLR4, leading to the activation of several MAPKs. The activation of those signaling pathways requires the recruitment of MyD88 and other adaptor molecules, which are likely to be affected by the inhibition of PI3K. Activated MAPKs orchestrate the production of IL-10, whilst limiting the induction of IL-12p40.

In the next chapter, evidence for the production of IL-10 from macrophages at the skin site of *S. mansoni* skin invasion will be sought.

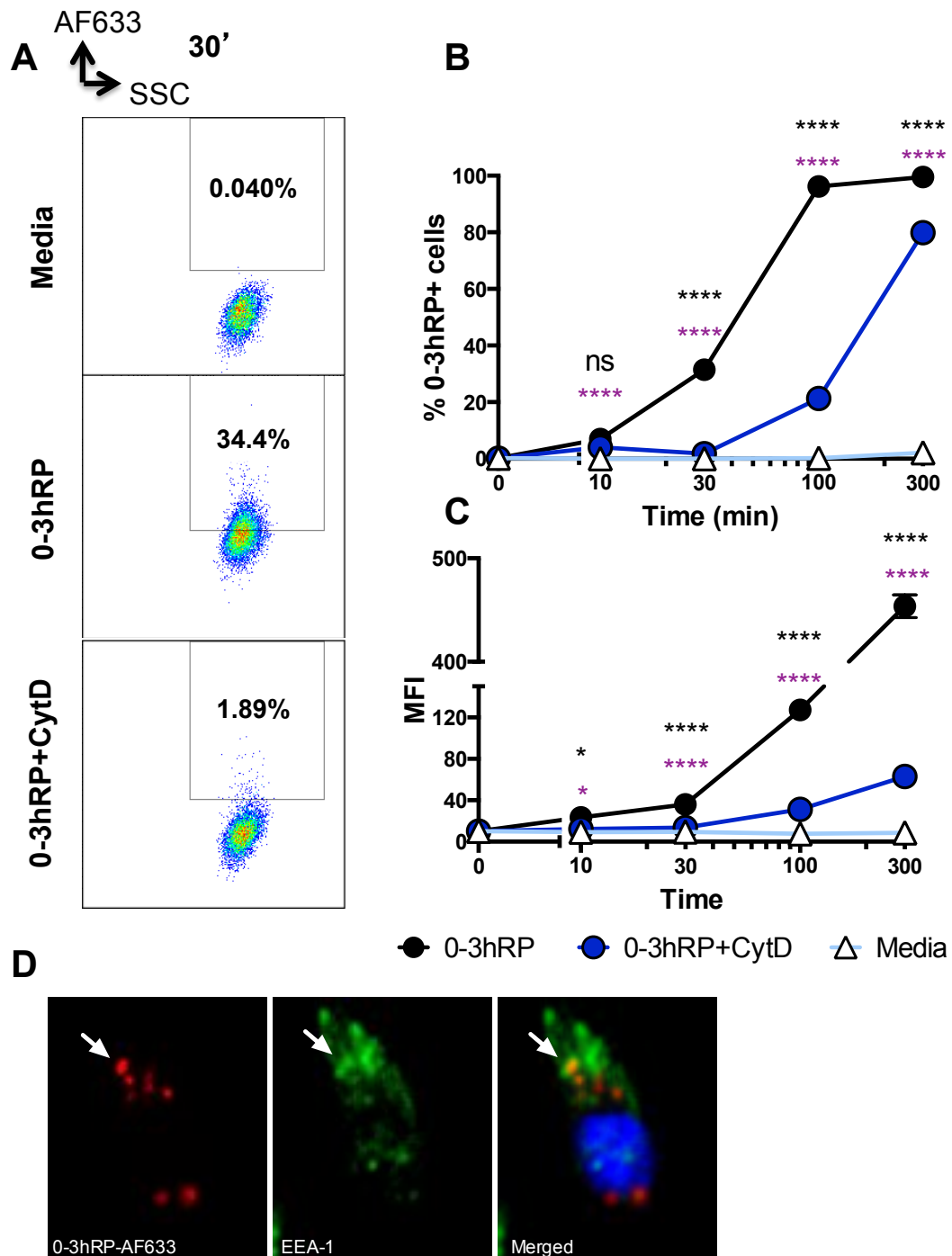


Figure 5.1 0-3hRP uptake by BMMφs requires actin polymerization

BMMφs pre-treated for 2 hours with Cytochalasin D (10μg/ml), washed and then were exposed to labeled 0-3hRP (50μg/ml) or Media control for different lengths of time. (A) Representative flow plots at 30min, (B) means ±SEM of percentages and (C) mean MFI ±SEM are given from three technical replicates. (D) A representative confocal image of a BMMφ containing labeled 0-3hRP (red) within EEA-1 positive endosomes (green) is also shown after 60min exposure to 0-3hRP. ANOVA and then Sidak's multiple comparisons test were performed to examine differences between the means of untreated BMMφs exposed to 0-3hRP compared to inhibitor treated BMMφs (significance in black) or compared to Media controls (significance in purple) at every time point (* = p<0.05; **** = p<0.0001; ns = p>0.05). Results are representative of three independent experiments.

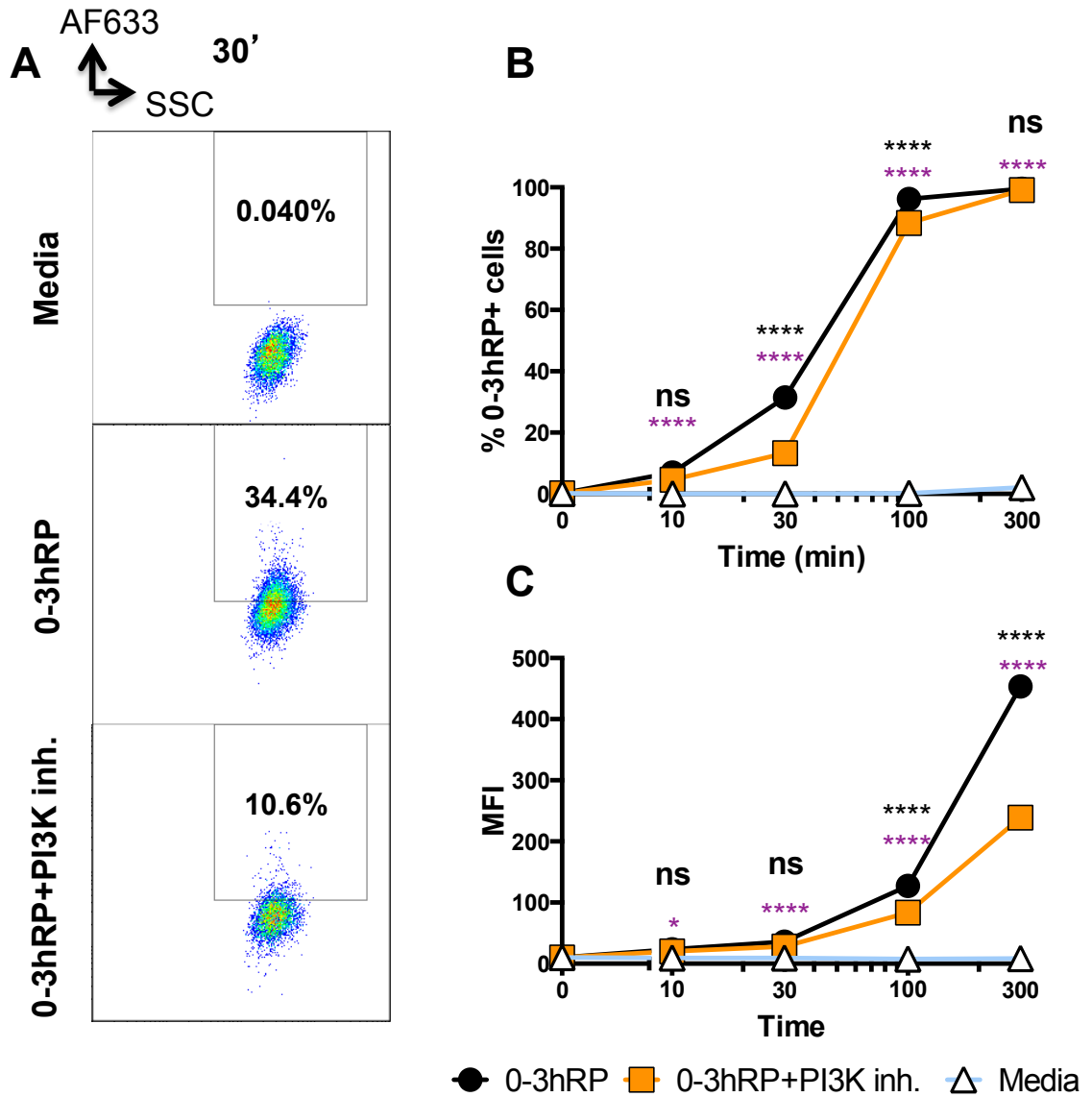


Figure 5.2 PI3K inhibition of BMMφs limits uptake of 0-3hRP

BMMφs pre-treated for 2 hours with a PI3K family inhibitor (LY294002 at 25μM) were exposed to labeled 0-3hRP (50μg/ml) or Media control for different lengths of time. (A) Representative flow plots at 30min, (B) means ±SEM of percentages and (C) mean MFI ±SEM are given from three technical replicates. ANOVA and then Sidak's multiple comparisons test were performed to examine differences between the means of untreated BMMφs exposed to 0-3hRP compared to inhibitor treated BMMφs (significance in black) or compared to Media controls (significance in purple) at every time point (* = p<0.05; **** = p<0.0001; ns = p>0.05). Results are representative of three independent experiments.

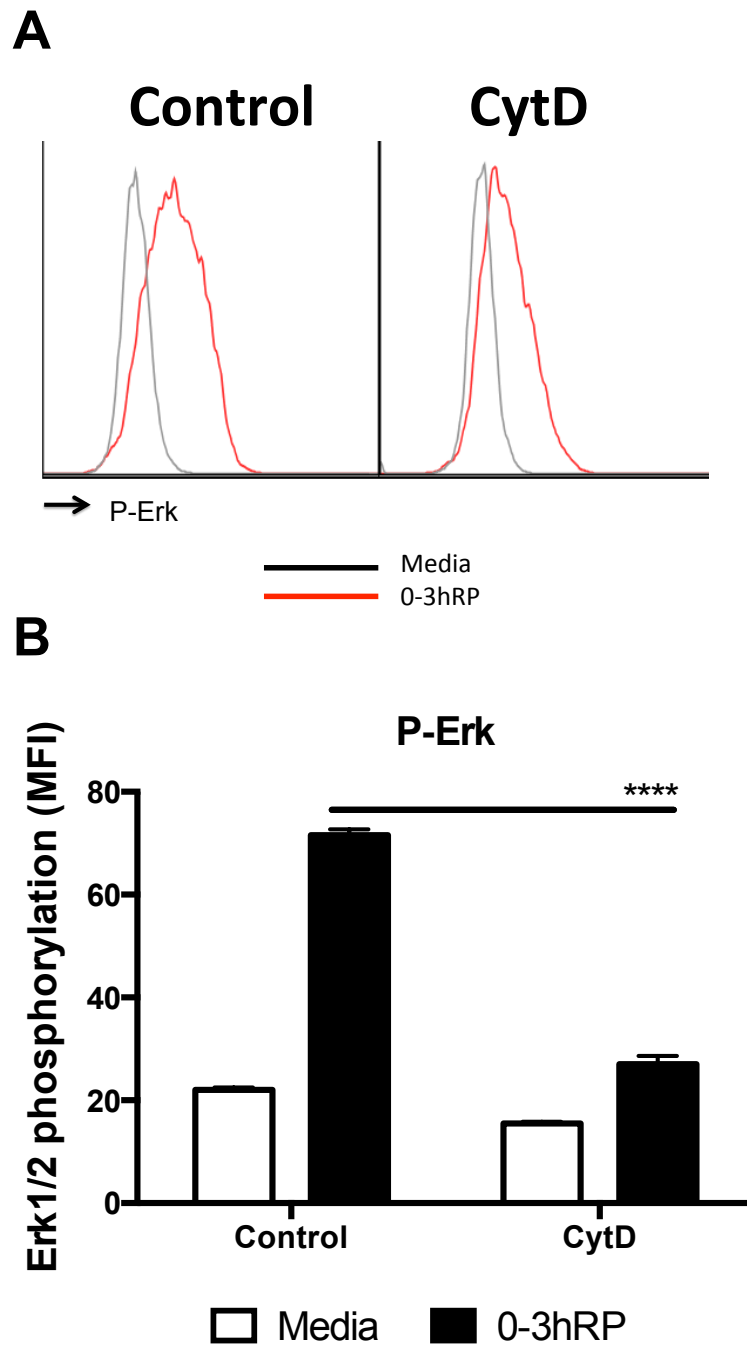


Figure 5.3 Chemical inhibition of uptake in BMMφs exposed to 0-3hRP limits Erk1/2 phosphorylation

BMMφs pre-treated for 2 hours with Cytochalasin D (10μg/ml) were exposed to 0-3hRP (50μg/ml) or left un-stimulated (Media) for 30min. BMMφs were then labeled with antibodies against P-Erk. **(A)** Representative overlaid histograms of 0-3hRP (red) or Media (black) samples and **(B)** means + SEM of MFIs are given from three technical replicates. ANOVA and then Dunnett's multiple comparisons test were performed to examine differences between the means of inhibitor treated stimulated cells compared to control cells (**** = $p < 0.0001$). Results are representative of three independent experiments.

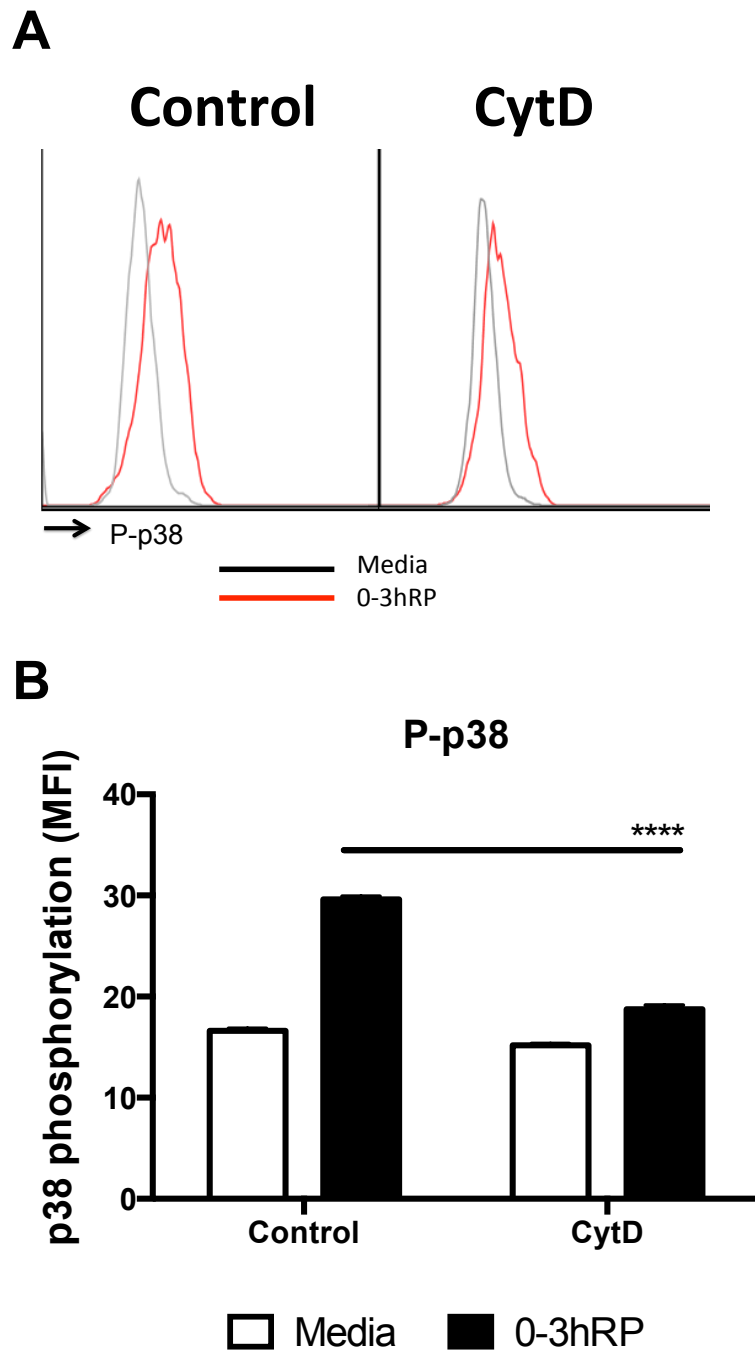


Figure 5.4 Chemical inhibition of uptake in BMMφs exposed to 0-3hRP limits p38 phosphorylation

BMMφs pre-treated for 2 hours with Cytochalasin D (10μg/ml) were exposed to 0-3hRP (50μg/ml) or left un-stimulated (Media) for 30min. BMMφs were then labeled with antibodies against P-p38. **(A)** Representative overlaid histograms of 0-3hRP (red) or Media (black) samples and **(B)** means + SEM of MFIs are given from three technical replicates. ANOVA and then Dunnett's multiple comparisons test were performed to examine differences between the means of inhibitor treated stimulated cells compared to control cells (**** = $p < 0.0001$). Results are representative of three independent experiments.

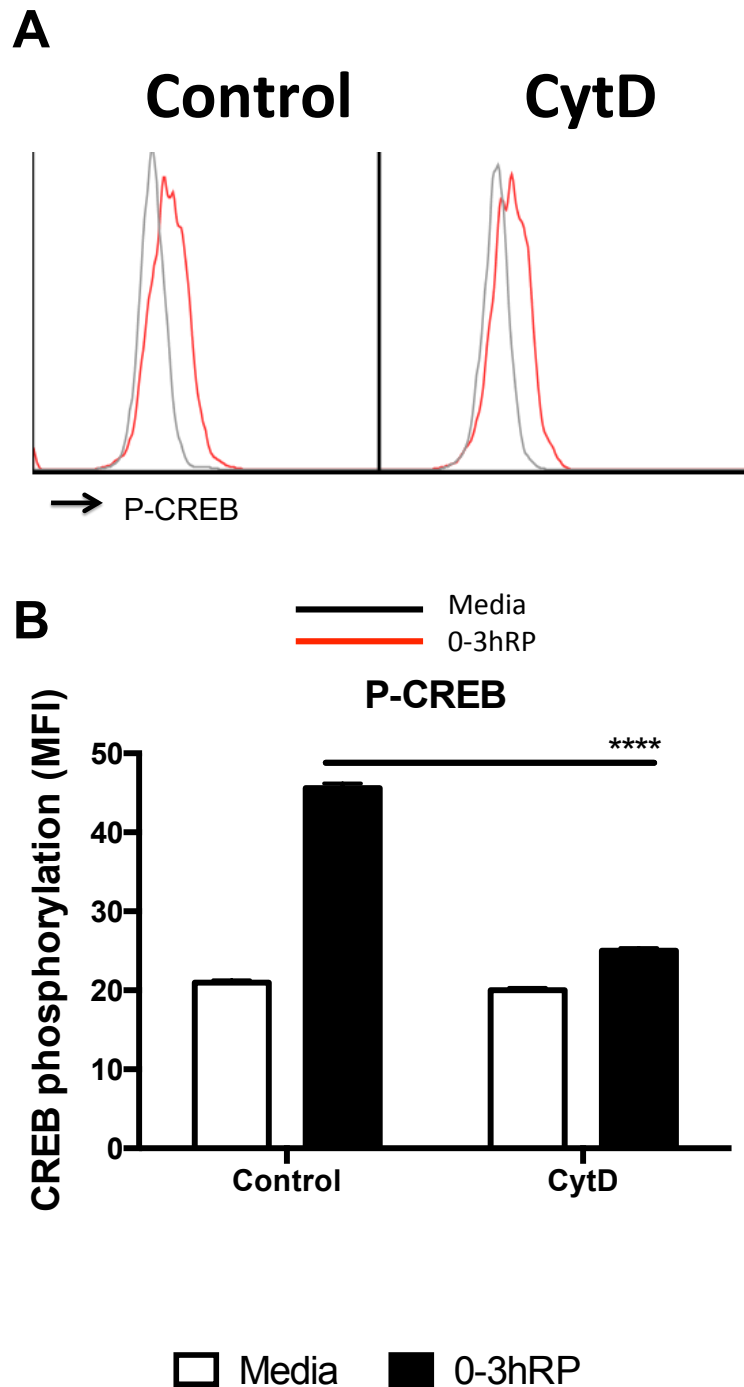


Figure 5.5 Chemical inhibition of uptake in BMMφs exposed to 0-3hRP limits CREB phosphorylation

BMMφs pre-treated for 2 hours with Cytochalasin D (10μg/ml) were exposed to 0-3hRP (50μg/ml) or left un-stimulated (Media) for 30min. BMMφs were then labeled with antibodies against P-CREB. (A) Representative overlaid histograms of 0-3hRP (red) or Media (black) samples and (B) means + SEM of MFIs are given from three technical replicates. ANOVA and then Dunnett's multiple comparisons test were performed to examine differences between the means of inhibitor treated stimulated cells compared to control cells (**** = $p < 0.0001$). Results are representative of three independent experiments.

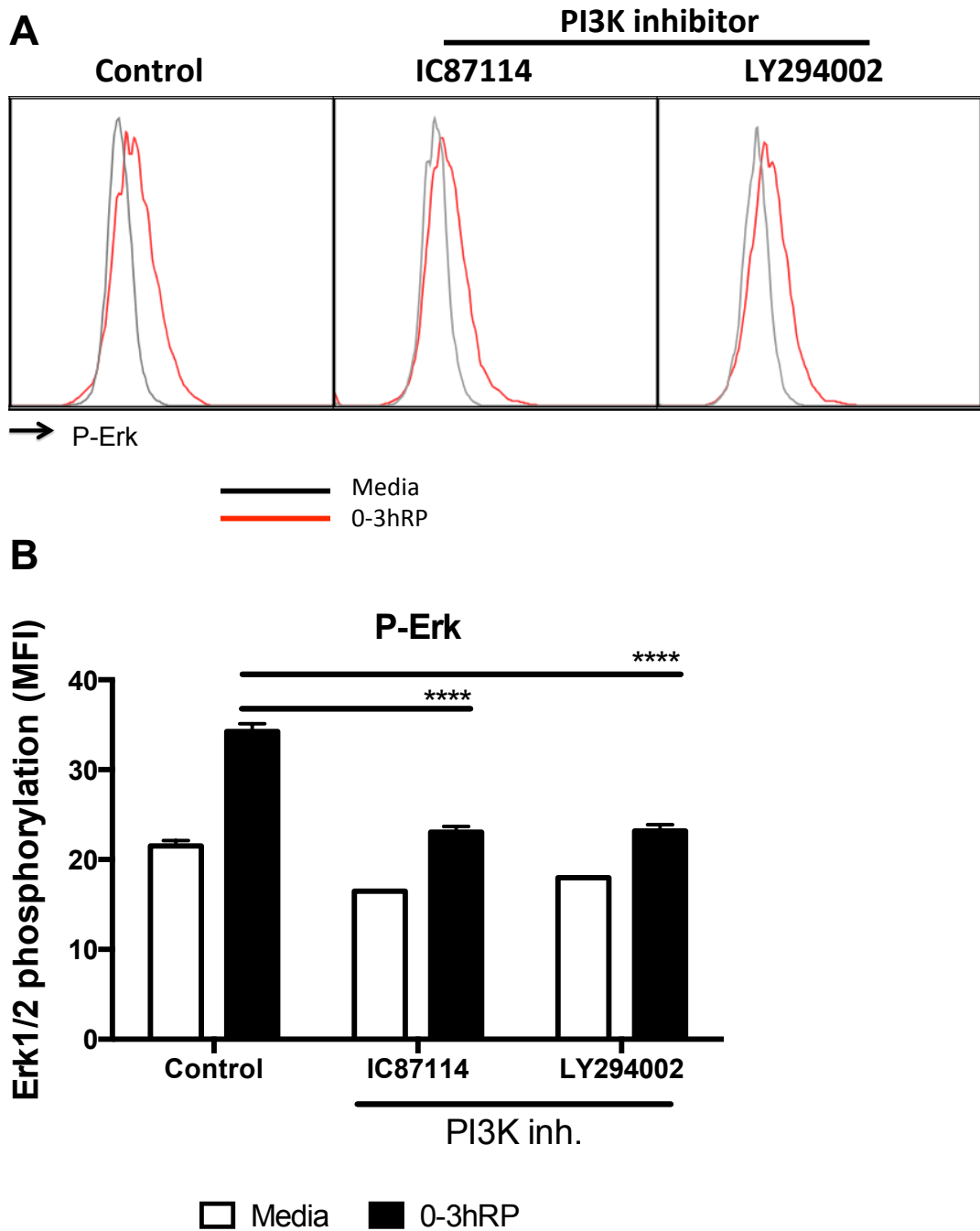


Figure 5.6 PI3K inhibition of BMMφs exposed to 0-3hRP limits Erk1/2 phosphorylation

BMMφs pre-treated for 2 hours with a PI3K family inhibitor (LY294002 at 25μM) or a p110-δ inhibitor (IC87114 at 5μg/ml) were exposed to 0-3hRP (50μg/ml) or left un-stimulated (Media) for 30min. BMMφs were then labeled with antibodies against P-Erk. **(A)** Representative overlaid histograms of 0-3hRP (red) and Media (black) and **(B)** means +SEM of MFIs are given for three technical replicates. ANOVA and then Dunnett's multiple comparisons test were performed to examine differences between the means of inhibitor treated stimulated cells compared to control cells (**** = $p < 0.0001$). Results are representative of three independent experiments.

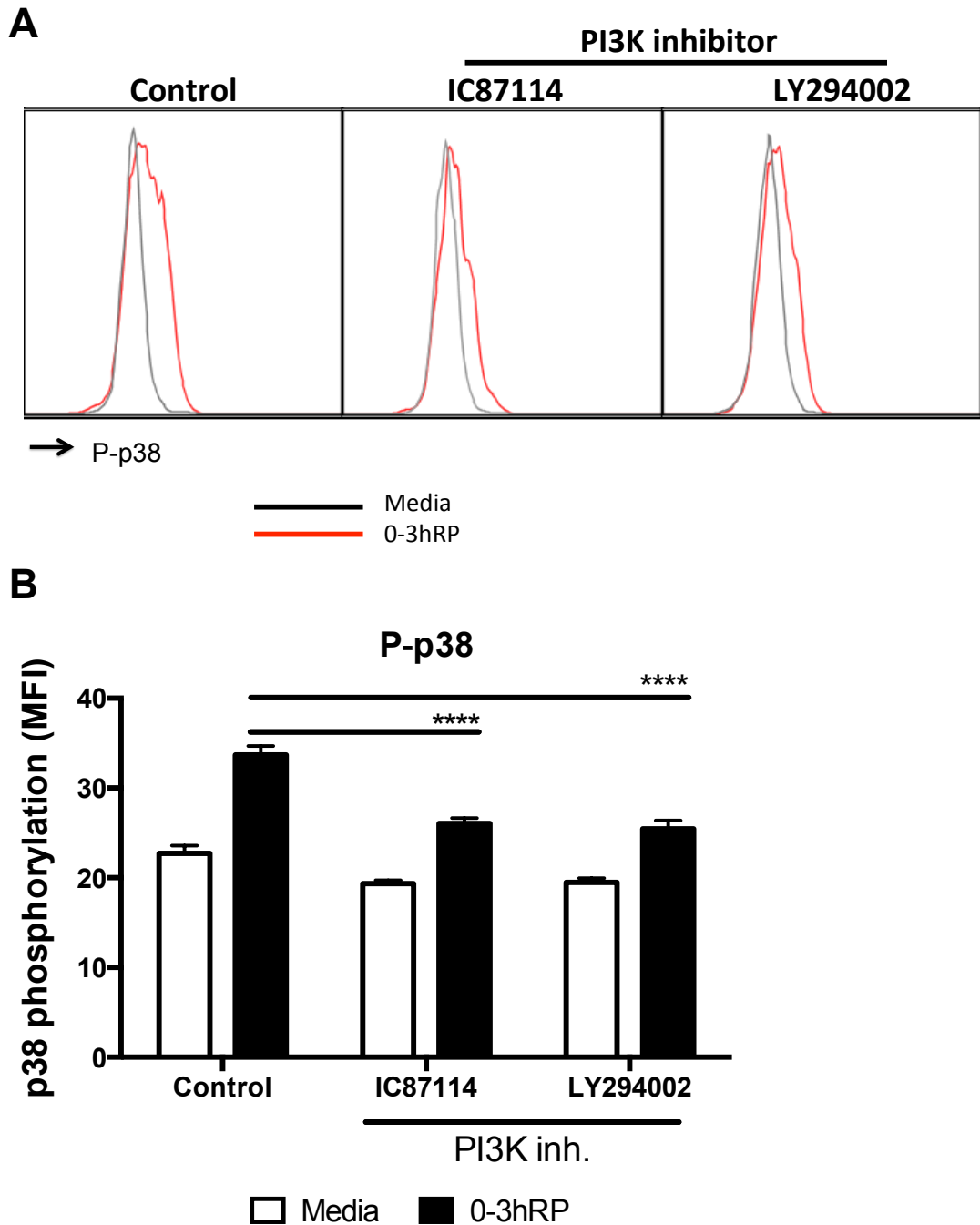


Figure 5.7 PI3K inhibition of BMMφs exposed to 0-3hRP limits p38 phosphorylation

BMMφs pre-treated for 2 hours with a PI3K family inhibitor (LY294002 at 25μM) or a p110-δ inhibitor (IC87114 at 5μg/ml) were exposed to 0-3hRP (50μg/ml) or left un-stimulated (Media) for 30min. BMMφs were then labeled with antibodies against P-p38. **(A)** Representative overlaid histograms of 0-3hRP (red) and Media (black) and **(B)** means +SEM of MFIs are given for three technical replicates. ANOVA and then Dunnett's multiple comparisons test were performed to examine differences between the means of inhibitor treated stimulated cells compared to control cells (**** = $p < 0.0001$). Results are representative of three independent experiments.

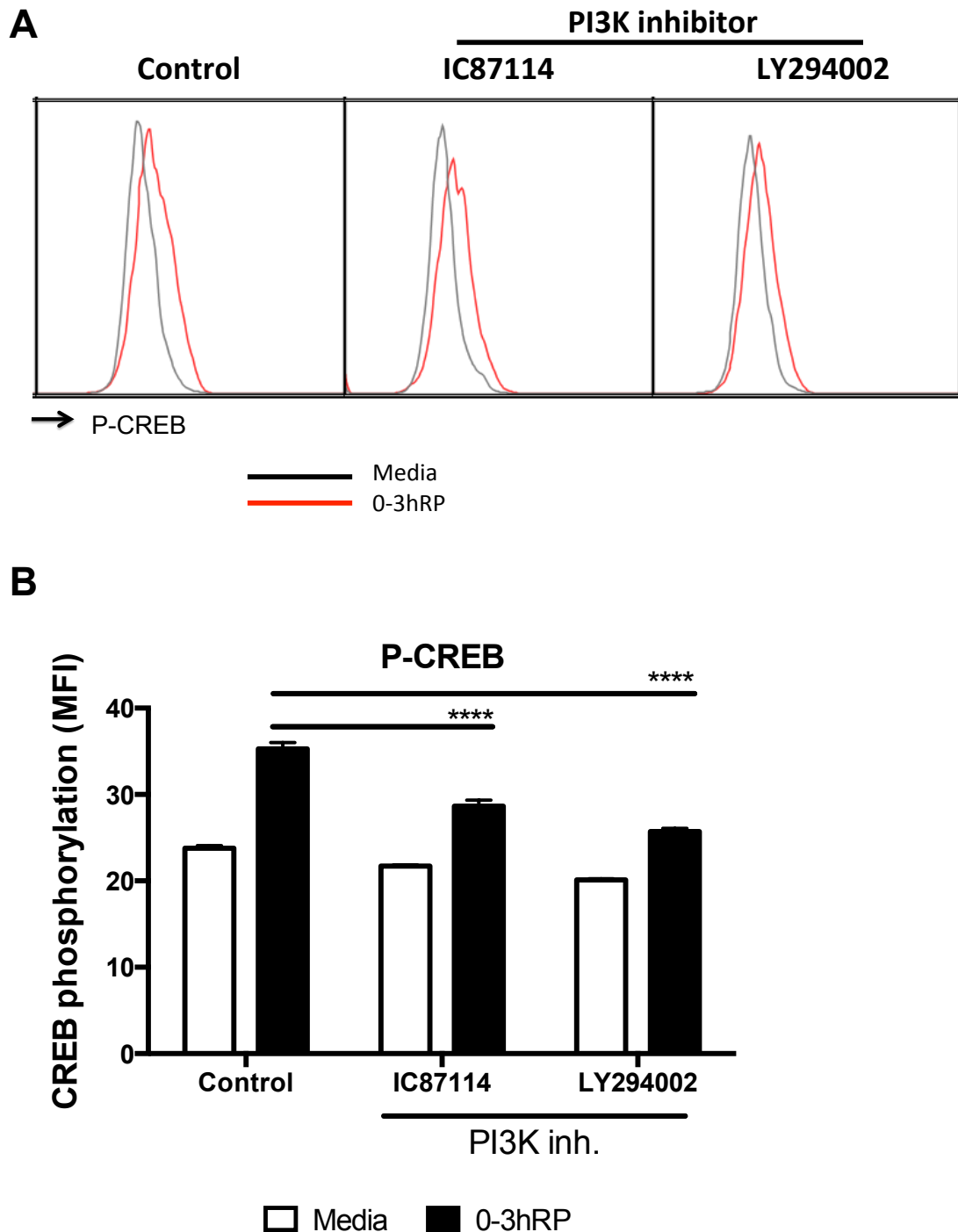


Figure 5.8 PI3K inhibition of BMMφs exposed to 0-3hRP limits CREB phosphorylation

BMMφs pre-treated for 2 hours with a PI3K family inhibitor (LY294002 at 25μM) or a p110-δ inhibitor (IC87114 at 5μg/ml) were exposed to 0-3hRP (50μg/ml) or left un-stimulated (Media) for 30min. BMMφs were then labeled with antibodies against P-CREB. **(A)** Representative overlaid histograms of 0-3hRP (red) and Media (black) and **(B)** means +SEM of MFIs are given for three technical replicates. ANOVA and then Dunnett's multiple comparisons test were performed to examine differences between the means of inhibitor treated stimulated cells compared to control cells (**** = $p < 0.0001$). Results are representative of three independent experiments.

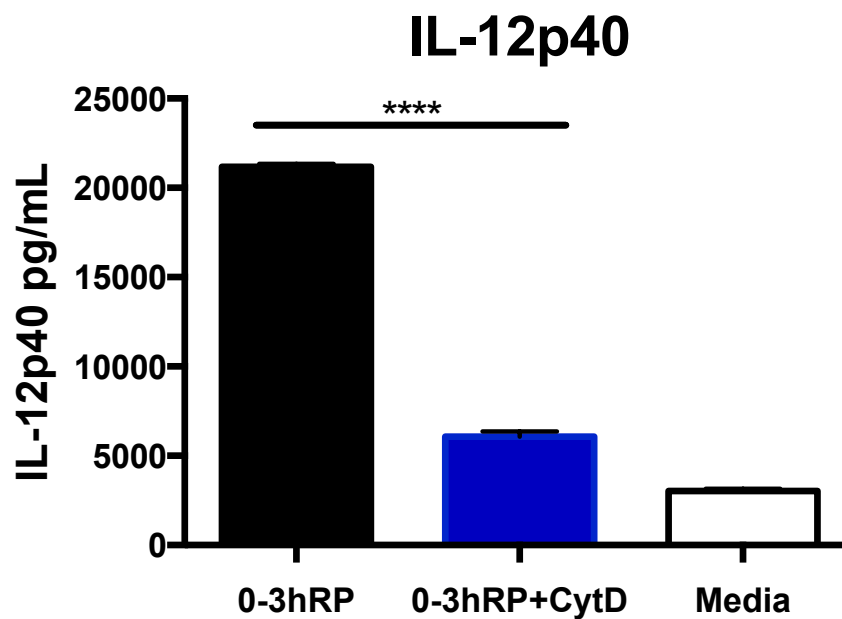
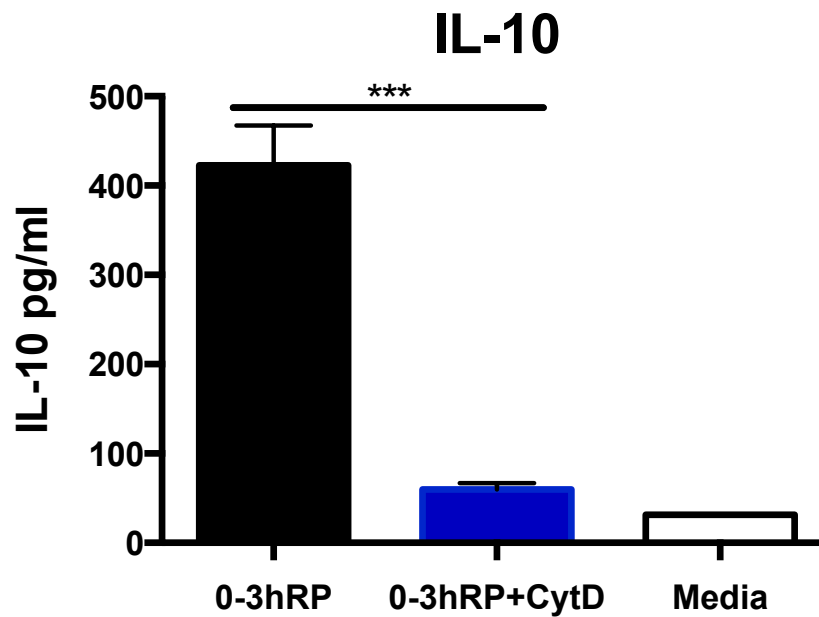


Figure 5.9 Chemical inhibition of 0-3hRP uptake inhibits cytokine production in BMMφs

BMMφs were pre-treated for 2 hours with Cytochalasin D (10μg/ml), exposed overnight to 0-3hRP (50μg/ml) or left un-stimulated (Media) and culture supernatants tested for IL-10 and IL-12p40 by ELISA. Means +SEM from three technical replicates are given. ANOVA and then Dunnett's multiple comparisons test were performed to examine differences between the means of CytD treated BMMφs compared to untreated control (*** = $p < 0.001$; **** = $p < 0.0001$). Results are representative of three independent experiments.

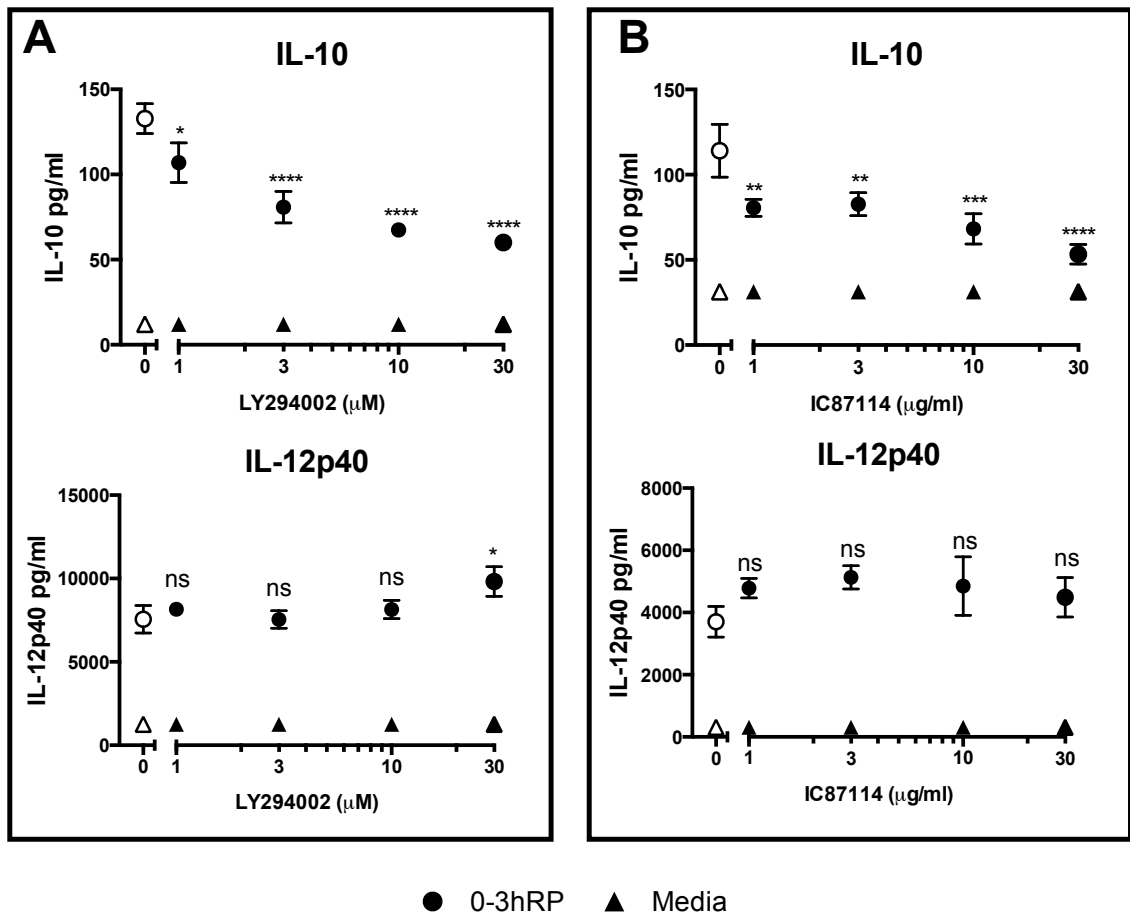


Figure 5.10 Chemical inhibition of PI3K regulates cytokine production in BMMφs exposed to 0-3hRP

BMMφs were pre-treated for 2 hours with increasing doses of (A) a PI3K family inhibitor (LY294002) or (B) a p110- δ inhibitor (IC87114), exposed overnight to 0-3hRP (50 μ g/ml) or left un-stimulated (Media) and culture supernatants tested for IL-10 and IL-12p40 by ELISA (detection limit for IL-10 ELISA was at 32pg/ml). Means \pm SEM from three technical replicates are given. BMMφs without pre-treatment with inhibitors are represented with open circles (0-3hRP) or open triangles (Media). ANOVA and then Dunnett's multiple comparisons test were performed to examine differences between the means of inhibitor treated cells compared to untreated control (* = $p < 0.05$; ** = $p < 0.01$; *** = $p < 0.001$; **** = $p < 0.0001$; ns = $p > 0.05$). Results are representative of three independent experiments.

6 Macrophages in the skin condition the immune response to *S. mansoni* cercariae by producing IL-10

6.1 Introduction

Immunological responses in the skin are unlike any other site, due to its special function as a barrier, both physically and immunologically (Nestle et al, 2009). The skin plays host to a billion bacteria per square inch, and must respond appropriately to both pathogens and commensal microbiota (Belkaid & Naik, 2013). This balance is achieved largely by a network of tissue resident immune cells that work to limit pathology (Belkaid et al, 2001; Malissen et al, 2014; Sanchez Rodriguez et al, 2014; Staumont-Salle et al, 2014).

S. mansoni cercariae penetrate mammalian skin by releasing molecules from their acetabular glands that aid remodeling of the extracellular matrix (Curwen et al, 2006; Paveley et al, 2009; Wilson, 2012) and to aid migration of larvae through the skin to reach blood vessels thereby facilitating onward migration (Cook et al, 2011; Coulson & Wilson, 1997; Incani & McLaren, 1984). Upon penetration of the skin different populations of cells are recruited to the site of infection, including several types of mononuclear cells (macrophages and dendritic cells), as well as eosinophils and neutrophils (Cook et al, 2011). Indeed, F4/80⁺, CD11c⁺, and Gr1⁺ cells (considered to be macrophages, dendritic cells and neutrophils respectively) have been shown to interact with and take up cercarial E/S products in the skin (Paveley et al, 2009). However, the relative roles of these cells in the course of *S. mansoni* skin infection, particularly macrophages, are not fully defined (see 1.2.3).

Several cytokines are produced in the skin as a cascade after infection with live *S. mansoni* cercariae, including IL-10, IL-12, IL-6, IL-1 β and IL-18, many of which reached their peaks of production 4 days after infection (Hogg et al, 2003a). In particular, IL-10 limits the amount of IL-12p40 produced *in vivo* after exposure to radiation-attenuated *S. mansoni* cercariae (Hogg et al, 2003a; Hogg et al, 2003b), which in turn affects the development of Th1 responses in the skin draining lymph nodes (Hogg et al, 2003a). IL-12p40 production in the skin after *S. mansoni* infection with radiation-attenuated cercariae is predominantly from a CD11b⁺CD11c⁺ population of dendritic cells (Hogg et al, 2003b).

Despite the importance of IL-10 production after *S. mansoni* infection (Turner et al, 2013; Wilson et al, 2011), the cellular source of this cytokine is known only in later stages (after 4 weeks) of the disease (Scheer et al, 2014). As IL-10 is difficult to detect by conventional intracellular cytokine staining, particularly in granulocytes, reporter mice have been employed to discover the cell types responsible for the production of this cytokine (Bouabe, 2012). Tiger mice (IL-10^{+gfp}) were developed to track the production of IL-10 by introducing GFP after the 5th exon of the IL-10 gene (Kamanaka et al, 2006). Consequently, IL-10 protein is fluorescent and can be visualized inside cells as it is being produced (Kamanaka et al, 2006). IL-10^{+gfp} mice have already been used to study the sources of IL-10 after 4 weeks of *S. mansoni* infection (Scheer et al, 2014).

BMMφs internalize *S. mansoni* E/S products (chapter V) and tightly regulate the production IL-10 by activating the transcription factor CREB in a TLR dependent manner (chapter IV). In this chapter, the source of IL-10 in the skin will be determined, with a view to link the *in vitro* production of IL-10 by BMMφs to their *in vivo* counterparts.

6.2 Chapter specific materials and methods

6.2.1 Skin infection with *S. mansoni* cercariae

S. mansoni cercariae were obtained as described previously (see 2.2) and diluted to 150 parasites/ml in water to perform percutaneous skin infection.

Female mice (6 weeks of age) from strains previously described (see 2.1) were anesthetized with an intra-peritoneal (i.p.) injection of Domitor (Medetomidine, Fort Dodge) at 0.1mg/kg plus Ketaset (Ketamine, Fort Dodge) at 90mg/kg. Both pinnae of anesthetized animals were moistened and submerged in 1ml of parasite-containing water for 20min. After infection of both ears, mice were revived by subcutaneous administration of 100µl of diluted (1:25) Antisedan (Zoetis) (regardless of weight).

6.2.2 Dermal exudate cells

Naïve, and infected mice (on days 1, 2 or 4 days post-exposure to *S. mansoni* cercariae), were humanly killed; pinnae were removed, briefly sterilized with ethanol, air-dried and split along the central cartilage into two halves to obtain dermal cell suspension as described previously (Cook et al, 2011; Mendez et al, 2004). Briefly, split pinnae were floated overnight at 37°C and 5% CO₂ on RPMI medium (Gibco) containing 10% FCS, 2mM L-Glutamine solution (Gibco), 50U/ml penicillin, 50µg/ml streptomycin and 50µM 2-mercaptoethanol (Complete RPMI) in non-adherent 24-well plates. Floating tissue was removed after 20 hours of incubation and supernatants containing dermal exudate cells (DEC) were centrifuged at 1000g for 7min at 4°C. Pelleted DEC were re-suspended in FACS buffer and counted using a hemocytometer, whilst cell-free culture supernatants were preserved at -20°C and analyzed for cytokines by ELISA as previously described (see 2.5). DEC were prepared for flow cytometry as detailed before (see 2.4).

6.2.2.1 Detection of intracellular IL-10 in DEC

Detection of IL-10 production in different cell types in DEC was achieved by using IL-10^{+gfp} mice (see 2.1). WT and IL-10^{+gfp} mice were infected and pinnae harvested as described above. Split pinnae were incubated with complete RPMI for 12 hours, prior to the addition of 1X Brefeldin A (BreA) (eBioscience)

following the manufacturer's instructions. After a further 8 hours DEC were prepared for flow cytometric analysis as described above.

6.3 Results

6.3.1 Different populations of cells in the skin change after *S. mansoni* infection

Skin infected with *S. mansoni* cercariae was analyzed by flow cytometry to determine the early changes to the composition of immune cells in the DEC. Typically, DEC were harvested, counted and labeled with a Live/Dead discrimination dye to select for viable cells, which were then gated based on size and granularity, and finally as singlets (Figure 6.1A). Subsequent gates for cells positive for different specific antibodies were made based on relevant isotype controls for each antibody (Figure 6.1B & C). This approach was common to all experiments.

6.3.1.1 *Global changes in DEC populations after S. mansoni cercariae infection*

Viable single DEC were initially separated based on the expression of F4/80 and MHC-II (Figure 6.1C, left plot), which produced 5 clearly distinguishable populations, some of which have been characterized previously elsewhere (Cook et al, 2011). These populations were F4/80⁻MHC-II⁻ cells (R1), F4/80⁺MHC-II⁻ eosinophils (R2), F4/80⁺MHC-II^{low} inflammatory monocytes (R3), F4/80⁻MHC-II^{high} DCs (R4) and F4/80⁺MHC-II^{high} cells (R4A). F4/80⁻MHC-II⁻ cells (R1) were further separated based on the expression of CD11b and CD4 (Figure 6.1C, right plot), resulting in four populations. CD11b⁻CD4⁻ cells comprised a small numbers (less than 1%) of CD3⁺CD8a⁺ presumably cytotoxic T lymphocytes and CD3⁻B220⁺ B lymphocytes, whilst the majority were uncharacterized cells (data not shown). CD11b^{mid}CD4⁻ cells were not positive for CD3, B220, NK1.1 or CD8, however, CD11b⁻CD4⁺ cells were all CD3⁺, compared to isotype control (Figure 6.1B, right plot), and so were considered to be CD4⁺ T lymphocytes (Figure 6.1D, left plot). Finally, CD11b^{high}CD4⁻ cells, which were also high for Gr1, were considered to be neutrophils (Figure 6.1D, right plot).

As infection progressed (for four days), the total number of cells in the skin increased compared to naïve tissues (Figure 6.2), but was only significantly greater on days 2 and 4 (both $p < 0.001$). The percentages (Figure 6.3) and numbers (Figure 6.4) of the aforementioned cell populations in DEC changed

dramatically after infection with *S. mansoni* cercariae. F4/80⁻MHC-II^{high} DCs in R4 increased significantly in proportion (Figure 6.3A) and number (Figure 6.4A) on day 2 after infection but did not change substantially by day 4. F4/80⁺MHC-II^{high} cells in R4A decrease significantly in proportion (Figure 6.3B, $p < 0.01$) on day 1 after infection compared to naïve. Thereafter, this population regained its previous abundance, with a significant increase between day 1 and 2 ($p < 0.05$), but no difference was detected by day 4, or indeed between days 2, 4 and naïve. Numbers of these F4/80⁺MHC-II^{high} cells increased significantly only by day 2 after infection ($p < 0.05$) and did not change by day 4 (Figure 6.4B).

Neutrophils (F4/80⁻MHC-II⁻CD11b^{high}) in R1, inflammatory monocytes (F4/80⁺MHC-II^{low}) in R3 and eosinophils (F4/80⁺MHC-II⁻) in R2 all increased significantly in proportion (Figure 6.3C, D & F) and number (Figure 6.4C, D & F) by day 1, and remained elevated on subsequent days, although R2 eosinophils decreased slightly on day 2 compared to day 1 as a proportion (Figure 6.3D). CD4⁺ T cells in R1 were only significantly higher as a proportion, or as numbers on day 4 after infection (Figure 6.3E & Figure 6.4E).

6.3.1.2 Further characterization of monocyte populations in the skin after *S. mansoni* cercariae infection

The three populations of mononuclear cells found in the skin after *S. mansoni* infection based on expression of F4/80 and MHC-II, were F4/80⁻MHC-II^{high}, F4/80⁺MHC-II^{low} and F4/80⁺MHC-II^{high} cells. To further characterize these mononuclear populations, CD11c expression (based on the MFI) on each population 4 days after infection was analyzed by flow cytometry (Figure 6.5). Indeed, CD11c was observed to be significantly elevated on F4/80⁻MHC-II^{high} cells compared to F4/80⁺MHC-II^{low} and F4/80⁺MHC-II^{high} cells (both $p < 0.0001$). F4/80⁻MHC-II^{high}CD11c^{high} cells are likely to be dendritic cells, as high CD11c expression is associated with DCs. The remaining monocyte populations could be a mixture of blood-recruited monocytes, tissue resident macrophages and other types of dendritic cells.

6.3.2 IL-10 is produced by whole skin biopsies after *S. mansoni* infection

6.3.2.1 *Skin infected with S. mansoni cercariae produces IL-10 and IL-12p40*

Cercarial E/S products are released as *S. mansoni* larvae penetrate the skin, causing tissue damage (see 1.2). As demonstrated in previous chapters (chapter III, IV & V), F4/80⁺ BMMφs produce IL-10 and IL-12p40 when exposed to these secretions. To test the ability of cells in the skin to produce these cytokines in response to larval invasion, supernatants from *in vitro*-cultured skin biopsies from infected mice were analysed for the presence of IL-10 and IL-12p40 by ELISA (2.5).

Significantly higher levels of IL-10 were produced by skin samples obtained 4 days after infection with *S. mansoni* cercariae compared to naïve biopsies (Figure 6.6A, $p < 0.01$). Likewise, IL-12p40 production was significantly increased in supernatants from infected skin (Figure 6.6B, $p < 0.01$).

6.3.2.2 *Dynamics of IL-10 production by infected skin in culture*

Unlike other strains of IL-10 reporter mice (Bouabe, 2012), IL-10^{+gfp} mice express one copy of IL-10 with a GFP construct after the 5th exon. To measure IL-10 produced by cells in these mice, it was necessary to initially determine the dynamics of IL-10 production. Consequently, culture supernatants from skin biopsies from infected mice (day 4) were tested for IL-10 at regular intervals. It was apparent that the bulk of IL-10 was detected after the initial 6 hours of culture (Figure 6.7A). Consequently, BreA was added to the media after 12 hours of incubation, and cells harvested 8 hours later (total = 20 hours).

Incubation with BreA resulted in a significant ($p < 0.05$) decrease in the amount of IL-10 secreted by infected skin as detected by ELISA (Figure 6.7B), with only a slight effect on the viability of DEC assessed by incorporation of Trypan blue (Sigma) using light microscopy or later by flow cytometry using fluorescent live/dead discrimination dyes (data not shown).

6.3.2.3 *IL-10 producing cells are increased in skin infected with S. mansoni cercariae*

Pinnae from WT and IL-10^{+gfp} *S. mansoni* infected mice were harvested 1, 2 or 4 days after infection and compared to samples from naïve mice. Pinnae were

split and cultured for a total of 20 hours in media in the absence of added parasite antigen, but with BreA added during the last 8 hours. WT controls were used to set GFP⁺ gates on live single cells obtained as described before (6.3.1) (Figure 6.8A).

GFP was detected in cells obtained from all groups of IL-10^{+gfp} mice including naïve compared to WT controls (Figure 6.8A & B). However, IL-10 positive cells were significantly increased in DEC on days 2 and 4 after infection ($p < 0.01-0.0001$), with the highest percentage and number being observed on day 4 (Figure 6.8B).

6.3.3 F4/80⁺ cells in the skin produce IL-10 in response to *S. mansoni* cercariae

Closer analysis of GFP⁺ cells with the markers described before (6.3.1.1), revealed that only two of the aforementioned populations were predominant in producing IL-10 in the skin after *S. mansoni* infection.

On the basis of F4/80 and MHC-II expression, GFP⁺ was exclusively detected in naïve DEC by F4/80⁺MHC-II^{high} cells (Figure 6.9A). Indeed, nearly 80% of GFP⁺ cells from naïve mice were F4/80⁺MHC-II^{high} (Figure 6.9C). However, 1, 2 or 4 days after *S. mansoni* infection, the detected GFP signal was split between GFP⁺ F4/80⁺MHC-II^{high} and GFP⁺ F4/80⁻MHC-II⁻ cells, which were all CD4⁺ (Figure 6.9B). On day 1, the contribution detected IL-10 from CD4⁺ T cells was similar to that of F4/80⁺MHC-II^{high} cells (Figure 6.9D). Subsequently, F4/80⁺MHC-II^{high} cells became the main source of IL-10 on day 2 after infection (Figure 6.9E) but by day 4 the main contribution to the production of IL-10 came from CD4⁺ T cells (Figure 6.9F), which coincides with the numerical expansion of the CD4⁺ T cell population (Figure 6.3G & Figure 6.4F). Nevertheless, GFP⁺ F4/80⁺MHC-II^{high} cells continued to be significantly more abundant than other mononuclear cells in the DEC (Figure 6.9F, $p < 0.01-0.0001$) and indeed the numbers of GFP⁺ F4/80⁺MHC-II^{high} cells on days 2 and 4 after infection was significantly greater than the number of these cells in naïve skin (Figure 6.10, $p < 0.01-0.001$).

In line with previous results (Figure 6.5), GFP⁺ F4/80⁺MHC-II^{high} cells had a significantly lower expression of CD11c than GFP⁺ F4/80⁻MHC-II^{high} cells (Figure 6.11, $p < 0.0001$), meaning they are likely to be tissue resident macrophages and not DCs.

6.3.4 Higher proportion CD3⁺CD4⁺ T cells in the skin produce IL-10 in response to *S. mansoni* cercariae

Analysis of GFP⁺ cells within each population revealed that only a small proportion of F4/80⁺MHC-II^{low} (R3), F4/80⁺MHC-II^{high} (R4) or F4/80⁺MHC-II^{high} (R4A) were positive for GFP⁺ as a percentage of the total population (~1%, data not shown). Further more, while numbers of GFP⁺ F4/80⁺MHC-II^{high} (R4A) cells were significantly higher on days 2 and 4 after infection compared to naïve (Figure 6.10), numbers of GFP⁺ F4/80⁺MHC-II^{low} (R3) and GFP⁺ F4/80⁺MHC-II^{high} (R4) were only significantly higher than naïve non day 4 after infection (data not shown).

However, the percentage of GFP⁺ cells within the CD3⁺CD4⁺ T cell population was greater than those found for these populations of monocytes. Indeed, on day 4 of infection ~7% of CD4⁺ T cells were positive for GFP⁺, and this was significantly different from naïve and on day 1 and 2 after infection (Figure 6.12A, p<0.001). Moreover, the number of GFP⁺ CD4⁺ T cells was also significantly increased on day 4 after infection compared to naïve, day 1 and day 2 (Figure 6.12B, p<0.0001). These findings highlight the significant contribution to the production of IL-10 by CD4⁺ T cells in the skin, specifically at the later stages of skin infection.

6.4 Discussion

6.4.1 *S. mansoni* infection alters the proportions and numbers of immune cells in the skin

S. mansoni larvae invade the host, releasing the contents of their acetabular glands and initiating an inflammatory process at the site of infection. Reports on the type and proportion of immune cells recruited to the skin after *S. mansoni* infection are scarce. The findings presented in this chapter are the first comprehensive report using modern tools to identify the populations of immune cells that are recruited to the site of infection. The first leukocytes recruited to the site are granulocytes, such as neutrophils and eosinophils, as well as a population of F4/80⁺MHC-II^{low}CD11c^{low} inflammatory monocytes. These three groups of immune cells predominantly remain in the skin as schistosomula migrate through this tissue, which occurs mostly within the first three days (Incani & McLaren, 1984; Mountford & Harrop, 1998; Wheeler & Wilson, 1979) and are likely to be the source of early pro-inflammatory cytokines in the skin such as IL-6 and IL-1 (Hogg et al, 2003a). Furthermore, neutrophils have been shown to take up the secretions of the parasite (Paveley et al, 2009) and alongside eosinophils and macrophages, could be involved in causing and repairing tissue damage (Chen et al, 2012). Moreover, eosinophils are often recruited to sites of helminth infection and are thought to mediate parasite clearance (Falcone et al, 2001; Gentil et al, 2014; Magalhães et al, 2010) which they could be attempting in the skin. Blood recruited monocytes, represented here by F4/80⁺MHC-II^{low}CD11c^{low} cells, are plastic and can adopt several phenotypes, including alternatively activated macrophages (Girgis et al, 2014), or more typical classically activated pro-inflammatory macrophages (Benoit et al, 2008; Gundra et al, 2014). In the multiple *S. mansoni* skin infection model, these cells appear to become alternatively activated (Cook et al, 2011).

As the infection progresses, other types of leukocytes are recruited to the site of infection, specifically cells with antigen presenting function. In the context of *S. mansoni* infection, these APCs include F4/80⁻MHC-II^{high}CD11c^{high} DCs, which are increased in the skin only after 2 days of infection. DCs play a fundamental role in the immune system by polarizing T helper cell responses, and have been heavily implicated in *S. mansoni* chronic infection (Cook et al, 2012; Everts et al, 2012; Pearce & MacDonald, 2002), as well as immune processes in

response to other helminthic parasites (Everts et al, 2010). The F4/80⁺MHC-II^{high}CD11c^{high} DCs are also likely to be the previously reported source of IL-12p40 (Hogg et al, 2003a), allowing them to polarize the infiltrating CD4⁺ T cells to Th1.

DCs are presumably responsible for the increased numbers and proportion of CD4⁺CD3⁺ T cells in the skin by driving local proliferation of antigen specific CD4⁺ T cells, as CD4⁺ T cells are dramatically elevated after 4 days of infection. Resident CD4⁺CD3⁺ T cells, whose numbers were unchanged at day 1 and 2 after infection, have vastly different roles than proliferative antigen specific infiltrating CD4⁺ T cells seen at day 4. Those tissue resident cells will include several populations of regulatory T cells, which are FoxP3⁺CD25⁺ (Belkaid et al, 2002; Campanelli et al, 2006), or Type 1 regulatory 1 (Tr1) cells, positive for CD223 and CD49b (Gagliani et al, 2013).

Yet another resident population of immune cells in the skin is the F4/80⁺MHC-II^{high}CD11c^{mid} mononuclear cells whose proportion is significantly reduced upon schistosoma infection. The number of these cells in the skin is initially unchanged, however it increases at day 2, restoring their original proportion. F4/80⁺MHC-II^{high}CD11c^{mid} cells are most likely to represent tissue resident F4/80⁺ macrophages, which have been the focus of intense research in recent years (Davies et al, 2013).

Tissue resident macrophages are able to proliferate *in situ* (Jenkins et al, 2011). They are seeded in most tissues from the embryonic state and maintain their levels through local proliferation (Jenkins et al, 2013; Schulz et al, 2012). However, in the skin, tissue resident macrophages come from the bone marrow (Jakubzick et al, 2013). Their role in infectious processes is still an area of heated debate. Some propose that it is blood-recruited monocytes that hold the most immunomodulatory role (Girgis et al, 2014; Gundra et al, 2014), yet others argue that resident macrophages are more important in helminth infections (Davies et al, 2013; Jenkins et al, 2011). Similar studies have not been conducted in the skin, however the evidence presented here shows that these cells are responding to *S. mansoni* infection alongside other mononuclear cells. Better markers for tissue resident macrophages would be required to conclusively demonstrate that these cells can be assigned that classification. In recent years, several new markers to discriminate between these cells and

other monocytes have been proposed (i.e. Ly6C, MerTK, CD115, CD64) (Girgis et al, 2014; Nascimento et al, 2014), yet they were not used in the present study.

Several populations of immune cells were found in the skin after *S. mansoni* infection based on expression of F4/80, MHC-II, CD11c, CD11b, CD4 and CD3. The remaining uncharacterized cells are likely to include basophils, mast cells, B cells, CD8⁺ T cells, $\gamma\delta$ T cells, NK cells and other innate lymphoid cells. However, these populations are small in number and difficult to characterize or find in the DEC. The identified populations responded robustly by increasing in number at different times and are likely to attempt parasite clearance (neutrophils and eosinophils), orchestrate adaptive immune responses (DCs and CD4⁺ T cells), condition the immune environment as a source of cytokines plus antigen presentation (inflammatory monocytes), and limit the amount of tissue damage plus inducing its repair (tissue residents macrophages and regulatory CD4⁺ T cells). The exact causes of the influx of immune cells into the skin after *S. mansoni* infection are unknown. Signals triggered by the parasite secretions, particularly the production of CCL2 by macrophages shown in 3.3.5.1, have the potential to account for the recruitment of monocytes. Moreover, levels of IL-5 are increased in the skin after *S. mansoni* infection (data not shown), which could explain the recruitment of eosinophils. However, a comprehensive study on the chemokines involved in this process has not been carried out.

6.4.2 *S. mansoni* infection triggers the production of IL-10 by tissue resident macrophages

Several cytokines are secreted by *S. mansoni* infected skin, including IL-1, IL-18, IL-6 and TNF- α (Hogg et al, 2003a). In this study, IL-10 and IL-12p40 were measured and both were found elevated on day 4 after cercarial invasion. Using IL-10 reporter mice, it was determined that IL-10 was produced in the skin as a response to infection as early as day 1, and that this production continued to increase until at least day 4.

The cellular source of IL-10, which has been investigated in later stages of *S. mansoni* infection (Scheer et al, 2014), and the importance of which in schistosomiasis has been highlighted frequently in this thesis (1.5.1), in the skin was completely unknown. Here it was shown, that two populations of immune

cells in the skin were responsible for the vast majority of IL-10 production; tissue resident F4/80⁺MHC-II^{high}CD11c^{mid} macrophages and CD4⁺ T cells.

IL-10 is important after primary *S. mansoni* skin infection by limiting the recruitment of neutrophils, preventing excessive tissue damage and dampening local proliferation of T cells. These features become further enhanced after multiple exposures to the parasite, as evidenced in IL-10 deficient animals (manuscript in preparation). Consequently the relative contribution to IL-10 production by populations of cells in *S. mansoni* infected skin and the mechanisms that drive that production need to be elucidated.

The production of IL-10 by CD4⁺ T cells was surprising as parasite antigen-specific cells would not have had enough time to clonally expand by day 1 and few DCs to prime T cells were available in the skin at this stage of the infection. Nevertheless, CD4⁺ T cells accounted for a significant portion of the initial production of IL-10 (day 1) in response to *S. mansoni* larvae. Consequently, it is likely that these rapidly responding CD4⁺ T cells are in fact tissue resident cells responding to the skin microbiota. Likely candidates for these cells are a number of regulatory T cells mentioned earlier, including FoxP3⁺CD25⁺ T cells (Belkaid et al, 2001; Belkaid & Naik, 2013; Campanelli et al, 2006; Naik et al, 2012; Sanchez Rodriguez et al, 2014) and suppressive Tr1 cells (Gagliani et al, 2013; Sabat et al, 2010). These cells have been shown to be detrimental for pathology by preventing parasite clearance in *Leishmania* infections (Belkaid et al, 2001; Campanelli et al, 2006), and can be retained in inflamed skin (Staumont-Salle et al, 2014; Suffia et al, 2005). The involvement of these IL-10⁺ CD4⁺ T cells in the early response to *S. mansoni* opens up an exciting possibility: namely, are schistosomula exploiting the tolerance induced by skin commensals to promote migration through the skin? Indeed, the absence of T regulatory cells has been shown to facilitate worm clearance in other settings (Sawant et al, 2014). To test this it would be necessary to carry out an infection in germ-free or antibiotic treated mice. However, cercariae are obtained from a non-sterile environment, so these experiments would also require a completely sterile life cycle of the parasite, which would be technically challenging and expensive.

By day 2, these tolerance-maintaining CD4⁺ T cells contribute significantly less to the production of IL-10. However, by day 4, when APCs have had a chance

to prime T cells, these activated *S. mansoni* specific CD4⁺ T cells become the main source of IL-10 in the skin. Indeed, the proportion of T cells that produced IL-10 increased as infection progressed beyond any other IL-10⁺ population. CD4⁺ T cells are also the main sources of IL-10 at later stages of *S. mansoni* infection in the mesenteric lymph node (Scheer et al, 2014). No IFN- γ or IL-4 could be detected at this stage by ELISA, and the vast majority of day 4 IL-10⁺ CD4⁺ T cells were not T regulatory cells (data not shown) leaving the question of what T helper cell subset these cells might be open. However, *in vitro* stimulation of DEC from infected mice has suggested that these T cells could be Th2 cells (manuscript in preparation). Consequently, the question of how these Th2 cells are primed/polarized in the skin is wide open, but the mechanism could involve elevated levels of IL-10 produced by local antigen presenting cells in response to cercarial E/S products.

As discussed earlier, the role of tissue resident macrophages is highly contentious. In naïve skin, a subset of F4/80⁺MHC-II^{high}CD11c^{mid} macrophages, probably tissue resident, produced IL-10, and is likely to be in response to the mechanical disruption of the tissue during skin biopsy processing. However, it is clear that these tissue resident macrophages, and not any other mononuclear cells in the DEC, are poised to respond to tissue damage by limiting inflammation in an IL-10 dependent manner.

However, F4/80⁺MHC-II^{high}CD11c^{mid} tissue resident macrophages produced elevated levels of IL-10 at every stage of infection in the skin compared to naïve DEC. The increase in numbers of GFP⁺ F4/80⁺MHC-II^{high}CD11c^{mid} macrophages at day 2 and 4 after cercarial invasion indicates that progressively more of these cells participate in the response to the invading larvae by limiting inflammation. Macrophage derived IL-10 has been shown to confer susceptibility to helminth infections (Specht et al, 2012), which adds weight to the potential role of this early IL-10 production in the course of *S. mansoni* infection. Unlike *in vitro* assays used in previous chapters, IL-10 production by skin F4/80⁺MHC-II^{high}CD11c^{mid} macrophages obtained *ex vivo* will be the result of several conflicting signals, including cercarial E/S products released during parasite penetration, antigens from migrating larvae through the skin, tissue damage caused by migrating larvae, and the presence of skin commensal microorganisms. Skin commensals are likely to be most relevant only on day 1

of infection, as seen with the early CD4⁺ T cell production of IL-10. Tissue damage induced by cercariae is an important factor, but it is likely to be dwarfed by the mechanical disruption of the tissue when samples were processed. Therefore, the dominant signal driving IL-10 production from these cells must be the schistosomula and/or their secretions. To determine whether myeloid or lymphoid derived IL-10 holds the balance of preventing excessive inflammation in the skin will require lineage specific IL-10 deficient animals. It is possible that early IL-10 by both macrophages and T cells (in a mixed response to commensals and *S. mansoni* E/S products) drives T cells towards a Th2 phenotype, with abundant secretion of IL-10.

6.5 Summary

S. mansoni infection in the skin induces significant changes in the populations of tissue resident cells and immune cells recruited to the site, or are proliferating locally. An inflammatory process marked by the arrival of neutrophils, eosinophils and inflammatory monocytes develops, alongside the appearance of DCs, and later CD4⁺ T cells. However, it falls to tissue resident macrophages and regulatory CD4⁺ T cells to produce the majority of IL-10 in response to the advancing cercariae. Each population is likely to be responding to different stimuli. Tissue resident macrophages will produce IL-10 in response to cercarial E/S products and skin microbiota, whereas CD4⁺ T cells would only respond to the latter on day 1. As the parasite migrates through the dermis, F4/80⁺MHC-II^{high}CD11c^{mid} macrophages produce more IL-10 than any other population of cells in the skin. By day 4 however, schistosoma antigen-specific CD4⁺ T cells will expand in the skin and produce IL-10 alongside tissue resident macrophages.

A mechanism by which tissue resident macrophages can recognize cercarial E/S products and produce IL-10 as a result of that interaction has been proposed using *in vitro* cultured BMMφs (Diagram 4.2). In combination, these findings demonstrate that macrophages within murine skin also produce IL-10 *in vivo* in response to *S. mansoni* E/S products.

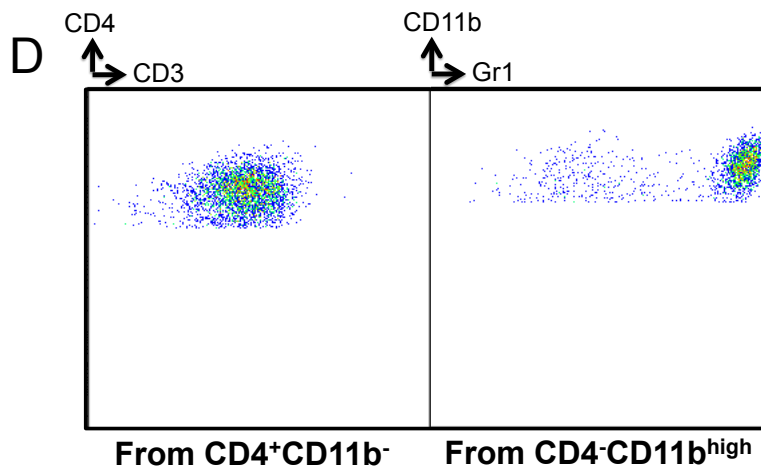
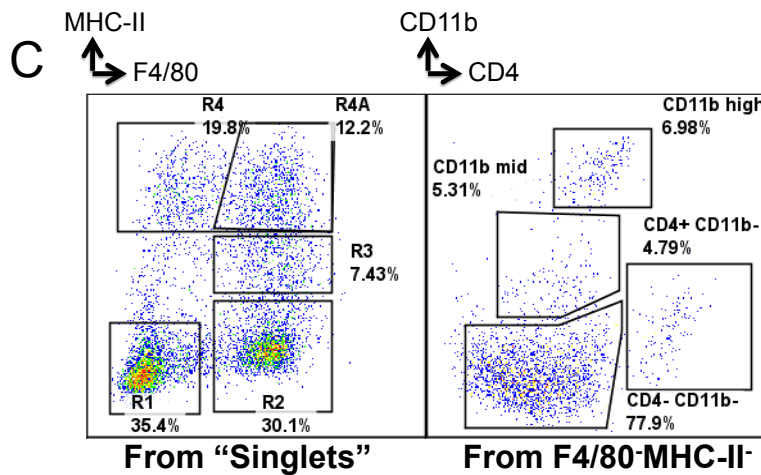
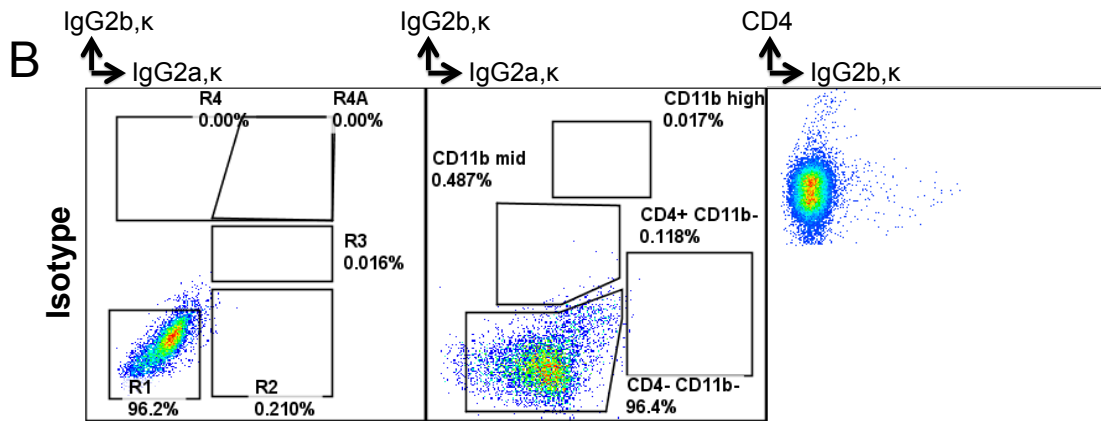
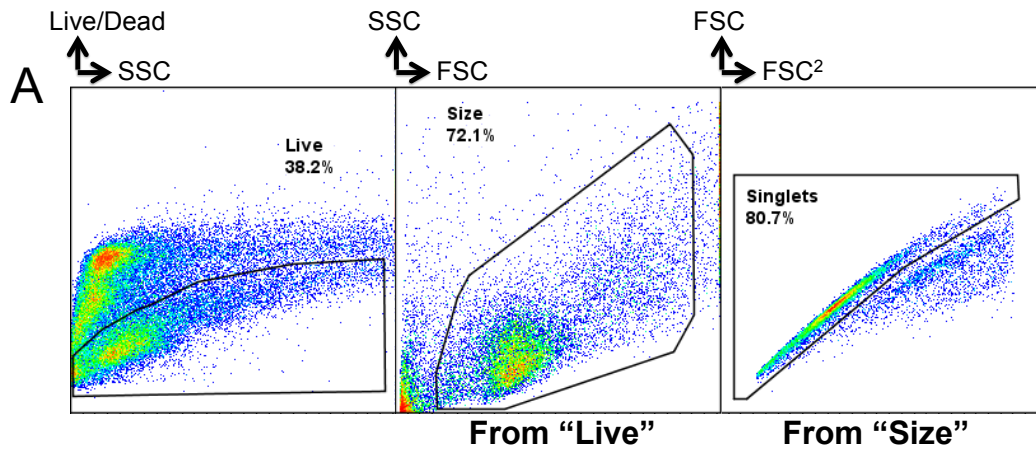


Figure 6.1 Flow cytometric analysis of cell populations in DEC after *S. mansoni* cercariae invasion

Pinnae from C57BL/6 mice were split longitudinally 4 days after infection with *S. mansoni* cercariae infection and floated overnight in complete RPMI. DEC, which had migrated from the split pinnae were, labeled with **(A)** live/dead discrimination dye, gated according to FSC and SSC, and selected for single cells. **(B)** Gating strategy was defined with respect to relevant isotype controls for antibodies as used in C. DEC were labeled for antibodies against **(C)** F4/80 and MHC-II (left-hand panel), and against CD11b plus CD4 (right-hand panel). **(D)** CD4⁺CD11b⁻ cells were subsequently analyzed for their expression of CD4⁺ and CD3 (left-hand panel); CD11b^{high} cells were subsequently analysed for their expression of Gr1 (right-hand panel). Representative flow plots of DEC from 1 pinna gated on live single cells are presented.

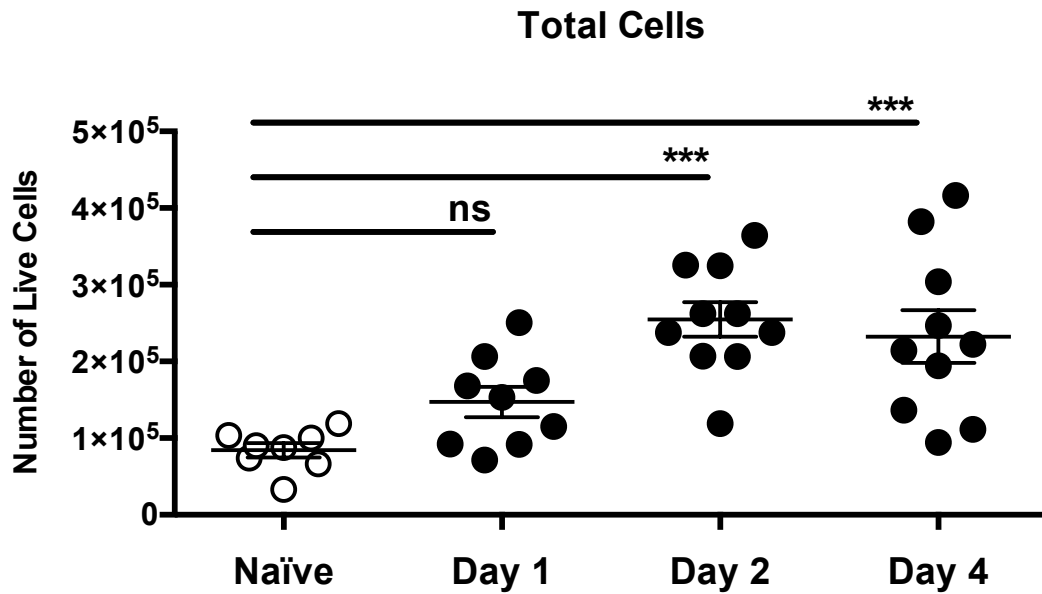


Figure 6.2 Total cell numbers in DEC after infection of pinnae with *S. mansoni* cercariae

Total number of DEC from naïve pinnae (open circles), or pinnae 1, 2 or 4 days after infection (closed circles) with *S. mansoni* cercariae. Mean \pm SEM from 4-5 mice (8-10 pinnae) are given. ANOVA and then Sidak's multiple comparisons test were performed to examine differences between the means of all infected groups compared to naïve (***) = $p < 0.001$; ns = $p > 0.05$).

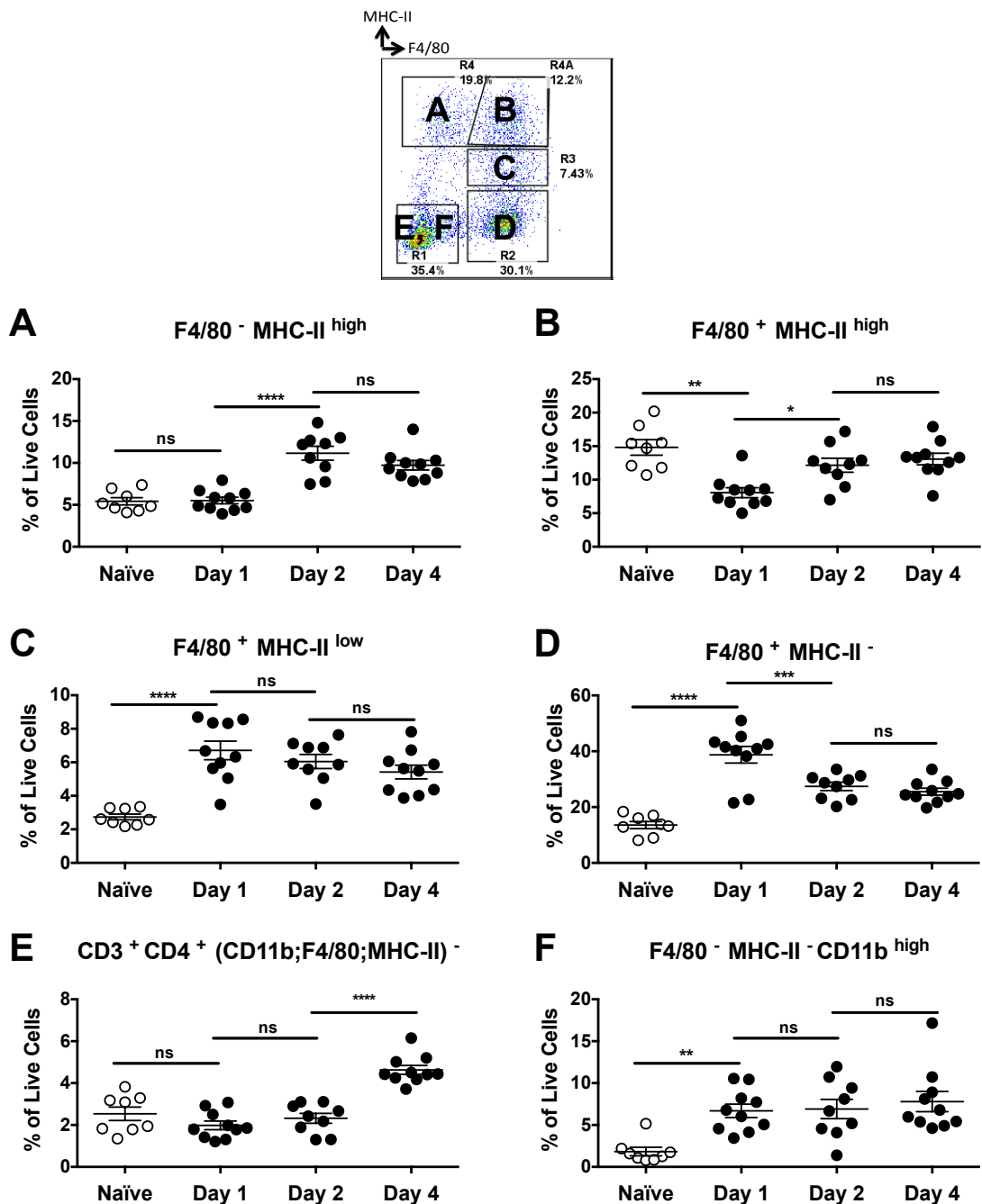


Figure 6.3 Proportions of cell populations in DEC after infection of pinnae with *S. mansoni* cercariae

DEC from naïve pinnae (open circles), or pinnae 1, 2 or 4 days after *S. mansoni* infection (closed circles) were grouped into five distinct populations based on the expression of F4/80, MHC-II, CD11b, CD4 and CD3. Mean \pm SEM of percentages from 4-5 mice (8-10 pinnae) of (A) F4/80⁻MHC-II^{high}, (B) F4/80⁺MHC-II^{high}, (C) F4/80⁺MHC-II^{low}, (D) F4/80⁺MHC-II⁻, (E) CD3⁺CD4⁺ (CD11b⁻F4/80⁻MHC-II⁻), (F) F4/80⁻MHC-II⁻CD11b^{high} are given. ANOVA and then Tukey's multiple comparisons test were performed to examine differences between the means of selected groups (* = p<0.05; ** = p<0.01; *** = p<0.001; **** = p<0.0001; ns = p>0.05). This experiment was repeated twice.

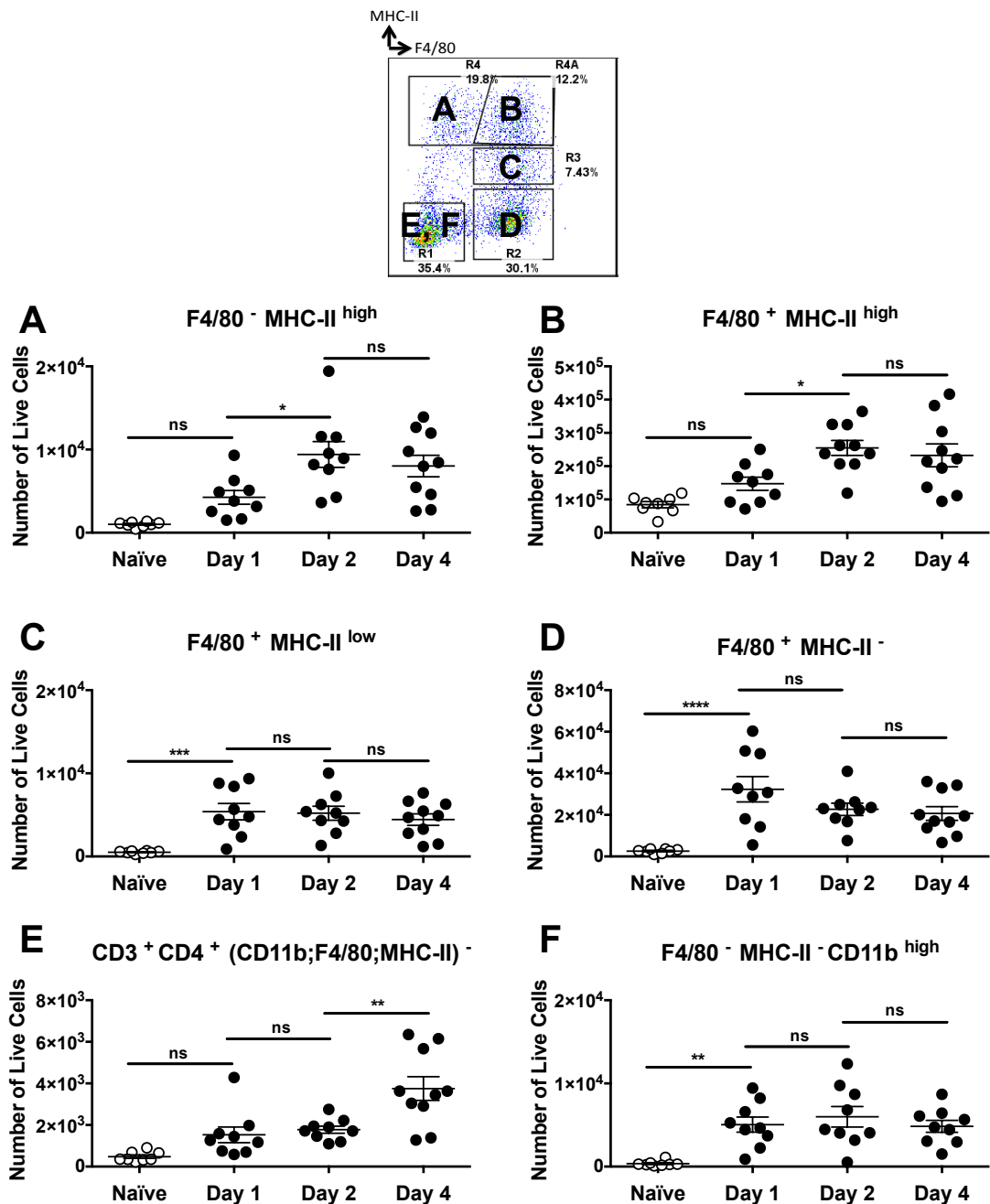


Figure 6.4 Numbers of cell populations in DEC after infection of pinnae with *S. mansoni* cercariae

DEC from naïve pinnae (open circles), or pinnae 1, 2 or 4 days after *S. mansoni* infection (closed circles) were grouped into five distinct populations based on the expression of F4/80, MHC-II, CD11b, CD4 and CD3. Mean \pm SEM of absolute numbers from 4-5 mice (8-10 pinnae) of (A) F4/80⁻MHC-II^{high}, (B) F4/80⁺MHC-II^{high}, (C) F4/80⁺MHC-II^{low}, (D) F4/80⁺MHC-II⁻, (E) CD3⁺CD4⁺ (CD11b⁻F4/80⁻MHC-II⁻), (F) F4/80⁻MHC-II⁻CD11b^{high} are given. ANOVA and then Tukey's multiple comparisons test were performed to examine differences between the means of selected groups (* = p<0.05; ** = p<0.01; *** = p<0.001; **** = p<0.0001; ns = p>0.05). This experiment was repeated twice.

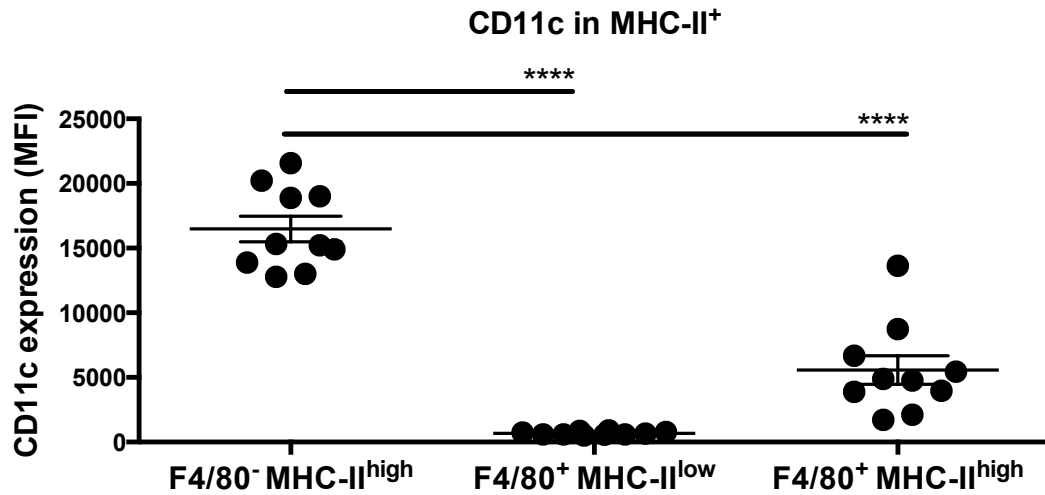


Figure 6.5 CD11c expression on MHC-II⁺ DEC populations recovered from mice 4 days after exposure of pinnae to *S. mansoni* cercariae

Three populations of cells with variable levels of MHC-II and F4/80 expression in DEC recovered on day 4 after exposure to *S. mansoni* cercariae were analyzed via flow cytometry for the expression of CD11c. Mean MFI ±SEM of each population from 5 mice (10 pinnae) are given. ANOVA and then Tukey's multiple comparisons test were performed to examine differences between the means of selected populations (* = p<0.05; ** = p<0.01; *** = p<0.001; **** = p<0.0001; ns = p>0.05). This experiment is representative of three independent experiments.

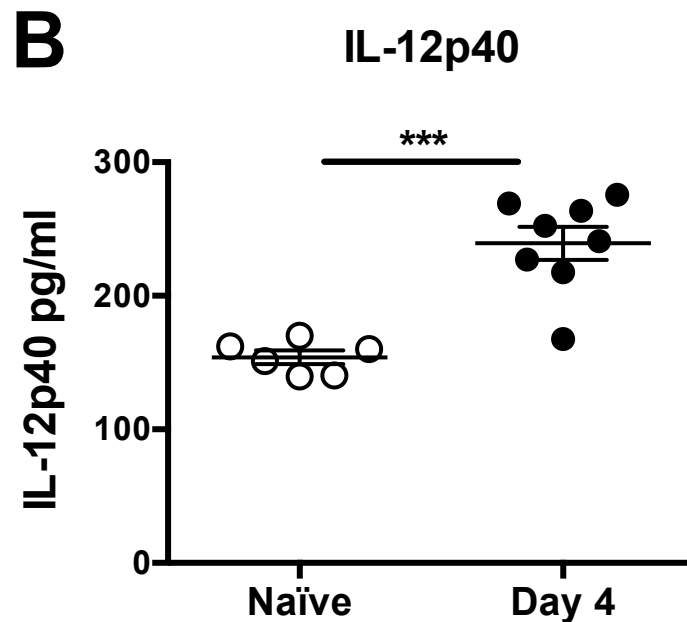
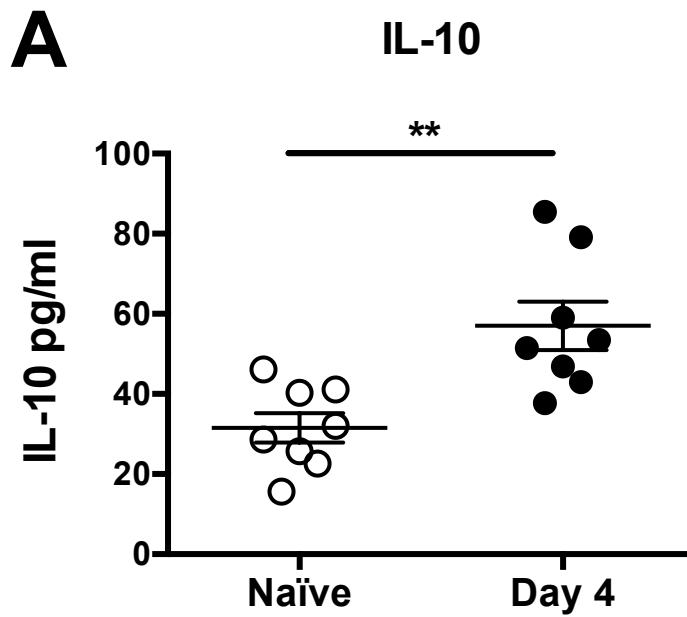


Figure 6.6 Cytokine production from *in vitro* cultured skin biopsies from mice infected with *S. mansoni* cercariae

Pinnae obtained from mice 4 days after exposure to *S. mansoni* cercariae were cultured *in vitro* overnight and supernatants tested for production of IL-10 and IL-12p40 by ELISA (detection limit for IL-10 ELISA was at 16pg/ml). Supernatants were from infected (closed circles) and age matched naïve control (open circles) mice. Means \pm SEM for each group of 3-4 mice (6-8 pinnae) are presented. Two tailed t-tests were performed to find statistically significant differences between the means for the two groups of mice (** = $p < 0.01$; *** = $p < 0.001$).

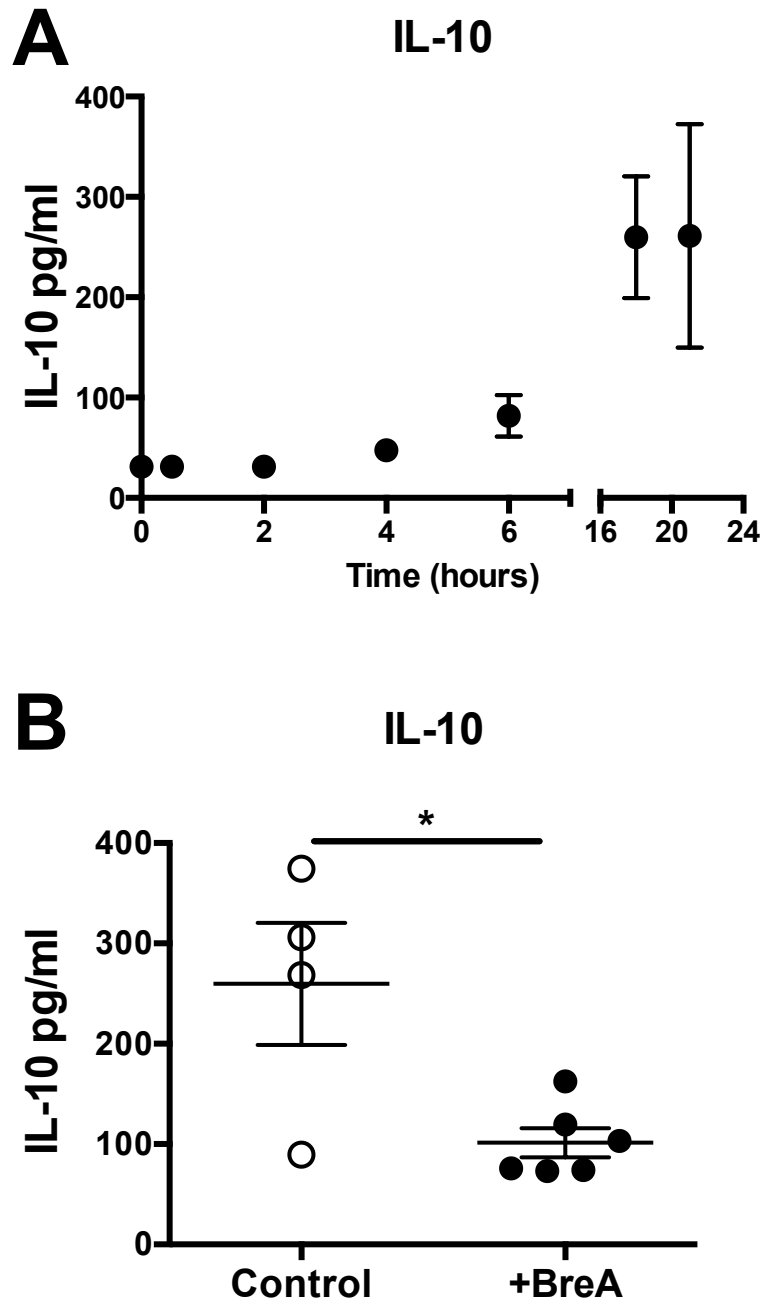


Figure 6.7 IL-10 production time course from skin infected with *S. mansoni* cercariae

(A) Culture supernatants were analyzed for IL-10 after 0.5, 2, 4, 6, 18 and 21 hours. Means \pm SEM for each time point of 2 mice (4 pinnae) are presented. (B) Brefeldin A (BreA) was added to culture supernatant (6 pinnae) at 12 hours of incubation (closed circles), and IL-10 production compared with un-treated cultures (open circles; 4 pinnae) when samples were taken after 20 hours of incubation. Two tailed t-tests were performed to examine differences between the means (* = $p < 0.05$).

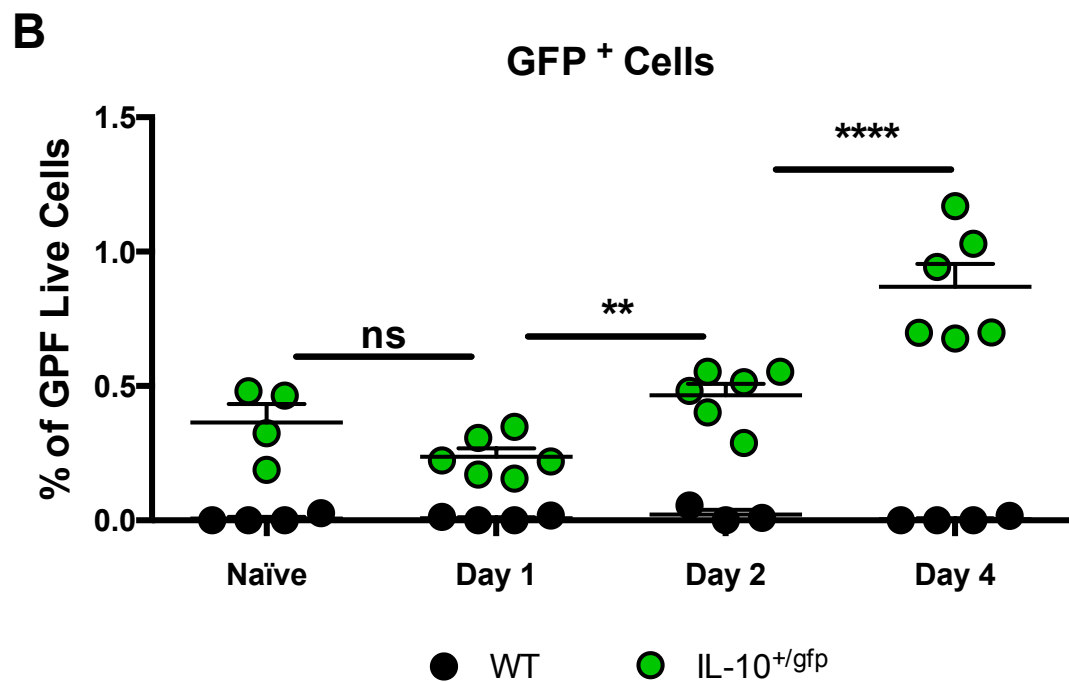
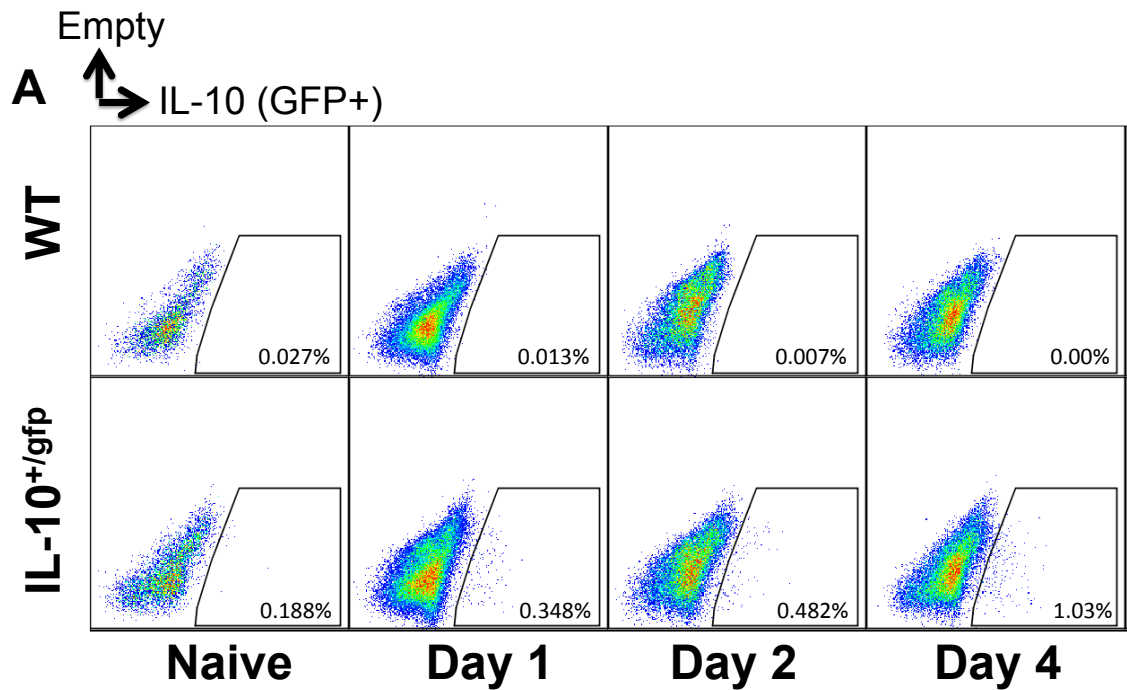


Figure 6.8 Proportions of GFP⁺DEC after infection with *S. mansoni* cercariae

(A) Representative flow plots from DEC from WT or IL-10^{+/gfp} naïve mice, or mice 1, 2 and 4 days after exposure to *S. mansoni* cercariae. Gates (and percentage values) represent proportion of GFP⁺DEC at each time point. (B) Mean ±SEM of percentages from 2-3 mice (4-6 pinnae) for WT (black) or IL-10^{+/gfp} (green) mice at each time point are given. ANOVA and then Sidak's multiple comparisons test were performed to examine differences between the means of selected groups (* = p<0.05; ** = p<0.01; *** = p<0.001; **** = p<0.0001; ns = p>0.05). This experiment was performed twice.

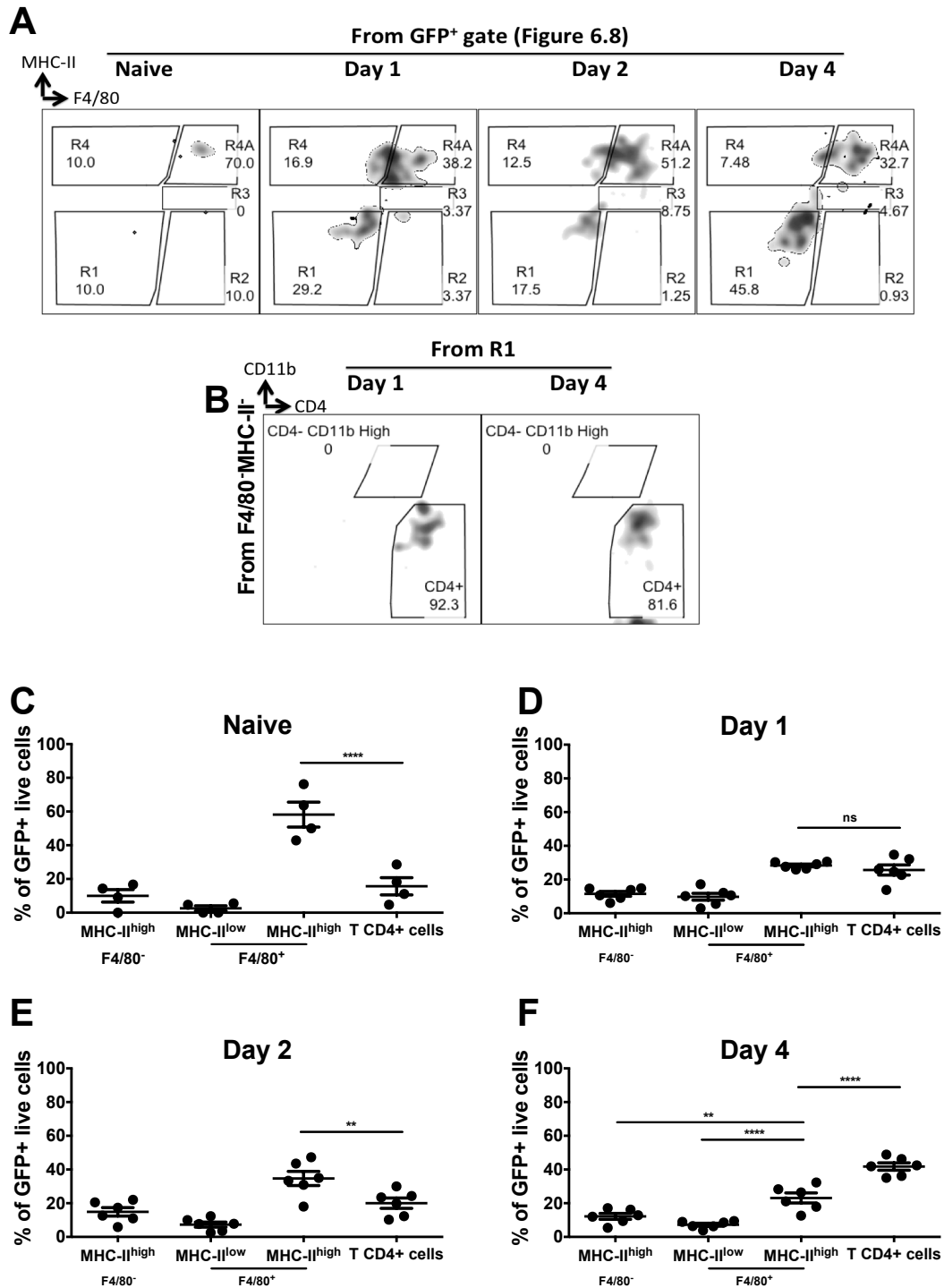


Figure 6.9 Proportions of GFP⁺ cell populations in DEC after exposure of pinnae to *S. mansoni* cercariae

(A-B) Representative flow plots from GFP⁺ DEC (gated for as shown in Figure 6.8), labeled with antibodies against MHC-II, F4/80, CD11b, and CD4, from IL-10^{+/gfp} naive mice or IL-10^{+/gfp} infected mice. (C-F) Proportions of different groups of cells obtained from naive mice and at day 1, 2 and 4 after infection with *S. mansoni* cercariae. Mean \pm SEM of percentages from 2-3 mice (4-6 pinnae) are given. ANOVA and then Sidak's multiple comparisons test were performed to examine differences between the means of selected groups (* = $p < 0.05$; ** = $p < 0.01$; *** = $p < 0.001$; **** = $p < 0.0001$; ns = $p > 0.05$). This experiment was performed twice.

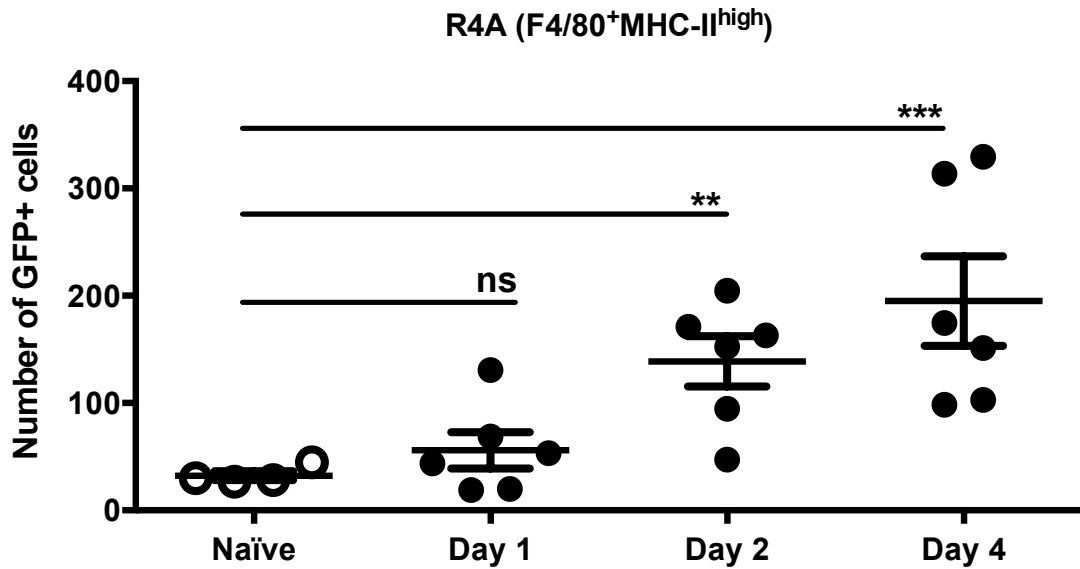


Figure 6.10 Number of GFP⁺ F4/80⁺MHC-II^{high} cells in DEC from mice after exposure *S. mansoni* cercariae

GFP⁺ F4/80⁺MHC-II^{high} cells in DEC from IL-10^{+/gfp} naïve mice (open circles) or IL-10^{+/gfp} mice infected for 1, 2 or 4 days (closed circles) were analyzed via flow cytometry, and in conjunction with cell counts used to calculate the total number of cells in each group. Mean ±SEM of numbers from 2-3 mice (4-6 pinnae) are given. ANOVA and then Dunnett's multiple comparisons test were performed to examine differences between the means of each group compared to naïve (** = p<0.01; *** = p<0.001).

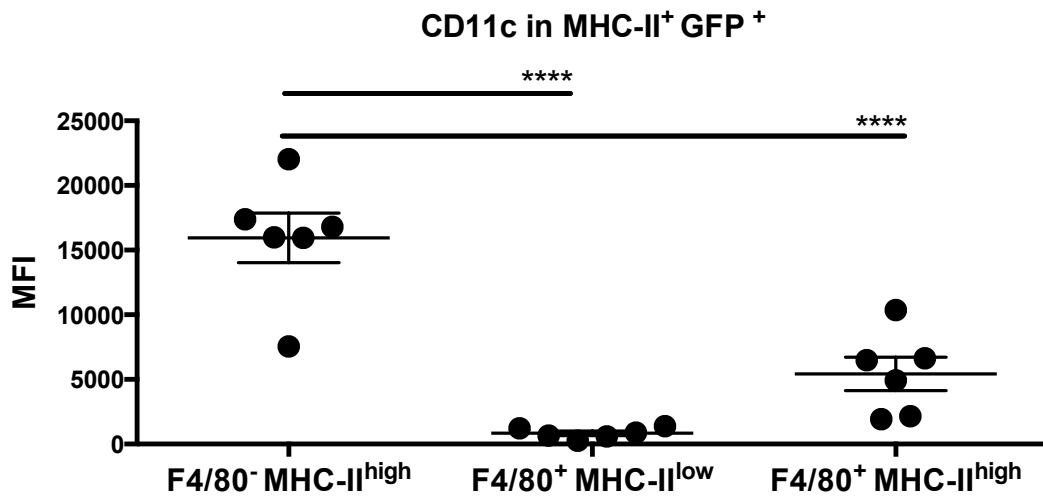


Figure 6.11 CD11c expression on MHC-II⁺GFP⁺ DEC populations from mice 4 days after exposure to *S. mansoni* cercariae

Three populations of GFP⁺ DEC with differential levels of MHC-II and F4/80 expression were analyzed via flow cytometry for the expression of CD11c. Mean MFI ±SEM of each population from 3 mice (6 pinnae) are given. ANOVA and then Tukey's multiple comparisons test were performed to examine differences between the means of selected groups (**** = p<0.0001).

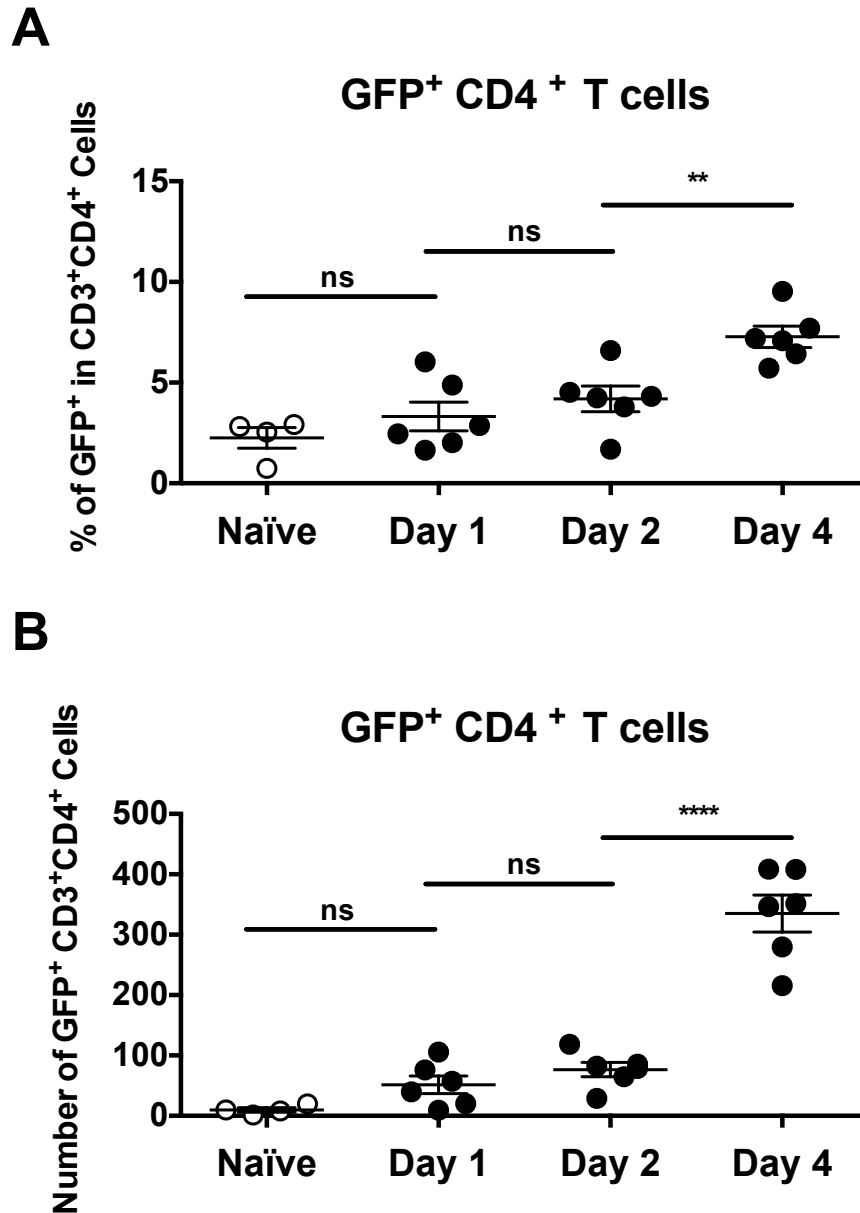


Figure 6.12 Percentages and number of GFP⁺ CD3⁺CD4⁺ cells in DEC from mice after exposure *S. mansoni* cercariae
 GFP⁺ CD3⁺CD4⁺ cells in DEC from IL-10^{+/gfp} naïve mice (open circles) or IL-10^{+/gfp} mice infected for 1, 2 or 4 days (closed circles) were analyzed via flow cytometry, and in conjunction with cell counts used to calculate the total number of cells in each group. Mean ±SEM of (A) percentages and (B) absolute numbers from 2-3 mice (4-6 pinnae) are given. ANOVA and then Sidak's multiple comparisons test were performed to examine differences between selected means (** = p<0.01; **** = p<0.0001).

7 Discussion

7.1 *S. mansoni* cercarial E/S products have a profound impact on macrophage phenotype

E/S products have diverse roles in the modulation of the immune response during different helminth infections and they can act on several different cells of the immune system (Hewitson et al, 2009). All *S. mansoni* life stages in the mammalian host secrete molecules into their environment (Wilson, 2012). For example, adult worms release a cysteine protease that is associated with a Th2 bias (de Oliveira Fraga et al, 2010). Also *S. mansoni* eggs are thought to secrete a chemokine binding protein which retains immune cells in the granulomas (Smith et al, 2005), whilst egg secretions have recently been proposed to facilitate the exit from the host through the Peyer's patches (Turner et al, 2012). It is therefore unsurprising that the E/S products released by invading *S. mansoni* larvae have a profound impact on macrophages.

0-3hRP elicited cytokine production in BMMφs was significantly different from other PAMPs, and was independent of possible endotoxin contamination. RNA levels of cytokines conventionally associated with innate immune cells, such as TNFα, IL-1 and IL-6 (Benoit et al, 2008; Hertzog et al, 2011; Ioannou & Voulgarelis, 2010; Rathinam et al, 2012; Ruland, 2011), were greatly increased in 0-3hRP stimulated cells (3.3.5.1). However, 0-3hRP consistently induced higher levels of IL-10 and lower levels of IL-12 than LPS (both as RNA and protein). IL-10 was produced first, in close association with the uptake of the secretions. This IL-10 induction bias underpins the special nature of 0-3hRP as an innate stimulus, driving a mixed immune response that has a strong anti-inflammatory component.

An exciting discovery was made using label-free quantitative proteomics of membrane proteins from 0-3hRP stimulated BMMφs. A significant increase in the expression of proteins linked with the metabolism of organic substances was demonstrated. This could mean that processing and responding to 0-3hRP is costly from an energy point of view, which occurs to a greater extent than responding to LPS. Moreover, SEA has been shown to up-regulate proteins involved with metabolic processes in dendritic cells (Ferret-Bernard et al, 2012), and a growing body of research is beginning to explore the interplay and intimate linkage between metabolism and the immune response (Arnoult et al,

2011; Everts et al, 2014; Ferret-Bernard et al, 2012; Gehart et al, 2010; Pulendran & Artis, 2012; Vanhaesebroeck et al, 2012; West et al, 2011). The enhanced metabolic activity in 0-3hRP stimulated BMMφs requires further exploration. For example, the use of targeted inhibitors acting on proteins associated with metabolism, or the use of genetically deficient BMMφs that lack one or more of those proteins would begin to address their potential role in the immune responses to 0-3hRP. Similarly, direct measures of metabolic activity in these cells (e.g. rate of extracellular acidification, or the rate of oxygen consumption) would confirm, or refute, my proteomic results, and highlight potential differences between the metabolic demands of 0-3hRP and other PAMPs.

0-3hRP stimulated macrophages also regulated membrane-associated proteins with known immunological functions. As such, MSR1 and CD36 are both scavenger receptors that could be implicated in uptake of 0-3hRP, as is the case with other ligands for these receptors (Baranova et al, 2012; Blanchet et al, 2014; Fonager et al, 2012; Mukhopadhyay et al, 2011; Oury, 2014; Sulahian et al, 2008). CD36 is also an accessory receptor to TLR2 (Lee et al, 2012), and the fact that its expression is reduced in response to 0-3hRP indicates that stimulated macrophages will have limited availability of this receptor on the surface. CD14 is perhaps the best characterized co-receptor for the TLR system (Akira & Takeda, 2004; Ambarus et al, 2012; Baumann et al, 2010; Ioannou & Voulgarelis, 2010; Valanne et al, 2011), and its expression is up-regulated in 0-3hRP treated BMMφs, further suggesting a role for this family of receptors in the recognition of parasite secretions. Although the contribution of CD14 and MSR1 to the responses observed in 0-3hRP stimulated BMMφs was not addressed in this work, blocking antibodies against both could provide initial evidence about their role in the recognition, or uptake of 0-3hRP. Moreover, as CD36 was observed to be down-regulated in stimulated BMMφs, a more appropriate experiment would be to use genetically modified BMMφs that over-express that protein.

Macrophages are dramatically altered by exposure to *S. mansoni* cercarial E/S products. These cells become highly active metabolically and start producing a mixture of pro and anti-inflammatory cytokines. Importantly, these changes do

not include increases in co-stimulatory molecules or MHC-II. Rather these cells start producing significant amounts of regulatory IL-10.

7.2 TLR2 and TLR4 drive the production of IL-10 by macrophages in response to cercarial E/S products

Macrophages exert a very detailed control over the production of IL-10 and IL-12p40 in response to *S. mansoni* cercarial E/S products. My studies show that BMMφs directly recognize 0-3hRP using TLR2 and TLR4, which are responsible for the production of IL-10 in a MyD88-dependent manner. Other studies on different ligands show that TLR2 can have a more regulatory role than TLR4, by limiting the ability of antigen presenting cells to induce a Th1 response (Agrawal et al, 2003; Gao et al, 2012; van Riet et al, 2009), blocking the production of pro-inflammatory cytokines (Correale & Farez, 2009), regulating susceptibility to bacterial infection (Blanchet et al, 2014), and/ or promoting the production of IL-10 (van Vliet et al, 2013). Indeed, TLR2 compared to TLR4, deficiency in BMMφs exposed to 0-3hRP resulted in a more pronounced defect in the induction of IL-10. Conversely, the absence of TLR2 had a relatively small effect on IL-12p40, unlike TLR4 that greatly reduced the production of this cytokine in response to 0-3hRP. Furthermore, at least one of the components of 0-3hRP, the protein Sm16, is able to block TLR4 driven cytokine production (8.4). Recombinant Sm16 can in fact significantly limit the LPS-IFN-γ driven oxidative burst and IL-12p40 production in macrophages. Moreover, this protein is significantly enriched in a fraction of 0-3hRP that was found to retain a higher proportion of the IL-10 inducing potential of the antigenic preparation (8.3). This Sm16 rich fraction, with the IL-10 inducing potential, was also able to block IL-12p40 production in response to LPS. Thus, TLR2 mediates IL-10 production by macrophages exposed to *S. mansoni* cercarial secretions, limiting their ability to contribute to the induction of Th1 responses.

Proteomic studies showed that BMMφs stimulated with 0-3hRP up-regulated proteins that modulate MAPK responses, a category absent from LPS-treated cells (3.3.3.2). In conjunction with the regulation of elements of the TLR system (CD14 and CD36) and the involvement of TLR2 and TLR4 in the production of IL-10 elicited by the parasite secretions, MAPKs appeared to be a likely link between the exposure to 0-3hRP and the downstream immune response.

Indeed, p105, Erk1/2, RSK, p38, and CREB have maximal phosphorylation 30min after stimulation with cercarial E/S products, as measured by flow cytometry, confirming data obtained using a proteome profiler array, where similarities in the phosphorylation of p38 α , MSK2, ERK2, RSK2 and CREB also suggested links in the activation of these kinases. The activation of these proteins was further demonstrated to depend directly upon MyD88 and is strongly impacted by the absence of TLR2, whose function is complemented by TLR4.

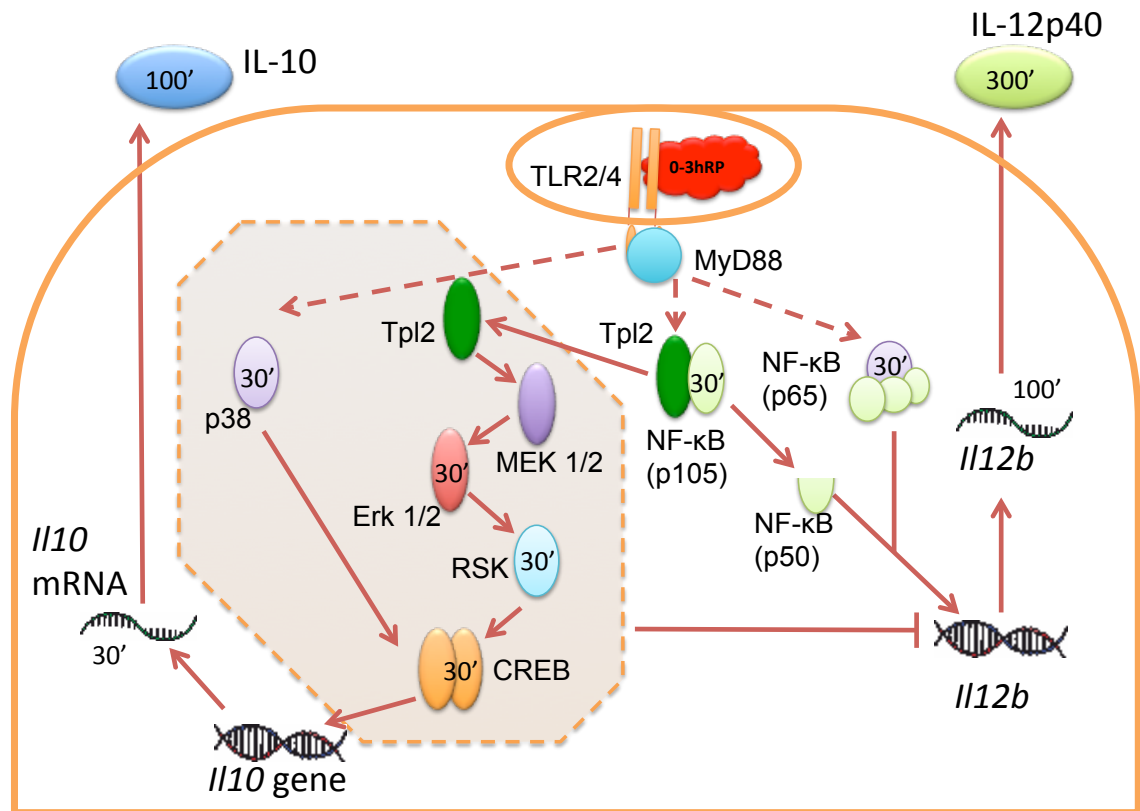
Activation of p38 downstream from TLRs is well characterized and mediated by the phosphorylation of MAP3K7. This protein will activate MKK3/6, which phosphorylates p38 and then activates several targets (Akira & Takeda, 2004; Arthur & Ley, 2013; Yang et al, 2010). p38 α is known to phosphorylate MSK2 (Yang et al, 2010) which has been reported to phosphorylate CREB downstream of p38 (Ananieva et al, 2008; Deak et al, 1998; Elcombe et al, 2013; Mayer et al, 2013). In addition, the phosphorylation of p105 results in its degradation into p50, releasing Tpl2 from an inactive cytoplasmic complex. The release of Tpl2, results in the activation of MEK1/2 and subsequent phosphorylation of Erk1/2, which can in turn activate RSK2 (Bain et al, 2007; Mayer et al, 2013; van Vliet et al, 2013). In BMM ϕ s exposed to cercarial E/S products, p105 and Erk1/2 phosphorylation leads to the activation of RSK and CREB. The association between Erk1/2 and CREB has been reported in the past with other innate immune stimuli, such as Zymosan or *Leishmania* parasites, and receptors including TLRs (Elcombe et al, 2013; Nandan et al, 2012; Nandan & Reiner, 2005; van Vliet et al, 2013), however, this association has not been reported in the context of helminth antigens.

The hierarchy of phosphorylation events and their link to cytokine production was established in macrophages exposed to 0-3hRP using a combination of genetically deficient mice and chemical inhibitors. The pathway of events that I propose (Diagram 7.1) shows how *S. mansoni* cercarial E/S products coordinate the production of IL-10, whilst limiting the production of IL-12p40.

The production of pro-inflammatory cytokines is likely to be a result of the phosphorylation of p65, which would associate with released p50 forming a heterodimer. The p50/p65 complex is a well-known transcription factor, and

among its prime targets are pro-inflammatory cytokines such as IL-1 β , IL-6 and importantly IL-12p40 (Cao et al, 2006; Hoesel & Schmid, 2013).

Diagram 7.1 IL-10 biogenesis in macrophages exposed to *S. mansoni* cercarial E/S products



*Main phosphorylation events (orange dashed line) in BMM ϕ s, which have taken up *S. mansoni* cercarial E/S products (red).*

Similar pathways have been proposed by others for ligands such as LPS or Zymosan (Arthur & Ley, 2013; Elcombe et al, 2013; Lucas et al, 2005; Mayer et al, 2013; van Vliet et al, 2013; Zhang et al, 2006), that included MSK1/2 (Ananieva et al, 2008), that was also found to be phosphorylated in response to 0-3hRP. However, no other study has demonstrated this pathway in the context of a helminth antigen, and only infrequently as a result of TLR signaling. Most studies have limited their demonstration of the link between IL-10 and CREB by using chemical inhibition, siRNA or genetically modified cells. However, only two studies showed an interaction between CREB and DNA from the IL-10 gene. One in a highly artificial system (Nandan et al, 2012) and the other in conjunction with another transcription factor (Ananieva et al, 2008).

Here it is demonstrated that in BMM ϕ s exposed to cercarial E/S products, phosphorylated CREB is recruited to the IL-10 promoter in a region that

overlaps with the first exon of the gene, which is different from what was reported in the past (Ananieva et al, 2008). This recruitment is apparent 30 minutes after stimulation with the parasite's secretions, at which point there is a peak in the activation of CREB. Both the abundant levels of phosphorylated CREB and its strong interaction with the IL-10 promoter, place this transcription factor in a privileged place to effectively regulate the transcription of this cytokine.

Phosphorylated CREB is unlikely to limit its role to IL-10 regulation in the context of 0-3hRP-stimulation. The most highly expressed transcript in 0-3hRP stimulated BMMφs after 30min was the transcription factor *Egr1*. Erk and CREB have been shown to be upstream from *Egr1* (Pagel & Deindl, 2011; Shen et al, 2011). *Egr1* targets several hundred genes and is often associated with tissue damage, however some of genes regulated by this protein are related to inflammation. However, the role of *Egr1* in that regulation is not clear (Fu et al, 2003). Thus, it is likely that 0-3hRP induced CREB activation enhances the transcription of *Egr1*.

As both *Egr1* and IL-10 appear to be under the control of phosphorylated CREB, a more detailed exploration of the genes regulated by this protein is required. ChIP-Seq would provide a comprehensive description of the regions of the chromatin with which this transcription factor is interacting in macrophages committed to the production of IL-10 in the manner proposed above (Diagram 7.1). Bioinformatic analysis of this information would arm us with the precise knowledge of how CREB phosphorylation in macrophages conditions the overall phenotype in these cells, greatly contributing to their plasticity. To that effect, DNA fragments precipitated with anti-P-CREB Ab from 0-3hRP stimulated BMMφs have been prepared and sent for sequencing (results pending).

7.3 Endosomal recognition of cercarial E/S products by macrophages is likely to play an important role in cytokine responses

The receptor(s) involved in the uptake of 0-3hRP is not fully known. Other *S. mansoni* antigens (i.e. SEA) can be internalized by CLRs (Everts et al, 2012; van Liempt et al, 2007). 0-3hRP is a similarly complex mixture of proteins (Curwen et al, 2006), some of which are glycosylated (Jang-Lee et al, 2007),

and partly requires the mannose receptor for internalization into macrophages (Paveley et al, 2011). Additionally, at least MSR1 is up-regulated by 0-3hRP (3.3.3.3) raising the possibility that this receptor could be involved in 0-3hRP uptake.

A growing body of literature has considered the possibility that TLRs abundant on the cell surface are also able to direct signaling pathways from endosomal compartments (Aksoy et al, 2012; Bonham et al, 2014; Kagan & Iwasaki, 2012). Indeed, some studies reveal the intricate interplay between TLRs on the surface and in the endosomes in responses to bacterial products (Wolf et al, 2011). In particular, TLR4 has been shown to accumulate in phagolysosomes (Kagan & Iwasaki, 2012), and helminth products can sequester TLR components limiting their responses to other stimuli (Pineda et al, 2014).

The activation of the MAPK pathway described (Diagram 7.1) linked with the early detection of IL-10 mRNA in response to the 0-3hRP, matches the uptake of 0-3hRP by BMMφs. Previous studies have shown that *S. mansoni* E/S products are taken up by macrophages in the skin and by BMMφs *in vitro* (Paveley et al, 2009). This uptake process requires both actin polymerization and PI3K signaling and involves the trafficking of 0-3hRP through early endosomes (as determined by EEA-1 staining, see 5.3.1.1). Furthermore, inhibition of uptake resulted in significant reductions in the activation of Erk1/2, p38 and CREB, and also the production of IL-10. With the knowledge that TLR2 and TLR4 are responsible for the activation of these signals and the production of IL-10, this evidence strongly supports the possibility that 0-3hRP is binding TLR2 or TLR4 in endosomes. Additional experiments would be required to demonstrate this, for example isolation of 0-3hRP loaded vesicles in macrophages followed by the detection of TLR2 or TLR4. In that manner, it is hoped to demonstrate which “cell surface” TLR is/are able to travel with their ligands to the endosome and use certain adaptor molecules to influence macrophage phenotype. As stated before, TLR4 has already been found in the endosomes (Aksoy et al, 2012), but similar studies are lacking for TLR2. Even if TLR2 or TLR4 were found in 0-3hRP loaded vesicles, teasing out the consequences of those potential interactions would require complex genetic manipulation of macrophages, a process primary cells are not amenable to, unlike some macrophage cell lines (e.g. RAW 264.7). Furthermore, discarding

the possibility that TLR2 or TLR4 are in fact acting in concert with an endosomal TLR would be required. This could be demonstrated by performing stimulation experiments with macrophages deficient for endosomal TLRs.

Unlike blocking actin polymerization, PI3K inhibition not only prevents phagocytosis, but also impacts the recruitment of adaptor molecules to different cellular compartments (Vanhaesebroeck et al, 2012). In fact, inhibition of p110- δ has been shown to prevent TLR4 internalization and enhance its ability to signal from the cell surface (Aksoy et al, 2012), while PI3K signaling is required for adequate recruitment of TIRAP to TLRs (Bonham et al, 2014). TOR is downstream of PI3K. The strong and prolonged activation of TOR, which started 30min after stimulation with 0-3hRP as demonstrated with the proteome profiler, further suggests that PI3K signaling plays a role in 0-3hRP responses. However, other members of this signaling pathway were not found to be active (such as the Akt family). To further elucidate the relevance of TOR activation in macrophages stimulated with 0-3hRP chemical inhibition of that molecule (i.e. Rapamycin) could be used.

PI3K signaling could be very relevant in orchestrating 0-3hRP trafficking through BMM ϕ s. 0-3hRP is delayed in appearing in early endosomes (Paveley et al, 2009) and it contains a significant portion of particulate material that has strong immunomodulatory power (8.3). The size and shape of this particulate material could play an important role in the phenotype of 0-3hRP stimulated cells, as observed with other particles (Flach et al, 2011). Detailed trafficking studies, involving confocal microscopy of macrophages labeled with antibodies against several components of the endocytosis pathway (e.g. RAB proteins and LAMP1) exposed to labeled parasite material would be necessary (in the presence and absence of selective PI3K inhibitors). Similarly, the naturally fluorescent properties of a fraction of 0-3hRP (see 8.3.6) could be exploited to investigate the relevance of particulate vs. soluble processing of 0-3hRP, by investigating the trafficking of each one in isolation and linking this differential processing with the distinctive stimulatory properties of the fractions of these cercarial secretions.

7.4 Macrophages in the skin are an important source of IL-10 in *S. mansoni* cercarial infection

Several cytokines are secreted by *S. mansoni* infected skin, including IL-1 β , IL-18, IL-6 and TNF- α (Hogg et al, 2003b) plus IL-12p40 and IL-10. Similarly, several distinct populations of immune cells were found in the skin after *S. mansoni* infection. These cells responded robustly by increasing in number, like neutrophils, eosinophils and inflammatory monocytes (likely to attempt parasite clearance), DCs and CD4⁺ T cells (probably orchestrating adaptive immune responses) and tissue resident macrophages (most likely limiting the amount of tissue damage plus inducing its repair). Detailed description of the earliest changes to skin immune cells after *S. mansoni* infection is scarce in modern literature. However, these novel findings require further investigation. Moreover, the cellular source of most of the cytokines in the skin remains unknown. Whilst it is likely that inflammatory monocytes, eosinophils and neutrophils are the primary producers of IL-1 β , TNF- α and IL-6 (Nestle et al, 2009), keratinocytes could be a potential source of IL-1 α (Pasparakis et al, 2014). Consequently, cytokine reporter mice should be employed to determine the source of these important early immune mediators. Alternatively, conditional cell-specific deficient animals could be employed to address the contribution of each cell type to the production of cytokines and the overall immune response in the skin after *S. mansoni* infection.

Importantly, three populations of mononuclear cells were found in the skin after *S. mansoni* infection. First, blood recruited F4/80⁺MHC-II^{low}CD11c^{low} cells that are plastic and can adopt several phenotypes including AAM ϕ s (Cook et al, 2011; Girgis et al, 2014), or CAM ϕ s (Benoit et al, 2008; Gundra et al, 2014). Second, DCs represented by F4/80⁻MHC-II^{high}CD11c^{high} cells, have an important role in polarizing the immune response (Agrawal et al, 2003; de Jong et al, 2002; MacDonald et al, 2002) and can also become alternatively activated (Cook et al, 2012). Finally, tissue resident macrophages, represented by F4/80⁺MHC-II^{high}CD11c^{mid} cells, which are able to proliferate *in situ* (Jenkins et al, 2011), are seeded in most tissues from the embryonic state and can maintain their levels through local proliferation (Jenkins et al, 2013; Schulz et al, 2012). However, in the skin tissue resident macrophages come from the bone marrow (Jakubzick et al, 2013). The role of this cell population in infectious processes is contentious, with some proposing that blood-recruited monocytes

hold the most immunomodulatory role (Girgis et al, 2014; Gundra et al, 2014), yet others argue that resident macrophages that have immune modulatory role are more important in helminth infections (Davies et al, 2013; Jenkins et al, 2011).

The full contribution of these three types of myeloid mononuclear cells to *S. mansoni* skin infection is unclear. However, the evidence presented here shows that despite the fact that all these cells are responding to *S. mansoni* (on the basis of their recruitment to the skin), only tissue resident F4/80⁺MHC-II^{high}CD11c^{mid} macrophages produce IL-10 in response to the infection, alongside CD4⁺ T cells.

Two kinds of CD4⁺ T cells were found in the skin as a source of IL-10. Initially, a tolerance-maintaining group of cells that produced IL-10 were observed, and were most likely to be in response to skin microbiota. Subsequently, a parasite - antigen specific group, developed and expanded to take over most of the production of this cytokine. Furthermore, IL-10 producing T cells in the skin can have a profound impact on the outcome of other infections (e.g. Leishmaniasis) (Belkaid et al, 2001).

The increase in numbers of IL-10 producing F4/80⁺MHC-II^{high}CD11c^{mid} tissue resident macrophages as the infection proceeded over the first few days indicates that progressively more of these cells participate in the response to invading larvae by limiting inflammation. Macrophage derived IL-10 is known to confer susceptibility to other helminth infections (Specht et al, 2012), which adds weight to the potential role of this early IL-10 production in the course of *S. mansoni* infection. As *S. mansoni* larvae release the contents of their acetabular glands during that invasion process providing the most potent source of parasite antigen in the skin, it is probable that these E/S products are the target for tissue resident macrophages.

A natural following step from these findings would be to ablate IL-10 production specifically in these F4/80⁺ cells and evaluate the consequences to the infection. Additionally, transgenic animals lacking components of the proposed signaling pathway (Diagram 7.1) would be useful, both by validating my results and investigating the role of tissue resident macrophage derived IL-10. Nonetheless, initial studies performed during my Ph.D. on TLR2 deficient mice showed little to no difference in the induction of IL-10 in infected skin compared

to naïve controls (data not shown). The redundancy in the TLR system, particularly in the proposed signaling pathway that is used by both TLR2 and TLR4, coupled with the potential role of commensal microbiota in the induction of IL-10, severely compromises the usefulness of single full TLR deficient animals. *In vivo* chemical inhibition of kinases would have similar impairments, plus significant off target effects, by affecting not only macrophages but all cells in the mouse.

In that context IL-10^{+gfp} animals lacking both TLR2 and TLR4 only on F4/80⁺ cells are likely to be a more reliable tool to investigate the contribution of these receptors in the induction of IL-10. Only inducible cell type specific deficient animals would be appropriate for intracellular components of the pathway (i.e. full CREB or Erk deficiency would be lethal at birth). Another exciting avenue to explore would be to use Förster resonance energy transfer (FRET) based technologies on transgenic mice expressing specific biosensors (such as Erk) to investigate signaling events in real time in the skin using multi-photon microscopy (as developed by others (Mizuno et al, 2014)). Consequently, my findings could be validated and expanded upon *in vivo*.

Concluding remarks

In conclusion, this work has exhaustively investigated the signaling pathways linked to the production of IL-10 by macrophages exposed to *S. mansoni* cercarial E/S products. Key findings from this work include:

1. A detailed description of global changes to the membrane proteome of 0-3hRP stimulated macrophages, which highlights the role of metabolism in immune responses.
2. A comprehensive mechanism that links TLR2 and TLR4 mediated, MyD88 dependent, MAPK phosphorylation in response to *S. mansoni* cercarial E/S products. The phosphorylation of these MAPKs leads to the activation CREB, which is recruited to the promoter of IL-10 to enhance the production of this cytokine,
3. A role for the engagement of TLR2 and/or TLR4 in the endosomes of macrophages, leading to the activation of the proposed signaling mechanism that links *S. mansoni* cercarial E/S products to the production of IL-10 highlighting in particular the importance of PI3K.
4. Confirmation that tissue resident macrophages produce IL-10 *in vivo* in response to *S. mansoni* cercarial E/S products, validating the *in vitro* studies and highlighting the different roles of tissue resident macrophages compared to recruited monocytes.

Overall, these findings enhance current knowledge of macrophage biology. My studies provide a possible mechanism, supported by others in the literature, that is integral to macrophages in the production of IL-10. As the synthesis of this cytokine, and control, is very context specific, this added knowledge might enable us to predict instances when therapeutic intervention to boost or limit the production of IL-10 by macrophages would be appropriate.

These findings also highlight the strategies that may be employed by helminth parasites to evade the immune system. For example, exploiting commensal skin micro-flora to generate a tolerant environment where larvae can penetrate our skin, is indeed an elegant mechanism that prevent excessive damage to *S. mansoni* cercariae. As these early events have the potential to impact the overall progression of the disease, targeting macrophage IL-10 production (with selective inhibitors of the pathway I proposed) could provide a post-exposure

prophylactic approach, in case of known accidental contact with cercariae contaminated water. However, this approach would be limited by the difficulty in targeting macrophages specifically, plus limiting IL-10 production could cause undesirable excessive tissue damage to the host.

Finally, my Ph.D. studies confirm the role of innate immune signaling in response to schistosoma larvae in the skin and emphasizes that, even in the absence of cues from the adaptive immune system, macrophages are versatile cells.

8 Appendices

8.1 Membrane protein analysis using label free proteomics

Table 8.1 LC-MS/MS pre-run of membrane protein enriched samples sorted based on Mascot score for hits in 0-3hRP treatment

Accession	Description	0-3hRP		LPS		Media	
		Mascot Score	Peptide Matches	Mascot Score	Peptide Matches	Mascot Score	Peptide Matches
MGI:87904	Actb Actin, cytoplasmic 1	1561	424	1609	506	1529	446
MGI:107801	Atp5b ATP synthase subunit beta	1271	93	1235	122	1256	179
MGI:96794	Lmna Isoform A of Lamin-A/C	1134	44	1162	38	1514	75
MGI:88115	Atp5a1 ATP synthase subunit alpha	966	58	945	61	1052	79
MGI:104808	Lcp1 Plastin-2	904	44	617	41	664	35
MGI:95835	Hspa5 78 kDa glucose-regulated protein precursor	861	29	580	33	714	42
MGI:99600	Aldh2 Aldehyde dehydrogenase	785	42	585	31	854	68
MGI:97167	Msn Moesin	704	34	802	54	715	46
MGI:96611	Itgb2 Integrin beta-2 precursor	681	21	773	24	678	28
MGI:105384	Hspa8 Heat shock cognate 71 kDa protein	630	20	446	21	344	19
MGI:87902	Acta1 Actin, alpha skeletal muscle	619	138	750	227	652	198
MGI:1352757	Iqgap1 Ras GTPase-activating-like protein IQGAP1	615	21	509	24	824	43
MGI:95834	Pdia3 Protein disulfide-isomerase A3 precursor	591	22	589	23	415	14
MGI:95772	Gnai2 Guanine nucleotide-binding protein G(i), alpha-2 subunit	590	18	413	17	649	30
MGI:1099832	Tln1 Talin-1	538	13	439	9	274	8
MGI:96242	Hspd1 Isoform 1 of 60 kDa heat shock protein	538	17	284	11	401	20
MGI:106504	Efhd2 SWIPROSIN 1	525	25	539	29	591	31
MGI:106915	Vdac2 Voltage-dependent anion-selective channel protein 2	503	15	377	16	430	24
MGI:5000466	Anpep Aminopeptidase N	495	20	624	26	589	27

MGI:97050	Mdh2 Malate dehydrogenase	492	19	637	28	697	47
MGI:96607	Itgam integrin alpha M	475	14	277	16	481	27
MGI:98932	Vim Vimentin	469	16	687	38	752	46
MGI:1353496	Slc25a5 ADP/ATP translocase 2	463	27	495	42	502	46
MGI:101757	Cfl1 Cofilin-1	452	21	0	0	351	17
MGI:88246	Anxa2 Annexin A2	435	18	325	16	383	24
MGI:2388633	Cltc Clathrin heavy chain 1	431	14	374	13	474	21
MGI:1350931	Tcirg1 T-cell, immune regulator 1, ATPase, H+ transporting, lysosomal V0 protein A3	425	13	297	11	359	15
MGI:95556	Flna filamin, alpha	421	11	0	0	0	0
MGI:107341	Ctss cathepsin S	417	21	391	27	459	29
MGI:88318	Cd14 Monocyte differentiation antigen CD14 precursor	415	14	278	18	180	8
MGI:105068	Rab7 Ras-related protein Rab-7a	391	13	289	26	355	27
	- 11 kDa protein	386	65	361	105	362	103
MGI:88562	Ctsd Cathepsin D precursor	383	30	329	42	490	60
MGI:107717	Myh9 Myosin-9	370	11	482	16	335	12
MGI:106222	Capza2 F-actin-capping protein subunit alpha-2	368	15	344	13	284	11
MGI:1316648	Ahnak AHNAK nucleoprotein isoform 1	367	13	551	22	1040	46
MGI:96778	Lgals3 Galectin-3	359	37	351	56	468	62
MGI:103206	Irg1 Immune-responsive gene 1 protein	354	9	391	13	0	0
MGI:2448383	Hist1h2bl;Hist1h2bf;Hist1h2bn;Hist1h2bj;LOC100046213 Histone H2B type 1-F/J/L	340	81	353	61	352	86
MGI:1891190	Ctsz Cathepsin Z	329	8	194	6	316	11
MGI:99523	Prdx1 Peroxiredoxin-1	322	20	411	24	426	23
MGI:97591	Pkm2 Isoform M2 of Pyruvate kinase isozymes M1/M2	316	11	171	6	154	5

MGI:88561	Ctsb Cathepsin B precursor	315	20	294	21	408	46
MGI:97783	Psap Sulfated glycoprotein 1 precursor	311	15	306	14	347	19
MGI:97572	Phb Prohibitin	307	10	420	12	309	15
MGI:95784	Gnb2 Guanine nucleotide-binding protein G(I)/G(S)/G(T) subunit beta-2	291	10	407	15	482	18
MGI:88105	Atp1a1 Sodium/potassium-transporting ATPase subunit alpha-1 precursor	291	8	405	10	610	20
MGI:1353495	Slc25a4 ADP/ATP translocase 1	291	19	250	24	324	26
MGI:96897	Lyz2 Lysozyme C	289	14	311	21	230	23
MGI:1917600	Basp1 Brain acid soluble protein 1	276	8	537	13	665	21
MGI:96832	Lsp1 Isoform 1 of Lymphocyte-specific protein 1	274	7	177	4	222	7
MGI:1353498	Slc25a3 Phosphate carrier protein	264	10	172	11	230	19
MGI:88261	Canx Calnexin precursor	261	5	196	12	128	8
MGI:106919	Vdac1 Isoform PI-VDAC1 of Voltage-dependent anion-selective channel protein 1	259	15	281	17	334	19
MGI:1345961	Coro1a Coronin-1A	257	12	329	12	329	11
MGI:96245	Hspa9 Stress-70 protein	256	8	271	11	425	19
MGI:106227	Capza1 F-actin-capping protein subunit alpha-1	247	7	191	6	86	4
MGI:95872	Gusb beta-glucuronidase	247	6	190	4	234	7
MGI:1918929	Atp5h ATP synthase subunit d, mitochondrial	239	10	130	6	139	6
MGI:109618	Atp6v1b2 Vacuolar ATP synthase subunit B, brain isoform	231	6	183	5	88	3
MGI:1931526	Hist1h1c Histone H1.2	231	12	224	14	0	0
MGI:1915835	Rtn4 RTN4	228	10	164	5	159	8
MGI:102520	Phb2 Prohibitin-2	223	7	219	9	236	11
MGI:2135593	Hadha Trifunctional enzyme subunit alpha	222	6	179	4	302	7
MGI:97464	P4hb prolyl 4-hydroxylase, beta polypeptide	219	5	179	5	117	4

MGI:106341	Atp5o ATP synthase subunit O	217	6	188	9	261	16
MGI:1928370	Rhog Rho-related GTP-binding protein RhoG precursor	217	7	87	3	100	4
MGI:1261437	Atp5c1 ATP synthase subunit gamma	216	10	161	6	261	14
MGI:102503	mt-Co2 Cytochrome c oxidase subunit 2	216	18	184	16	202	24
MGI:1915113	Slc25a11 Mitochondrial 2-oxoglutarate/malate carrier protein	209	6	51	3	257	8
MGI:2442982	Rab8b Ras-related protein Rab-8B	207	14	0	0	143	10
MGI:1096881	Eef1a1 Elongation factor 1-alpha 1	203	10	173	7	248	9
MGI:1861461	Hist1h1b Histone H1.5	201	9	150	8	226	11
MGI:96745	Lamp1 lysosomal membrane glycoprotein 1	200	13	303	24	282	28
MGI:97842	Rab1 Ras-related protein Rab-1A	200	10	231	16	205	19
MGI:106922	Vdac3 Voltage-dependent anion channel 3	199	10	132	9	157	11
MGI:108563	Sirpa 56 kDa protein	199	5	141	3	194	6
MGI:108109	Ywhag 14-3-3 protein gamma	198	6	0	0	158	8
MGI:88252	Calr Calreticulin precursor	198	8	181	8	238	9
MGI:105066	Rab10 Ras-related protein Rab-10	197	8	0	0	0	0
MGI:107899	Cd36 Platelet glycoprotein 4	192	8	194	10	327	24
MGI:1201778	Atp6v0d1 Vacuolar proton pump subunit d 1	191	7	200	11	187	9
MGI:109484	Ywhaz 14-3-3 protein zeta/delta	191	9	78	3	228	10
MGI:98084	Rpn1 Dolichyl-diphosphooligosaccharide--protein glycosyltransferase subunit 1 precursor	190	5	225	7	227	7
MGI:1890773	Actn4 Alpha-actinin-4	187	8	34	1	64	3
MGI:894689	Ywhae 14-3-3 protein epsilon	184	7	0	0	82	7
MGI:88574	Cybb Cytochrome b-245 heavy chain	183	5	89	3	128	3
MGI:3606192	H2afj;LOC632401 H2A histone family, member J	182	20	135	14	158	28
MGI:1931527	Hist1h1e Histone H1.4	181	10	199	11	225	18

MGI:1923558	Rab1b Ras-related protein Rab-1B	179	10	0	0	254	15
MGI:2443191	Aadacl1 Arylacetamide deacetylase-like 1	173	4	82	2	84	3
MGI:98817	Hsp90b1 Endoplasmin precursor	170	6	216	7	211	8
MGI:97846	Rac2 Ras-related C3 botulinum toxin substrate 2 precursor	169	7	0	0	0	0
MGI:1345964	Coro1c Coronin-1C	169	7	118	3	195	6
MGI:1927636	Rplp0 60S acidic ribosomal protein P0	167	4	132	4	147	6
MGI:94893	- Cytochrome b5 reductase 3	166	4	116	4	138	3
MGI:107876	Uqcrc1 Cytochrome b-c1 complex subunit 1	166	5	0	0	123	5
MGI:894315	Rap1b; Ras-related protein Rap-1b precursor	165	6	128	7	238	7
MGI:95781	Gnb1 Guanine nucleotide-binding protein G(I)/G(S)/G(T) subunit beta-1	165	5	266	11	299	12
MGI:98352	Sod2 Superoxide dismutase [Mn]	164	8	109	6	67	2
MGI:96073	Hexa Beta-hexosaminidase subunit alpha precursor	163	6	54	2	168	9
MGI:1929693	Slc37a2 Isoform 2 of Sugar phosphate exchanger 2	159	8	57	3	137	18
MGI:109318	Myl6 Isoform Smooth muscle of Myosin light polypeptide 6	158	6	171	6	200	9
MGI:88529	Cs Citrate synthase	157	3	85	3	196	9
MGI:98887	Ubc;Gm1821;Uba52;Ubb hypothetical protein LOC666586	157	10	171	17	212	15
MGI:2144765	Pld4 Isoform 1 of Phospholipase D4	155	4	173	3	157	8
MGI:104652	Capzb Isoform 2 of F-actin-capping protein subunit beta	154	4	193	9	241	7
MGI:96163	Hmox1 Heme oxygenase 1	152	6	48	1	0	0
MGI:1935159	EG628438;Hspe1-rs1 CPN10-like protein	151	5	109	6	0	0
MGI:1915213	Npc2 Epididymal secretory protein E1 precursor	150	4	114	5	108	3
MGI:87880	Aco2 Aconitate hydratase, mitochondrial precursor	149	4	0	0	184	7

MGI:2448320	Hist1h3c;Hist1h3b;Hist1h3f;Hist2h3c2;Hist2h3b;Hist1h3d;Hist1h3e;Hist2h3c1 Histone H3.2	149	15	164	20	136	25
MGI:1923686	Tufm Isoform 1 of Elongation factor Tu	149	4	0	0	78	3
MGI:98869	Tuba1a Tubulin alpha-1A chain	148	7	90	5	89	3
MGI:109194	Ywhah 14-3-3 protein eta	147	5	116	4	214	12
MGI:105306	Rab5c Ras-related protein Rab-5C	146	4	184	7	167	6
MGI:96074	Hexb Beta-hexosaminidase subunit beta precursor	143	4	203	6	253	8
MGI:1934765	Gpnmb Transmembrane glycoprotein NMB precursor	139	34	157	35	190	56
MGI:97845	Rac1 RAS-related C3 botulinum substrate 1	138	6	141	6	154	13
MGI:107460	Cox6b1 Cytochrome c oxidase subunit VIb isoform 1	136	5	106	8	126	14
MGI:97748	Ctsa Lysosomal protective protein precursor	134	5	30	2	32	2
MGI:109553	Ctsc Dipeptidyl-peptidase 1 precursor	128	4	70	2	66	3
MGI:1312985	Tagln2 Transgelin-2	127	3	27	1	37	1
MGI:106211	Cdc42 Isoform 2 of Cell division control protein 42 homolog precursor	126	5	28	1	59	3
MGI:3647311	EG623365 hypothetical protein isoform 1	126	9	139	10	0	0
MGI:1349450	Vat1 Synaptic vesicle membrane protein VAT-1 homolog	126	3	136	6	186	8
MGI:1921367	Actr3 Actin-related protein 3	125	3	191	6	129	6
MGI:2136381	Hadhb Trifunctional enzyme subunit beta	123	4	108	4	174	7
MGI:95403	Stom Erythrocyte band 7 integral membrane protein	121	6	190	4	252	13
MGI:1344426	Mbc2 Isoform 1 of Extended-synaptotagmin-1	120	3	101	2	90	2
MGI:96819	Anxa1 Annexin A1	119	4	90	2	152	5
MGI:97750	Ppib peptidylprolyl isomerase B	118	5	146	6	101	3
MGI:1919020	Ap2b1 Isoform 1 of AP-2 complex subunit beta-1	116	1	48	2	80	2
MGI:88473	Cox4i1 Cytochrome c oxidase subunit 4 isoform 1	116	6	113	5	141	9

MGI:2442910	9130404D14Rik Niban-like protein 1	113	6	36	1	76	2
MGI:96247	Hsp90ab1 Heat shock protein 84b	113	5	54	3	78	3
MGI:88342	Cd68 Macrosialin	109	7	105	5	125	8
MGI:1914436	Rplp2 60S acidic ribosomal protein P2	105	2	99	3	126	5
MGI:1931523	Hist1h1a Histone H1.1	103	4	70	5	112	9
MGI:95753	Glud1 Glutamate dehydrogenase 1	101	2	35	1	470	12
MGI:99554	Lgals3bp Mama protein	100	2	0	0	0	0
MGI:95904	H2-K1 42 kDa protein	100	4	0	0	0	0
MGI:88251	Calm3;Calm2;Calm1 calmodulin 1	99	3	79	3	26	1
MGI:1891435	Usmg5 Up-regulated during skeletal muscle growth protein 5	98	3	83	2	109	4
MGI:96907	Marcks Myristoylated alanine-rich C-kinase substrate	96	5	82	3	0	0
MGI:106912	Emr1 EGF-like module-containing mucin-like hormone receptor-like 1 precursor	95	3	143	3	0	0
MGI:1888388	H2afz Histone H2A.Z	95	8	0	0	131	13
MGI:1919619	Ehd4 EH-domain containing 4-KJR (Fragment)	94	3	138	3	86	2
MGI:88474	Cox5a Cytochrome c oxidase subunit 5A	93	3	140	7	158	12
MGI:1920973	Sh3bgrl3 SH3 domain-binding glutamic acid-rich-like protein 3	91	5	51	2	63	4
MGI:96392	Icam1 Isoform 1 of Intercellular adhesion molecule 1 precursor	91	3	116	4	0	0
MGI:99431	Arf1 ADP-ribosylation factor 1	91	2	0	0	65	2
MGI:1338859	P2rx4 purinergic receptor P2X, ligand-gated ion channel 4	90	3	0	0	0	0
MGI:1347344	Gla alpha-galactosidase A	90	2	0	0	29	1
MGI:96748	Lamp2 Isoform LAMP-2A of Lysosome-associated membrane glycoprotein 2 precursor	89	5	170	9	167	13

MGI:1915339	Arpc4 Actin-related protein 2/3 complex subunit 4	89	4	39	2	46	2
MGI:1194924	Cd180 CD180 antigen precursor	87	3	105	1	159	2
MGI:2138133	Lrrc59 Leucine-rich repeat-containing protein 59	87	3	68	1	69	2
MGI:1921262	Rap2b Ras-related protein Rap-2b precursor	84	3	91	7	68	3
MGI:109175	Dab2 Isoform p93 of Disabled homolog 2	84	2	0	0	87	4
MGI:1201780	Atp6v1a Isoform 1 of Vacuolar ATP synthase catalytic subunit A	83	2	79	4	101	4
MGI:97810	Ptprc Isoform 2 of Leukocyte common antigen precursor	83	3	107	2	229	8
MGI:95912	H2-Q2;H2-L;H2-Q1 H-2 class I histocompatibility antigen, L-D alpha chain precursor	81	4	0	0	52	2
MGI:88338	Cd44 CD44 antigen isoform c	78	1	81	4	72	3
MGI:1194505	C1qbp complement component 1, q subcomponent binding protein	77	3	28	3	68	8
MGI:95498	Fcgr1 High affinity immunoglobulin gamma Fc receptor I precursor	75	4	94	6	105	3
MGI:1914253	Uqcrc2 Cytochrome b-c1 complex subunit 2	74	2	219	4	117	4
MGI:95832	Grn granulin	74	6	110	6	92	8
MGI:1890149	Tpm3 Isoform 2 of Tropomyosin alpha-3 chain	73	3	0	0	161	6
MGI:97143	Marcks11 MARCKS-related protein	71	2	116	3	0	0
MGI:1919103	Pdia6 thioredoxin domain containing 7	71	3	48	2	42	1
MGI:1316715	Cox7a2 Cytochrome c oxidase polypeptide VIIa-liver/heart	71	3	57	2	63	3
MGI:1923959	Arpc2 Actin-related protein 2/3 complex subunit 2	65	2	26	1	45	3
MGI:1913325	Chchd3 Coiled-coil-helix-coiled-coil-helix domain-containing protein 3	65	1	54	1	110	4
MGI:88339	Cd48 CD48 antigen precursor	64	1	0	0	0	0
MGI:1858210	Stx7 Syntaxin-7	64	1	55	1	100	4

MGI:1923864	Immt Isoform 1 of Mitochondrial inner membrane protein	63	1	50	1	119	5
MGI:1914195	Sdha Succinate dehydrogenase [ubiquinone] flavoprotein subunit	62	2	42	1	63	1
MGI:1913697	Mgst3 Microsomal glutathione S-transferase 3	61	1	50	1	49	1
MGI:107777	Atp5j;LOC674583 ATP synthase-coupling factor 6	61	4	164	5	173	11
MGI:894326	Atp6v1e1 Vacuolar proton pump subunit E 1	61	4	27	1	0	0
MGI:1344382	Creg1 Protein CREG1 precursor	60	2	0	0	0	0
MGI:1201689	Tapbp Isoform Short of Tapasin precursor	59	1	91	3	0	0
MGI:2148924	Clic1 Chloride intracellular channel protein 1	59	1	0	0	31	1
MGI:1333768	Krt6b Keratin, type II cytoskeletal 6B	59	2	25	1	54	10
MGI:98073	Rpl7 60S ribosomal protein L7	58	1	68	2	38	1
MGI:95496	Fcer1g High affinity immunoglobulin epsilon receptor subunit gamma precursor	58	4	75	5	75	3
MGI:3607712	Krt73 Keratin, type II cytoskeletal 73	57	1	65	1	77	3
MGI:87866	Acadl Long-chain specific acyl-CoA dehydrogenase	55	1	46	1	97	3
MGI:106092	Etfa Electron transfer flavoprotein subunit alpha	53	3	0	0	119	3
MGI:97552	Pgam1 Phosphoglycerate mutase 1	53	1	0	0	0	0
MGI:96160	Hmga1 Isoform HMG-I of High mobility group protein HMG-I/HMG-Y	52	2	37	1	42	3
MGI:1926952	Cyb5 Cytochrome b5	51	1	179	2	25	1
MGI:98257	Msr1 macrophage scavenger receptor 1 isoform a	49	1	99	3	0	0
MGI:1328323	Syngr1 Isoform 1A of Synaptogyrin-1	49	1	25	1	43	2
MGI:1915009	5033414D02Rik Uncharacterized protein C9orf46 homolog	49	1	0	0	0	0
MGI:1913358	Ndufa9 NADH dehydrogenase [ubiquinone] 1 alpha subcomplex subunit 9	49	2	48	1	55	1
MGI:1354721	Slc25a13 Calcium-binding mitochondrial carrier	48	1	0	0	152	7

	protein Aralar2						
MGI:1196297	Hgsnat Heparan-alpha-glucosaminide N-acetyltransferase	48	1	0	0	42	1
MGI:96610	Itgb1 Integrin beta-1 precursor	48	2	24	1	0	0
MGI:2443807	Osbpl8 oxysterol-binding protein-like protein 8 isoform b	48	1	0	0	0	0
MGI:1316658	Cyba Isoform 1 of Cytochrome b-245 light chain	48	2	62	3	62	3
MGI:1914647	Erp29 5 kDa protein	47	1	26	1	25	1
MGI:3040672	Rpl23a 60S ribosomal protein L23a	47	1	47	1	0	0
MGI:1913758	2400001E08Rik UPF0404 protein C11orf59 homolog	46	2	49	2	40	2
MGI:1333782	Pld3 Phospholipase D3	46	1	0	0	43	1
MGI:99435	Arf6 ADP-ribosylation factor 6	46	2	0	0	27	1
MGI:88271	Cat Catalase	45	1	0	0	32	1
MGI:88262	Cap1 Adenylyl cyclase-associated protein 1	45	1	58	3	69	3
MGI:1932697	Mapbpip Mitogen-activated protein-binding protein-interacting protein	45	1	50	2	78	2
MGI:106028	Rhoc Rho-related GTP-binding protein RhoC precursor	45	1	26	1	0	0
MGI:1855697	Atp5e ATP synthase subunit epsilon, mitochondrial	45	1	0	0	45	1
MGI:1914930	Sdhb Succinate dehydrogenase [ubiquinone] iron-sulfur subunit	44	1	0	0	0	0
MGI:1913293	Atp5d ATP synthase subunit delta	44	2	97	3	49	1
MGI:1927558	Atp5j2 ATP synthase subunit f	44	2	45	2	48	2
MGI:107788	Atp1b3 Sodium/potassium-transporting ATPase subunit beta-3	43	2	0	0	0	0
MGI:1914291	Oxct1 Succinyl-CoA:3-ketoacid-coenzyme A transferase 1	43	2	32	1	92	3

MGI:88475	Cox5b cytochrome c oxidase, subunit Vb	42	2	47	3	78	7
MGI:2443241	Ndufs1 NADH-ubiquinone oxidoreductase 75 kDa subunit	42	1	0	0	104	3
MGI:1926967	Hsd17b12 Isoform 1 of Estradiol 17-beta-dehydrogenase 12	41	1	0	0	0	0
MGI:104819	Hnrnpa2b1 Isoform 3 of Heterogeneous nuclear ribonucleoproteins A2/B1	41	1	0	0	60	2
MGI:1915021	Arpc5 Actin-related protein 2/3 complex subunit 5	41	1	26	1	0	0
MGI:2442032	Daglb Sn1-specific diacylglycerol lipase beta	40	1	0	0	0	0
MGI:1346330	Banf1 Barrier-to-autointegration factor	40	1	0	0	25	1
MGI:1923442	Abhd12 Abhydrolase domain-containing protein 12	40	1	0	0	0	0
MGI:97555	Pgk1 Phosphoglycerate kinase 1	39	2	0	0	0	0
MGI:2148491	Acaa1b;Acaa1a 3-ketoacyl-CoA thiolase A	39	1	0	0	0	0
MGI:95393	EG433182;Eno1;LOC100044223 Alpha-enolase	38	1	0	0	0	0
MGI:96693	Krt19 Keratin, type I cytoskeletal 19	38	2	82	4	33	2
MGI:105941	Mpp1 55 kDa erythrocyte membrane protein	38	1	31	1	41	1
MGI:106636	Atp5k ATP synthase subunit e	38	2	0	0	71	3
MGI:1098259	Capg Macrophage-capping protein	38	2	78	3	53	2
MGI:1932395	Rrbp1 Isoform 3 of Ribosome-binding protein 1	38	1	35	1	82	2
MGI:97356	Nme2 Nucleoside diphosphate kinase B	37	2	36	1	139	4
MGI:106612	Myo1c Isoform B of Myosin-Ic	37	1	113	3	57	3
MGI:102705	Gng2 Guanine nucleotide-binding protein G(I)/G(S)/G(O) subunit gamma-2 precursor	37	2	69	3	38	3
MGI:99778	Gpd2 Glycerol phosphate dehydrogenase 2	37	1	0	0	0	0
MGI:3582693	Tor1aip1 Torsin-1A-interacting protein 1	37	1	0	0	0	0
MGI:1921867	Scpep1 serine carboxypeptidase 1	37	1	25	1	0	0
MGI:95665	Gba Glucosylceramidase precursor	37	1	0	0	0	0

MGI:2178103	Arhgdia Rho GDP-dissociation inhibitor 1	36	1	0	0	0	0
MGI:99702	Bax Apoptosis regulator BAX	36	1	0	0	0	0
MGI:1194508	Ddost Dolichyl-diphosphooligosaccharide--protein glycosyltransferase 48 kDa subunit precursor	36	1	68	2	86	5
MGI:1355332	Myadm Myeloid-associated differentiation marker	36	1	86	1	37	1
MGI:3032636	Ugt1a6b;Ugt1a7c;Ugt1a10;Ugt1a5;Ugt1a2;Ugt1a9;LOC632297;Ugt1a1 UDP-glucuronosyltransferase 1-7C precursor	36	1	47	1	40	2
MGI:1913391	Ifitm3 INTERFERON-INDUCIBLE PROTEIN	36	2	45	1	25	1
MGI:1890889	Ndufs5;BC002163 NADH dehydrogenase [ubiquinone] iron-sulfur protein 5	36	1	0	0	33	1
MGI:3045213	Tlr13 Toll-like receptor 13 precursor	36	1	0	0	0	0
MGI:1913826	Uqcrh Cytochrome b-c1 complex subunit 6	36	1	52	1	27	1
MGI:1913540	Atp6v1g1 Vacuolar proton pump subunit G 1	35	1	46	2	38	2
MGI:1913394	Atp6v1f Vacuolar proton pump subunit F	35	1	0	0	0	0
MGI:1333743	Mpeg1 macrophage expressed gene 1	35	2	90	3	0	0
MGI:1270152	Reep5 receptor accessory protein 5	35	1	25	1	0	0
MGI:2143132	Plekho2 46 kDa protein	35	1	0	0	63	2
MGI:107812	Tubb5 Tubulin beta-5 chain	34	3	0	0	139	3
MGI:103016	Ppp1ca Serine/threonine-protein phosphatase PP1-alpha catalytic subunit	33	1	0	0	0	0
MGI:1919292	Cotl1 Coactosin-like protein	33	1	38	1	51	1
MGI:96685	Krt10 keratin complex 1, acidic, gene 10	32	1	0	0	55	2
MGI:1337100	Wdr1 WD repeat-containing protein 1	32	1	32	1	0	0
MGI:1345283	Slc25a1 solute carrier family 25 (mitochondrial carrier; citrate transporter), member 1	32	1	69	3	65	3
MGI:104560	Nsf Vesicle-fusing ATPase	31	1	0	0	95	2
MGI:104568	Hcls1 Hematopoietic lineage cell-specific protein	30	1	58	2	55	2

MGI:3643413	EG268795 hypothetical protein isoform 2	30	1	66	1	64	2
MGI:3644100	EG619883 similar to ribosomal protein L30	30	1	43	1	0	0
MGI:1333871	Hsd17b10 3-hydroxyacyl-CoA dehydrogenase type-2	30	1	0	0	0	0
MGI:101847	Mnda;Ifi205 Interferon-activable protein 205-A	30	1	0	0	0	0
MGI:1298382	Plp2 Proteolipid protein 2	30	1	38	2	0	0
MGI:1919022	1300012G16Rik Isoform 1 of Putative phospholipase B-like 2 precursor	29	1	0	0	0	0
MGI:104614	Cox6c Cytochrome c oxidase polypeptide VIc	29	1	0	0	0	0
MGI:99529	Cd63 Cd63 antigen, full insert sequence	28	1	25	2	44	3
MGI:97298	Sept2 Septin-2	28	1	0	0	0	0
MGI:2443286	Slc2a6 solute carrier family 2 (facilitated glucose transporter), member 6	28	1	32	2	0	0
MGI:103226	LOC100048613;Cox7c Cytochrome c oxidase subunit 7C	27	1	0	0	31	1
MGI:1351597	Atp5l ATP SYNTHASE, H+ TRANSPORTING, MITOCHONDRIAL F0 COMPLEX, SUBUNIT G	27	2	0	0	0	0
MGI:1336171	Gng12 Guanine nucleotide-binding protein G(I)/G(S)/G(O) subunit gamma-12 precursor	27	1	0	0	0	0
MGI:107686	Ndufa4 NADH dehydrogenase [ubiquinone] 1 alpha subcomplex subunit 4	27	1	0	0	131	8
MGI:1277124	Asah1 Acid ceramidase precursor	27	1	0	0	48	2
MGI:1913963	Actr2 Actin-related protein 2	27	1	28	1	0	0
MGI:1350927	Rpl8 60S ribosomal protein L8	26	1	38	1	0	0
MGI:97286	Ncl Nucleolin	26	1	0	0	29	1
MGI:1890156	Stx8 Syntaxin-8	26	1	0	0	0	0
MGI:3646088	EG622339 predicted gene, EG622339	26	2	0	0	25	2
MGI:98445	Surf4 Surfeit locus protein 4	26	1	0	0	64	1

MGI:2136742	Pcdhb8 Protocadherin beta 8	26	1	0	0	0	0
MGI:2385030	Krt79 Keratin, type II cytoskeletal 79	25	2	0	0	0	0
MGI:1261415	Sgpl1 Sphingosine-1-phosphate lyase 1	25	1	90	4	25	1
MGI:1914745	Tmem167b UPF0373 protein C1orf119 homolog precursor	25	1	0	0	0	0
MGI:98003	Rpl18 60S ribosomal protein L18	25	1	54	3	58	2
MGI:1931052	Aldoat2 Fructose-bisphosphate aldolase	24	1	71	1	76	2
MGI:96429	Ifi204 72 kDa protein	24	1	0	0	0	0
MGI:88348	Cd9 CD9 antigen	24	1	58	1	41	1
MGI:101757	LOC100048522 similar to Cofilin-1	0	0	296	16	0	0
MGI:95556	Flna Isoform 1 of Filamin-A	0	0	643	15	775	18
MGI:95896	H2-Q2;H2-L; H-2D cell surface glycoprotein (Fragment)	0	0	193	11	0	0
MGI:95896	H2-D1 MRNA, . precursor	0	0	156	7	0	0
MGI:1913677	Cyb5b Cytochrome b5 type B precursor	0	0	73	5	81	5
MGI:1915615	Rab14 Ras-related protein Rab-14	0	0	80	5	74	4
MGI:3648759	Glyceraldehyde-3-phosphate dehydrogenase (GAPDH) isoform 1	0	0	151	5	0	0
MGI:96103	Hk1 Isoform HK1-SA of Hexokinase-1	0	0	114	4	149	5
MGI:1915974	Arl8a ADP-ribosylation factor-like protein 8A	0	0	127	4	41	3
MGI:1338859	P2rx4 P2X purinoceptor	0	0	58	3	0	0
MGI:1343142	Arcp1b Arpc1b protein	0	0	59	3	57	1
MGI:1913695	Cyc1 Isoform 1 of Cytochrome c1, heme protein	0	0	67	3	0	0
MGI:96759	Ldha L-lactate dehydrogenase A chain	0	0	77	3	68	2
MGI:95499	Fcgr2b Fc receptor, IgG, low affinity IIb isoform 1	0	0	78	3	0	0
MGI:1920960	Tubb2b Tubulin beta-2B chain	0	0	100	3	0	0
MGI:95792	Got2 Aspartate aminotransferase	0	0	102	3	192	11

MGI:1196457	Atpif1 ATPase inhibitor	0	0	32	2	31	2
MGI:1855694	Isg15; Ubiquitin cross-reactive protein precursor	0	0	39	2	0	0
MGI:98809	Tpm1 Isoform 1 of Tropomyosin alpha-1 chain	0	0	44	2	0	0
MGI:1917160	Slc25a24 Calcium-binding mitochondrial carrier protein SCaMC-1	0	0	45	2	82	3
MGI:1859821	Prdx5 Isoform Mitochondrial of Peroxiredoxin-5	0	0	47	2	54	3
MGI:108057	Rpl6 60S ribosomal protein L6	0	0	49	2	0	0
MGI:96904	M6pr Cation-dependent mannose-6-phosphate receptor precursor	0	0	49	2	0	0
MGI:1915831	Tmed10 Isoform 1 of Transmembrane emp24 domain-containing protein 10 precursor	0	0	52	2	40	2
MGI:1915599	Ndufs3 NADH dehydrogenase [ubiquinone] iron-sulfur protein 3	0	0	52	2	111	3
MGI:2137679	Sfxn3 Isoform 1 of Sideroflexin-3	0	0	52	2	34	1
MGI:103286	Atp6v0a1 Isoform A1-II of Vacuolar proton translocating ATPase 116 kDa subunit a isoform 1	0	0	53	2	45	2
MGI:96955	Slc3a2 CD98 heavy chain	0	0	56	2	35	1
MGI:1100495	Atp5f1 ATP synthase subunit b	0	0	57	2	57	3
MGI:1926080	Slc25a12 Calcium-binding mitochondrial carrier protein Aralar1	0	0	68	2	0	0
MGI:2143132	Plekho2 Pleckstrin homology domain-containing family O member 2	0	0	68	2	0	0
MGI:106008	Anxa5 Annexin A5	0	0	75	2	0	0
MGI:104563	Napa Alpha-soluble NSF attachment protein	0	0	75	2	78	3
MGI:106920	Tmpo Isoform Beta of Lamina-associated polypeptide 2 isoforms beta/delta/epsilon/gamma	0	0	98	2	128	4
MGI:2445284	Lrrc25 Leucine-rich repeat-containing protein 25 precursor	0	0	108	2	0	0

MGI:1194884	Evl Isoform 2 of Ena/VASP-like protein	0	0	25	1	0	0
MGI:106098	Etfb Electron transfer flavoprotein subunit beta	0	0	25	1	27	2
MGI:1916800	Bst2 Bone marrow stromal antigen 2 precursor	0	0	26	1	0	0
MGI:1099464	Ssr4 signal sequence receptor, delta	0	0	26	1	0	0
MGI:107567	Irgm Isoform 1 of Immunity-related GTPase family M protein	0	0	27	1	0	0
MGI:1928375	Arpc3 Actin-related protein 2/3 complex subunit 3	0	0	28	1	0	0
MGI:1859307	Unc93b1 Isoform 1 of Protein unc-93 homolog B1	0	0	29	1	0	0
MGI:99262	Rpl22;mCG_130059 60S ribosomal protein L22	0	0	30	1	0	0
MGI:1298405	Ap2m1 AP-2 complex subunit mu-1	0	0	30	1	77	2
MGI:1277214	Sept11 Isoform 3 of Septin-11	0	0	31	1	0	0
MGI:1351455	Rpl13a 60S ribosomal protein L13a	0	0	31	1	25	1
MGI:1328317	Trex1 Three prime repair exonuclease 1	0	0	32	1	0	0
MGI:1353561	Vapa Vesicle-associated membrane protein-associated protein A	0	0	32	1	0	0
MGI:101912	Dad1 Dolichyl-diphosphooligosaccharide--protein glycosyltransferase subunit DAD1	0	0	32	1	0	0
MGI:1931071	Sec61a2 Sec61, alpha subunit 2	0	0	33	1	30	2
MGI:3646682	LOC675192;EG668182 hypothetical protein	0	0	34	1	0	0
MGI:98085	Rpn2 Dolichyl-diphosphooligosaccharide--protein glycosyltransferase subunit 2 precursor	0	0	34	1	51	1
MGI:1276534	Bcat2 Branched-chain-amino-acid aminotransferase	0	0	35	1	0	0
MGI:1929899	Sqrdl Sulfide:quinone oxidoreductase	0	0	35	1	0	0
MGI:88578	Cycc Cytochrome c, somatic	0	0	36	1	57	2
MGI:2149821	Hsd17b11 Isoform 1 of Estradiol 17-beta-dehydrogenase 11 precursor	0	0	36	1	0	0
MGI:1914518	2900073G15Rik myosin light chain, regulatory B-like	0	0	37	1	0	0

MGI:88336	Cd40 Isoform I of Tumor necrosis factor receptor superfamily member 5 precursor	0	0	37	1	0	0
MGI:107505	Alox5ap Arachidonate 5-lipoxygenase-activating protein	0	0	38	1	57	1
MGI:894311	Lilrb3 paired-Ig-like receptor B	0	0	38	1	0	0
MGI:1913404	Tmem14c Transmembrane protein 14C	0	0	41	1	0	0
MGI:1915903	Samm50 Sorting and assembly machinery component 50 homolog	0	0	41	1	25	1
MGI:96795	Lmnb1 Lamin-B1	0	0	42	1	52	2
MGI:95762	Gm2a Ganglioside GM2 activator precursor	0	0	46	1	27	1
MGI:1098623	Acaa2 3-ketoacyl-CoA thiolase, mitochondrial	0	0	48	1	131	3
MGI:1913775	Timm50 Import inner membrane translocase subunit TIM50	0	0	48	1	33	1
MGI:1914761	Tmed9 1 Glycoprotein 25L2 homolog	0	0	50	1	43	1
MGI:1913462	Sec61b Protein transport protein Sec61 subunit beta	0	0	50	1	0	0
MGI:3648523	EG432798 similar to ribosomal protein L27A	0	0	51	1	51	1
MGI:3646154	EG241053 similar to ribosomal protein L12	0	0	51	1	39	1
MGI:1349419	Aifm1 Apoptosis-inducing factor 1	0	0	51	1	37	1
MGI:1913296	Ndufb5 NADH dehydrogenase [ubiquinone] 1 beta subcomplex subunit 5	0	0	61	1	41	1
MGI:95394	Eno2 Enolase	0	0	63	1	25	1
MGI:107502	Hist1h1d Histone H1.3	0	0	0	0	292	22
MGI:104680	Hspe1 10 kDa heat shock protein, mitochondrial	0	0	0	0	268	21
MGI:95773	Gnai3 Guanine nucleotide-binding protein G	0	0	0	0	207	12
MGI:107450	Dld Dihydrolipoyl dehydrogenase	0	0	0	0	138	3
MGI:1097712	Npc1 Niemann-Pick C1 protein precursor	0	0	0	0	101	2
MGI:1915084	Idh3a Isoform 1 of Isocitrate dehydrogenase [NAD] subunit alpha	0	0	0	0	91	1

MGI:1313266	Alcam CD166 antigen precursor	0	0	0	0	89	3
MGI:1913944	Uqcfs1 Cytochrome b-c1 complex subunit Rieske	0	0	0	0	88	3
MGI:88232	C5ar1 complement component 5, receptor 1	0	0	0	0	82	4
MGI:1315197	Hk2 Hexokinase-2	0	0	0	0	74	3
MGI:1096342	Rhoa Transforming protein RhoA precursor	0	0	0	0	73	3
MGI:96414	Idh2 Isocitrate dehydrogenase [NADP]	0	0	0	0	72	3
MGI:1927091	Myo1g Myosin-Ig	0	0	0	0	70	2
MGI:1929260	Mtch2 Mitochondrial carrier homolog 2	0	0	0	0	70	1
MGI:96113	Hmgb1; High mobility group protein B1	0	0	0	0	70	2
MGI:1927234	Suc1g1 Succinyl-CoA ligase [GDP-forming] subunit alpha	0	0	0	0	62	1
MGI:99926	mt-Atp8 ATP synthase protein 8	0	0	0	0	56	2
MGI:2137677	Sfxn1 Sideroflexin-1	0	0	0	0	52	2
MGI:99425	Rab11b Ras-related protein Rab-11B	0	0	0	0	52	2
MGI:1926170	Dlst Isoform 1 of Dihydrolipoyllysine-residue succinyltransferase component of 2- oxoglutarate dehydrogenase complex	0	0	0	0	51	2
MGI:894297	Clta Clathrin light chain A	0	0	0	0	50	4
MGI:1933395	Lactb;LOC677144 Serine beta-lactamase-like protein LACTB	0	0	0	0	49	1
MGI:1921372	Tmem43 Transmembrane protein 43	0	0	0	0	49	1
MGI:1917529	Krt78 keratin Kb40	0	0	0	0	49	1
MGI:87870	Acat1 Acetyl-CoA acetyltransferase	0	0	0	0	48	1
MGI:1890682	Evi2b EVI2B protein precursor	0	0	0	0	47	2
MGI:103294	Prg2 Bone marrow proteoglycan precursor	0	0	0	0	45	1
MGI:1913739	Rpl35; 60S ribosomal protein L35	0	0	0	0	45	1
MGI:3026965	Ccdc109a Isoform 1 of Coiled-coil domain-	0	0	0	0	44	1

	containing protein 109A						
MGI:2136460	Echs1 Enoyl-CoA hydratase, mitochondrial precursor	0	0	0	0	43	1
MGI:105368	Atp2b2 Plasma membrane calcium-transporting ATPase 2	0	0	0	0	42	1
MGI:1929464	Sec11a Signal peptidase complex catalytic subunit SEC11A	0	0	0	0	40	1
MGI:1914434	Ndufa13 NADH dehydrogenase [ubiquinone] 1 alpha subcomplex subunit 13	0	0	0	0	40	2
MGI:1890463	Ear6 Eosinophil-associated ribonuclease 6	0	0	0	0	40	1
MGI:2385311	Dlat Dihydrolipoyllysine-residue acetyltransferase component of pyruvate dehydrogenase complex	0	0	0	0	40	1
MGI:1922169	4930471M23Rik Uncharacterized protein C2orf18 homolog precursor	0	0	0	0	39	1
MGI:97532	Pdha1 Pyruvate dehydrogenase E1 component subunit alpha	0	0	0	0	34	1
MGI:1913745	Ndufb3 NADH dehydrogenase [ubiquinone] 1 beta subcomplex subunit 3	0	0	0	0	32	1
MGI:97394	Oat Ornithine aminotransferase	0	0	0	0	31	1
MGI:1888994	Fmn1 Isoform 1 of Formin-like protein 1	0	0	0	0	31	1
MGI:1277989	Shmt2 Serine hydroxymethyltransferase	0	0	0	0	28	1
MGI:109356	Snap23 synaptosomal-associated protein	0	0	0	0	28	1
MGI:1346518	Scamp2 Secretory carrier-associated membrane protein 2	0	0	0	0	28	1
MGI:3616088	Ogdhl oxoglutarate dehydrogenase-like	0	0	0	0	28	1
MGI:1321389	Vamp3 Vesicle-associated membrane protein 3	0	0	0	0	28	1
MGI:1915513	Pdhb Pyruvate dehydrogenase E1 component subunit beta	0	0	0	0	28	2

MGI:101761	Hmga2 High mobility group protein HMGI-C	0	0	0	0	27	1
MGI:1914864	Atp6v1h Vacuolar proton pump subunit H	0	0	0	0	27	1
MGI:108403	Rpo1-3; RNA polymerase 1-3	0	0	0	0	26	1
MGI:2679150	Oog1 protein isoform 2	0	0	0	0	25	1
MGI:1916931	Cdk3 Isoform 1 of Cell division protein kinase 3	0	0	0	0	25	1
MGI:3037658	H2afy3 H2A histone family, member Y3, full insert sequence	0	0	0	0	24	1

Table 8.2 Biological process GO terms for regulated proteins

Biological Process			
0-3hRP		LPS	
Term	Genes	Term	Genes
Up-regulated			
GO:0065007: biological regulation	Capza2, Capzb, Cd14, Ctss, Cybb, H2-D1, Hsp90b1, Hspa8, Ifitm3, Lcp1, Msn, Msr1, Pdia3, Prdx1, Psap, Rap1b, Sod2, Tln1, Vdac2	GO:0065007: biological regulation	Cd14, H2-D1, Ifitm3, Msr1, Prdx1
GO:0050896: response to stimulus	Cd14, Cybb, H2-D1, Hsp90b1, Hspa8, Ifitm3, Lcp1, Lyz2, Pdia3, Pkm, Prdx1, Psap, Rap1b, Sod2	GO:0050896: response to stimulus	Cd14, H2-D1, Ifitm3, Prdx1
GO:0008152: metabolic process	Atp6v1b2, Ctss, Cybb, Hsp90b1, Hspa8, Lap1, Lyz2, Pdia3, Pkm, Prdx1, Psap, Rap1b, Sod2	GO:0002376: immune system process	Cd14, H2-D1, Ifitm3, Prdx1

GO:0044237: cellular metabolic process	Atp6v1b2, Ctss, Cybb, Hsp90b1, Hspa8, Lyz2, Pdia3, Pkm, Prdx1, Psap, Rap1b, Sod2	GO:0006950: response to stress	Cd14, Ifitm3, Prdx1
GO:0071704: organic substance metabolic process	Atp6v1b2, Ctss, Hsp90b1, Hspa8, Lap1, Lyz2, Pdia3, Pkm, Psap, Rap1b, Sod2	GO:0044763: single-organism cellular process	Atp6v1b2, Ifitm3, Prdx1
GO:0006950: response to stress	Cd14, Cybb, Hsp90b1, Hspa8, Ifitm3, Lcp1, Lyz2, Pdia3, Pkm, Prdx1, Sod2	GO:0045087: innate immune response	Cd14, Ifitm3, Prdx1
GO:0023051: regulation of signaling	Capzb, Pdia3, Prdx1, Psap, Rap1b, Sod2, Vdac2	GO:0008152: metabolic process	Atp6v1b2, Prdx1
GO:0002376: immune system process	Cd14, Cybb, H2-D1, Ifitm3, Lcp1, Prdx1, Sod2	GO:0002252: immune effector process	Ifitm3, Prdx1
GO:0045087: innate immune response	Cd14, Cybb, Ifitm3, Prdx1	GO:0009605: response to external stimulus	Cd14, Ifitm3
GO:0009605: response to external stimulus	Cd14, Ifitm3, Lyz2, Sod2		

GO:0043408: regulation of MAPK cascade	Prdx1, Psap, Rap1b		
GO:0002252: immune effector process	Ifitm3, Lcp1, Prdx1		
Down-regulated			
GO:0050896: response to stimulus	Cd36, Idh2, Lmna	GO:0008150: biological_process	Aldh2, Atp5b, Glud1, Gpnmb, Lmna, Mdh2
GO:0006950: response to stress	Cd36, Idh2, Lmna	GO:0008152: metabolic process	Aldh2, Atp5b, Glud1, Mdh2
GO:0023052: signaling	Cd36, Lmna	GO:0071704: organic substance metabolic process	Atp5b, Glud1, Mdh2
GO:0007165: signal transduction	Cd36, Lmna	GO:0044237: cellular metabolic process	Atp5b, Glud1, Mdh2
GO:0006357: regulation of transcription from RNA polymerase II promoter	Cd36, Lmna	GO:0050896: response to stimulus	Glud1, Lmna
GO:0051716: cellular response to stimulus	Cd36, Lmna	GO:0023051: regulation of signaling	Glud1, Lmna

Table 8.3 Cellular localization GO terms for regulated proteins

Cellular localization			
0-3hRP		LPS	
Term	Genes	Term	Genes
Up-regulated			
GO:0016020: membrane	Atp6v1b2, Capza2, Capzb, Cd14, Cox6b1, Ctss, Cybb, Efhd2, H2-D1, Hsp90b1, Ifitm3, Lcp1, Lrrc25, Lrrc59, Mpeg1, Msn, Msr1, Pkm, Rap1b, Sod2, Tcirg1, Tln1, Vdac2	GO:0016020: membrane	Atp6v1b2, Cd14, H2-D1, Ifitm3, Lrrc25, Msr1
GO:0031982: vesicle	Actg1, Atp6v1b2, Capza2, Capzb, Cd14, H2-D1, Hsp90b1, Hspa8, Ifitm3, Lcp1, Lyz2, Msn, Msr1, Pdia3, Pkm, Prdx1, Psap, Rap1b, Tagln2, Tln1	GO:0031982: vesicle	Atp6v1b2, Cd14, H2-D1, Ifitm3, Msr1, Prdx1

GO:0005886: plasma membrane	Atp6v1b2, Cd14, Cybb, H2-D1, Hsp90b1, Ifitm3, Lcp1, Msn, Msr1, Pkm, Rap1b, Tcirg1, Tln1	GO:0005886: plasma membrane	Atp6v1b2, Cd14, H2-D1, Ifitm3, Msr1
GO:0005739: mitochondrion	Cox6b1, Cybb, Lrrc59, Pkm, Prdx1, Psap, Sod2, Tcirg1, Vdac2	GO:0005829: cytosol	Atp6v1b2, Msr1, Prdx1
GO:0042995: cell projection	Atp6v1b2, Capzb, Cybb, Hspa8, Lcp1, Lyz2, Msn, Pkm, Tln1	GO:0009986: cell surface	Cd14, H2-D1, Ifitm3
GO:0005829: cytosol	Atp6v1b2, Hsp90b1, Hspa8, Lcp1, Msr1, Prdx1	GO:0005634: nucleus	Ifitm3, Prdx1
GO:0009986: cell surface	Cd14, Ctss, H2-D1, Ifitm3, Msn, Pdia3	GO:0005764: lysosome	Atp6v1b2, Ifitm3
GO:0005783: endoplasmic reticulum	Cybb, Hsp90b1, Ifitm3, Lrrc59, Lyz2, Pdia3		
GO:0005634: nucleus	Hspa8, Ifitm3, Lrrc59, Pkm, Prdx1		

GO:0005764: lysosome	Atp6v1b2, Ctss, Ifitm3, Psap, Tcirg1		
GO:0005794: Golgi apparatus	Cybb, Lyz2		
Down-regulated			
GO:0044444: cytoplasmic part	Cd36, Idh2, Lmna	GO:0043226: organelle	Aldh2, Atp5b, Glud1, Gpnmb, Lmna, Mdh2
GO:0016020: membrane	Cd36, Lmna	GO:0016020: membrane	Atp5b, Glud1, Gpnmb, Mdh2
GO:0005739: mitochondrion	Cd36, Idh2	GO:0005739: mitochondrion	Aldh2, Atp5b, Glud1, Mdh2
		GO:0031982: vesicle	Aldh2, Atp5b, Gpnmb, Mdh2
		GO:0005886: plasma membrane	Atp5b, Gpnmb, Mdh2

8.2 Kinase proteome profiler

Table 8.4 Kinase proteome profiler coordinates and phosphorylation sites

Coordinate	Target/Control	Alternate Nomenclature	Phosphorylation Site Detected
A1, A2	Positive Control	Control (+)	—
A21, A22	Positive Control	Control (+)	—
B3, B4	Akt1	PKB α , RAC α	S473
B5, B6	Akt2	PKB β , RAC β	S474
B7, B8	Akt3	PKB γ , RAC γ	S472
B9, B10	Akt pan	—	S473, S474, S472
B11, B12	CREB	—	S133
B13, B14	ERK1	MAPK3, p44 MAPK	T202/Y204
B15, B16	ERK2	MAPK1, p42 MAPK	T185/Y187
B17, B18	GSK-3 α/β	GSK3 α /GSK3 β	S21/S9
B19, B20	GSK-3 β	GSK3B β	S9
C3, C4	HSP27	HSPB1, SRP27	S78/S82
C5, C6	JNK1	MAPK8, SAPK1 γ	T183/Y185
C7, C8	JNK2	MAPK9, SAPK1 α	T183/Y185
C9, C10	JNK3	MAPK10, SAPK1 β	T221/Y223
C11, C12	JNK pan	—	T183/Y185, T221/Y223
C13, C14	MKK3	MEK3, MAP2K3	S218/T222
C15, C16	MKK6	MEK6, MAP2K6	S207/T211
C17, C18	MSK2	RSKb, RPS6KA4	S360
D3, D4	p38 α	MAPK14, SAPK2A, CSBP1	T180/Y182

D5, D6	p38 β	MAPK11, SAPK2B, p38-2	T221/Y223
D7, D8	p38 δ	MAPK13, SAPK4	S360
D9, D10	p38 γ	MAPK13, SAPK3, ERK6	T183/Y185
D11, D12	p53	—	S46
D13, D14	p70 S6 Kinase	S6K1, p70a, RPS6KB1	T421/S424
D15, D16	RSK1	MAPKAPK1a, RPS6KA1	S380
D17, D18	RSK2	ISPK-1, RPS6KA3	S386
D19, D20	TOR	—	S2448
E19, E20	PBS	Control (-)	—
F1, F2	Positive Control	Control (+)	—

8.3 Fractionation of *S. mansoni* cercarial E/S products

To investigate the role of different components of *S. mansoni* cercarial E/S products in the responses observed in BMM ϕ s, 0-3hRP was fractionated into a soluble preparation (0-3hRP_S) and a pellet (0-3hRP_P) by using ultracentrifugation.

8.3.1 Fractionation of 0-3hRP

0-3hRP was fractionated by centrifugation at 100,000g for 1 hour at 4°C into a soluble preparation and a pellet. The soluble 0-3hRP preparation was denoted as 0-3hRP_S, whilst the pellet was re-suspended in PBS and denoted as 0-3hRP_P. The protein content of both preparations was quantified as specified before (2.2.1).

8.3.2 SDS polyacrylamide gel electrophoresis (PAGE) of fractions

0-3hRP and its fractions were prepared for gel electrophoresis by taking 20 μ g of protein from each preparation, mixing it with 1X LDS sample buffer® (Life Technologies) plus 1X NuPAGE® Sample Reducing Agent (Life Technologies) and boiling it for 5min at 95°C. Prepared samples and Novex® Sharp Pre-stained Protein Standard (Life Technologies) were loaded onto 4-12% NuPAGE® Bis-Tris Precast Gels (Life Technologies) and run for 2h at 200V in 1X NuPAGE® MOPS SDS Running Buffer (Life Technologies).

Gels were directly imaged in a Personal Molecular Imager (BioRad) using a 638nm excitation laser and images acquired with QuantityOne® software (Biorad).

Alternatively, gels were stained over night using Brilliant Blue G concentrate (SIGMA) and then de-stained washing several times in a 25% Methanol 10% Acetic acid solution. Stained gels were imaged using a GelDoc® and ImageLab® by Biorad.

8.3.3 Differential effects of soluble and pellet fractions of *S. mansoni* E/S products on cytokine production

BMM ϕ s were exposed overnight to 50 μ g/ml 0-3hRP, 50 μ g/ml 0-3hRP_S, 25 μ g/ml 0-3hRP_P or left un-stimulated (Media), and culture supernatants tested for production of IL-10 and IL-12p40. 0-3hRP_P was used at a lower dose (25 μ g/ml) due to limited availability of the material. IL-10 production was strikingly different

in BMM ϕ s exposed to the different preparations (Figure 8.1A). 0-3hRP_P induced 10-fold more IL-10 than either 0-3hRP, or 0-3hRP_S, which were not significantly different compared to each other ($p>0.05$). Conversely, IL-12p40 production was significantly reduced in BMM ϕ s exposed to 0-3hRP_P compared to 0-3hRP stimulated cells (Figure 8.1B, $p<0.01$), whilst the effect of 0-3hRP_S on BMM ϕ s was comparable to that of 0-3hRP.

Therefore, it appears that the IL-10 inducing feature of 0-3hRP is significantly enriched in 0-3hRP_P.

8.3.4 0-3hRP_P inhibits TLR4 mediated IL-12p40 production in BMM ϕ exposed to LPS

As described in previous chapters (4.3.5.3), MAPK activation in response to 0-3hRP in BMM ϕ s is able to limit the induction of IL-12p40 and this ability is linked to the signaling events that lead to the production of IL-10. As IL-10 induction is significantly increased in response to 0-3hRP_P, the capacity of this preparation to inhibit IL-12p40 was tested.

BMM ϕ s exposed overnight to LPS (1ng/ml) and increasing doses of 0-3hRP_P were tested for the production of IL-12p40 and IL-10 by ELISA. PMB (2 μ g/ml) was used as a positive control for inhibition. 0-3hRP_P was able to significantly reduce the amount of IL-12p40 produced by BMM ϕ s exposed to LPS (Figure 8.2A, $p<0.0001$). At the highest dose of 0-3hRP_P (50 μ g/ml), IL-12p40 production was still higher than the PMB control, which was expected, as 0-3hRP_P alone is able to induce IL-12p40 (Figure 8.1B). Likewise, IL-10 production was significantly enhanced in response to greater concentrations of 0-3hRP_P (Figure 8.2B, $p<0.0001$).

Notably, IL-12p40 production was already significantly impaired compared to LPS only at 2 μ g/ml of 0-3hRP_P ($p<0.0001$), whilst IL-10 levels at that dose were not significantly different compared to LPS only BMM ϕ s. This further supports the notion that IL-12p40 inhibition occurs as a result of 0-3hRP driven MAPK activation in BMM ϕ s, and not as an IL-10 feedback loop, as demonstrated before (4.3.5.3).

Unlike 0-3hRP_P, 0-3hRP was not able to inhibit IL-12p40 production in response to LPS by BMM ϕ s (Figure 8.3).

8.3.5 Protein profile of different fractions *S. mansoni* E/S products

As the ability to induce IL-10 in BMM ϕ s was not equally distributed between the fractions obtained from 0-3hRP, the distribution of proteins was qualitatively assessed by SDS PAGE.

Each fraction contained a different quantity of protein (Figure 8.4A), with 0-3hRP_S retaining close to 75% of the protein available in the original 0-3hRP preparation. After fractionating, 20 μ g of 0-3hRP and the same amount from each fraction were analyzed by electrophoresis as described before (8.3.2) and stained with Brilliant Blue G (Figure 8.4B). In agreement with the estimated protein content of unfractionated 0-3hRP, most bands were also present in 0-3hRP_S, whereas only two of the most dominant bands were clearly visible in 0-3hRP_P (marked with arrows). Both bands were identified using MS/MS. The higher molecular weight band (a) was Invadolysin (M08) (Sm_90100) with a Mascot score of 826 and 7 peptides identified. The lower molecular weight band (b) contained two hits: cercarial elastase 2a (mascot score 405, 3 peptides) and Sm16 (mascot score 70, 2 peptides).

8.3.6 0-3hRP_P fluoresces naturally

In the course of experimental work with 0-3hRP_P, it became apparent that this preparation was emitting light when it was excited with different lasers. Consequently, this feature of the secretions was analysed using a fluorimeter.

Equal volumes of 0-3hRP (Figure 8.5A), 0-3hRP_S (Figure 8.5B) and 0-3hRP_P (Figure 8.5C) were analyzed using a Fluoromax 4 (Horiba). Emission data was collected between 420nm and 750nm with excitations at 415nm (top), 488nm (middle) and 633nm (bottom). A limited amount of fluorescence was detectable in 0-3hRP and 0-3hRP_S around 500nm, with no discernible peaks. However, both 0-3hRP and 0-3hRP_P had a clear emission peak at 675nm that was absent from 0-3hRP_S. This emission was excited by all three lasers, and was greatest when excited with the 633nm laser. In all cases, 0-3hRP_P exhibited greater levels of fluorescence than 0-3hRP.

This fluorescence was not restricted to the antigenic preparation in solution, but was also clear when BMM ϕ s internalized the secretions. BMM ϕ s exposed overnight to 0-3hRP, 0-3hRP_P or left un-stimulated (Media), were analyzed with flow cytometry as described before (2.4), leaving the 633nm/680nm

(Excitation/Emission) channel free. As expected, 0-3hRP and 0-3hRP_P stimulated BMMφs were positive in the 633nm/680nm channel, with 0-3hRP_P exposure resulting in higher levels of fluorescence (Figure 8.6A). Consequently, 0-3hRP_P stimulated BMMφs were sorted based on the brightness of the fluorescence (Figure 8.6B) and imaged using confocal microscopy (Figure 8.6C).

In line with the results obtained with flow cytometry, 0-3hRP_P exposed BMMφs contained differing levels of the fluorescent material, with the brightest cells as judged by flow cytometry (right) containing the most material as observed with confocal microscopy (Figure 8.6C, right panel). Flow cytometric analysis of the middle group (Figure 8.6C, middle panel) and the low group (Figure 8.6C, left panel) also correlated to the results obtained by confocal microscopy. Closer examination of bright cells (Figure 8.6D) revealed that 0-3hRP_P could be localized in discrete bright spots, or diffused throughout the cytoplasm.

Finally, all fractions were loaded onto a protein gel and imaged without staining in a Personal Molecular Imager (Biorad) (see 8.3.2) with an excitation of 635nm and emission of 685nm. Two bands between 10 and 20kDa were strongly positive in both 0-3hRP and 0-3hRP_P, but not in 0-3hRP_S (Figure 8.7, red arrows). These bands are in the same region as the band identified earlier (8.3.5) so they could be Sm16 or cercarial elastase.

In short, the component of 0-3hRP that is responsible for the induction of IL-10 is enriched in the pellet fraction of this preparation. The ability to induce IL-10 production is linked with the potential to block IL-12p40, which is indeed also an effect of 0-3hRP_P. Additionally, this material naturally fluoresces, and its uptake by BMMφs can be measured using flow cytometry. Furthermore, increased uptake of naturally fluorescent 0-3hRP coincided with an increase in MAPK activation (data not shown).

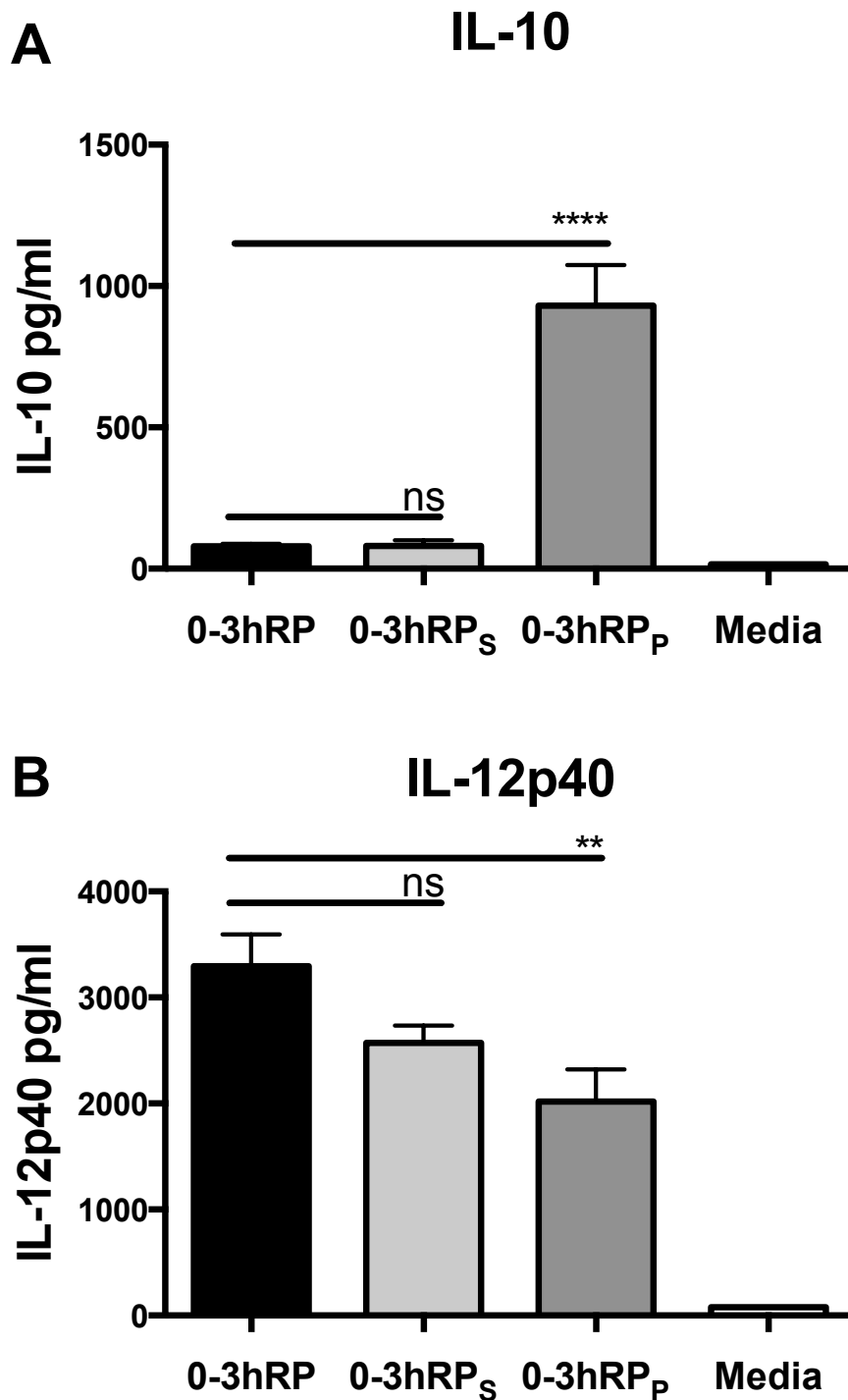


Figure 8.1 BMM ϕ s exposed to 0-3hRP fractions secrete differing quantities of IL-10 and IL-12p40

Supernatants from BMM ϕ s exposed to 0-3hRP (50 μ g/ml), 0-3hRP_S (50 μ g/ml), 0-3hRP_P (25 μ g/ml) or left un-stimulated (Media) were tested for the production of (A) IL-10 and (B) IL-12p40. Means +SEM of 6 technical replicates are presented. ANOVA and then Dunnett's multiple comparisons test were performed to examine differences between the means of cells stimulated with fractions compared to cells stimulated with whole preparation (** = $p < 0.01$; **** = $p < 0.0001$; ns = $p > 0.05$). Results are representative of three independent experiments.

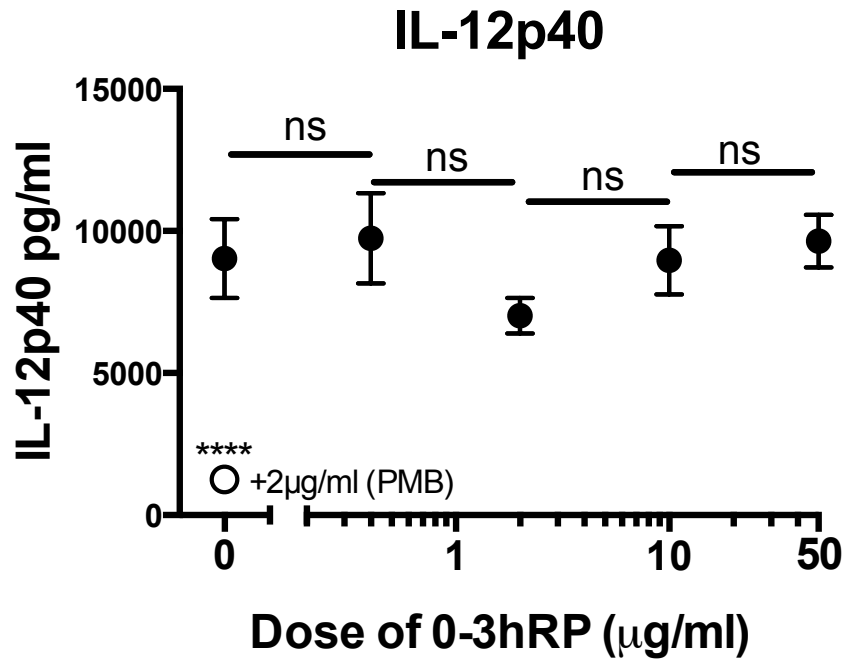


Figure 8.3 0-3hRP does not impair IL-12p40 production in BMMφs exposed to LPS

Supernatants from BMMφs exposed to LPS (1ng/ml) and increasing doses of 0-3hRP, or PMB (2µg/ml) (open circles), were tested the production of IL-12p40. Means ±SEM of 6 technical replicates are presented. ANOVA and then Tukey's multiple comparisons test were performed to examine differences between selected means (ns = $p > 0.05$). Results are representative of two independent experiments.

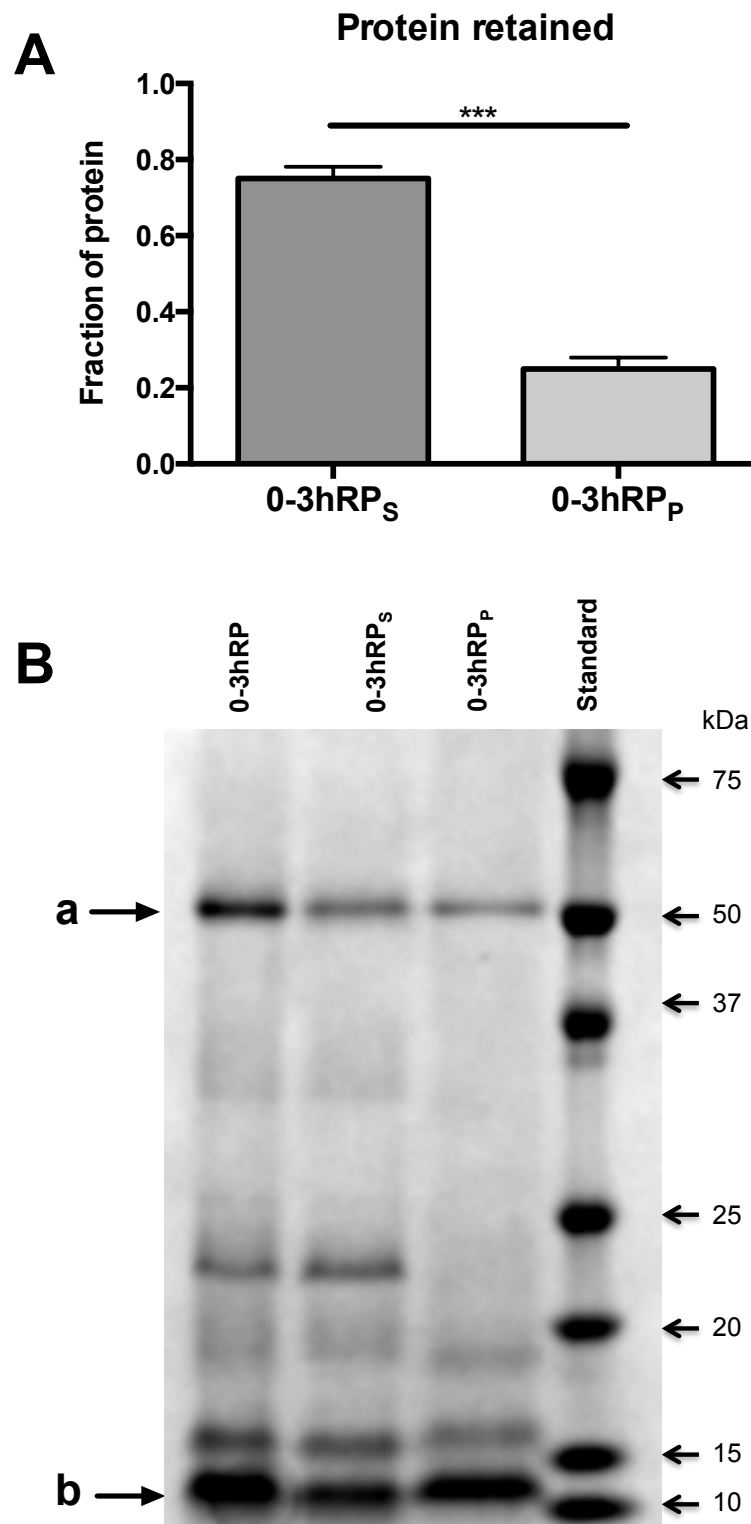


Figure 8.4 0-3hRP fractions retain different levels of proteins

Three preparations of 0-3hRP were fractionated using ultracentrifugation and fractions restored to the original volume of each preparation. **(A)** The protein content of each resulting fraction was determined using a BCA assay and expressed as a percentage of the total protein present in the original preparation. Unpaired t-test was performed to find statistically significant differences between the means (***) = $p < 0.001$). **(B)** 20 μ g of 0-3hRP and each fraction were analyzed in a protein gel stained with Brilliant Blue G.

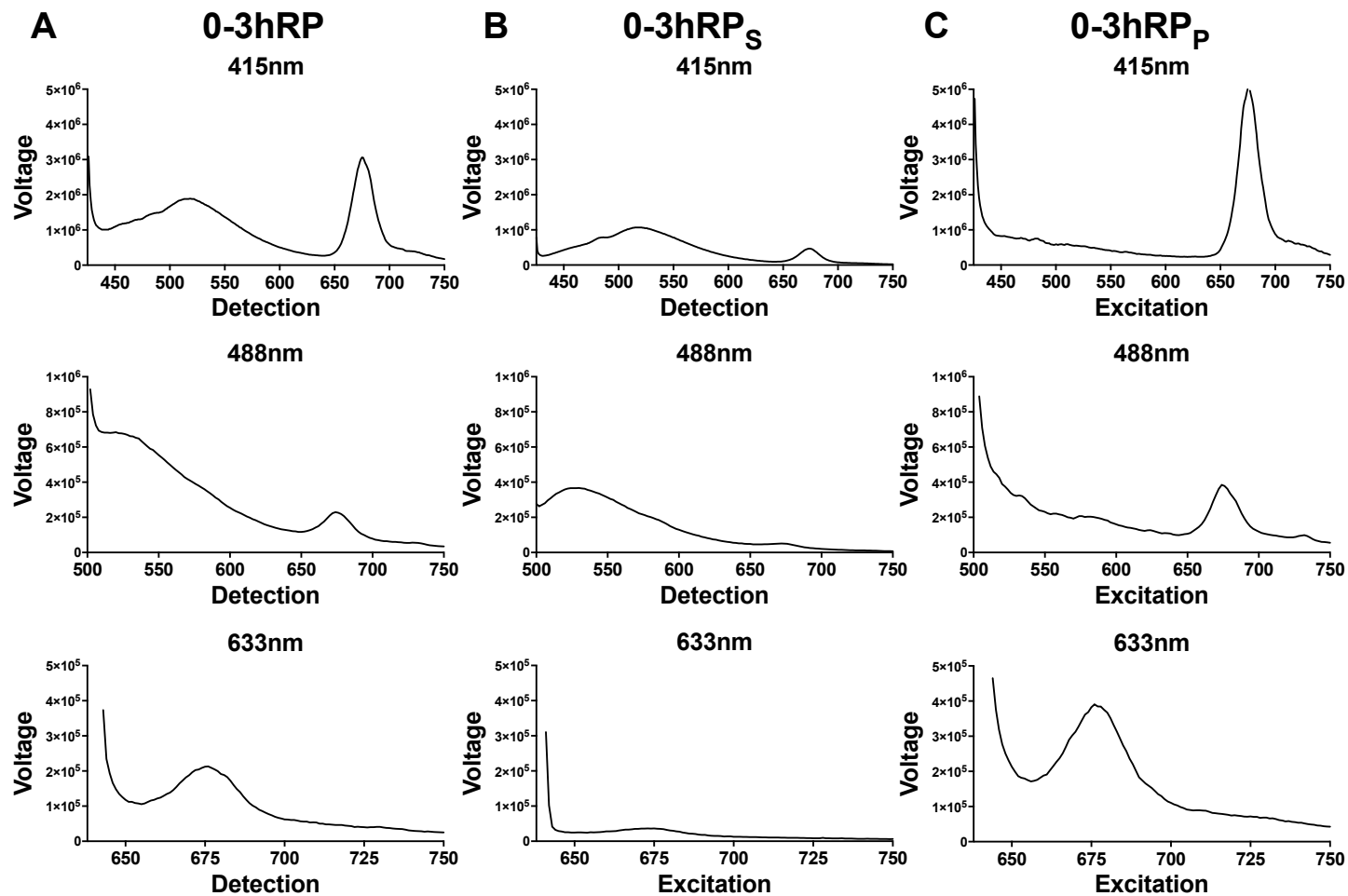


Figure 8.5 0-3hRP naturally emits red fluorescence

(A) 0-3hRP, (B) 0-3hRP_S and (C) 0-3hRP_P were analyzed using a fluorimeter to determine their absorption/emission profile after excitation at (top) 415nm, (middle) 488nm or (bottom) 633nm.

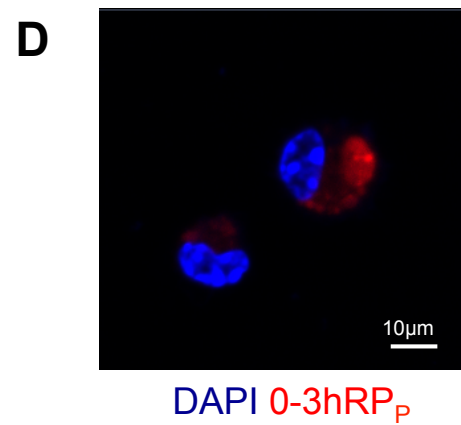
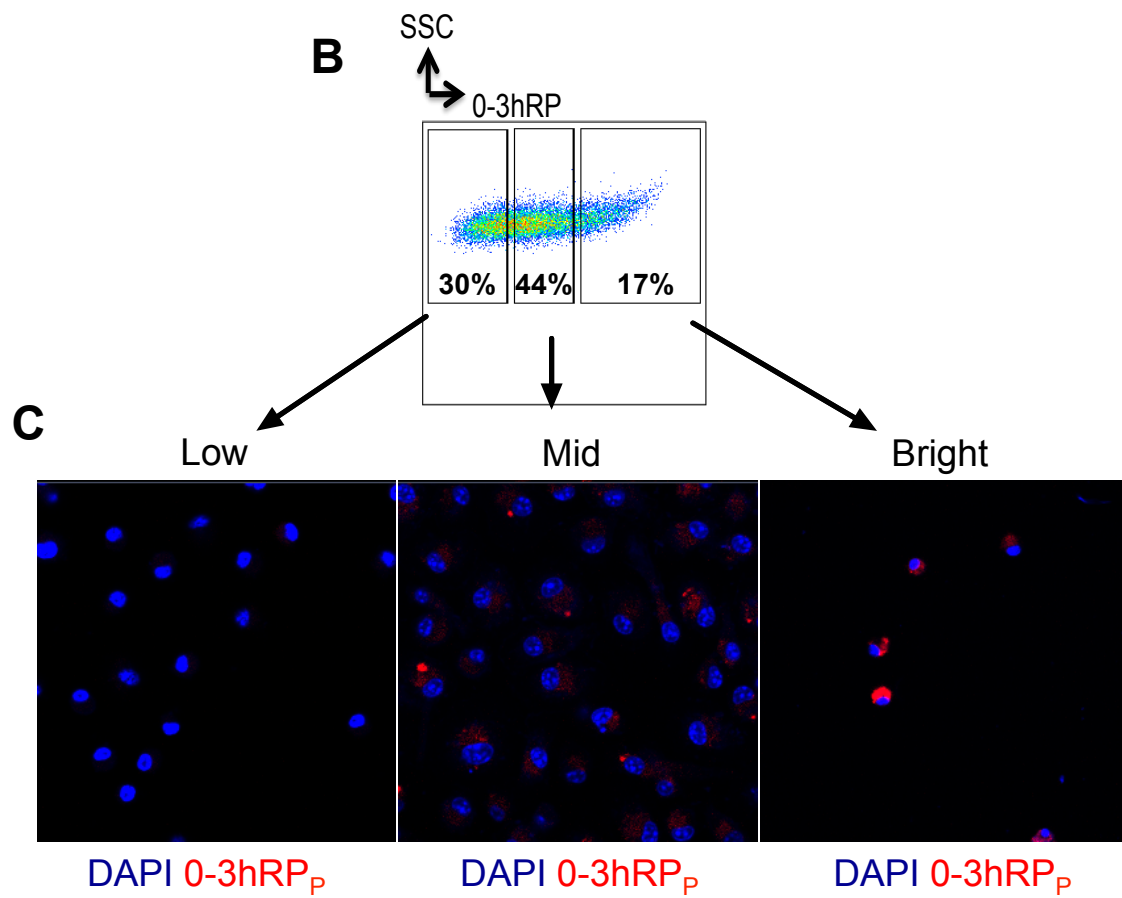
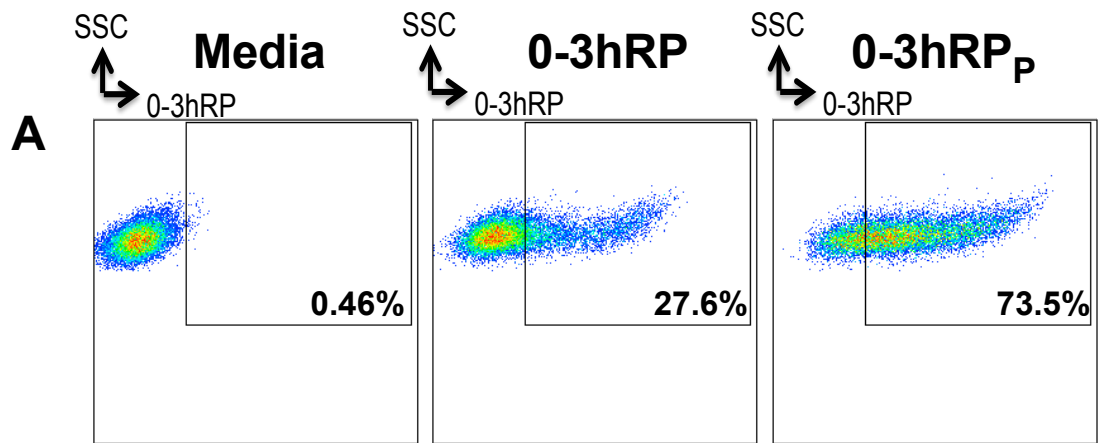


Figure 8.6 0-3hRP fluorescence is detectable inside BMMφs

(A) BMMφs exposed overnight to 0-3hRP (50μg/ml), 0-3hRP_P (25μg/ml) or left un-stimulated (Media) were analyzed using flow cytometry. (B) BMMφs exposed overnight to 0-3hRP_P (25μg/ml) sorted using fluorescence activated cell sorting into three groups were based on levels of 0-3hRP_P-associated fluorescence. (C & D) Each group was analyzed using confocal microscopy to confirm internalization of fluorescent material. (D) Higher resolution image of bright cells reveals diffuse fluorescence in the cytoplasm and concentrated fluorescence in punctae.

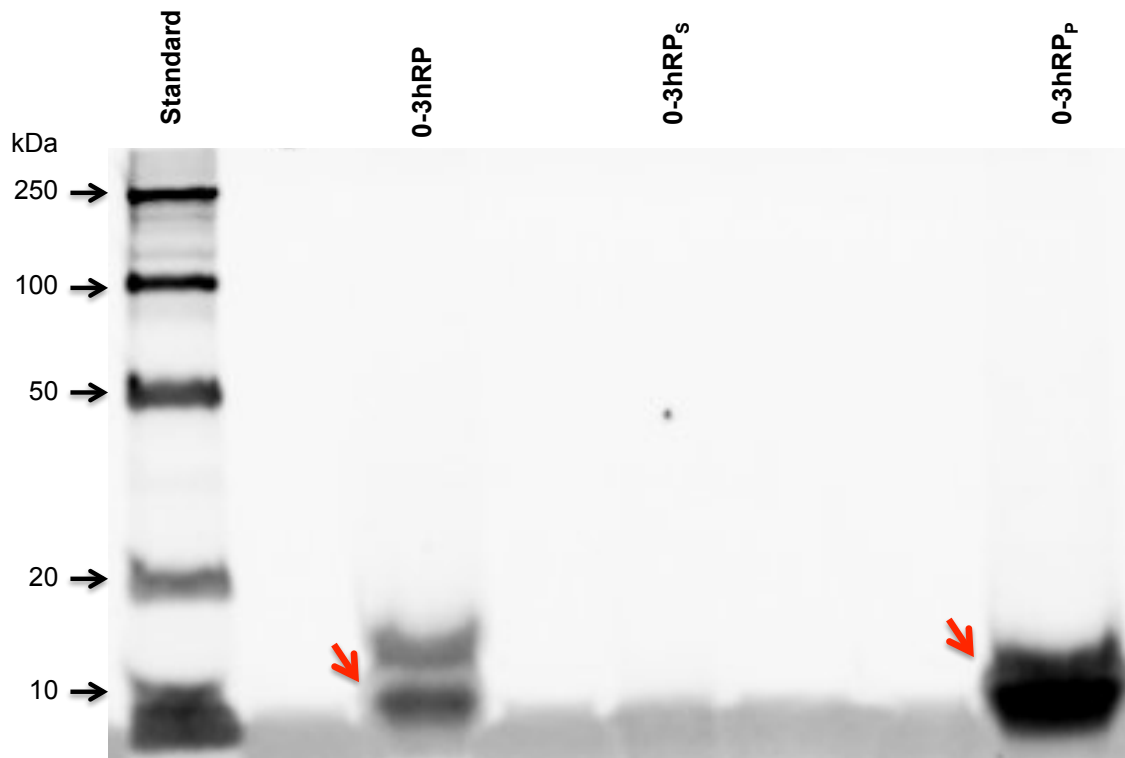


Figure 8.7 0-3hRP naturally emits red fluorescence which can be detected on a protein gel as discrete bands

10 μ g/ml of 0-3hRP, 0-3hRP_S and 0-3hRP_P were analyzed on a protein gel and imaged without staining on a Personal Molecular Imager (Biorad) using a 635nm excitation laser and detecting at 680nm. Result is representative of three individual experiments.

8.4 Sm16, a protein in 0-3hRP_p, inhibits BMM ϕ activation by TLR ligands

As explained above, fractions of 0-3hRP revealed differential abilities to modulate cytokine responses by stimulated BMM ϕ s (8.3). In particular, 0-3hRP_p was able to prevent LPS induced production of IL-12p40. This fraction contained at least two enriched proteins: Invadolysin and Sm16. The latter protein has been studied in most detail previously and was found to have a profound effect on human macrophages, predominantly by inhibiting TLR induced cytokine production (Brännström et al, 2009; Holmfeldt et al, 2007). Therefore, it was decided to perform a direct comparison between 0-3hRP and recombinant Sm16 (rSm16).

8.4.1 Western blot analysis of fractions

0-3hRP and its fractions were resolved using protein electrophoresis as described before (8.3.2) and transferred onto a nitrocellulose membrane using an iBlot® Transfer Stack (Life Technologies) as specified by the manufacturer. Membranes were then analyzed by western blot by using the SnapID® system (Millipore). Initially membranes are blocked in vacuum with a 1% BSA solution in PBS, then rabbit anti-rSm16 antibody (1:5000) (donated by Dr Martin Gullberg, Umeå University, Sweden) was added in vacuum for 10min followed by 4 washes in 0.05% Tween in PBS. Membranes were incubated in vacuum with goat anti rabbit antibody (1:30000) conjugated to horseradish peroxidase for 10min followed by 4 washes in 0.05% Tween in PBS.

SuperSignal® West Pico (Thermo Scientific) chemiluminescence reagent was used to reveal the antibody labelling of proteins on the membranes using X-ray film imaging (GE Healthcare). Equal volumes of Luminol/Enhancer Solution and Stable Peroxidase solution were mixed and incubated with labelled/probed membranes for 5min. Chemiluminescence reagent was removed by washing and X-ray film finally exposed for different lengths of time prior to development.

8.4.2 Sm16 is present in 0-3hRP_p

Increasing amounts of 0-3hRP fractions were analyzed on a protein gel, as described before (8.3.2), alongside increasing amounts of rSm16 (kindly donated by Dr Martin Gullberg) (Figure 8.8A). rSm16 had a molecular weight between 15kDa and 20kDa judged by comparison with the protein standard

(expected molecular weight of 16kDa). This was higher than the band identified in section 8.3.5, which was between 10kDa and 15kDa (Figure 8.4B, arrow b). Nonetheless, both 0-3hRP_S and 0-3hRP_P contained a band of a similar molecular weight as rSm16 (Figure 8.8A, red arrows), therefore it was presumed likely that the fractions of 0—3hRP contained Sm16. Densitometry analysis performed of the selected bands, allowed the construction of a standard curve based on the amount of rSm16 loaded onto the gel and the resulting pixel intensity (Figure 8.8B). A linear regression, with an adequate fit ($R^2=0.999$), produced an equation to estimate the amount of Sm16 in the 0-3hRP fractions based on pixel intensities, which showed that the putative Sm16 band was significantly enriched in 0-3hRP_P as a fraction of the total protein, compared to 0-3hRP_S (Figure 8.8C, $p<0.05$). The putative band for Sm16 in the 15 μ g lane of 0-3hRP_P was excluded from the analysis as it appeared elongated.

However, it is likely that more than one protein is contained in the aforementioned band. Consequently, western blot analysis was performed (8.4.1), on a gel where equivalent amounts of both fractions were loaded (i.e. fractions were diluted to the volume of the original preparation). Indeed, using an anti-rSm16 antibody, the native form of this protein was detected in both 0-3hRP_S and 0-3hRP_P (Figure 8.9A). Moreover, densitometry analysis of the blot, using rSm16 pixel intensity as a normalizer, suggested that Sm16 was significantly enriched as a proportion (greater than 5 fold) in 0-3hRP_P compared to 0-3hRP_S (Figure 8.9B, $p<0.0001$).

8.4.3 Sm16 blocks cytokine production in response to TLR4 and TLR3, but not TLR2 ligands in BMM ϕ s

0-3hRP_P's ability to block LPS induced IL-12p40 production could be a result of the enrichment of Sm16 in that fraction. Consequently, the capacity of Sm16 to prevent TLR signaling in murine macrophages was tested.

BMM ϕ s were exposed overnight to LPS (1ng/ml) and increasing doses of rSm16 and culture supernatants tested for IL-12p40 and IL-10 by ELISA. rSm16 was able to reduce the amount of IL-12p40 produced by BMM ϕ s exposed to LPS to media levels at all doses used (Figure 8.10A). Likewise, IL-10 production was ablated in response to all concentrations of rSm16 (Figure 8.10A).

An intermediate dose of rSm16 (10µg/ml) was taken forward for all other experiments, where the ability of this protein to block TLR driven cytokine production in response to other ligands was tested. rSm16 was dissolved in a phosphate buffer (pH 7.5) containing 0.45M NaCl to prevent aggregation. To rule out any effects of this buffer, BMMφs exposed to all TLR ligands were given an equivalent amount of this buffer as a negative control (Buffer control). As before, BMMφs exposed to LPS were unable to produce IL-12p40 and IL-10 when rSm16 was present in the culture, whereas Buffer control had no effect (Figure 8.11A & B). rSm16 had no effect on cytokine production of BMMφs exposed to Pam₃CSK₄ (Figure 8.11C & D). However, Poly I:C treated BMMφs were unable to produce IL-12p40 and IL-10 when rSm16 was given at the same time, whilst no impairment was observed with Buffer control (Figure 8.11E & F).

8.4.4 Sm16 is able to prevent BMMφ activation in the context of IFN-γ stimulation

Macrophage function is modulated *in vivo* by several cytokines, specially IL-4 and IFN-γ (see 1.3.1). IFN-γ boosts the pro-inflammatory phenotype of macrophages and works in tandem with innate stimuli, such as LPS, to provide a necessary second signal for complete oxidative burst (see 1.3.1). Consequently, the effects of rSm16 on BMMφ-activation in the context of IFN-γ stimulation were investigated.

Culture supernatants from BMMφs exposed overnight to LPS or Media, +/- IFN-γ (25U/ml), +/- rSm16 were tested for IL-12p40 by ELISA and Nitric oxide (NO₂⁻) production by commercially available Greiss reaction (Life Technologies). As before, IL-12p40 production was ablated by rSm16 in LPS stimulated BMMφs (Figure 8.12A). IFN-γ activation resulted in a marked increase in the production of IL-12p40 by macrophages stimulated with LPS, but not Media alone. Nevertheless, rSm16 was able to significantly reduce IL-12p40 production in LPS treated IFN-γ stimulated BMMφs (Figure 8.12A, p<0.0001).

A small amount of NO₂⁻ was produced in response to LPS, that could be significantly reduced by rSm16 in BMMφs (Figure 8.12B, p<0.01). IFN-γ activation greatly enhanced the detected levels of NO₂⁻ in LPS stimulated BMMφs; however, rSm16 was able to significantly reduce that response (Figure 8.12B, p<0.0001).

In short, rSm16 was able to significantly reduce the activation of BMMφs in response to innate stimuli even in the context of potent IFN-γ stimulation.

8.4.5 TLR2 is not required for rSm16 effect on cytokine production in BMMφs

rSm16 was able to prevent TLR4 and TLR3 mediated cytokine production in BMMφs, but no defect was observed when a TLR2 ligand was used. Earlier, 0-3hRP was shown to be recognized both by TLR2 and TLR4 (see 4.3.2), therefore the effect of exogenous rSm16 on 0-3hRP cytokine induction was tested.

BMMφs exposed overnight to 0-3hRP and rSm16 produced significantly less IL-12p40 than BMMφs exposed to 0-3hRP alone (Figure 8.13A, $p < 0.01$). However, IL-10 production in response to 0-3hRP was significantly increased when rSm16 was added to the culture (Figure 8.13B, $p < 0.001$). Buffer control had no effect on either cytokine. Unlike Pam₃CSK₄, which is only recognized by TLR2, 0-3hRP uses both TLR2 and TLR4. TLR4 deficiency had a greater impact in IL-12p40 production than TLR2 in BMMφs stimulated with 0-3hRP. Whereas TLR2 deficiency had a greater effect on IL-10 production than TLR4 in BMMφs exposed to 0-3hRP. As cytokine production was not ablated by rSm16 in BMMφs exposed to 0-3hRP, and Sm16 blocks TLR4 stimulation, these results confirm TLR2 is involved in the recognition of 0-3hRP. The observed increase in IL-10 induced by co-stimulation with rSm16 and 0-3hRP indicates that TLR4 signaling could be antagonizing the production of IL-10 in BMMφs. The reduction in IL-12p40 in these co-stimulated cells also implies that TLR4 is responsible partly for the induction of this cytokine in response to 0-3hRP.

As 0-3hRP is recognized by TLR2 (see 4.3.2), and rSm16 is unable to block signaling from that receptor, the role of TLR2 in the effects of the recombinant protein were tested. TLR2^{-/-} BMMφs, obtained as described before (2.3), were exposed overnight to LPS and Poly I:C and culture supernatants tested for IL-12p40. Both ligands induced a robust IL-12p40 production in TLR2^{-/-} BMMφs, however, rSm16 was able to completely ablate the production of this cytokine (Figure 8.14). Therefore, rSm16 acts on BMMφs independently of TLR2. rSm16 inhibition of Poly I:C induced cytokines was also evident in TLR4^{-/-} BMMφs (data not shown).

8.4.6 Sm16 is taken up by BMM ϕ s into a distinct processing pathway

0-3hRP uptake has been shown to be important for triggering of downstream signals (see chapter V) and others have described its delayed processing in BMM ϕ s, marked by a prolonged stay in early endosomes (Paveley et al, 2009). Other inhibitory helminth products sequester TLR signaling machinery through endocytosis (Pineda et al, 2014). Consequently, the uptake and processing of rSm16 was investigated.

BMM ϕ s were exposed for 10 and 100min to rSm16 labeled with AF594 and analyzed with confocal microscopy as described before (5.2.3), with antibodies for EEA-1 (Figure 8.15B) and relevant no primary antibody controls (Figure 8.15A). rSm16 was closely associated with EEA-1 at 10 and 100min after stimulation. Closer analysis of confocal images revealed that EEA-1 could be seen surrounding rSm16 (Figure 8.16, white arrows on inserts), indicative of the latter protein being present in early endosomes positive for EEA-1. EEA-1 is not a membrane protein, but rather it associates with the outside of the endosome. Typical staining with EEA-1 is for this protein to surround the cargo (Beas et al, 2012). This prolonged retention of rSm16 in these compartments, was reminiscent of previous similar observations for 0-3hRP (Paveley et al, 2009).

To further study the cellular fate of rSm16, BMM ϕ s were exposed to this labeled protein and FITC conjugated DEXTRAN (DEXTRAN^{FITC}) (SIGMA) as a control for readily processed cargo. Both stimuli were removed after 100min, and the cells imaged at frequent intervals (Figure 8.17). At 10 and 60min after removal, both rSm16 and DEXTRAN^{FITC} were found in different compartments of BMM ϕ s. rSm16 was more abundant in the periphery of the cell, whereas DEXTRAN^{FITC} was closer to the nucleus, although by 100min after stimuli removal, only a faint signal was detected from DEXTRAN^{FITC}. rSm16 was also greatly reduced, yet foci were still visible in the perinuclear region (Figure 8.17).

In summary, 0-3hRP_P contains a significantly higher proportion of Sm16, which has potent inhibitory activity on TLR4 and TLR3 induced signaling. This activity is not mediated by direct interaction with TLR2 or TLR4 and is able to enhance 0-3hRP driven IL-10 production, strongly suggesting that Sm16 works in tandem with the signaling events triggered by 0-3hRP to induce that cytokine. Furthermore, rSm16 is quickly internalized by BMM ϕ s and placed in early endosomes, leading to a delayed processing pathway compared to other cargo.

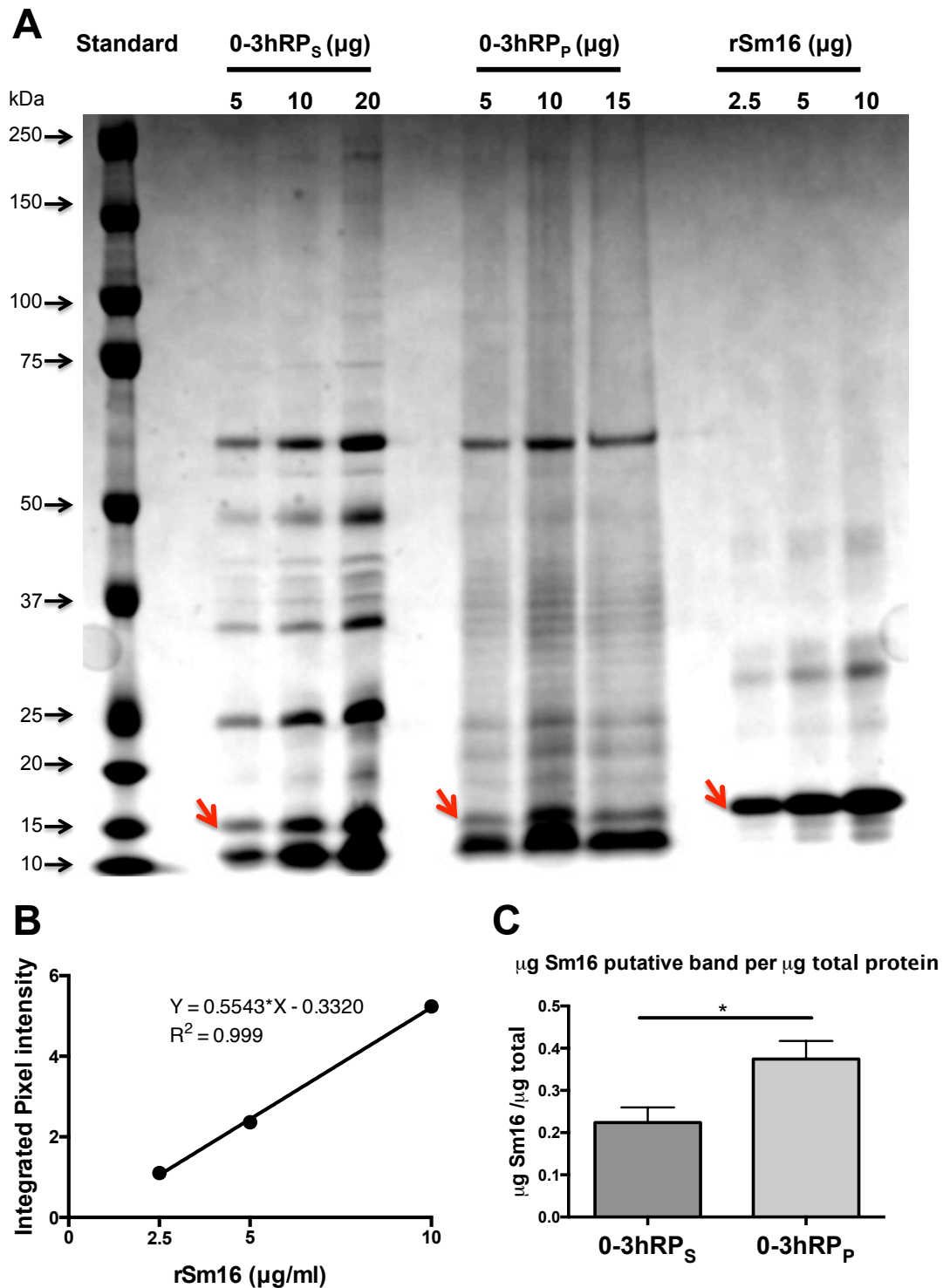


Figure 8.8 0-3hRP fractions protein profile comparison to rSm16

(A) 0-3hRP was fractionated using ultracentrifugation and resulting 0-3hRP_S and 0-3hRP_P analyzed in a protein SDS PAGE gel stained with Brilliant Blue G alongside rSm16. (B) A standard curve was constructed based on densitometry analysis of dominant band in rSm16 lanes (red arrow) and a linear regression was performed to obtain an equation (displayed on graph) to fit the curve. (C) Densitometry analysis of Sm16 equivalent bands in 0-3hRP fractions (red arrows) was used to estimate the μg of putative Sm16 per μg of total protein. Mean +SEM are presented and an unpaired t-test performed to examine statistically significant differences between them (* = $p < 0.05$).

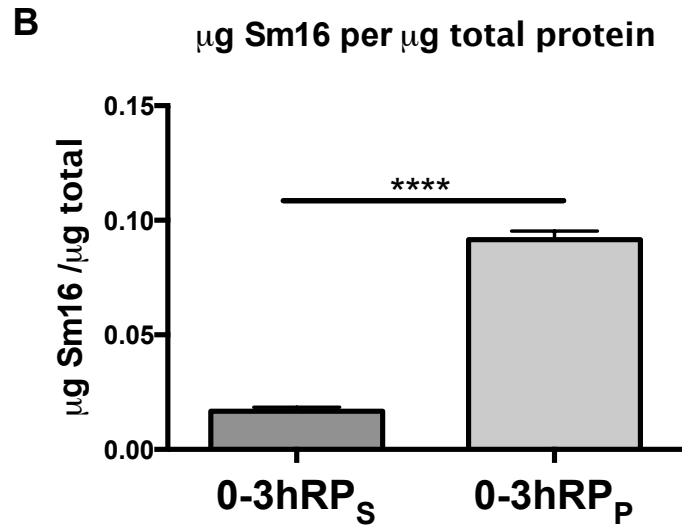
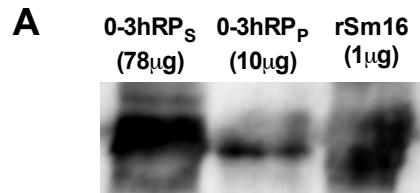


Figure 8.9 Sm16 abundance in 0-3hRP fractions

0-3hRP was fractionated using ultracentrifugation and resulting 0-3hRP_S (78μg) and 0-3hRP_P (10μg) were analyzed in a protein gel alongside rSm16 (1μg). **(A)** Western blot analysis of said gel was performed with rabbit anti-rSm16 antibody (1:5000), with the corresponding goat anti rabbit HRP (1:30000) secondary antibody. **(B)** Based on densitometry analysis of rSm16, the relative concentration of Sm16 in both fractions was estimated. Mean +SEM are presented and an unpaired t-test performed to examine statistically significant differences between them (**** = p<0.0001).

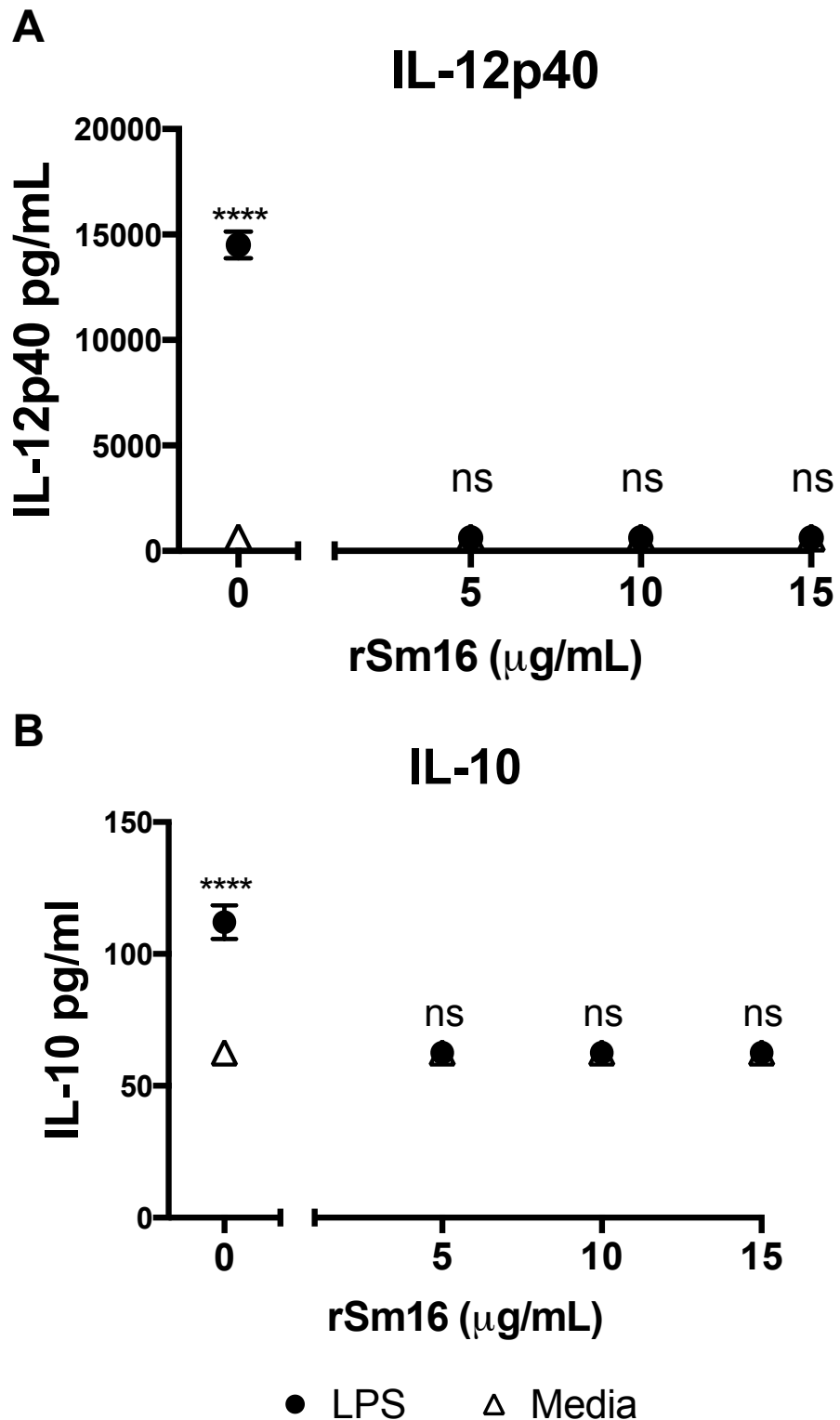


Figure 8.10 rSm16 blocks cytokine production in BMM ϕ s exposed to LPS
 Supernatants from BMM ϕ s exposed to LPS (1ng/ml) or Media (open triangles) and increasing doses of rSm16 were tested for the presence of **(A)** IL-12p40 and **(B)** IL-10. Means \pm SEM of 3 technical replicates are presented. ANOVA and then Tukey's multiple comparisons test were performed to examine differences between the means compared to Media control (**** = $p < 0.0001$; ns = $p > 0.05$). Results are representative of three independent experiments.

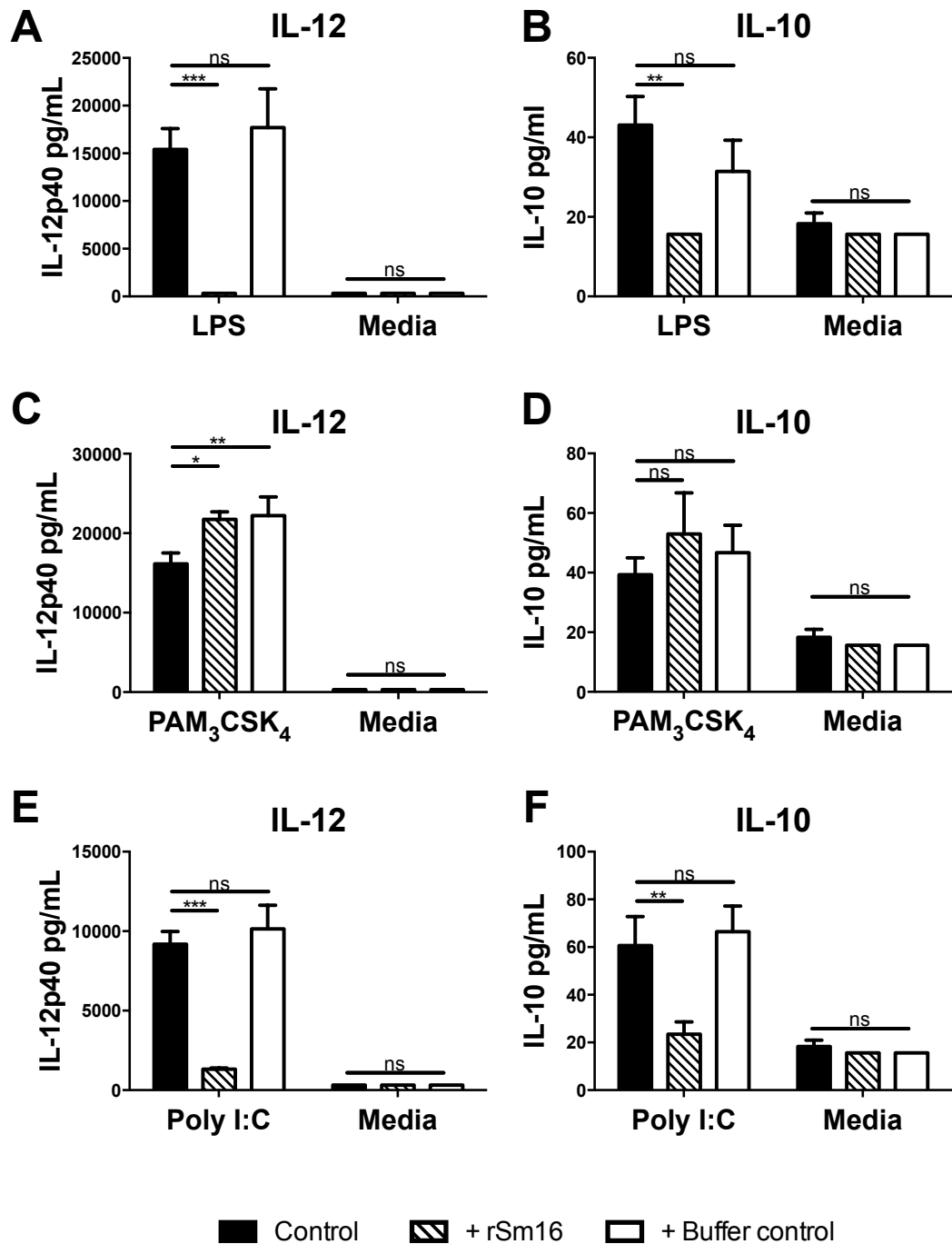


Figure 8.11 rSm16 blocks cytokine production in BMMφs exposed to TLR4 and TLR3, but not TLR2 ligands

Supernatants from BMMφs exposed to (A-B) LPS (1ng/ml), (C-D) Pam₃CSK₄ (5μg/ml), (E-F) Poly I:C (25μg/ml) or Media plus rSm16 (10μg/ml) (hatched bars) or an equivalent volume of protein buffer (open bars) were tested for the presence of (A, C, E) IL-12p40 and (B, D, F) IL-10 (limit of detection of 16pg/ml). Means ±SEM of 3 technical replicates are presented. ANOVA and then Dunnett's multiple comparisons test were performed to examine differences between selected means (* = p<0.05; ** = p<0.01; *** = p<0.001; **** = p<0.0001; ns = p>0.05). Results are representative of three independent experiments.

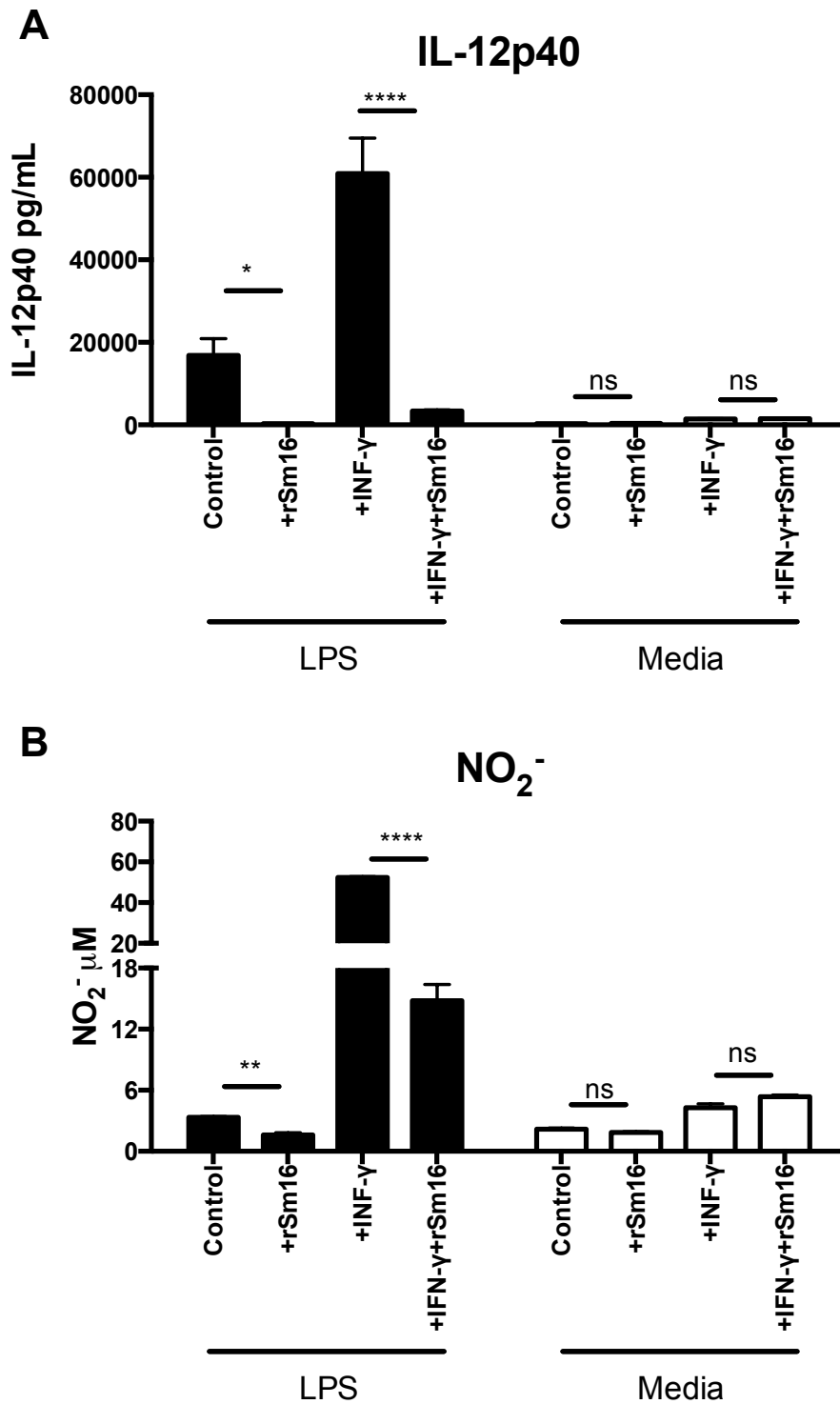


Figure 8.12 rSm16 blocks both cytokine production and oxidative burst in BMM ϕ exposed to LPS and IFN- γ

Supernatants from BMM ϕ s exposed to LPS (1ng/ml) or left un-stimulated (Media) plus recombinant IFN- γ (25U/ml) and/or rSm16 (10 μ g/ml) were tested for the production of (A) IL-12p40 by ELISA and (B) nitric oxide (NO₂⁻) by Greiss reaction. Means \pm SEM of 3 technical replicates are presented. ANOVA and then Sidak's multiple comparisons test were performed to examine differences between selected means (* = $p < 0.05$; ** = $p < 0.01$; *** = $p < 0.001$; **** = $p < 0.0001$; ns = $p > 0.05$). Results are representative of three independent experiments.

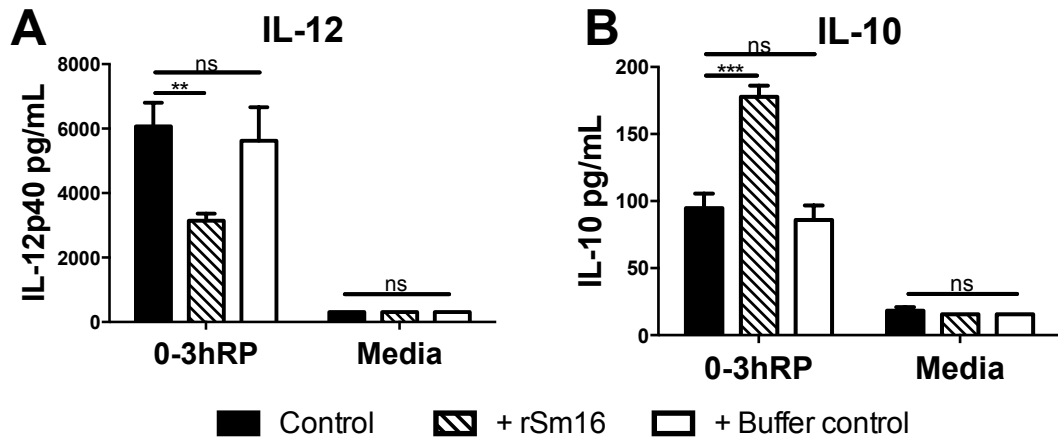


Figure 8.13 rSm16 has differential effect on cytokine production in BMMφs exposed to 0-3hRP

Supernatants from BMMφs exposed to 0-3hRP (50μg/ml) with PMB (2μg/ml) or left un-stimulated (Media) plus rSm16 (10μg/ml) (hatched bars) or an equivalent volume of protein buffer (open bars) were tested for the production of **(A)** IL-12p40 and **(B)** IL-10. Means ±SEM of 3 technical replicates are presented. ANOVA and then Dunnett's multiple comparisons test were performed to examine differences between selected means (* = p<0.05; ** = p<0.01; *** = p<0.001; **** = p<0.0001; ns = p>0.05). Results are representative of three independent experiments.

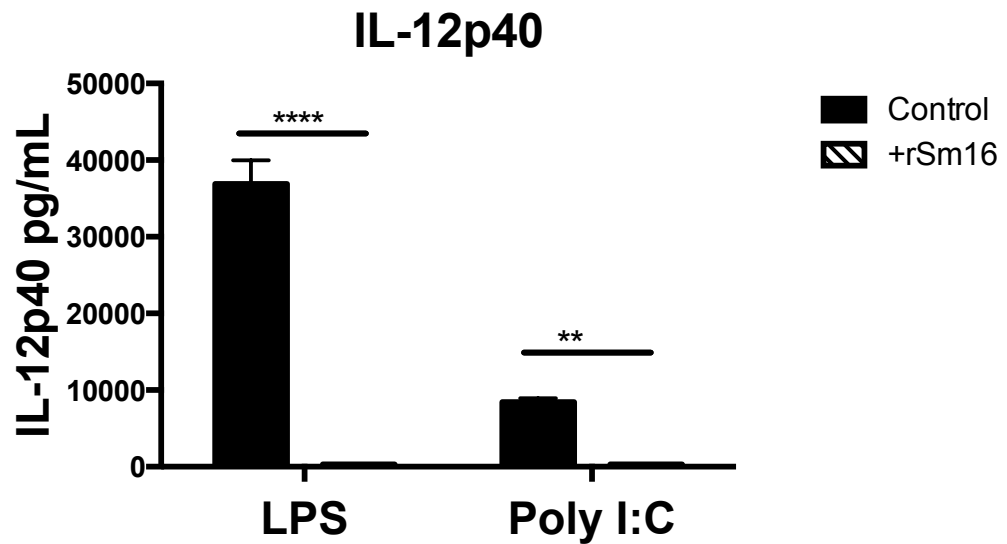


Figure 8.14 rSm16 blocks IL-12p40 production in BMMφs exposed to TLR4 and TLR3 ligands in a TLR2 independent manner

Supernatants from BMMφs from TLR2^{-/-} mice exposed to LPS (1ng/ml) or Poly I:C (25μg/ml) (solid bars), plus rSm16 (10μg/ml) (hatched bars), were tested for IL-12p40 by ELISA. Means ±SEM of 3 technical replicates are presented. ANOVA and then Dunnett's multiple comparisons test were performed to examine differences between selected means (** = p<0.01; **** = p<0.0001). Results are representative of two independent experiments.

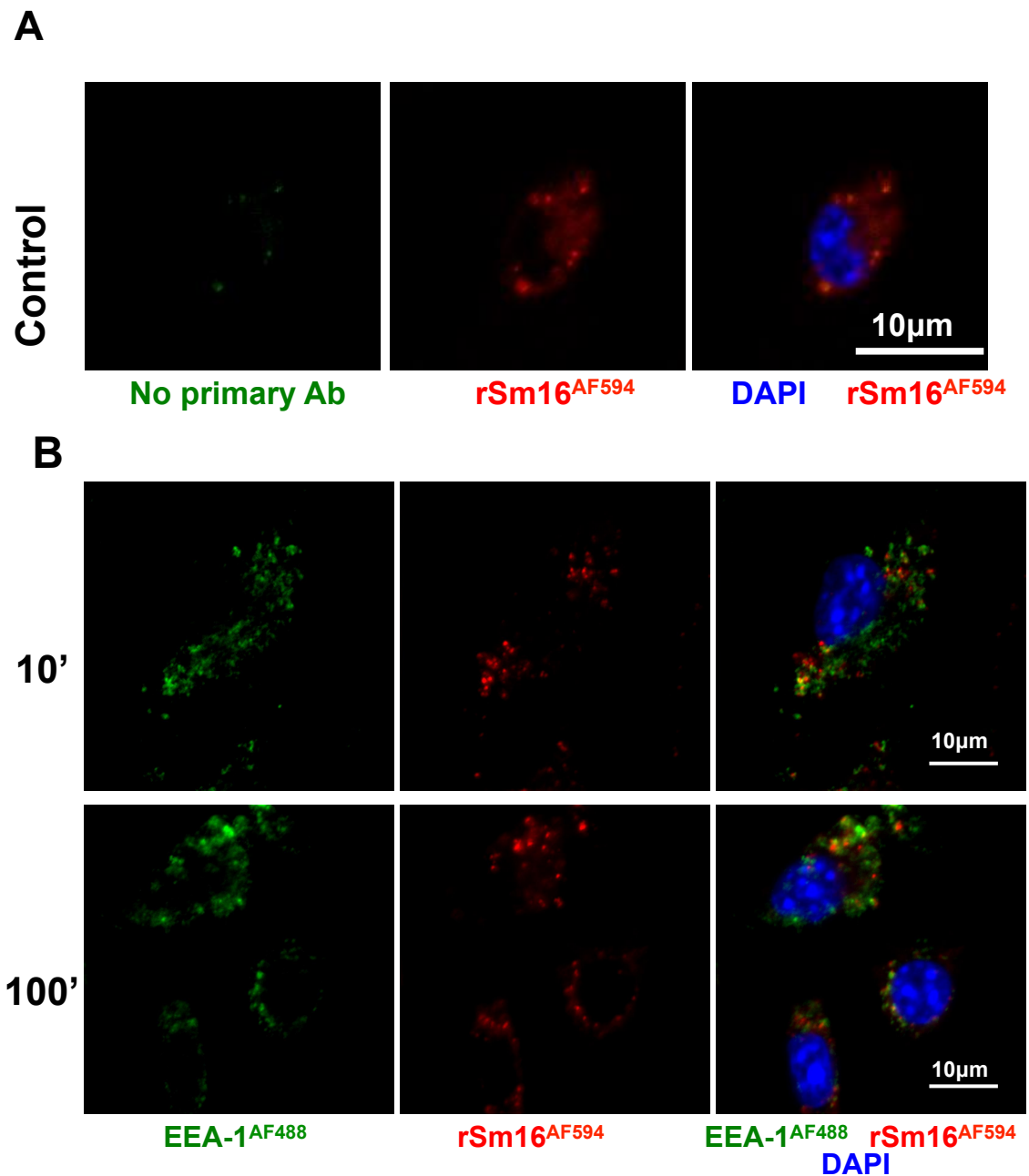


Figure 8.15 Uptake of fluorescently labelled rSm16 by BMMφs

BMMφs exposed to labeled rSm16^{AF594} (red) and dyed with nuclear stain DAPI (blue) were analyzed by confocal microscopy (63X objective, 38.8μm x 38.8μm). **(A)** Representative no primary antibody controls are given for EEA-1 staining. **(B)** Representative confocal images of BMMφs containing labeled rSm16 within EEA-1 positive endosomes (green) after 10min and 100min.

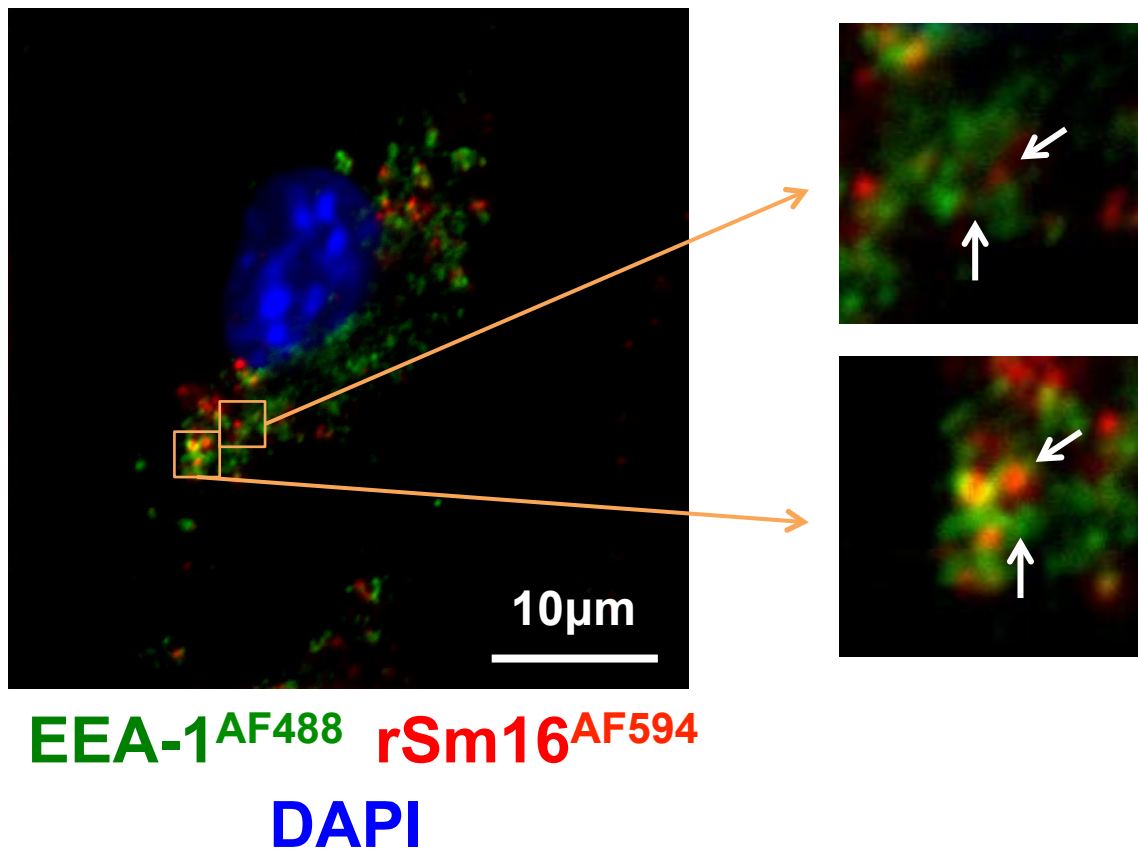


Figure 8.16 High resolution image of vesicles containing rSm16 in BMMφs
BMMφs exposed for 10min to labeled rSm16 (red) and dyed with nuclear stain DAPI (blue) were analyzed by confocal microscopy (63X objective, 38.8μm x 38.8μm). Intracellular EEA-1 positive structures containing labeled Sm16 are highlighted (2μm x 2μm).

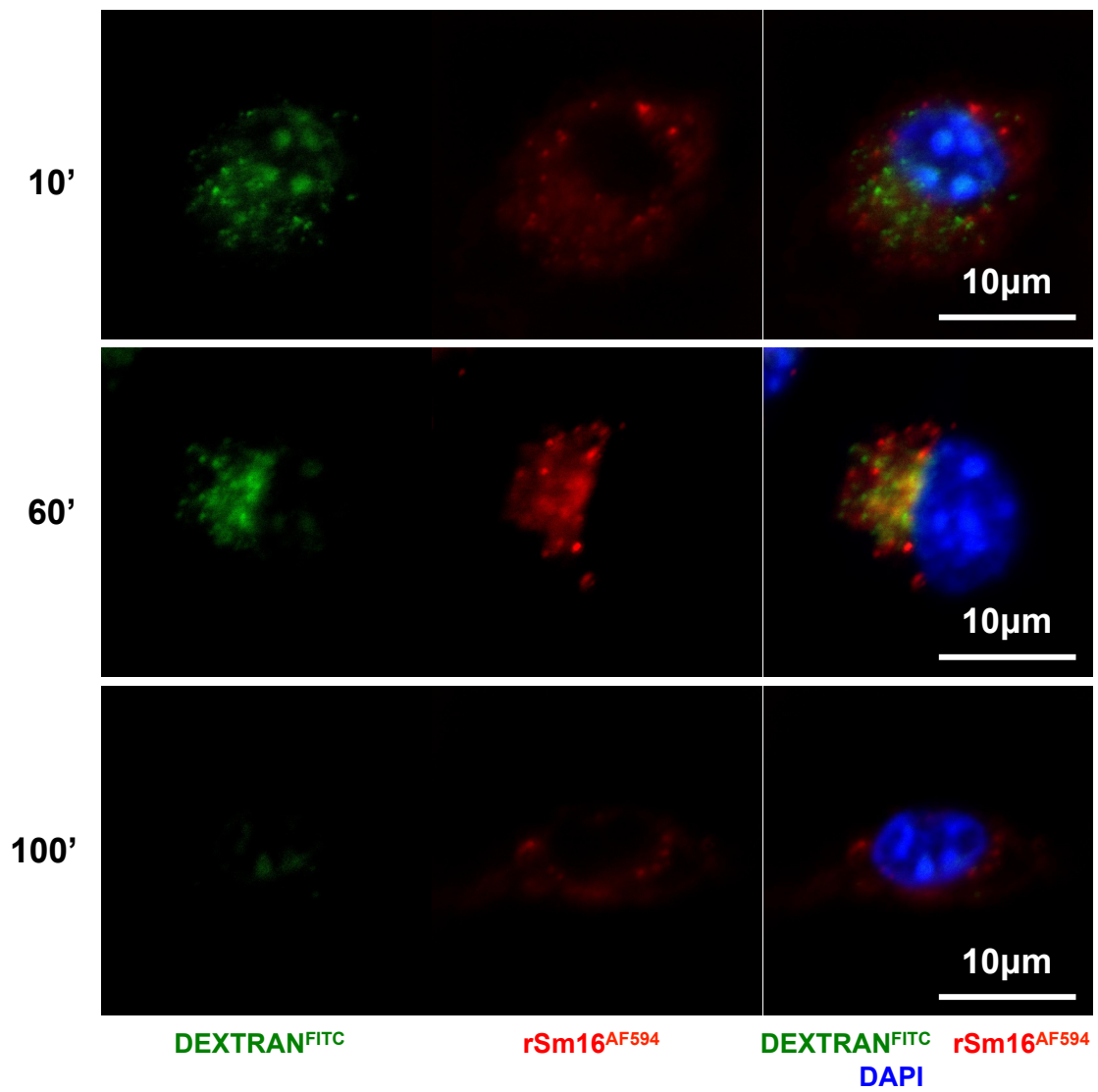


Figure 8.17 Intracellular trafficking of rSm16 is delayed compared to dextran processing

BMMφs were exposed for 100min to labeled rSm16 (red) and DEXTRAN^{FITC} (green). Stimuli were then removed and cells washed and imaged after 10, 60 and 100min. Representative confocal images of BMMφs dyed with nuclear stain DAPI (blue) at each time point are presented (63X objective, 24μm x 24μm).

List of Abbreviations

-/-	Full genetic deficiency
°	Degree
~	Approximately
0-3hRP	Cercarial E/S Products
0-3hRP _P	Insoluble 0-3hRP
0-3hRP _S	Soluble 0-3hRP
2ME	2-mercaptoethanol
AAM ϕ s	Alternatively activated macrophages
ANOVA	Analysis of Variance
AP-1	Activator protein 1
Arg-1	Arginase 1
BgM ϕ s	BioGel elicited macrophages
BMM ϕ s	Bone marrow derived macrophages
BreA	Brefeldin A
BSA	Bovine serum albumin
C/EBP β	CCAAT/enhancer binding protein β
CAM ϕ s	Classically activated macrophages
CD	Cluster of Differentiation
ChIP	Chromatin Immunoprecipitation
CLR	C-type lectin receptors
CREB	cAMP response element binding
CSF-1	Macrophage colony stimulating factor
CytD	Cytochalasin D
DC SIGN	Dendritic Cell-Specific Intercellular adhesion molecule-3-Grabbing Non-integrin
DCs	Dendritic cells
DEC	Dermal Exudate Cells

DETC	Dendritic epidermal T cells
DEXTRAN ^{FITC}	FITC conjugated dextran
DNA	Deoxyribonucleic Acid
EEA-1	Early endosome antigen 1
Egr1	Early growth response protein 1
Erk	Extracellular signal-regulated kinase
FACS buffer	1% FCS in PBS
FASP	Filtered assisted samples preparation
FCS	Foetal calf serum
Fix/Perm	Fixation/Permeabilization
FSC	Forward Scatter
<i>g</i>	Gravities
GAPDH	Glyceraldehyde-3-phosphate dehydrogenase
GFP	Green fluorescent protein
GO	Gene ontology
HRP	Horseradish peroxidase
i.p.	Intra-peritoneal
IFN- γ	Interferon gamma
Ig	Immunoglobulin
IKK β	Inhibitor of nuclear factor kappa B kinase β
IL-	Interleukin
IL-10 ^{+gfp}	IL-10 reporter mice heterozygous for GFP
IL-4ra	IL-4 receptor alpha
ILCs	Innate Lymphoid cells
inh.	Inhibitor
iNOS	Inducible nitric oxide synthase
IPI	International protein index
IRAK1	Interleukin-1 receptor-associated kinase 1

JAK1	Janus kinase 1
kDa	Kilo Daltons
L-Glut	L-Glutamine
LBP	LPS binding protein
LC-MS/MS	Liquid chromatography – mass spectrometry
LCs	Langerhans cells
LPS	Lipopolysaccharide
mAb	Monoclonal antibody
MAP2K	Mitogen associated protein kinase kinase
MAP3K	Mitogen activated protein kinase kinase kinase
Map3K7	Mitogen activated protein kinase kinase kinase 7
MAPK	Mitogen activated protein kinase
MAPKAP	MAPK activated-protein kinase
MD2	Lymphocyte antigen 96
MEK1/2	Mitogen activated protein kinase kinase 1/2
MFI	Median Fluorescence Intensity
MFI	Median fluorescence intensity
MGI	Mouse Genome Informatics
MHC-II	Major histocompatibility complex class II
min	Minutes
ml	Milliliter
MR	Macrophage mannose receptor
MSK	Mitogen- and stress-activated protein kinase
MyD88	Myeloid differentiation protein 88
NF-κB	Nuclear factor κ B
NLR	NOD like receptor
No Ab	No antibody

NOD	Nucleotide oligomerization domain
Nrp-1	Neuropilin-1
ns	Not significant
ON	Overnight
P-	Phosphorylated
P-Akt	Phosphorylated Akt
P-CREB	Phosphorylated CREB
P-Erk	Phosphorylated Erk1/2
P-p105	Phosphorylated p105
P-p38	Phosphorylated p38
P-p65	Phosphorylated p65
pAb	Polyclonal antibody
PAMP	Pathogen associated molecular pattern
PBS	Phosphate buffered saline
PCR	Polymerase chain reaction
Perm	Permeabilization
PFA	Paraformaldehyde
PI3K	Phosphatidylinositol-4,5-bisphosphate 3-kinase
PMB	Polymixin B
Poly I:C	Polyinosinic:polycytidylic acid
PRR	Pattern recognition receptor
qPCR	Quantitative real time PCR
RAF	Proto-oncogene serine/threonine-protein kinase
Rag	Recombination-activation gene
Relm α	Resistin like molecule α
RNA	Ribonucleic Acid
RSK	Ribosomal s6 kinase
rSm16	Recombinant Sm16

SEA	<i>S. mansoni</i> egg antigen
SEM	Standard error of the mean
SHP1	Src homology region 2 domain-containing phosphatase-1
SR-AI/MSR1	Macrophage scavenger receptor 1
SSAP	Soluble schistosomula antigen preparation
SSC	Side Scatter
STAT3	Signal transducer and activator of transcription 3
Th	T helper
TIRAP	Toll-interleukin 1 receptor (TIR) domain containing adaptor protein
TLR	Toll-like receptor
TNF- α	Tumor necrosis factor alpha
Tpl2	Tumor progression locus 2
Tr1	Type 1 regulatory
TRAF 6	TNF receptor associated factor 6
TRAM	TRIF related adaptor molecule
TRIF	TIR-domain-containing adapter-inducing interferon β
TSLP	Thymic stromal lymphopietin
TYK2	Tyrosine kinase 2
VLAD	Visual Annotation Display
Ym1	Chitinase like 3
Zym	Zymosan A
α -CD36	Antibody against CD36
α -CREB	Antibody against CREB
α -P-CREB	Antibody against phosphorylated CREB
α -Pol II	Antibody against RNA Polymerase II

References

- Abram CL, Roberge GL, Pao LI, Neel BG, Lowell CA (2013) Distinct roles for neutrophils and dendritic cells in inflammation and autoimmunity in motheaten mice. *Immunity* **38**: 489-501
- Adachi O, Kawai T, Takeda K, Matsumoto M, Tsutsui H, Sakagami M, Nakanishi K, Akira S (1998) Targeted disruption of the MyD88 gene results in loss of IL-1- and IL-18-mediated function. *Immunity* **9**: 143-150
- Aebersold R, Mann M (2003) Mass spectrometry-based proteomics. *Nature* **422**: 198-207
- Agrawal S, Agrawal A, Doughty B, Gerwitz A, Blenis J, Van Dyke T, Pulendran B (2003) Cutting edge: different Toll-like receptor agonists instruct dendritic cells to induce distinct Th responses via differential modulation of extracellular signal-regulated kinase-mitogen-activated protein kinase and c-Fos. *J Immunol* **171**: 4984-4989
- Akira S, Takeda K (2004) Toll-like receptor signalling. *Nature Reviews Immunology* **4**: 499-511
- Aksoy E, Taboubi S, Torres D, Delbaue S, Hachani A, Whitehead MA, Pearce WP, Berenjano IM, Nock G, Filloux A, Beyaert R, Flamand V, Vanhaesebroeck B (2012) The p110delta isoform of the kinase PI(3)K controls the subcellular compartmentalization of TLR4 signaling and protects from endotoxic shock. *Nat Immunol* **13**: 1045-1054
- Albanesi C, Scarponi C, Giustizieri ML, Girolomoni G (2005) Keratinocytes in inflammatory skin diseases. *Current drug targets Inflammation and allergy* **4**: 329-334
- Alessandrini A, De Haseth S, Fray M, Miyajima M, Colvin RB, Williams WW, Benedict Cosimi A, Benichou G (2011) Dendritic cell maturation occurs through the inhibition of GSK-3beta. *Cell Immunol* **270**: 114-125
- Allen JE, Maizels RM (2011) Diversity and dialogue in immunity to helminths. *Nat Rev Immunol* **11**: 375-388
- Ambarus CA, Krausz S, van Eijk M, Hamann J, Radstake TR, Reedquist KA, Tak PP, Baeten DL (2012) Systematic validation of specific phenotypic markers for in vitro polarized human macrophages. *J Immunol Methods* **375**: 196-206

Ananieva O, Darragh J, Johansen C, Carr JM, McIlrath J, Park JM, Wingate A, Monk CE, Toth R, Santos SG, Iversen L, Arthur JS (2008) The kinases MSK1 and MSK2 act as negative regulators of Toll-like receptor signaling. *Nat Immunol* **9**: 1028-1036

Antoniv TT, Ivashkiv LB (2011) Interleukin-10-induced gene expression and suppressive function are selectively modulated by the PI3K-Akt-GSK3 pathway. *Immunology* **132**: 567-577

Arnoult D, Soares F, Tattoli I, Girardin SE (2011) Mitochondria in innate immunity. *EMBO Rep* **12**: 901-910

Arthur JS, Ley SC (2013) Mitogen-activated protein kinases in innate immunity. *Nat Rev Immunol* **13**: 679-692

Bailey MJ, Lacey DC, de Kok BV, Veith PD, Reynolds EC, Hamilton JA (2011) Extracellular proteomes of M-CSF (CSF-1) and GM-CSF-dependent macrophages. *Immunol Cell Biol* **89**: 283-293

Bain J, Plater L, Elliott M, Shpiro N, Hastie CJ, McLauchlan H, Klevernic I, Arthur JS, Alessi DR, Cohen P (2007) The selectivity of protein kinase inhibitors: a further update. *Biochem J* **408**: 297-315

Balce DR, Li B, Allan ER, Rybicka JM, Krohn RM, Yates RM (2011) Alternative activation of macrophages by IL-4 enhances the proteolytic capacity of their phagosomes through synergistic mechanisms. *Blood*

Bandyopadhyay S, Chiang CY, Srivastava J, Gersten M, White S, Bell R, Kurschner C, Martin CH, Smoot M, Sahasrabudhe S, Barber DL, Chanda SK, Ideker T (2010) A human MAP kinase interactome. *Nature Methods* **7**: 801-U850

Baranova IN, Vishnyakova TG, Bocharov AV, Leelahavanichkul A, Kurlander R, Chen Z, Souza AC, Yuen PS, Star RA, Csako G, Patterson AP, Eggerman TL (2012) Class B scavenger receptor types I and II and CD36 mediate bacterial recognition and proinflammatory signaling induced by *Escherichia coli*, lipopolysaccharide, and cytosolic chaperonin 60. *J Immunol* **188**: 1371-1380

Barron L, Wynn TA (2011) Macrophage activation governs schistosomiasis-induced inflammation and fibrosis. *Eur J Immunol* **41**: 2509-2514

Bartels K, Grenz A, Eltzschig HK (2013) Hypoxia and inflammation are two sides of the same coin. *Proc Natl Acad Sci U S A* **110**: 18351-18352

Baumann CL, Aspalter IM, Sharif O, Pichlmair A, Blüml S, Grebien F, Bruckner M, Pasierbek P, Aumayr K, Planyavsky M, Bennett KL, Colinge J, Knapp S, Superti-Furga G (2010) CD14 is a coreceptor of Toll-like receptors 7 and 9. *J Exp Med* **207**: 2689-2701

Beardmore VA, Hinton HJ, Eftychi C, Apostolaki M, Armaka M, Darragh J, McIlrath J, Carr JM, Armit LJ, Clacher C, Malone L, Kollias G, Arthur JS (2005) Generation and characterization of p38beta (MAPK11) gene-targeted mice. *Mol Cell Biol* **25**: 10454-10464

Beas AO, Taupin V, Teodorof C, Nguyen LT, Garcia-Marcos M, Farquhar MG (2012) Galphas promotes EEA1 endosome maturation and shuts down proliferative signaling through interaction with GIV (Girdin). *Molecular biology of the cell* **23**: 4623-4634

Belkaid Y, Hoffmann KF, Mendez S, Kamhawi S, Udey MC, Wynn TA, Sacks DL (2001) The role of interleukin (IL)-10 in the persistence of *Leishmania major* in the skin after healing and the therapeutic potential of anti-IL-10 receptor antibody for sterile cure. *J Exp Med* **194**: 1497-1506

Belkaid Y, Naik S (2013) Compartmentalized and systemic control of tissue immunity by commensals. *Nat Immunol* **14**: 646-653

Belkaid Y, Piccirillo CA, Mendez S, Shevach EM, Sacks DL (2002) CD4⁺CD25⁺ regulatory T cells control *Leishmania major* persistence and immunity. *Nature* **420**: 502-507

Benoit M, Desnues B, Mege JL (2008) Macrophage polarization in bacterial infections. *Journal of Immunology* **181**: 3733-3739

Berriman M, Haas BJ, LoVerde PT, Wilson RA, Dillon GP, Cerqueira GC, Mashiyama ST, Al-Lazikani B, Andrade LF, Ashton PD, Aslett MA, Bartholomeu DC, Blandin G, Caffrey CR, Coghlan A, Coulson R, Day TA, Delcher A, DeMarco R, Djikeng A, Eyre T, Gamble JA, Ghedin E, Gu Y, Hertz-Fowler C, Hirai H, Hirai Y, Houston R, Ivens A, Johnston DA, Lacerda D, Macedo CD, McVeigh P, Ning Z, Oliveira G, Overington JP, Parkhill J, Pertea M, Pierce RJ, Protasio AV, Quail MA, Rajandream MA, Rogers J, Sajid M, Salzberg SL, Stanke M, Tivey AR, White O, Williams DL, Wortman J, Wu W, Zamanian M, Zerlotini A, Fraser-Liggett CM, Barrell BG, El-Sayed NM (2009) The genome of the blood fluke *Schistosoma mansoni*. *Nature* **460**: 352-358

Blanchet C, Jouvion G, Fitting C, Cavillon JM, Adib-Conquy M (2014) Protective or deleterious role of scavenger receptors SR-A and CD36 on host

resistance to *Staphylococcus aureus* depends on the site of infection. *PLoS One* **9**: e87927

Bodenmiller B, Aebersold R (2010) QUANTITATIVE ANALYSIS OF PROTEIN PHOSPHORYLATION ON A SYSTEM-WIDE SCALE BY MASS SPECTROMETRY-BASED PROTEOMICS. In *Methods in Enzymology, Vol 470: Guide to Yeast Genetics*: Vol. 470, pp 317-334. San Diego: Elsevier Academic Press Inc

Bonham KS, Orzalli MH, Hayashi K, Wolf AI, Glanemann C, Weninger W, Iwasaki A, Knipe DM, Kagan JC (2014) A promiscuous lipid-binding protein diversifies the subcellular sites of toll-like receptor signal transduction. *Cell* **156**: 705-716

Booth M, Mwatha JK, Joseph S, Jones FM, Kadzo H, Ileri E, Kazibwe F, Kemijumbi J, Kariuki C, Kimani G, Ouma JH, Kabatereine NB, Vennervald BJ, Dunne DW (2004) Periportal fibrosis in human *Schistosoma mansoni* infection is associated with low IL-10, low IFN-gamma, high TNF-alpha, or low RANTES, depending on age and gender. *J Immunol* **172**: 1295-1303

Bouabe H (2012) Cytokine reporter mice: the special case of IL-10. *Scand J Immunol* **75**: 553-567

Braem K, Luyten FP, Lories RJ (2011) Blocking p38 signalling inhibits chondrogenesis in vitro but not ankylosis in a model of ankylosing spondylitis in vivo. *Ann Rheum Dis*

Brännström K, Sellin ME, Holmfeldt P, Brattsand M, Gullberg M (2009) The *Schistosoma mansoni* protein Sm16/SmSLP/SmSPO-1 assembles into a nine-subunit oligomer with potential To inhibit Toll-like receptor signaling. *Infect Immun* **77**: 1144-1154

Burton OT, Gibbs S, Miller N, Jones FM, Wen L, Dunne DW, Cooke A, Zaccane P (2010) Importance of TLR2 in the direct response of T lymphocytes to *Schistosoma mansoni* antigens. *Eur J Immunol* **40**: 2221-2229

Bustinduy AL, Thomas CL, Fiutem JJ, Parraga IM, Mungai PL, Muchiri EM, Mutuku F, Kitron U, King CH (2011) Measuring fitness of Kenyan children with polyparasitic infections using the 20-meter shuttle run test as a morbidity metric. *PLoS Negl Trop Dis* **5**: e1213

Campanelli AP, Roselino AM, Cavassani KA, Pereira MS, Mortara RA, Brodskyn CI, Goncalves HS, Belkaid Y, Barral-Netto M, Barral A, Silva JS (2006) CD4+CD25+ T cells in skin lesions of patients with cutaneous

leishmaniasis exhibit phenotypic and functional characteristics of natural regulatory T cells. *J Infect Dis* **193**: 1313-1322

Cao S, Liu J, Song L, Ma X (2005) The protooncogene c-Maf is an essential transcription factor for IL-10 gene expression in macrophages. *J Immunol* **174**: 3484-3492

Cao S, Zhang X, Edwards JP, Mosser DM (2006) NF-kappaB1 (p50) homodimers differentially regulate pro- and anti-inflammatory cytokines in macrophages. *J Biol Chem* **281**: 26041-26050

Cardoso LS, Araujo MI, Goes AM, Pacifico LG, Oliveira RR, Oliveira SC (2007) Polymyxin B as inhibitor of LPS contamination of *Schistosoma mansoni* recombinant proteins in human cytokine analysis. *Microb Cell Fact* **6**: 1

Caulada-Benedetti Z, al-Zamel F, Sher A, James S (1991) Comparison of Th1- and Th2-associated immune reactivities stimulated by single versus multiple vaccination of mice with irradiated *Schistosoma mansoni* cercariae. *J Immunol* **146**: 1655-1660

Chang HD, Helbig C, Tykocinski L, Kreher S, Koeck J, Niesner U, Radbruch A (2007) Expression of IL-10 in Th memory lymphocytes is conditional on IL-12 or IL-4, unless the IL-10 gene is imprinted by GATA-3. *Eur J Immunol* **37**: 807-817

Chen F, Liu Z, Wu W, Rozo C, Bowdridge S, Millman A, Van Rooijen N, Urban JF, Jr., Wynn TA, Gause WC (2012) An essential role for T(H)2-type responses in limiting acute tissue damage during experimental helminth infection. *Nat Med* **18**: 260-266

Chow A, Brown BD, Merad M (2011) Studying the mononuclear phagocyte system in the molecular age. *Nat Rev Immunol* **11**: 788-798

Colley DG, Bustinduy AL, Secor WE, King CH (2014) Human schistosomiasis. *Lancet*

Consortium EP, Birney E, Stamatoyannopoulos JA, Dutta A, Guigo R, Gingeras TR, Margulies EH, Weng Z, Snyder M, Dermitzakis ET, Thurman RE, Kuehn MS, Taylor CM, Neph S, Koch CM, Asthana S, Malhotra A, Adzhubei I, Greenbaum JA, Andrews RM, Flicek P, Boyle PJ, Cao H, Carter NP, Cielland GK, Davis S, Day N, Dharmi P, Dillon SC, Dorschner MO, Fiegler H, Giresi PG, Goldy J, Hawrylycz M, Haydock A, Humbert R, James KD, Johnson BE, Johnson EM, Frum TT, Rosenzweig ER, Karnani N, Lee K, Lefebvre GC, Navas PA, Neri F, Parker SC, Sabo PJ, Sandstrom R, Shafer A, Vetrie D, Weaver M, Wilcox S, Yu M, Collins FS, Dekker J, Lieb JD, Tullius TD, Crawford GE,

Sunyaev S, Noble WS, Dunham I, Denoeud F, Reymond A, Kapranov P, Rozowsky J, Zheng D, Castelo R, Frankish A, Harrow J, Ghosh S, Sandelin A, Hofacker IL, Baertsch R, Keefe D, Dike S, Cheng J, Hirsch HA, Sekinger EA, Lagarde J, Abril JF, Shahab A, Flamm C, Fried C, Hackermuller J, Hertel J, Lindemeyer M, Missal K, Tanzer A, Washietl S, Korbel J, Emanuelsson O, Pedersen JS, Holroyd N, Taylor R, Swarbreck D, Matthews N, Dickson MC, Thomas DJ, Weirauch MT, Gilbert J, Drenkow J, Bell I, Zhao X, Srinivasan KG, Sung WK, Ooi HS, Chiu KP, Foissac S, Alioto T, Brent M, Pachter L, Tress ML, Valencia A, Choo SW, Choo CY, Ucla C, Manzano C, Wyss C, Cheung E, Clark TG, Brown JB, Ganesh M, Patel S, Tammana H, Chrast J, Henrichsen CN, Kai C, Kawai J, Nagalakshmi U, Wu J, Lian Z, Lian J, Newburger P, Zhang X, Bickel P, Mattick JS, Carninci P, Hayashizaki Y, Weissman S, Hubbard T, Myers RM, Rogers J, Stadler PF, Lowe TM, Wei CL, Ruan Y, Struhl K, Gerstein M, Antonarakis SE, Fu Y, Green ED, Karaoz U, Siepel A, Taylor J, Liefer LA, Wetterstrand KA, Good PJ, Feingold EA, Guyer MS, Cooper GM, Asimenos G, Dewey CN, Hou M, Nikolaev S, Montoya-Burgos JI, Loytynoja A, Whelan S, Pardi F, Massingham T, Huang H, Zhang NR, Holmes I, Mullikin JC, Ureta-Vidal A, Paten B, Sringhaus M, Church D, Rosenbloom K, Kent WJ, Stone EA, Program NCS, Baylor College of Medicine Human Genome Sequencing C, Washington University Genome Sequencing C, Broad I, Children's Hospital Oakland Research I, Batzoglou S, Goldman N, Hardison RC, Haussler D, Miller W, Sidow A, Trinklein ND, Zhang ZD, Barrera L, Stuart R, King DC, Ameer A, Enroth S, Bieda MC, Kim J, Bhingee AA, Jiang N, Liu J, Yao F, Vega VB, Lee CW, Ng P, Shahab A, Yang A, Moqtaderi Z, Zhu Z, Xu X, Squazzo S, Oberley MJ, Inman D, Singer MA, Richmond TA, Munn KJ, Rada-Iglesias A, Wallerman O, Komorowski J, Fowler JC, Couttet P, Bruce AW, Dovey OM, Ellis PD, Langford CF, Nix DA, Euskirchen G, Hartman S, Urban AE, Kraus P, Van Calcar S, Heintzman N, Kim TH, Wang K, Qu C, Hon G, Luna R, Glass CK, Rosenfeld MG, Aldred SF, Cooper SJ, Halees A, Lin JM, Shulha HP, Zhang X, Xu M, Haidar JN, Yu Y, Ruan Y, Iyer VR, Green RD, Wadelius C, Farnham PJ, Ren B, Harte RA, Hinrichs AS, Trumbower H, Clawson H, Hillman-Jackson J, Zweig AS, Smith K, Thakkapallayil A, Barber G, Kuhn RM, Karolchik D, Armengol L, Bird CP, de Bakker PI, Kern AD, Lopez-Bigas N, Martin JD, Stranger BE, Woodroffe A, Davydov E, Dimas A, Eyraes E, Hallgrimsdottir IB, Huppert J, Zody MC, Abecasis GR, Estivill X, Bouffard GG, Guan X, Hansen NF, Idol JR, Maduro VV, Maskeri B, McDowell JC, Park M, Thomas PJ, Young AC, Blakesley RW, Muzny DM, Sodergren E, Wheeler DA, Worley KC, Jiang H, Weinstock GM, Gibbs RA, Graves T, Fulton R, Mardis ER, Wilson RK, Clamp M, Cuff J, Gnerre S, Jaffe DB, Chang JL, Lindblad-Toh K, Lander ES, Koriabine M, Nefedov M, Osoegawa K, Yoshinaga Y, Zhu B, de Jong PJ (2007) Identification and analysis of functional elements in 1% of the human genome by the ENCODE pilot project. *Nature* **447**: 799-816

Cook PC, Aynsley SA, Turner JD, Jenkins GR, Van Rooijen N, Leeto M, Brombacher F, Mountford AP (2011) Multiple helminth infection of the skin causes lymphocyte hypo-responsiveness mediated by Th2 conditioning of dermal myeloid cells. *PLoS Pathog* **7**: e1001323

Cook PC, Jones LH, Jenkins SJ, Wynn TA, Allen JE, Macdonald AS (2012) Alternatively activated dendritic cells regulate CD4+ T-cell polarization in vitro and in vivo. *Proc Natl Acad Sci U S A* **109**: 9977-9982

Cooperstock MS (1974) Inactivation of endotoxin by polymyxin B. *Antimicrob Agents Chemother* **6**: 422-425

Correale J, Farez M (2009) Helminth antigens modulate immune responses in cells from multiple sclerosis patients through TLR2-dependent mechanisms. *J Immunol* **183**: 5999-6012

Coulson PS, Smythies LE, Betts C, Mabbott NA, Sternberg JM, Wei XG, Liew FY, Wilson RA (1998) Nitric oxide produced in the lungs of mice immunized with the radiation-attenuated schistosome vaccine is not the major agent causing challenge parasite elimination. *Immunology* **93**: 55-63

Coulson PS, Wilson RA (1997) Recruitment of lymphocytes to the lung through vaccination enhances the immunity of mice exposed to irradiated schistosomes. *Infect Immun* **65**: 42-48

Cremer TJ, Shah P, Cormet-Boyaka E, Valvano MA, Butchar JP, Tridandapani S (2011) Akt-Mediated Proinflammatory Response of Mononuclear Phagocytes Infected with *Burkholderia cenocepacia* Occurs by a Novel GSK3 β -Dependent, I κ B Kinase-Independent Mechanism. *J Immunol* **187**: 635-643

Curwen RS, Ashton PD, Sundaralingam S, Wilson RA (2006) Identification of novel proteases and immunomodulators in the secretions of schistosome cercariae that facilitate host entry. *Molecular & Cellular Proteomics* **5**: 835-844

Davicino RC, Elicabe RJ, Di Genaro MS, Rabinovich GA (2011) Coupling pathogen recognition to innate immunity through glycan-dependent mechanisms. *Int Immunopharmacol* **11**: 1457-1463

Davies LC, Jenkins SJ, Allen JE, Taylor PR (2013) Tissue-resident macrophages. *Nat Immunol* **14**: 986-995

de Jong EC, Vieira PL, Kalinski P, Schuitemaker JH, Tanaka Y, Wierenga EA, Yazdanbakhsh M, Kapsenberg ML (2002) Microbial compounds selectively induce Th1 cell-promoting or Th2 cell-promoting dendritic cells in vitro with diverse th cell-polarizing signals. *J Immunol* **168**: 1704-1709

de Oliveira Fraga LA, Lamb EW, Moreno EC, Chatterjee M, Dvorak J, Delcroix M, Sajid M, Caffrey CR, Davies SJ (2010) Rapid induction of IgE responses to a worm cysteine protease during murine pre-patent schistosome infection. *BMC Immunol* **11**: 56

de Waal Malefyt R, Haanen J, Spits H, Roncarolo MG, te Velde A, Figdor C, Johnson K, Kastelein R, Yssel H, de Vries JE (1991) Interleukin 10 (IL-10) and viral IL-10 strongly reduce antigen-specific human T cell proliferation by diminishing the antigen-presenting capacity of monocytes via downregulation of class II major histocompatibility complex expression. *J Exp Med* **174**: 915-924

Deak M, Clifton AD, Lucocq LM, Alessi DR (1998) Mitogen- and stress-activated protein kinase-1 (MSK1) is directly activated by MAPK and SAPK2/p38, and may mediate activation of CREB. *EMBO J* **17**: 4426-4441

Deryugina EI, Ratnikov BI, Bourdon MA, Gilmore GL, Shadduck RK, Muller-Sieburg CE (1995) Identification of a growth factor for primary murine stroma as macrophage colony-stimulating factor. *Blood* **86**: 2568-2578

Dewals BG, Marillier RG, Hoving JC, Leeto M, Schwegmann A, Brombacher F (2010) IL-4/Ralpha-independent expression of mannose receptor and Ym1 by macrophages depends on their IL-10 responsiveness. *PLoS Negl Trop Dis* **4**: e689

Dillon S, Agrawal A, Van Dyke T, Landreth G, McCauley L, Koh A, Maliszewski C, Akira S, Pulendran B (2004) A Toll-like receptor 2 ligand stimulates Th2 responses in vivo, via induction of extracellular signal-regulated kinase mitogen-activated protein kinase and c-Fos in dendritic cells. *J Immunol* **172**: 4733-4743

Domon B, Aebersold R (2006) Review - Mass spectrometry and protein analysis. *Science* **312**: 212-217

Donnelly S, O'Neill SM, Stack CM, Robinson MW, Turnbull L, Whitchurch C, Dalton JP (2010) Helminth cysteine proteases inhibit TRIF-dependent activation of macrophages via degradation of TLR3. *J Biol Chem* **285**: 3383-3392

Dorsey CH, Cousin CE, Lewis FA, Stirewalt MA (2002) Ultrastructure of the *Schistosoma mansoni* cercaria. *Micron* **33**: 279-323

Downes JE, Marshall-Clarke S (2010) Innate immune stimuli modulate bone marrow-derived dendritic cell production in vitro by toll-like receptor-dependent and -independent mechanisms. *Immunology* **131**: 513-524

Dumitru CD, Ceci JD, Tsatsanis C, Kontoyiannis D, Stamatakis K, Lin JH, Patriotis C, Jenkins NA, Copeland NG, Kollias G, Tscholis PN (2000) TNF-alpha induction by LPS is regulated posttranscriptionally via a Tpl2/ERK-dependent pathway. *Cell* **103**: 1071-1083

Elcombe SE, Naqvi S, Van Den Bosch MW, Mackenzie KF, Cianfanelli F, Brown GD, Arthur JS (2013) Dectin-1 Regulates IL-10 Production via a MSK1/2 and CREB Dependent Pathway and Promotes the Induction of Regulatory Macrophage Markers. *PLoS One* **8**: e60086

Everts B, Amiel E, Huang SC, Smith AM, Chang CH, Lam WY, Redmann V, Freitas TC, Blagih J, van der Windt GJ, Artyomov MN, Jones RG, Pearce EL, Pearce EJ (2014) TLR-driven early glycolytic reprogramming via the kinases TBK1-IKKvarepsilon supports the anabolic demands of dendritic cell activation. *Nat Immunol* **15**: 323-332

Everts B, Husaarts L, Driessen NN, Meevissen MH, Schramm G, van der Ham AJ, van der Hoeven B, Scholzen T, Burgdorf S, Mohrs M, Pearce EJ, Hokke CH, Haas H, Smits HH, Yazdanbakhsh M (2012) Schistosome-derived omega-1 drives Th2 polarization by suppressing protein synthesis following internalization by the mannose receptor. *J Exp Med*

Everts B, Perona-Wright G, Smits HH, Hokke CH, van der Ham AJ, Fitzsimmons CM, Doenhoff MJ, van der Bosch J, Mohrs K, Haas H, Mohrs M, Yazdanbakhsh M, Schramm G (2009) Omega-1, a glycoprotein secreted by *Schistosoma mansoni* eggs, drives Th2 responses. *J Exp Med* **206**: 1673-1680

Everts B, Smits HH, Hokke CH, Yazdanbakhsh M (2010) Helminths and dendritic cells: sensing and regulating via pattern recognition receptors, Th2 and Treg responses. *Eur J Immunol* **40**: 1525-1537

Fairfax K, Nascimento M, Huang SC, Everts B, Pearce EJ (2012) Th2 responses in schistosomiasis. *Seminars in immunopathology* **34**: 863-871

Falcone FH, Loke P, Zang X, MacDonald AS, Maizels RM, Allen JE (2001) A *Brugia malayi* homolog of macrophage migration inhibitory factor reveals an important link between macrophages and eosinophil recruitment during nematode infection. *J Immunol* **167**: 5348-5354

Farhan H, Wendeler MW, Mitrovic S, Fava E, Silberberg Y, Sharan R, Zerial M, Hauri HP (2010) MAPK signaling to the early secretory pathway revealed by kinase/phosphatase functional screening. *J Cell Biol* **189**: 997-1011

Ferragine CE, Walls CD, Davies SJ (2013) Modulation of innate antigen-presenting cell function by pre-patent schistosome infection. *PLoS Negl Trop Dis* **7**: e2136

Ferret-Bernard S, Castro-Borges W, Dowle AA, Sanin DE, Cook PC, Turner JD, Macdonald AS, Thomas JR, Mountford AP (2012) Plasma membrane proteomes of differentially matured dendritic cells identified by LC-MS/MS combined with iTRAQ labelling. *J Proteomics* **75**: 938-948

Flach TL, Ng G, Hari A, Desrosiers MD, Zhang P, Ward SM, Seamone ME, Vilaysane A, Mucsi AD, Fong Y, Prenner E, Ling CC, Tschopp J, Muruve DA, Amrein MW, Shi Y (2011) Alum interaction with dendritic cell membrane lipids is essential for its adjuvant activity. *Nat Med* **17**: 479-487

Fonager J, Pasini EM, Braks JA, Klop O, Ramesar J, Remarque EJ, Vroegrijk IO, van Duinen SG, Thomas AW, Khan SM, Mann M, Kocken CH, Janse CJ, Franke-Fayard BM (2012) Reduced CD36-dependent tissue sequestration of Plasmodium-infected erythrocytes is detrimental to malaria parasite growth in vivo. *J Exp Med* **209**: 93-107

Fu M, Zhu X, Zhang J, Liang J, Lin Y, Zhao L, Ehrenguber MU, Chen YE (2003) Egr-1 target genes in human endothelial cells identified by microarray analysis. *Gene* **315**: 33-41

Fuentes-Duculan J, Suarez-Farinas M, Zaba LC, Nograles KE, Pierson KC, Mitsui H, Pensabene CA, Kzhyshkowska J, Krueger JG, Lowes MA (2010) A subpopulation of CD163-positive macrophages is classically activated in psoriasis. *The Journal of investigative dermatology* **130**: 2412-2422

Gagliani N, Magnani CF, Huber S, Gianolini ME, Pala M, Licona-Limon P, Guo B, Herbert DR, Bulfone A, Trentini F, Di Serio C, Bacchetta R, Andreani M, Brockmann L, Gregori S, Flavell RA, Roncarolo MG (2013) Coexpression of CD49b and LAG-3 identifies human and mouse T regulatory type 1 cells. *Nat Med* **19**: 739-746

Galli SJ, Borregaard N, Wynn TA (2011) Phenotypic and functional plasticity of cells of innate immunity: macrophages, mast cells and neutrophils. *Nat Immunol* **12**: 1035-1044

Gao Y, Zhang M, Chen L, Hou M, Ji M, Wu G (2012) Deficiency in TLR2 but not in TLR4 impairs dendritic cells derived IL-10 responses to schistosome antigens. *Cell Immunol* **272**: 242-250

Gazzinelli RT, Oswald IP, James SL, Sher A (1992) IL-10 inhibits parasite killing and nitrogen oxide production by IFN-gamma-activated macrophages. *J Immunol* **148**: 1792-1796

Gehart H, Kumpf S, Ittner A, Ricci R (2010) MAPK signalling in cellular metabolism: stress or wellness? *EMBO Rep* **11**: 834-840

Gentil K, Lentz CS, Rai R, Muhsin M, Kamath AD, Mutluer O, Specht S, Hubner MP, Hoerauf A (2014) Eotaxin-1 is involved in parasite clearance during chronic filarial infection. *Parasite Immunol* **36**: 60-77

Ghigo C, Mondor I, Jorquera A, Nowak J, Wienert S, Zahner SP, Clausen BE, Luche H, Malissen B, Klauschen F, Bajenoff M (2013) Multicolor fate mapping of Langerhans cell homeostasis. *J Exp Med*

Girgis NM, Gundra UM, Ward LN, Cabrera M, Frevert U, Loke P (2014) Ly6Chigh Monocytes Become Alternatively Activated Macrophages in Schistosome Granulomas with Help from CD4+ Cells. *PLoS Pathog* **10**: e1004080

Goh F, Irvine KM, Lovelace E, Donnelly S, Jones MK, Brion K, Hume DA, Kotze AC, Dalton JP, Ingham A, Sweet MJ (2009) Selective induction of the Notch ligand Jagged-1 in macrophages by soluble egg antigen from *Schistosoma mansoni* involves ERK signalling. *Immunology* **127**: 326-337

Goodridge HS, Reyes CN, Becker CA, Katsumoto TR, Ma J, Wolf AJ, Bose N, Chan AS, Magee AS, Danielson ME, Weiss A, Vasilakos JP, Underhill DM (2011) Activation of the innate immune receptor Dectin-1 upon formation of a 'phagocytic synapse'. *Nature* **472**: 471-475

Goodridge HS, Wilson EH, Harnett W, Campbell CC, Harnett MM, Liew FY (2001) Modulation of macrophage cytokine production by ES-62, a secreted product of the filarial nematode *Acanthocheilonema viteae*. *J Immunol* **167**: 940-945

Gordon S (2003) Alternative activation of macrophages. *Nature Reviews Immunology* **3**: 23-35

Gordon S, Martinez F (2010) Alternative activation of macrophages: mechanism and functions. *Immunity* **32**: 593-604

Gringhuis SI, den Dunnen J, Litjens M, van Het Hof B, van Kooyk Y, Geijtenbeek TB (2007) C-type lectin DC-SIGN modulates Toll-like receptor

signaling via Raf-1 kinase-dependent acetylation of transcription factor NF-kappaB. *Immunity* **26**: 605-616

Gryseels B, Polman K, Clerinx J, Kestens L (2006) Human schistosomiasis. *Lancet* **368**: 1106-1118

Gundra UM, Girgis NM, Ruckerl D, Jenkins S, Ward LN, Kurtz ZD, Wiens KE, Tang MS, Basu-Roy U, Mansukhani A, Allen JE, Loke P (2014) Alternatively activated macrophages derived from monocytes and tissue macrophages are phenotypically and functionally distinct. *Blood* **123**: e110-122

Gwinn DM, Shackelford DB, Egan DF, Mihaylova MM, Mery A, Vasquez DS, Turk BE, Shaw RJ (2008) AMPK phosphorylation of raptor mediates a metabolic checkpoint. *Mol Cell* **30**: 214-226

Haas W, Haeberlein S (2009) Penetration of cercariae into the living human skin: *Schistosoma mansoni* vs. *Trichobilharzia szidati*. *Parasitology research* **105**: 1061-1066

Hammer M, Mages J, Dietrich H, Servatius A, Howells N, Cato AC, Lang R (2006) Dual specificity phosphatase 1 (DUSP1) regulates a subset of LPS-induced genes and protects mice from lethal endotoxin shock. *J Exp Med* **203**: 15-20

Herbert DR, Holscher C, Mohrs M, Arendse B, Schwegmann A, Radwanska M, Leeto M, Kirsch R, Hall P, Mossman H, Claussen B, Forster I, Brombacher F (2004) Alternative macrophage activation is essential for survival during schistosomiasis and downmodulates T helper 1 responses and immunopathology. *Immunity* **20**: 623-635

Hertzog PJ, Mansell A, van Driel IR, Hartland EL (2011) Sculpting the immune response to infection. *Nat Immunol* **12**: 579-582

Hesse M, Piccirillo CA, Belkaid Y, Prufer J, Mentink-Kane M, Leusink M, Cheever AW, Shevach EM, Wynn TA (2004) The pathogenesis of schistosomiasis is controlled by cooperating IL-10-producing innate effector and regulatory T cells. *J Immunol* **172**: 3157-3166

Hewitson JP, Grainger JR, Maizels RM (2009) Helminth immunoregulation: the role of parasite secreted proteins in modulating host immunity. *Mol Biochem Parasitol* **167**: 1-11

Hewitson JP, Hamblin PA, Mountford AP (2007) In the absence of CD154, administration of interleukin-12 restores Th1 responses but not protective immunity to *Schistosoma mansoni*. *Infect Immun* **75**: 3539-3547

Hinz M, Scheidereit C (2014) The I κ B kinase complex in NF- κ B regulation and beyond. *EMBO Rep* **15**: 46-61

Hoesel B, Schmid JA (2013) The complexity of NF- κ B signaling in inflammation and cancer. *Molecular cancer* **12**: 86

Hogg KG, Kumkate S, Anderson S, Mountford AP (2003a) Interleukin-12 p40 secretion by cutaneous CD11c⁺ and F4/80⁺ cells is a major feature of the innate immune response in mice that develop Th1-mediated protective immunity to *Schistosoma mansoni*. *Infect Immun* **71**: 3563-3571

Hogg KG, Kumkate S, Mountford AP (2003b) IL-10 regulates early IL-12-mediated immune responses induced by the radiation-attenuated schistosome vaccine. *Int Immunol* **15**: 1451-1459

Hokke CH, Deelder AM (2001) Schistosome glycoconjugates in host-parasite interplay. *Glycoconjugate Journal* **18**: 573-587

Holmfeldt P, Brannstrom K, Sellin ME, Segerman B, Carlsson SR, Gullberg M (2007) The *Schistosoma mansoni* protein Sm16/SmSLP/SmSPO-1 is a membrane-binding protein that lacks the proposed microtubule-regulatory activity. *Mol Biochem Parasitol* **156**: 225-234

Hoshino K, Takeuchi O, Kawai T, Sanjo H, Ogawa T, Takeda Y, Takeda K, Akira S (1999) Cutting edge: Toll-like receptor 4 (TLR4)-deficient mice are hyporesponsive to lipopolysaccharide: evidence for TLR4 as the Lps gene product. *J Immunol* **162**: 3749-3752

Hotez PJ (2009) Mass drug administration and integrated control for the world's high-prevalence neglected tropical diseases. *Clin Pharmacol Ther* **85**: 659-664

Hotez PJ, Brindley PJ, Bethony JM, King CH, Pearce EJ, Jacobson J (2008) Helminth infections: the great neglected tropical diseases. *J Clin Invest* **118**: 1311-1321

Huotari J, Helenius A (2011) Endosome maturation. *EMBO J* **30**: 3481-3500

Incanni RN, McLaren DJ (1984) Histopathological and ultrastructural studies of cutaneous reactions elicited in naive and chronically infected mice by invading schistosomes of *Schistosoma mansoni*. *Int J Parasitol* **14**: 259-276

Ioannou S, Voulgarelis M (2010) Toll-like receptors, tissue injury, and tumorigenesis. *Mediators Inflamm* **2010**

Iwasaki H, Takeuchi O, Teraguchi S, Matsushita K, Uehata T, Kuniyoshi K, Satoh T, Saitoh T, Matsushita M, Standley DM, Akira S (2011) The IkappaB kinase complex regulates the stability of cytokine-encoding mRNA induced by TLR-IL-1R by controlling degradation of regnase-1. *Nat Immunol* **12**: 1167-1175

Jakubzick C, Gautier EL, Gibbings SL, Sojka DK, Schlitzer A, Johnson TE, Ivanov S, Duan Q, Bala S, Condon T, van Rooijen N, Grainger JR, Belkaid Y, Ma'ayan A, Riches DW, Yokoyama WM, Ginhoux F, Henson PM, Randolph GJ (2013) Minimal differentiation of classical monocytes as they survey steady-state tissues and transport antigen to lymph nodes. *Immunity* **39**: 599-610

James SL, Cheever AW, Caspar P, Wynn TA (1998) Inducible nitric oxide synthase-deficient mice develop enhanced type 1 cytokine-associated cellular and humoral immune responses after vaccination with attenuated *Schistosoma mansoni* cercariae but display partially reduced resistance. *Infect Immun* **66**: 3510-3518

Jang-Lee J, Curwen RS, Ashton PD, Tissot B, Mathieson W, Panico M, Dell A, Wilson RA, Haslam SM (2007) Glycomics analysis of *Schistosoma mansoni* egg and cercarial secretions. *Molecular & Cellular Proteomics* **6**: 1485-1499

Jenkins SJ, Allen JE (2010) Similarity and diversity in macrophage activation by nematodes, trematodes, and cestodes. *J Biomed Biotechnol* **2010**: 262609

Jenkins SJ, Hewitson JP, Ferret-Bernard S, Mountford AP (2005) Schistosome larvae stimulate macrophage cytokine production through TLR4-dependent and -independent pathways. *Int Immunol* **17**: 1409-1418

Jenkins SJ, Mountford AP (2005) Dendritic cells activated with products released by schistosome larvae drive Th2-type immune responses, which can be inhibited by manipulation of CD40 costimulation. *Infect Immun* **73**: 395-402

Jenkins SJ, Ruckerl D, Cook PC, Jones LH, Finkelman FD, van Rooijen N, MacDonald AS, Allen JE (2011) Local macrophage proliferation, rather than recruitment from the blood, is a signature of TH2 inflammation. *Science* **332**: 1284-1288

Jenkins SJ, Ruckerl D, Thomas GD, Hewitson JP, Duncan S, Brombacher F, Maizels RM, Hume DA, Allen JE (2013) IL-4 directly signals tissue-resident macrophages to proliferate beyond homeostatic levels controlled by CSF-1. *J Exp Med* **210**: 2477-2491

John D, Fischer MR, von Stebut E (2013) Model for generation of large numbers of primary, inflammatory skin-derived neutrophils, and macrophages. *Methods Mol Biol* **961**: 403-410

Joshi AD, Schaller MA, Lukacs NW, Kunkel SL, Hogaboam CM (2008) TLR3 modulates immunopathology during a *Schistosoma mansoni* egg-driven Th2 response in the lung. *Eur J Immunol* **38**: 3436-3449

Joshi T, Butchar JP, Tridandapani S (2006) Fcγ receptor signaling in phagocytes. *International journal of hematology* **84**: 210-216

Kagan JC, Iwasaki A (2012) Phagosome as the organelle linking innate and adaptive immunity. *Traffic* **13**: 1053-1061

Kamanaka M, Kim ST, Wan YY, Sutterwala FS, Lara-Tejero M, Galan JE, Harhaj E, Flavell RA (2006) Expression of interleukin-10 in intestinal lymphocytes detected by an interleukin-10 reporter knockin tiger mouse. *Immunity* **25**: 941-952

Kane CM, Cervi L, Sun J, McKee AS, Masek KS, Shapira S, Hunter CA, Pearce EJ (2004) Helminth antigens modulate TLR-initiated dendritic cell activation. *Journal of Immunology* **173**: 7454-7461

Knudsen GM, Medzihradzky KF, Lim KC, Hansell E, McKerrow JH (2005) Proteomic analysis of *Schistosoma mansoni* cercarial secretions. *Molecular & Cellular Proteomics* **4**: 1862-1875

Kufer TA, Sansonetti PJ (2011) NLR functions beyond pathogen recognition. *Nat Immunol* **12**: 121-128

Kuhn R, Lohler J, Rennick D, Rajewsky K, Muller W (1993) Interleukin-10-deficient mice develop chronic enterocolitis. *Cell* **75**: 263-274

Kumar S, Jiang MS, Adams JL, Lee JC (1999) Pyridinylimidazole compound SB 203580 inhibits the activity but not the activation of p38 mitogen-activated protein kinase. *Biochem Biophys Res Commun* **263**: 825-831

Kumkate S, Jenkins GR, Paveley RA, Hogg KG, Mountford AP (2007) CD207+ Langerhans cells constitute a minor population of skin-derived antigen-presenting cells in the draining lymph node following exposure to *Schistosoma mansoni*. *Int J Parasitol* **37**: 209-220

Laird MH, Rhee SH, Perkins DJ, Medvedev AE, Piao W, Fenton MJ, Vogel SN (2009) TLR4/MyD88/PI3K interactions regulate TLR4 signaling. *J Leukoc Biol* **85**: 966-977

Landt SG, Marinov GK, Kundaje A, Kheradpour P, Pauli F, Batzoglou S, Bernstein BE, Bickel P, Brown JB, Cayting P, Chen Y, DeSalvo G, Epstein C, Fisher-Aylor KI, Euskirchen G, Gerstein M, Gertz J, Hartemink AJ, Hoffman MM, Iyer VR, Jung YL, Karmakar S, Kellis M, Kharchenko PV, Li Q, Liu T, Liu XS, Ma L, Milosavljevic A, Myers RM, Park PJ, Pazin MJ, Perry MD, Raha D, Reddy TE, Rozowsky J, Shores N, Sidow A, Slattery M, Stamatoyannopoulos JA, Tolstorukov MY, White KP, Xi S, Farnham PJ, Lieb JD, Wold BJ, Snyder M (2012) ChIP-seq guidelines and practices of the ENCODE and modENCODE consortia. *Genome research* **22**: 1813-1831

Lawrenz M, Visekruna A, Kuhl A, Schmidt N, Kaufmann SH, Steinhoff U (2012) Genetic and pharmacological targeting of TPL-2 kinase ameliorates experimental colitis: a potential target for the treatment of Crohn's disease? *Mucosal Immunol* **5**: 129-139

Lee CC, Avalos AM, Ploegh HL (2012) Accessory molecules for Toll-like receptors and their function. *Nat Rev Immunol* **12**: 168-179

Leelahavanichkul A, Bocharov AV, Kurlander R, Baranova IN, Vishnyakova TG, Souza AC, Hu X, Doi K, Vaisman B, Amar M, Sviridov D, Chen Z, Remaley AT, Csako G, Patterson AP, Yuen PS, Star RA, Eggerman TL (2012) Class B scavenger receptor types I and II and CD36 targeting improves sepsis survival and acute outcomes in mice. *J Immunol* **188**: 2749-2758

Li Q, Singh CR, Ma S, Price ND, Jagannath C (2011) Label-free proteomics and systems biology analysis of mycobacterial phagosomes in dendritic cells and macrophages. *J Proteome Res*

Liu YC, Simmons DP, Li X, Abbott DW, Boom WH, Harding CV (2012) TLR2 signaling depletes IRAK1 and inhibits induction of type I IFN by TLR7/9. *J Immunol* **188**: 1019-1026

Livak KJ, Schmittgen TD (2001) Analysis of relative gene expression data using real-time quantitative PCR and the 2^{(-Delta Delta C(T))} Method. *Methods* **25**: 402-408

Loke P, Gallagher L, Nair MG, Zang X, Brombacher F, Mohrs M, Allison JP, Allen JE (2007) Alternative activation is an innate response to injury that requires CD4(+) T cells to be sustained during chronic infection. *Journal of Immunology* **179**: 3926-3936

Lucas M, Zhang X, Prasanna V, Mosser DM (2005) ERK activation following macrophage FcγR ligation leads to chromatin modifications at the IL-10 locus. *J Immunol* **175**: 469-477

MacDonald AS, Straw AD, Dalton NM, Pearce EJ (2002) Cutting edge: Th2 response induction by dendritic cells: a role for CD40. *J Immunol* **168**: 537-540

Mackay LK, Rahimpour A, Ma JZ, Collins N, Stock AT, Hafon ML, Vega-Ramos J, Lauzurica P, Mueller SN, Stefanovic T, Tschärke DC, Heath WR, Inouye M, Carbone FR, Gebhardt T (2013) The developmental pathway for CD103(+)CD8+ tissue-resident memory T cells of skin. *Nat Immunol* **14**: 1294-1301

MacKenzie KF, Clark K, Naqvi S, McGuire VA, Noehren G, Kristariyanto Y, van den Bosch M, Mudaliar M, McCarthy PC, Pattison MJ, Pedrioli PG, Barton GJ, Toth R, Prescott A, Arthur JS (2013) PGE₂ induces macrophage IL-10 production and a regulatory-like phenotype via a protein kinase A-SIK-CRTC3 pathway. *J Immunol* **190**: 565-577

Magalhães KG, Almeida PE, Atella GC, Maya-Monteiro CM, Castro-Faria-Neto HC, Pelajo-Machado M, Lenzi HL, Bozza MT, Bozza PT (2010) Schistosomal - derived lysophosphatidylcholine are involved in eosinophil activation and recruitment through Toll - like receptor-2-dependent mechanisms. *J Infect Dis* **202**: 1369-1379

Malissen B, Tamoutounour S, Henri S (2014) The origins and functions of dendritic cells and macrophages in the skin. *Nat Rev Immunol* **14**: 417-428

Mallick P, Kuster B (2010) Proteomics: a pragmatic perspective. *Nat Biotechnol* **28**: 695-709

Marshall FA, Pearce EJ (2008) Uncoupling of induced protein processing from maturation in dendritic cells exposed to a highly antigenic preparation from a helminth parasite. *J Immunol* **181**: 7562-7570

Martinez FO, Helming L, Gordon S (2009) Alternative Activation of Macrophages: An Immunologic Functional Perspective. *Annual Review of Immunology* **27**: 451-483

Martinez-Pomares L, Linehan SA, Taylor PR, Gordon S (2001) Binding properties of the mannose receptor. *Immunobiology* **204**: 527-535

Mayer TZ, Simard FA, Cloutier A, Vardhan H, Dubois CM, McDonald PP (2013) The p38-MSK1 signaling cascade influences cytokine production through CREB and C/EBP factors in human neutrophils. *J Immunol* **191**: 4299-4307

McKerrow JH, Caffrey C, Kelly B, Loke P, Sajid M (2006) Proteases in parasitic diseases. *Annu Rev Pathol* **1**: 497-536

McKerrow JH, Salter J (2002) Invasion of skin by *Schistosoma* cercariae. *Trends Parasitol* **18**: 193-195

Medina EA, Morris IR, Berton MT (2010) Phosphatidylinositol 3-Kinase Activation Attenuates the TLR2-Mediated Macrophage Proinflammatory Cytokine Response to Francisella tularensis Live Vaccine Strain. *J Immunol* **185**: 7562-7572

Meevissen MH, Driessen NN, Smits HH, Versteegh R, van Vliet SJ, van Kooyk Y, Schramm G, Deelder AM, Haas H, Yazdanbakhsh M, Hokke CH (2012) Specific glycan elements determine differential binding of individual egg glycoproteins of the human parasite *Schistosoma mansoni* by host C-type lectin receptors. *Int J Parasitol*

Meevissen MH, Yazdanbakhsh M, Hokke CH (2011) *Schistosoma mansoni* egg glycoproteins and C-type lectins of host immune cells: Molecular partners that shape immune responses. *Exp Parasitol*

Meissner F, Scheltema RA, Mollenkopf HJ, Mann M (2013) Direct proteomic quantification of the secretome of activated immune cells. *Science* **340**: 475-478

Mendez S, Reckling SK, Piccirillo CA, Sacks D, Belkaid Y (2004) Role for CD4(+) CD25(+) regulatory T cells in reactivation of persistent leishmaniasis and control of concomitant immunity. *J Exp Med* **200**: 201-210

Meng G, Zhang F, Fuss I, Kitani A, Strober W (2009) A mutation in the Nlrp3 gene causing inflammasome hyperactivation potentiates Th17 cell-dominant immune responses. *Immunity* **30**: 860-874

Mentink-Kane MM, Cheever AW, Wilson MS, Madala SK, Beers LM, Ramalingam TR, Wynn TA (2011) Accelerated and progressive and lethal liver

fibrosis in mice that lack interleukin (IL)-10, IL-12p40, and IL-13. *Gastroenterology* **141**: 2200-2209

Mizuno R, Kamioka Y, Kabashima K, Imajo M, Sumiyama K, Nakasho E, Ito T, Hamazaki Y, Okuchi Y, Sakai Y, Kiyokawa E, Matsuda M (2014) In vivo imaging reveals PKA regulation of ERK activity during neutrophil recruitment to inflamed intestines. *J Exp Med* **211**: 1123-1136

Mountford AP, Harrop R (1998) Vaccination against Schistosomiasis: The case for Lung-stage Antigens. *Parasitol Today* **14**: 109-114

Mukhopadhyay S, Varin A, Chen Y, Liu B, Tryggvason K, Gordon S (2011) SR-A/MARCO-mediated ligand delivery enhances intracellular TLR and NLR function, but ligand scavenging from cell surface limits TLR4 response to pathogens. *Blood* **117**: 1319-1328

Murray PJ, Wynn TA (2011) Protective and pathogenic functions of macrophage subsets. *Nat Rev Immunol* **11**: 723-737

Mutapi F, Rujeni N, Bourke C, Mitchell K, Appleby L, Nausch N, Midzi N, Mdluza T (2011) Schistosoma haematobium Treatment in 1-5 Year Old Children: Safety and Efficacy of the Antihelminthic Drug Praziquantel. *PLoS Negl Trop Dis* **5**: e1143

Muzio M, Ni J, Feng P, Dixit VM (1997) IRAK (Pelle) family member IRAK-2 and MyD88 as proximal mediators of IL-1 signaling. *Science* **278**: 1612-1615

Naik S, Bouladoux N, Wilhelm C, Molloy MJ, Salcedo R, Kastenmuller W, Deming C, Quinones M, Koo L, Conlan S, Spencer S, Hall JA, Dzutsev A, Kong H, Campbell DJ, Trinchieri G, Segre JA, Belkaid Y (2012) Compartmentalized control of skin immunity by resident commensals. *Science* **337**: 1115-1119

Nandan D, Camargo de Oliveira C, Moeenrezakhanlou A, Lopez M, Silverman JM, Subek J, Reiner NE (2012) Myeloid cell IL-10 production in response to leishmania involves inactivation of glycogen synthase kinase-3beta downstream of phosphatidylinositol-3 kinase. *J Immunol* **188**: 367-378

Nandan D, Reiner NE (2005) Leishmania donovani engages in regulatory interference by targeting macrophage protein tyrosine phosphatase SHP-1. *Clinical Immunology* **114**: 266-277

Nascimento M, Huang SC, Smith A, Everts B, Lam W, Bassity E, Gautier EL, Randolph GJ, Pearce EJ (2014) Ly6Chi monocyte recruitment is responsible for

Th2 associated host-protective macrophage accumulation in liver inflammation due to schistosomiasis. *PLoS Pathog* **10**: e1004282

Nestle FO, Di Meglio P, Qin JZ, Nickoloff BJ (2009) Skin immune sentinels in health and disease. *Nat Rev Immunol* **9**: 679-691

Oeckinghaus A, Hayden MS, Ghosh S (2011) Crosstalk in NF-kappaB signaling pathways. *Nat Immunol* **12**: 695-708

Okazawa H, Motegi S, Ohyama N, Ohnishi H, Tomizawa T, Kaneko Y, Oldenborg PA, Ishikawa O, Matozaki T (2005) Negative regulation of phagocytosis in macrophages by the CD47-SHPS-1 system. *J Immunol* **174**: 2004-2011

Oury C (2014) CD36: linking lipids to the NLRP3 inflammasome, atherogenesis and atherothrombosis. *Cell Mol Immunol* **11**: 8-10

Pagel JI, Deindl E (2011) Early growth response 1--a transcription factor in the crossfire of signal transduction cascades. *Indian J Biochem Biophys* **48**: 226-235

Park SH, Park-Min KH, Chen J, Hu X, Ivashkiv LB (2011) Tumor necrosis factor induces GSK3 kinase-mediated cross-tolerance to endotoxin in macrophages. *Nat Immunol* **12**: 607-615

Pasparakis M, Haase I, Nestle FO (2014) Mechanisms regulating skin immunity and inflammation. *Nat Rev Immunol* **14**: 289-301

Patel VJ, Thalassinos K, Slade SE, Connolly JB, Crombie A, Murrell JC, Scrivens JH (2009) A comparison of labeling and label-free mass spectrometry-based proteomics approaches. *J Proteome Res* **8**: 3752-3759

Paveley RA, Aynsley SA, Cook PC, Turner JD, Mountford AP (2009) Fluorescent imaging of antigen released by a skin-invading helminth reveals differential uptake and activation profiles by antigen presenting cells. *PLoS Negl Trop Dis* **3**: e528

Paveley RA, Aynsley SA, Turner JD, Bourke CD, Jenkins SJ, Cook PC, Martinez-Pomares L, Mountford AP (2011) The Mannose Receptor (CD206) is an important pattern recognition receptor (PRR) in the detection of the infective stage of the helminth *Schistosoma mansoni* and modulates IFN γ production. *Int J Parasitol* **41**: 1335-1345

Pearce EJ, MacDonald AS (2002) The immunobiology of schistosomiasis. *Nat Rev Immunol* **2**: 499-511

Pemberton RM, Smythies LE, Mountford AP, Wilson RA (1991) Patterns of cytokine production and proliferation by T lymphocytes differ in mice vaccinated or infected with *Schistosoma mansoni*. *Immunology* **73**: 327-333

Pena OM, Pistolic J, Raj D, Fjell CD, Hancock RE (2011) Endotoxin Tolerance Represents a Distinctive State of Alternative Polarization (M2) in Human Mononuclear Cells. *J Immunol*

Perona-Wright G, Jenkins SJ, MacDonald AS (2006) Dendritic cell activation and function in response to *Schistosoma mansoni*. *Int J Parasitol* **36**: 711-721

Pesce JT, Ramalingam TR, Mentink-Kane MM, Wilson MS, El Kasmi KC, Smith AM, Thompson RW, Cheever AW, Murray PJ, Wynn TA (2009) Arginase-1-expressing macrophages suppress Th2 cytokine-driven inflammation and fibrosis. *PLoS Pathog* **5**: e1000371

Phythian-Adams AT, Cook PC, Lundie RJ, Jones LH, Smith KA, Barr TA, Hochweller K, Anderton SM, Hammerling GJ, Maizels RM, MacDonald AS (2010) CD11c depletion severely disrupts Th2 induction and development in vivo. *J Exp Med* **207**: 2089-2096

Pineda MA, Lumb F, Harnett MM, Harnett W (2014) ES-62, a therapeutic anti-inflammatory agent evolved by the filarial nematode *Acanthocheilonema viteae*. *Mol Biochem Parasitol* **194**: 1-8

Pinto R, Herold S, Cakarova L, Hoegner K, Lohmeyer J, Planz O, Pleschka S (2011) Inhibition of influenza virus-induced NF-kappaB and Raf-MEK-ERK activation can reduce both virus titers and cytokine expression simultaneously in vitro and in vivo. *Antiviral Res*

Protasio AV, Tsai IJ, Babbage A, Nichol S, Hunt M, Aslett MA, De Silva N, Velarde GS, Anderson TJ, Clark RC, Davidson C, Dillon GP, Holroyd NE, LoVerde PT, Lloyd C, McQuillan J, Oliveira G, Otto TD, Parker-Manuel SJ, Quail MA, Wilson RA, Zerlotini A, Dunne DW, Berriman M (2012) A systematically improved high quality genome and transcriptome of the human blood fluke *Schistosoma mansoni*. *PLoS Negl Trop Dis* **6**: e1455

Pulendran B, Artis D (2012) New paradigms in type 2 immunity. *Science* **337**: 431-435

Puneet P, McGrath MA, Tay HK, Al-Riyami L, Rzepecka J, Moochhala SM, Pervaiz S, Harnett MM, Harnett W, Melendez AJ (2011) The helminth product ES-62 protects against septic shock via Toll-like receptor 4-dependent autophagosomal degradation of the adaptor MyD88. *Nat Immunol* **12**: 344-351

Ramalingam TR, Pesce JT, Sheikh F, Cheever AW, Mentink-Kane MM, Wilson MS, Stevens S, Valenzuela DM, Murphy AJ, Yancopoulos GD, Urban JF, Jr., Donnelly RP, Wynn TA (2008) Unique functions of the type II interleukin 4 receptor identified in mice lacking the interleukin 13 receptor alpha1 chain. *Nat Immunol* **9**: 25-33

Rathinam VA, Vanaja SK, Fitzgerald KA (2012) Regulation of inflammasome signaling. *Nat Immunol* **13**: 333-332

Redpath SA, Fonseca NM, Perona-Wright G (2014) Protection and pathology during parasite infection: IL-10 strikes the balance. *Parasite Immunol* **36**: 233-252

Retra K, van Riet E, Adegnik AA, Everts B, van Geest S, Kremsner PG, van Hellemond JJ, van der Kleij D, Tielens AG, Yazdanbakhsh M (2008) Immunologic activity of schistosomal and bacterial TLR2 ligands in Gabonese children. *Parasite Immunol* **30**: 39-46

Richter J, Correia Dacal AR, Vergetti Siqueira JG, Poggensee G, Mannsmann U, Deelder A, Feldmeier H (1998) Sonographic prediction of variceal bleeding in patients with liver fibrosis due to *Schistosoma mansoni*. *Tropical medicine & international health : TM & IH* **3**: 728-735

Robitaille AM, Christen S, Shimobayashi M, Cornu M, Fava LL, Moes S, Prescianotto-Baschong C, Sauer U, Jenoe P, Hall MN (2013) Quantitative phosphoproteomics reveal mTORC1 activates de novo pyrimidine synthesis. *Science* **339**: 1320-1323

Rojas López M, Duque Correa MA (2007) Alternative macrophage activation: the diversity of one cell involved in innate immunity in response to its environmental complexity. *Inmunología* **26**: 14

Rommel C, Clarke BA, Zimmermann S, Nuñez L, Rossman R, Reid K, Moelling K, Yancopoulos GD, Glass DJ (1999) Differentiation stage-specific inhibition of the Raf-MEK-ERK pathway by Akt. *Science* **286**: 1738-1741

Ruland J (2011) Return to homeostasis: downregulation of NF-kappaB responses. *Nat Immunol* **12**: 709-714

Sabat R, Grütz G, Warszawska K, Kirsch S, Witte E, Wolk K, Geginat J (2010) Biology of interleukin-10. *Cytokine Growth Factor Rev* **21**: 331-344

Sadler CH, Rutitzky LI, Stadecker MJ, Wilson RA (2003) IL-10 is crucial for the transition from acute to chronic disease state during infection of mice with *Schistosoma mansoni*. *Eur J Immunol* **33**: 880-888

Salmeron A, Ahmad TB, Carlile GW, Pappin D, Narsimhan RP, Ley SC (1996) Activation of MEK-1 and SEK-1 by Tpl-2 proto-oncoprotein, a novel MAP kinase kinase kinase. *EMBO J* **15**: 817-826

Salter JP, Lim KC, Hansell E, Hsieh I, McKerrow JH (2000) Schistosome invasion of human skin and degradation of dermal elastin are mediated by a single serine protease. *J Biol Chem* **275**: 38667-38673

Sanchez Rodriguez R, Pauli ML, Neuhaus IM, Yu SS, Arron ST, Harris HW, Yang SH, Anthony BA, Sverdrup FM, Krow-Lucal E, Mackenzie TC, Johnson DS, Meyer EH, Lohr A, Hsu A, Koo J, Liao W, Gupta R, Debbaneh MG, Butler D, Huynh M, Levin EC, Leon A, Hoffman WY, McGrath MH, Alvarado MD, Ludwig CH, Truong HA, Maurano MM, Gratz IK, Abbas AK, Rosenblum MD (2014) Memory regulatory T cells reside in human skin. *J Clin Invest* **124**: 1027-1036

Saraiva M, Christensen JR, Tsytsykova AV, Goldfeld AE, Ley SC, Kioussis D, O'Garra A (2005) Identification of a macrophage-specific chromatin signature in the IL-10 locus. *J Immunol* **175**: 1041-1046

Saraiva M, Christensen JR, Veldhoen M, Murphy TL, Murphy KM, O'Garra A (2009) Interleukin-10 production by Th1 cells requires interleukin-12-induced STAT4 transcription factor and ERK MAP kinase activation by high antigen dose. *Immunity* **31**: 209-219

Saraiva M, O'Garra A (2010) The regulation of IL-10 production by immune cells. *Nat Rev Immunol* **10**: 170-181

Sato M, Sano H, Iwaki D, Kudo K, Konishi M, Takahashi H, Takahashi T, Imaizumi H, Asai Y, Kuroki Y (2003) Direct binding of Toll-like receptor 2 to zymosan, and zymosan-induced NF-kappa B activation and TNF-alpha secretion are down-regulated by lung collectin surfactant protein A. *J Immunol* **171**: 417-425

Sawant DV, Gravano DM, Vogel P, Giacomini P, Artis D, Vignali DA (2014) Regulatory T Cells Limit Induction of Protective Immunity and Promote Immune Pathology following Intestinal Helminth Infection. *J Immunol* **192**: 2904-2912

Scheer S, Gross S, Mouahid G, Mone H, Lamers MC (2014) A novel tool to identify the relative contribution of lymphoid cell types that contribute to IL-10 production during the infection with *Schistosoma mansoni*: The TIGER index. *J Immunol Methods*

Schulz C, Gomez Perdiguero E, Chorro L, Szabo-Rogers H, Cagnard N, Kierdorf K, Prinz M, Wu B, Jacobsen SE, Pollard JW, Frampton J, Liu KJ, Geissmann F (2012) A lineage of myeloid cells independent of Myb and hematopoietic stem cells. *Science* **336**: 86-90

Schwartz DA (1981) Helminths in the induction of cancer II. *Schistosoma haematobium* and bladder cancer. *Tropical and geographical medicine* **33**: 1-7

Shen N, Shao Y, Lai SS, Qiao L, Yang RL, Xue B, Pan FY, Chen HQ, Li CJ (2011) GGPPS, a new EGR-1 target gene, reactivates ERK 1/2 signaling through increasing Ras prenylation. *Am J Pathol* **179**: 2740-2750

Shi Z, Cai Z, Sanchez A, Zhang T, Wen S, Wang J, Yang J, Fu S, Zhang D (2011) A novel Toll-like receptor that recognizes vesicular stomatitis virus. *J Biol Chem* **286**: 4517-4524

Shilo BZ, Schejter ED (2011) Regulation of developmental intercellular signalling by intracellular trafficking. *EMBO J* **30**: 3516-3526

Shoemaker J, Saraiva M, O'Garra A (2006) GATA-3 directly remodels the IL-10 locus independently of IL-4 in CD4⁺ T cells. *J Immunol* **176**: 3470-3479

Smith P, Fallon RE, Mangan NE, Walsh CM, Saraiva M, Sayers JR, McKenzie AN, Alami A, Fallon PG (2005) *Schistosoma mansoni* secretes a chemokine binding protein with antiinflammatory activity. *J Exp Med* **202**: 1319-1325

Specht S, Taylor MD, Hoeve MA, Allen JE, Lang R, Hoerauf A (2012) Over expression of IL-10 by macrophages overcomes resistance to murine filariasis. *Exp Parasitol* **132**: 90-96

Staubert-Salle D, Fleury S, Lazzari A, Molendi-Coste O, Hornez N, Lavogiez C, Kanda A, Wartelle J, Fries A, Pennino D, Mionnet C, Prawitt J, Bouchaert E, Delaporte E, Glaichenhaus N, Staels B, Julia V, Dombrowicz D (2014) CX3CL1 (fractalkine) and its receptor CX3CR1 regulate atopic dermatitis by controlling effector T cell retention in inflamed skin. *J Exp Med* **211**: 1185-1196

Stephens L, Ellson C, Hawkins P (2002) Roles of PI3Ks in leukocyte chemotaxis and phagocytosis. *Curr Opin Cell Biol* **14**: 203-213

Strippoli R, Benedicto I, Perez Lozano ML, Pellinen T, Sandoval P, Lopez-Cabrera M, del Pozo MA (2012) Inhibition of transforming growth factor-activated kinase 1 (TAK1) blocks and reverses epithelial to mesenchymal transition of mesothelial cells. *PLoS One* **7**: e31492

Suffia I, Reckling SK, Salay G, Belkaid Y (2005) A role for CD103 in the retention of CD4+CD25+ Treg and control of Leishmania major infection. *J Immunol* **174**: 5444-5455

Sulahian TH, Imrich A, DeLoid G, Winkler AR, Kobzik L (2008) Signaling pathways required for macrophage scavenger receptor-mediated phagocytosis: analysis by scanning cytometry. *Respiratory Research* **9**: 15

Svajger U, Obermajer N, Anderluh M, Kos J, Jeras M (2011) DC-SIGN ligation greatly affects dendritic cell differentiation from monocytes compromising their normal function. *J Leukoc Biol*

Takeuchi O, Hoshino K, Kawai T, Sanjo H, Takada H, Ogawa T, Takeda K, Akira S (1999) Differential roles of TLR2 and TLR4 in recognition of gram-negative and gram-positive bacterial cell wall components. *Immunity* **11**: 443-451

Thomas KE, Galligan CL, Newman RD, Fish EN, Vogel SN (2006) Contribution of interferon-beta to the murine macrophage response to the toll-like receptor 4 agonist, lipopolysaccharide. *J Biol Chem* **281**: 31119-31130

Traub LM (2011) Regarding the amazing choreography of clathrin coats. *PLoS Biol* **9**: e1001037

Turner JD, Meurs L, Dool P, Bourke CD, Mbow M, Dieye TN, Mboup S, Polman K, Mountford AP (2013) Schistosome infection is associated with enhanced whole-blood IL-10 secretion in response to cercarial excretory/secretory products. *Parasite Immunol* **35**: 147-156

Turner JD, Narang P, Coles MC, Mountford AP (2012) Blood flukes exploit Peyer's Patch lymphoid tissue to facilitate transmission from the mammalian host. *PLoS Pathog* **8**: e1003063

Valanne S, Wang JH, Rämetsä M (2011) The Drosophila Toll signaling pathway. *J Immunol* **186**: 649-656

van Berlo D, Knaapen AM, van Schooten FJ, Schins RPF, Albrecht C (2010) NF-kappa B dependent and independent mechanisms of quartz-induced proinflammatory activation of lung epithelial cells. *Particle and Fibre Toxicology* **7**

van der Kleij D, Latz E, Brouwers JF, Kruize YC, Schmitz M, Kurt-Jones EA, Espevik T, de Jong EC, Kapsenberg ML, Golenbock DT, Tielens AG, Yazdanbakhsh M (2002) A novel host-parasite lipid cross-talk. Schistosomal lyso-phosphatidylserine activates toll-like receptor 2 and affects immune polarization. *J Biol Chem* **277**: 48122-48129

van Liempt E, van Vliet SJ, Engering A, Garcia Vallejo JJ, Bank CM, Sanchez-Hernandez M, van Kooyk Y, van Die I (2007) Schistosoma mansoni soluble egg antigens are internalized by human dendritic cells through multiple C-type lectins and suppress TLR-induced dendritic cell activation. *Mol Immunol* **44**: 2605-2615

van Riet E, Everts B, Retra K, Phylipsen M, van Hellemond JJ, Tielens AG, van der Kleij D, Hartgers FC, Yazdanbakhsh M (2009) Combined TLR2 and TLR4 ligation in the context of bacterial or helminth extracts in human monocyte derived dendritic cells: molecular correlates for Th1/Th2 polarization. *BMC Immunol* **10**: 9

van Vliet SJ, Bay S, Vuist IM, Kalay H, Garcia-Vallejo JJ, Leclerc C, van Kooyk Y (2013) MGL signaling augments TLR2-mediated responses for enhanced IL-10 and TNF-alpha secretion. *J Leukoc Biol* **94**: 315-323

Vanhaesebroeck B, Stephens L, Hawkins P (2012) PI3K signalling: the path to discovery and understanding. *Nat Rev Mol Cell Biol* **13**: 195-203

Vlahos CJ, Matter WF, Hui KY, Brown RF (1994) A specific inhibitor of phosphatidylinositol 3-kinase, 2-(4-morpholinyl)-8-phenyl-4H-1-benzopyran-4-one (LY294002). *J Biol Chem* **269**: 5241-5248

Wang H, Brown J, Martin M (2011) Glycogen synthase kinase 3: a point of convergence for the host inflammatory response. *Cytokine* **53**: 130-140

Warner N, Nunez G (2013) MyD88: A Critical Adaptor Protein in Innate Immunity Signal Transduction. *J Immunol* **190**: 3-4

Watts C (2011) The endosome-lysosome pathway and information generation in the immune system. *Biochim Biophys Acta*

Wen AY, Sakamoto KM, Miller LS (2010) The Role of the Transcription Factor CREB in Immune Function. *J Immunol* **185**: 6413-6419

Wesche H, Henzel WJ, Shillinglaw W, Li S, Cao Z (1997) MyD88: an adapter that recruits IRAK to the IL-1 receptor complex. *Immunity* **7**: 837-847

West AP, Brodsky IE, Rahner C, Woo DK, Erdjument-Bromage H, Tempst P, Walsh MC, Choi Y, Shadel GS, Ghosh S (2011) TLR signalling augments macrophage bactericidal activity through mitochondrial ROS. *Nature* **472**: 476-480

Wheater PR, Wilson RA (1979) *Schistosoma mansoni*: a histological study of migration in the laboratory mouse. *Parasitology* **79**: 49-62

Whitfield TW, Wang J, Collins PJ, Partridge EC, Aldred SF, Trinklein ND, Myers RM, Weng Z (2012) Functional analysis of transcription factor binding sites in human promoters. *Genome Biol* **13**: R50

Wilson MS, Cheever AW, White SD, Thompson RW, Wynn TA (2011) IL-10 Blocks the Development of Resistance to Re-Infection with *Schistosoma mansoni*. *PLoS Pathog* **7**: e1002171

Wilson RA (1990) Leaky livers, portal shunting and immunity to schistosomes. *Parasitol Today* **6**: 354-358

Wilson RA (2012) Virulence factors of schistosomes. *Microbes Infect* **14**: 1442-1450

Wolf AJ, Arruda A, Reyes CN, Kaplan AT, Shimada T, Shimada K, Arditi M, Liu G, Underhill DM (2011) Phagosomal degradation increases TLR access to bacterial ligands and enhances macrophage sensitivity to bacteria. *J Immunol* **187**: 6002-6010

Wynn TA, Chawla A, Pollard JW (2013) Macrophage biology in development, homeostasis and disease. *Nature* **496**: 445-455

Wynn TA, Cheever AW, Williams ME, Hieny S, Caspar P, Kuhn R, Muller W, Sher A (1998) IL-10 regulates liver pathology in acute murine Schistosomiasis *mansoni* but is not required for immune down-modulation of chronic disease. *J Immunol* **160**: 4473-4480

Xu J, Yang Y, Qiu G, Lal G, Wu Z, Levy DE, Ochando JC, Bromberg JS, Ding Y (2009) c-Maf regulates IL-10 expression during Th17 polarization. *J Immunol* **182**: 6226-6236

Yan DM, Dai RY, Duan CY, Chen SK, Liu YP, Chen CN, Li H (2010) [Cross-talk between PI3K/Akt and MEK/ERK pathways regulates human hepatocellular carcinoma cell cycle progression under endoplasmic reticulum stress]. *Zhonghua Gan Zang Bing Za Zhi* **18**: 909-914

Yang Z, Zhang X, Darrah P, Mosser D (2010) The Regulation of Th1 Responses by the p38 MAPK. *J Immunol* **185**: 6205-6213

Yarovinsky F, Zhang D, Andersen JF, Bannenberg GL, Serhan CN, Hayden MS, Hieny S, Sutterwala FS, Flavell RA, Ghosh S, Sher A (2005) TLR11 activation of dendritic cells by a protozoan profilin-like protein. *Science* **308**: 1626-1629

Yip KY, Cheng C, Bhardwaj N, Brown JB, Leng J, Kundaje A, Rozowsky J, Birney E, Bickel P, Snyder M, Gerstein M (2012) Classification of human genomic regions based on experimentally determined binding sites of more than 100 transcription-related factors. *Genome Biol* **13**: R48

Yu M, Qi X, Moreno JL, Farber DL, Keegan AD (2011) NF- κ B Signaling Participates in Both RANKL- and IL-4-Induced Macrophage Fusion: Receptor Cross-Talk Leads to Alterations in NF- κ B Pathways. *J Immunol* **187**: 1797-1806

Yuk JM, Shin DM, Lee HM, Kim JJ, Kim SW, Jin HS, Yang CS, Park KA, Chanda D, Kim DK, Huang SM, Lee SK, Lee CH, Kim JM, Song CH, Lee SY, Hur GM, Moore DD, Choi HS, Jo EK (2011) The orphan nuclear receptor SHP acts as a negative regulator in inflammatory signaling triggered by Toll-like receptors. *Nat Immunol* **12**: 742-751

Zhang M, Gao Y, Du X, Zhang D, Ji M, Wu G (2011) Toll-like receptor (TLR) 2 and TLR4 deficiencies exert differential in vivo effects against *Schistosoma japonicum*. *Parasite Immunol* **33**: 199-209

Zhang X, Edwards JP, Mosser DM (2006) Dynamic and transient remodeling of the macrophage IL-10 promoter during transcription. *J Immunol* **177**: 1282-1288